CELL JOURNAL

(Yakhteh)

Vol 25, No 10, October 2023, Serial Number: 117
Pages: 665-740

ISSN: 2228-5806
eISSN: 2228-5814

www.celljournal.org

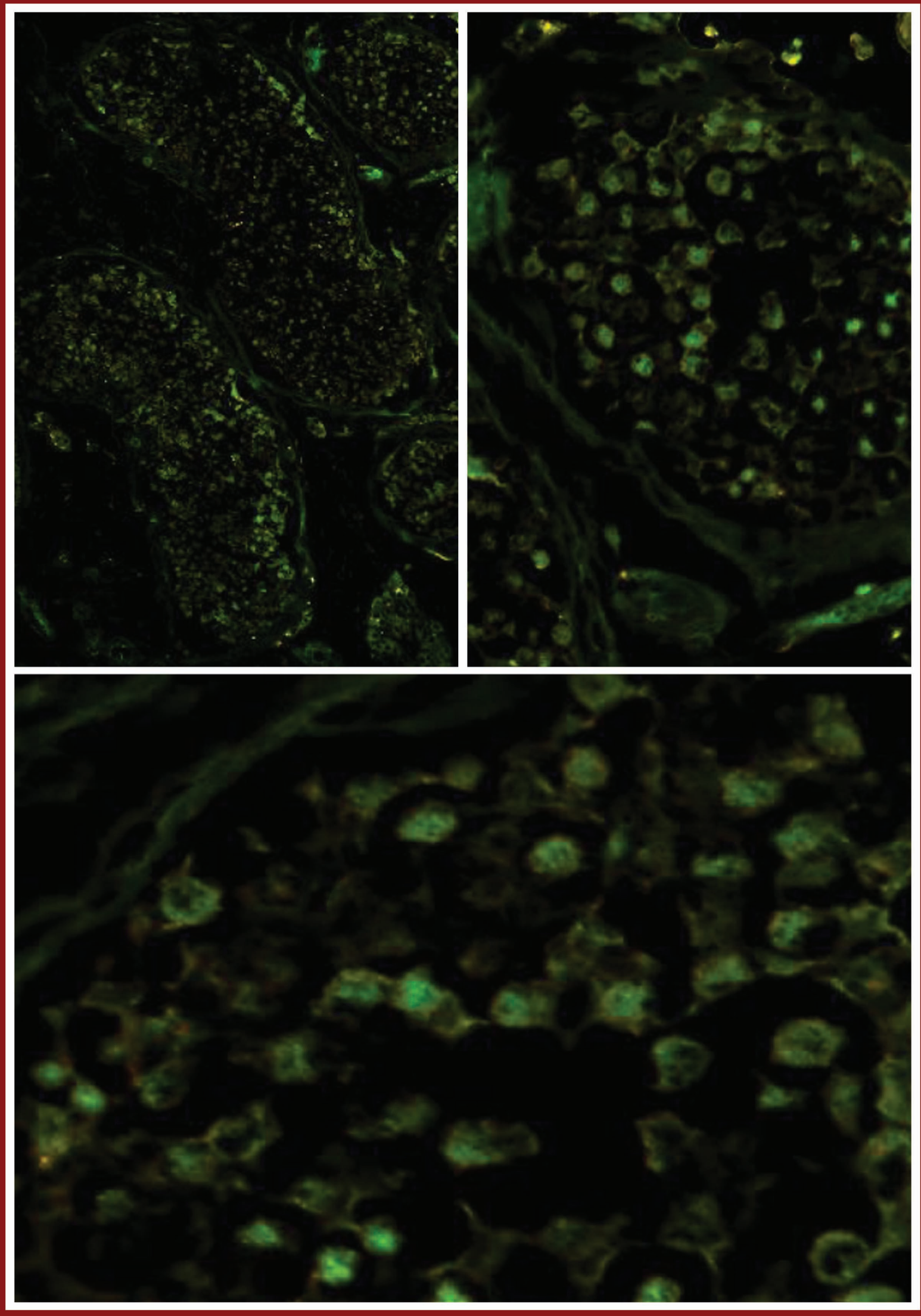

A monthly publication of the Royan Institute

پژوهشگاه رویان

Cell Journal (Yakhteh)

Guide for Authors

Aims and Scope: The "Cell Journal (Yakhteh)" is a peer review and monthly English publication of Royan Institute of Iran. The aim of the journal is to disseminate information by publishing the most recent scientific research studies based on medical and developmental biology including cell therapy and regenerative medicine, stem cell biology reproductive medicine, medical genetics, immunology, oncology, clinical biochemistry, neuroscience, and tissue engineering. **Cell J**, has been certified by the Ministry of Culture and Islamic Guidance since 1999 and accredited as a scientific and research journal by HBI (Health and Biomedical Information) Journal Accreditation Commission since 2000 which is an open access journal. **This journal holds the membership of the Committee on Publication Ethics (COPE).**

1. Types of articles

The articles in the field of Cellular and Molecular can be considered for publications in **Cell J.** These articles are as below:

A. Original articles

Original articles are scientific reports of the original research studies. The article consists of English Abstract (structured), Introduction, Materials and Methods, Results, Discussion, Conclusion, Acknowledgements, Author's Contributions, and References **(Up to 40).**

B. Review articles

Review articles are the articles written by well experienced authors and those who have excellence in the related fields. The corresponding author of the review article must be one of the authors of at least three published articles appearing in the references. The review article consists of English Abstract (unstructured), Introduction, Conclusion, Author's Contributions, and References **(Up to 90).**

C. Systematic Reviews

Systematic reviews are a type of literature review that collect and critically analyzes multiple research studies or papers. The Systematic reviews consist of English Abstract (unstructured), Introduction, Materials and Methods, Results, Discussion, Conclusion, Acknowledgements, Author's Contributions, and References **(Up to 90).**

D. Short communications

Short communications are articles containing new findings. Submissions should be brief reports of ongoing researches. The short communication consists of English Abstract (unstructured), the body of the manuscript (should not hold heading or subheading), Acknowledgements, Author's Contributions, and References **(Up to 30).**

E. Case reports

Case reports are short discussions of a case or case series with unique features not previously described which make an important teaching point or scientific observation. They may describe novel techniques or use equipment, or new information on diseases of importance. It consists of English Abstracts (Unstructured), Introduction, Case Report, Discussion, Acknowledgements, Author's Contributions, and References **(Up to 30).**

F. Commentary

Commentaries are short articles containing a contemporary issue that is relevant to the journal's scope and also expressing a personal opinion or a new perspective about existing research on a particular topic. The Commentary consists of English Abstract (unstructured), the body of the manuscript (should not hold heading or subheading), Acknowledgements, Author's Contributions, and References **(Up to 30).**

G. Editorial

Editorials are articles should be written in relevant and new data of journals' filed by either the editor in chief or the editorial board.

H. Imaging in biology

Images in biology should focus on a single case with an interesting illustration such as a photograph, histological specimen or investigation. Color images are welcomed. The text should be brief and informative.

I. Letter to the editors

Letter to the editors are in response to previously published **Cell J** articles, and may also include interesting cases that do not meet the requirement of being truly exceptional, as well as other brief technical or clinical notes of general interest.

J. Debate

Debates are articles which show a discussion of the positive and negative view of the author concerning all aspect of the issue relevant to scientific research.

2. Submission process

It is recommended to see the guidelines for reporting different kinds of manuscripts. This guide explains how to prepare the manuscript for submission. Before submitting, we suggest authors to familiarize themselves with **Cell J** format and content by reading the journal via the website (www.celljournal.com). The corresponding author ensures that all authors are included in the author list and agree with its order, and they must be aware of the manuscript submission.

A. Author contributions statements

It is essential for authors to include a statement of responsibility in the manuscript that specifies all the authors' contributions. This participation must include: Conceptualization, Methodology, Software, Validation, Formal analysis, Investigation, Resources, Data Curation, Writing - Original Draft, Writing - Review & Editing, Visualization, Supervision, Project administration, and Funding acquisition. Authors who do not meet the above criteria should be acknowledged in the Acknowledgments section.

B. Cover letter and copyright

Each manuscript should be accompanied by a cover letter, signed by all authors specifying the following statement: "The manuscript has been seen and approved by all authors and is not under active consideration for publication. It has neither been accepted for publication nor published in another journal fully or partially (except in abstract form). **Also, no manuscript would be accepted in case it has been pre-printed or submitted to other websites.** I hereby assign the copyright of the enclosed manuscript to **Cell J.**" The corresponding author must confirm the proof of the manuscript before online publishing. It is needed to suggest three peer reviewers in the field of their manuscript.

C. Manuscript preparation

Authors whose first language is not English encouraged to consult a native English speaker in order to confirm his manuscripts to American or British (not a mixture) English usage and grammar. It is necessary to mention that we will check the plagiarism of your manuscript by iThenticate Software. The manuscript should be prepared in accordance with the "International Committee of Medical Journal Editors (ICMJE)". Please send your manuscript in two formats word and PDF (including: title, name of all the authors with their degree, abstract, full text, references, tables and figures) and also send tables and figures separately in the site. The abstract and text pages should have consecutive line numbers in the left margin beginning with the title page and continuing through the last page of the written text. Each abbreviation must be defined in the abstract and text when they are mentioned for the first time. Avoid using abbreviation in the title. Please use the international and standard abbreviations and symbols

It should be added that an essential step toward the integration and linking of scientific information reported in published literature is using standardized nomenclature in all fields of science and medicine. Species names must be italicized (*e.g., Homo sapiens*) and also the full genus and species written out in full, both in the title of the manuscript and at the first mention of an organism in a paper.

It is necessary to mention that genes, mutations, genotypes, and alleles must be indicated in italics. Please use the recommended name by consulting the appropriate genetic nomenclature database, e.g., HUGO for human genes. In another words; if it is a human gene, you must write all the letters in capital and italic (*e.g., OCT4, c-MYC*). If not, only write the first letter in capital and italic (*e.g., Oct4, c-Myc*). **In addition, protein designations are the same as the gene symbol but are not italicized.**

Of note, Cell J will only consider publishing genetic association study papers that are novel and statistically robust. Authors are advised to adhere to the recommendations outlined in the STREGA statement (http://www.strega-statement.org). The following criteria must be met for all submissions:

1. Hardy-Weinberg Equilibrium (HWE) calculations must be carried out and reported along with the P-values if applicable [see Namipashaki et al. 2015 (Cell J, Vol 17, N 2, Pages: 187-192) for a discussion].

2. Linkage disequilibrium (LD) structure between SNPs (if multiple SNPs are reported) must be presented.

3. Appropriate multiple testing correction (if multiple independent SNPs are reported) must be included.

Submissions that fail to meet the above criteria will be rejected before being sent out for review.

Each of the following manuscript components should begin in the following sequence:

Authors' names and order of them must be carefully considered (full name(s), highest awarded academic degree(s), email(s), and institutional affiliation(s) of all the authors in English. Also, you must send mobile number and full postal address of the corresponding author).

Changes to Authorship such as addition, deletion or rearrangement of author names must be made only before the manuscript has been accepted in the case of approving by the journal editor. In this case, the corresponding author must explain the reason of changing and confirm them (which has been signed by all authors of the manuscript). If the manuscript has already been published in an online issue, an erratum is needed. Please contact us via info@celljournal.org in case of any changes (corrections, retractions, erratum, etc.).

Title is providing the full title of the research (do not use abbreviations in title).

Running title is providing a maximum of 7 words (no more than 50 characters).

Abstract must include Objective, Materials and Methods, Results, and Conclusion (no more than 300 words).

Keywords, three to five, must be supplied by the authors at the foot of the abstract chosen from the Medical Subject Heading (MeSH). Therefore; they must be specific and relevant to the paper.

The following components should be identified after the abstract:

Introduction: The Introduction should provide a brief background to the subject of the paper, explain the importance of the study, and state a precise study question or purpose.
Materials and Methods: It includes the exact methods or observations of experiments. If an apparatus is used, its manufacturer's name and address should be stipulated in parenthesis. If the method is established, give reference but if the method is new, give enough information so that another author can perform it. If a drug is used, its generic name, dose, and route of administration must be given. Standard units of measurements and chemical symbols of elements do not need to be defined.

Statistical analysis: Type of study and statistical methods should be mentioned and specified by any general computer program used.

Ethical considerations*:* Please state that informed consent was obtained from all human adult participants and from the parents or legal guardians of minors and include the name of the appropriate institutional review board that approved the project. It is necessary to indicate in the text that the maintenance and care of experimental animals complies with National Institutes of Health guidelines for the humane use of laboratory animals, or those of your Institute or agency.

Clinical trial registration: All of the Clinical Trials performing in Iran must be registered in Iranian Registry of Clinical Trials (www.irct.ir). The clinical trials performed abroad, could be considered for publication if they register in a registration site approved by WHO or www.clinicaltrials.gov. If you are reporting phase II or phase III randomized controlled trials, you must refer to the CONSORT Statement for recommendations to facilitate the complete and transparent reporting of trial findings. Reports that do not conform to the CONSORT guidelines may need to be revised before peer-reviewing.

Results: They must be presented in the form of text, tables, and figures. Take care that the text does not repeat data that are presented in tables and/or figures. Only emphasize and summarize the essential features of the main results. Tables and figures must be numbered consecutively as appeared in the text and should be organized in separate pages at the end of the manuscript while their location should be mentioned in the main text.

Tables and figures: If the result of your manuscript is too short, it is better to use the text instead of tables & figures. Tables should have a short descriptive heading above them and also any footnotes. Figure's caption should contain a brief title for the whole figure and continue with a short explanation of each part and also the symbols used (no more than 100 words). All figures must be prepared based on cell journal's guideline in color (no more than 6 Figures and Tables) and also in TIF format with 300 DPI resolution.

Of Note: Please put the tables & figures of the result in the results section not any other section of the manuscript.

Supplementary materials would be published on the online version of the journal. This material is important to the understanding and interpretation of the report and should not repeat material within the print article. The amount of supplementary material should be limited. Supplementary material should be original and not previously published and will undergo editorial and peer review with the main manuscript. Also, they must be cited in the manuscript text in parentheses, in a similar way as when citing a figure or a table. Provide a caption for each supplementary material submitted.

Discussion: It should emphasize the present findings and the variations or similarities with other researchers done by other researchers. The detailed results should not be repeated in the discussion again. It must emphasize the new and important aspects of the study.

Conclusion: It emphasizes the new and important aspects of the study. All conclusions are justified by the results of the study.

Acknowledgements: This part includes a statement thanking those who contributed substantially with work relevant to the study but does not have authorship criteria. It includes those who provided technical help, writing assistance and name of departments that provided only general support. You must mention financial support in the study. Otherwise; write this sentence "There is no financial support in this study".

Conflict of interest: Any conflict of interest (financial or otherwise) and sources of financial support must be listed in the Acknowledgements. It includes providers of supplies and services from a commercial organization. Any commercial affiliation must be disclosed, regardless of providing the funding or not.

Of Note: If you have already any patent related to the subject of your manuscript, or you are going to apply for such a patent, it must be mentioned in this part.

References: The references must be written based on the Vancouver style. Thus the references are cited numerically in the text and listed in the bibliography by the order of their appearance. The titles of journals must be abbreviated according to the style used in the list of Journals Indexed in PubMed. Write surname and initials of all authors when there are six or less. In the case of seven or more authors, the names of the first six authors followed by "et al." must be listed. You can download Endnote file for Journal references style: endnote file

The reference of information must be based on the following order:

Article:

Surname(s) and first letter of name &middle name(s) of author(s) .Manuscript title. Journal title (abbr).publication date (year); Volume & Issue: Page number.

Example: Manicardi GC, Bianchi PG, Pantano S, Azzoni P, Bizzaro D, Bianchi U, et al. Presence of endogenous nicks in DNA of ejaculated human spermatozoa and its relationship to chromomycin A3 accessibility. Biol Reprod. 1995; 52(4): 864-867.

Book:

Surname(s) and first letter of name & middle name(s) of author(s).Book title. Edition. Publication place: publisher name; publication date (year); Page number.

Example: Edelman CL, Mandle CL. Health promotion throughout the lifespan. 2nd ed. ST Louis: Mosby; 1998; 145-163.

Chapter of book:

Surname(s) and first letter of name & middle name(s) of author(s).Chapter title. In: Surname(s) and first letter of name & middle name(s) of editor(s), editors. Book title. Edition. Publication place: publisher name; publication date (year); Page number.

Example: Phillips SJ, Whisnant JP. Hypertension and stroke. In: Laragh JH, Brenner BM, editors. Hypertension: pathophysiology, diagnosis, and management. 2nd ed. New York: Raven Press; 1995; 465-478.

Abstract book:

Example: Amini rad O.The antioxidant effect of pomegranate juice on sperm parameters and fertility potential in mice. Cell J. 2008;10 Suppl 1:38.

Thesis:

Name of author. Thesis title. Degree. City name. University. Publication date (year).

Example: Eftekhari Yazdi P. Comparison of fragment removal and co-culture with Vero cell monolayers on development of human fragmented embryos. Presented for the Ph.D., Tehran. Tarbiyat Modarres University. 2004.

Internet references

Article:

Example: Jahanshahi A, Mirnajafi-Zadeh J, Javan M, Mohammad-Zadeh M, Rohani M. Effect of low-frequency stimulation on adenosineA1 and A2A receptors gene expression in dentate gyrus of perforant path kindled rats. Cell J. 2008; 10 (2): 87-92. Available from: http://www.celljournal.org. (20 Oct 2008).

Book:

Example: Anderson SC, Poulsen KB. Anderson's electronic atlas of hematology.[CD-ROM]. Philadelphia: Lippincott Williams & Wilkins; 2002.

D. Proofs are sent by email as PDF files and should be checked and returned within 72 hours of receipt. It is the authors' responsibility to check that all the text and data as contained in the page proofs are correct and suitable for publication. **We are requested to pay particular attention to author's names and affiliations as it is essential that these details be accurate when the article is published.**

E. Pay for publication: Publishing an article in **Cell J** requires Article Processing Charges (APC) that will be billed to the submitting author following the acceptance of an article for publication. For more information please see www.celljournal.org.

F. Ethics of scientific publication: Manuscripts that have been published elsewhere with the same intellectual material will refer to duplicate publication. If authors have used their own previously published work or work that is currently under review, as the basis for a submitted manuscript, they are required to cite the previous work and indicate how their submitted

manuscript offers novel contributions beyond those of the previous work. Research and publication misconduct is considered a serious breach of ethics.

The Journal systematically employs iThenticate, plagiarism detection and prevention software designed to ensure the originality of written work before publication. Plagiarism of text from a previously published manuscript by the same or another author is a serious publication offence. Some parts of text may be used, only where the source of the quoted material is clearly acknowledged.

3. General information

A. You can send your manuscript via online submission system which is available on our website. If the manuscript is not prepared according to the format of **Cell J**, it will be returned to authors.

B. The order of article appearance in the Journal is not demonstrating the scientific characters of the authors.

C. Cell J has authority to accept or reject the manuscript.

D. Corresponding authors should send the manuscripts via the Online Manuscript Submission System. All submissions will be evaluated by the associated editor in order to check scope and novelty. If the manuscript suits the journal criteria, the associated editor would select the single-blind peer-reviewers. The reviewers of the manuscript must not share information about the review with anyone without permission of the editors and authors. If three reviewers pass their judgments on the manuscript, it will be presented to the associated editor of **Cell J**. In the case of having a favorable judgment on the manuscript, reviewers' comments will be presented to the corresponding author (the identification of the reviewers will not be revealed). After receiving the revision, the associated editor would choose the final reviewer among the previous ones. The final decision will be taken by editor-in-chief based on the final reviewer's comments. The review process takes between 2 to 4 months in **Cell J**. The executive member of journal will contact the corresponding author directly within 3-4 weeks by email. If authors do not receive any reply from journal office after the specified time, they can contact the journal office. Finally, the executive manager will respond promptly to authors' request.

After receiving the acceptance letter, the abstract of the paper would be published electronically. The paper will be in a queue to be published in one Cell J. At last, the corresponding author should verify a proof copy of the paper in order to be published.

The Final Checklist

The authors must ensure that before submitting the manuscript for publication, they have to consider the following parts:

1. The first page of manuscript should contain title, name of the author/coauthors, their academic qualifications, designation & institutions they are affiliated with, mailing address for future correspondence, email address, phone, and fax number.

2. Text of manuscript and References prepared as stated in the "guide for authors" section.

3. Tables should be on a separate page. Figures must be sent in color and also in JPEG (Jpg) format.

4. Cover Letter should be uploaded with the signature of all authors.

5. An ethical committee letter should be inserted at the end of the cover letter.

The Editor-in-Chief: Ahmad Hosseini, Ph.D.

Cell Journal *(Yakhteh)*

P.O. Box: 16635-148, Iran

Tel/Fax: + 98-21-22510895

Emails: info@celljournal.org

journals@celljournal.org

Dr. Saeed Kazemi Ashtiani

IN THE NAME OF GOD

Gone But not Forgotten

In the memory of the late Director of Royan Institute, Founder of Stem Cells Research in Iran and Chairman of ***Cell Journal*** *(Yakhteh)*. May he rest in peace.

PUBLISHED & SPONSORED BY:
Publication of Royan Institute (ACECR)

Indexed in:
1. Thomson Reuters (ISI)
2. PubMed
3. PubMed Central (PMC)
4. National Library Medicine (NLM)
5. Biosis Preview
6. Index Medicus for the Eastern Mediterranean Region (IMEMR)
7. Regional Information Center for Sciences and Technology (RICeST)
8. Index Copernicus International
9. Cambridge Scientific Abstract (CSA)
10. EMBASE
11. Scopus
12. Cinahl Database
13. Google Scholar
14. Chemical Abstract Service (CAS)
15. Proquest
16. Directory of Open Access Journals (DOAJ)
17. Open Academic Journals Index (OAJI)
18. Directory of Research Journals Indexing (DRJI)
19. Scientific Information Database (SID)
20. Iranmedex
21. Islamic World Science Citation Center (ISC)
22. Magiran
23. Science Library Index
24. Biological Abstracts
25. Essential Science Indicators
26. EuroPub

Editorial Office Address (Dr. Ahmad Hosseini):
Royan Institute, P.O.Box: 16635-148,
Tehran, Iran
Tel & Fax: (+9821)22510895
Website: www.celljournal.org
Emails: info@celljournal.org
journals@celljournal.org

Printing Company:
Naghshe e Johar Co.
No. 103, Fajr alley, Tehranpars Street,
Tehran, Iran.

Cell Journal(Yakhteh), Vol 25, No 10, October 2023, Serial Number: 117, Pages: 665-740

CONTENTS

Original Articles

Commentary

Cell J
Cell Journal(Yakhteh)
Homepage: https://www.celljournal.org/
Original Article
Vol 25, No 10, October 2023, Pages: 665-673

CRISPR/Cas9-Mediated Generation of *COL7A1*-Deficient Keratinocyte Model of Recessive Dystrophic Epidermolysis Bullosa

Farzad Alipour, Ph.D.[1, 2], Mana Ahmadraji, M.Sc.[2], Elham Yektadoust, M.Sc.[2], Parvaneh Mohammadi, Ph.D.[2, 3], Hossein Baharvand, Ph.D.[2, 4], Mohsen Basiri, Ph.D.[2, 5*]

1. Department of Applied Cell Sciences, Faculty of Basic Sciences and Advanced Medical Technologies, Royan Institute, ACECR, Tehran, Iran
2. Department of Stem Cells and Developmental Biology, Cell Science Research Center, Royan Institute for Stem Cell Biology and Technology, ACECR, Tehran, Iran
3. Experimental Medicine and Therapy Research, University of Regensburg, Regensburg, Germany
4. Department of Developmental Biology, School of Basic Sciences and Advanced Technologies in Biology, University of Science and Culture, Tehran, Iran
5. Advanced Therapy Medicinal Product Technology Development Center (ATMP-TDC), Royan Institute for Stem Cell Biology and Technology, ACECR, Tehran, Iran

Abstract

Objective: Recessive dystrophic epidermolysis bullosa (RDEB) is a genetic skin fragility and ultimately lethal blistering disease caused by mutations in the *COL7A1* gene which is responsible for coding type VII collagen. Investigating the pathological mechanisms and novel candidate therapies for RDEB could be fostered by new cellular models. The aim of this study was to employ CRISPR/Cas9 technology in the development of immortalized *COL7A1*-deficient keratinocyte cell lines intended for application as a cellular model for RDEB in *ex vivo* studies.

Materials and Methods: In this experimental study, we used transient transfection to express *COL7A1*-targeting guide RNA (gRNA) and Cas9 in HEK001 immortalized keratinocyte cell line followed by enrichment with fluorescent-activated cell sorting (FACS) via GFP expressing cells (GFP^+ HEK001). Homogenous single-cell clones were then isolated, genotyped, and evaluated for type VII collagen expression. We performed a scratch assay to confirm the functional effect of *COL7A1* knockout.

Results: We achieved 46.1% ($P<0.001$) efficiency of in/del induction in the enriched transfected cell population. Except for 4% of single nucleotide insertions, the remaining in/dels were deletions of different sizes. Out of nine single expanded clones, two homozygous and two heterozygous *COL7A1*-deficient cell lines were obtained with defined mutation sequences. No off-target effect was detected in the knockout cell lines. Immunostaining and western blot analysis showed lack of type VII collagen (COL7A1) protein expression in these cell lines. We also showed that *COL7A1*-deficient cells had higher motility compared to their wild-type counterparts.

Conclusion: We reported the first isogenic immortalized *COL7A1*-deficient keratinocyte lines that provide a useful cell culture model to investigate aspects of RDEB biology and potential therapeutic options.

Keywords: COL7A1, CRISPR/Cas9, Keratinocyte, Recessive Dystrophic Epidermolysis Bullosa

Citation: **Alipour F, Ahmadraji M, Yektadoust E, Mohammadi P, Baharvand H, Basiri M. CRISPR/Cas9-mediated generation of COL7A1-deficient keratinocyte model of recessive dystrophic epidermolysis bullosa. Cell J. 2023; 25(10): 665-674. doi: 10.22074/CELLJ.2023.1989321.1225**

Introduction

Epidermolysis bullosa (EB) is a group of inherited skin blistering diseases, characterized by fragility of the skin due to defective epithelial cell adhesion leading to blister, erosion, and ulcers (1). In this group of diseases, 16 genes have thus far been detected that their protein expressions in keratinocyte and fibroblast participated in the cell cytoskeleton and extracellular matrix. According to phenotypic heterogeneity, there are four main subtypes including EB simplex (EBS), junctional EB (JEB), dystrophic EB (DEB), and Kindler syndrome (2). The severest form of these diseases is recessive dystrophic EB (RDEB), caused by loss of function mutations in *COL7A1*, the gene coding for type VII collagen protein (3). This protein is the main component of anchoring fibrils which is crucial for the adherence of the dermal-epidermal basement membrane. Mutations in *COL7A1* cause a variety of severities where truncated forms manifest a relatively milder forms and complete lack of the protein results in severest forms of RDEB (4).

Experimental studies on rare genetic disorders, such as

Received: 07/February/2023, Revised: 15/June/2023, Accepted: 06/August/2023
***Corresponding Address: P.O.Box: 16635-148, Department of Stem Cells and Developmental Biology, Cell Science Research Center, Royan Institute for Stem Cell Biology and Technology, ACECR, Tehran, Iran**
Email: basiri@royaninstitute.org

Royan Institute
Cell Journal (Yakhteh)

RDEB confront ethical and practical challenges including paucity of available stable patient donors, technical inconsistency in sampling and cell isolation, patient discomfort, and variability in the severity of disease between patients (5). Moreover, obtaining RDEB primary cells are mostly challenging due to inefficient and labor-consuming isolation, expansion, and limited proliferation capacity. These show the need for cell lines which could easily be handled for experimental purposes (6). Although animal models are available for EB disorders, they exhibit some shortcomings such as imperfection in development, stillbirth, and deficiency in the recapitulation of disease phenotype (7). Therefore, there is a need to establish new cellular RDEB models to study pathological pathways and evaluate potential therapeutic approaches.

Gene editing technologies, such as clustered regularly interspaced short palindromic repeats (CRISPR)/CRISPR associated protein 9 (Cas9) technology, have provided a straightforward means to introduce mutations to normal cells for modeling purposes. Site-specific double-strand break (DSB) induced by CRISPR/Cas9 complex undergoes the error-prone non-homologous end joining (NHEJ) DNA repair, which may result in insertion-deletion (in/del) mutations. A portion of in/del mutations causes frameshift or other types of detrimental changes in the gene sequence (8). Introducing mutations to the disease-related genes in the context of a normal cell line has been used as a powerful method to generate isogenic cellular models for different diseases (9-14).

The aim of this study was to generate immortalized *COL7A1*-deficient keratinocytes, as a cellular model for RDEB, using CRISPR/Cas9 technology. Since truncated *COL7A1* mutants represent mild manifestations of the disease and might hamper future investigations on exogenous type VII collagen therapeutics, we aimed to eliminate expression of the whole protein by targeting the first exon. The resultant *COL7A1*-deficient keratinocyte cell lines were then characterized in terms of genotype and type VII collagen expression.

Materials and Methods

Guide RNA design and construction

To induce frameshift on the transcription sequence of *COL7A1*, we designed one guide RNA (gRNA; 5′-ACTGCCTAGGATGACGCTG-3′) targeting the first exon of *COL7A1* gene, based on minimal off-target activity by CRISPOR online bioinformatic tool (15). Designed complementary sense (ghCOL7A1-S) and antisense (ghCOL7A1-A) oligonucleotides (Table S1, See Supplementary Online Information at www.celljournal.org) incubated to hybridize together and constitute a double-strand oligonucleotide. The hybridized double-stranded (ghCOL7A1-S+ghCOL7A1-A) DNA fragment cloned into the Esp3I (BsmBI) restriction sites of the LentiCRISPRv2GFP (Addgene plasmid # 82416) using a simultaneous digestion-ligation reaction as described previously (16). Briefly, a mixture of 10 pmol of the insert DNA fragment, 1 µg of LentiCRISPRv2GFP plasmid, 5 units of Esp3I enzyme, 1 unit of T4 DNA ligase, 1 µl of 10X FastDigest buffer, and 1 µl of 10X T4 DNA ligase buffer (all reagents from Thermo Fisher Scientific, USA) in a total volume of 20 µl was incubated in 37°C for 3 hours. The reaction product containing the recombinant plasmid (LentiCRISPRv2GFP-ghCOL7A1) was transformed into chemo-competent *E. coli* cells. Restriction mapping and sequencing were done on single clones for verification of the correct gRNA sequence in the vector.

Cell culture

Immortalized keratinocyte (HEK001) cell line (CRL-2404, ATCC) was cultured on DMEM/F12 medium (Thermo Fisher Scientific), containing 10% (v/v) fetal bovine serum (Thermo Fisher Scientific), 2 mM GlutaMAX (Thermo Fisher Scientific), 1% (v/v) NEAA (Thermo Fisher Scientific), 1% (v/v) Pen/Strep (Thermo Fisher Scientific) and supplemented with KGM-GoldsingleQuots (Lonza, Switzerland), containing Bovine pituitary extract (BPE), insulin (5 mg/ml), epidermal growth factor (EGF, 10 ng/ml), epinephrine, hydrocortisone (0.4 mg/ml), transferrin (17). The cells were incubated at 37°C in a 5% (vol/vol) CO_2 incubator during the performance of experiments.

Transfection of HEK001 cells

HEK001 cells were cultured in a 100 mm culture dish to reach 70-90% confluency. Two to three hours before transfection, the media was replaced with a fresh complete medium without antibiotics. HEK001 cells were transfected with LentiCRISPRv2GFP-ghCOL7A1 plasmid using lipofectamine 2000 Transfection Reagent (Thermo Fisher Scientific) according to the manufacturer's instructions. Briefly, a transfection medium was prepared by adding 24 µg of vector and 24 µl of lipofectamine 2000 to 1 ml base medium of DMEM/F12 in two separate tubes followed by 10 minutes incubation. The vector-containing medium was added to the lipofectamine tube and incubated for another 15 minutes. Transfection medium was added to cells gently and incubated overnight. The next day, the medium was replaced with a fresh keratinocyte growth medium and the cells were grown for another 36 hours. All Incubation was done at 37°C in a humidified 5% (vol/vol) CO_2 incubator.

Single-cell clone isolation

Since in our hand, single HEK001 cells had reduced viability right after FACS isolation, we used a limited dilution method (18, 19) to obtain single-cell clones. Two days after transfection by LentiCRISPRv2GFP-ghCOL7A1 plasmid, around 2×10^5 HEK001 cells expressed GFP (GFP^+ HEK001) isolated by FACS Aria II cell sorter (BD Biosciences, USA) and cultured in one well of a 24-well plate. When 70-90% confluency was reached, the cells were detached by trypsin (Thermo Fisher Scientific), counted, and serially diluted in complete media to obtain a cell suspension of 5 cells/

ml. Then, 100 µl of this suspension was manually seeded in each well of a 96-well plate to obtain an average of 0.5 cells per well. The wells containing truly single cells were determined using an inverted microscope (Olympus, Japan). Selected single-cell clones were then serially expanded into 48-, 24-, 12-, and 6-well plates for downstream analyses.

Sanger sequencing and targeting efficiency assessment

Genome extraction was done with a commercial genome extraction kit (Favorgen Biotech Corporation, Taiwan) according to the manufacturer's instructions. Briefly, 106 cells were resuspended in the lysis buffer of the kit and incubated for 10 minutes to obtain clear cell lysate. Genomic DNA was isolated from the cell lysate using silica columns and washing buffers provided in the kit. The gRNA target region was amplified by polymerase chain reaction (PCR) using COL7A1-F1 and COL7A1-R1 primers (Table S1, See Supplementary Online Information at www.celljournal.org) with the following PCR condition: 95°C for 10 minutes, 35 cycles of 95°C for 30 seconds, 60°C for 30 seconds, 72°C for 45 seconds and then 72°C for 10 minutes. The PCR product was subjected to Sanger sequencing using COL7A1-F2 and COL7A1-R2 primers (Table S1, See Supplementary Online Information at www.celljournal.org). Sequencing data were analyzed for insertion/deletion events and targeting efficiency using the Tracking of in/dels by Decomposition (TIDE) analysis method (20).

Off-target prediction and sequencing

Potential off-target sites in the human genome were predicted using CRISPOR bioinformatic tool (15). Four off-target sites in the exonic regions of *FAT3*, *ANKZF1*, *AXIN2*, and *NPHP4* genes were evaluated with PCR and sequencing. PCR program was done as follows: 95°C for 10 minutes, 35 cycles of 95°C for 30 seconds, 60°C for 30 seconds, and 72°C for 45 seconds, followed by a final extension step at 72°C for 10 minutes. The PCR products were subjected to Sanger sequencing. The primers used for the PCR and sequencing reactions are listed in Table S1 (See Supplementary Online Information at www.celljournal.org).

Immunofluorescence staining

The cells were fixed with paraformaldehyde 4% at 4°C for 20 minutes, washed three times with phosphate buffer saline (PBS) containing 0.05% Tween 20 (PBST, Sigma, Germany), and then permeabilized with 0.5% Triton X-100 (Sigma) at room temperature for 10 minutes. Blocking was performed with goat serum 10% at 37°C for 60 minutes and incubated with rabbit polyclonal antibody against type VII collagen (ab93350, Abcam, UK) at 1:100 dilution, for overnight at 4°C. The following day, the cells were incubated with Alexa Fluor 546-conjugated goat anti-rabbit secondary antibody (A11035, Thermo Fisher Scientific) at 1:500 dilution for 45 minutes at room temperature, and subsequently, nuclei were stained with DAPI 20 mg/ml (Sigma). The cells were analyzed by Olympus IX71S1F-3 inverted fluorescence microscope (Olympus, Japan) equipped with a 100 W Mercury light source (Olympus) as a source of excitation radiation and Olympus U-TV0.63XC image acquisition system. The staining observed by 10X objective lenses for GFP (excitation 460-490 nm, emission 520 nm, exposure time 500 mseconds), Alexa Flour 546 (excitation 510-555 nm, Emission 590 nm, exposure time 500 mseconds) in exposure time (500 mseconds) and DAPI (excitation 330-385 nm, emission 420 nm, exposure time 10 mseconds).

Western blot analysis

To extract total protein, cell pellets were lysed by adding cell lysis buffer (7 M urea, 2 M thiourea, 4% CHAPS, 30 mM Tris, 40 mM dithiothreitol) and 1X cocktail protease inhibitor, vortexing for 5 minutes on ice, sonicating for 5 minutes on ice, followed by centrifuging at 14000 g for 15 minutes and transferring the supernatant to new tubes. Protein concentration was measured by pierce BCA assay (Thermo Fisher Scientific). Protein samples were denatured at 50°C for 60 minutes in 50 µl 5X loading buffer [Laemmle 5X buffer: 0.5 M Tris-HCl, pH=6.8, 10% glycerol, 2% sodium dodecyl sulfate (SDS), 0.025% bromophenol blue and 50 mM dithiothreitol], then separated by loading on 8% SDS-polyacrylamide gel electrophoresis (SDS-PAGE), 100 V, 2 hours, followed by electrotransfer to polyvinylidene fluoride membranes at 15 V and 15°C, overnight. Membranes were blocked with 2% BSA in Tris-buffered saline containing 0.05% Tween (TBST) 20 at room temperature for 2 hours, followed by adding primary antibody rabbit anti-COL7A1 (ab93350, Abcam) at 1:1000 dilution in TBST and they were subsequently incubated overnight. A polyclonal β-tubulin antibody (sc15335, Santa Cruz, USA) at 1:1000 dilution served as loading control. The next day, after washing three times in TBST 0.1%, the blots were incubated at room temperature for 1 hour, with HRP-conjugated donkey anti-rabbit secondary antibody at 1:50000 dilution in TBST, followed by three washes. To detect the desired band, SuperSignal West Femto Maximum Sensitivity substrate (Thermo Scientific) was added, and Chemiluminescent signals were captured by the Alliance Q9 Advanced Uvitec System (UVItec Ltd, UK).

Statistical analysis

TIDE analysis uses a built-in two-tailed t test of the variance-covariance matrix of the standard errors to calculate p-values for the frequency of each in/del mutation (20). To compare the normalized percentage of cell-free area in the scratch assay, we performed a two-way ANOVA followed by Sidak's multiple comparison test using GraphPad Prism 8.0.2 (GraphPad Software Inc., USA). The adjusted P values less than 0.01 were considered statistically significant.

Ethics approval

The study was approved by the Ethical Committee

of Royan Institute (Tehran, Iran) -Academic Center for Education, Culture, and Research (IR.ACECR.ROYAN.REC.1398.076).

Results

Guide RNA Design and generation of *COL7A1* knockout HEK001 cells

To knock out the *COL7A1* gene in HEK001 immortalized keratinocytes, we designed a gRNA targeting the first exon of the gene. The corresponding sequence subcloned under a U6 promoter in an expression plasmid vector containing Cas9 coding sequence linked to GFP through a self-splitting 2A linker (Fig.1A, B). Transfection of HEK001 cells by this vector resulted in a population of GFP$^+$ cells with a transduction efficiency of 14.1 % (Fig.1C). To enrich the gene-modified cells GFP$^+$ cells were isolated by FACS (Fig.1D).

Sequencing analysis of the pool population of transfected cells

To assess targeting efficiency in the transfected HEK001 cells, genomic DNA of the isolated GFP$^+$ cells was extracted and PCR amplicon spanning gRNA targeted site was sequenced by Sanger sequencing. Results showed a composite sequence trace after the break site resulted from the presence of in/del mutations in the pool population of the transfected cells (Fig.2A). Decomposition of the sequence trace data (Fig.2B) showed that overall editing (in/del) efficiency was 46.1% ($P<0.001$) with more frequent deletion events compared to nucleotide insertions (Fig.2C). We did not detect insertion of more than one nucleotide in the bulk population. Single nucleotide insertion was observed in 4.0% ($P<0.001$) of the sequences, containing either T or A nucleotide insertions (Fig.2D).

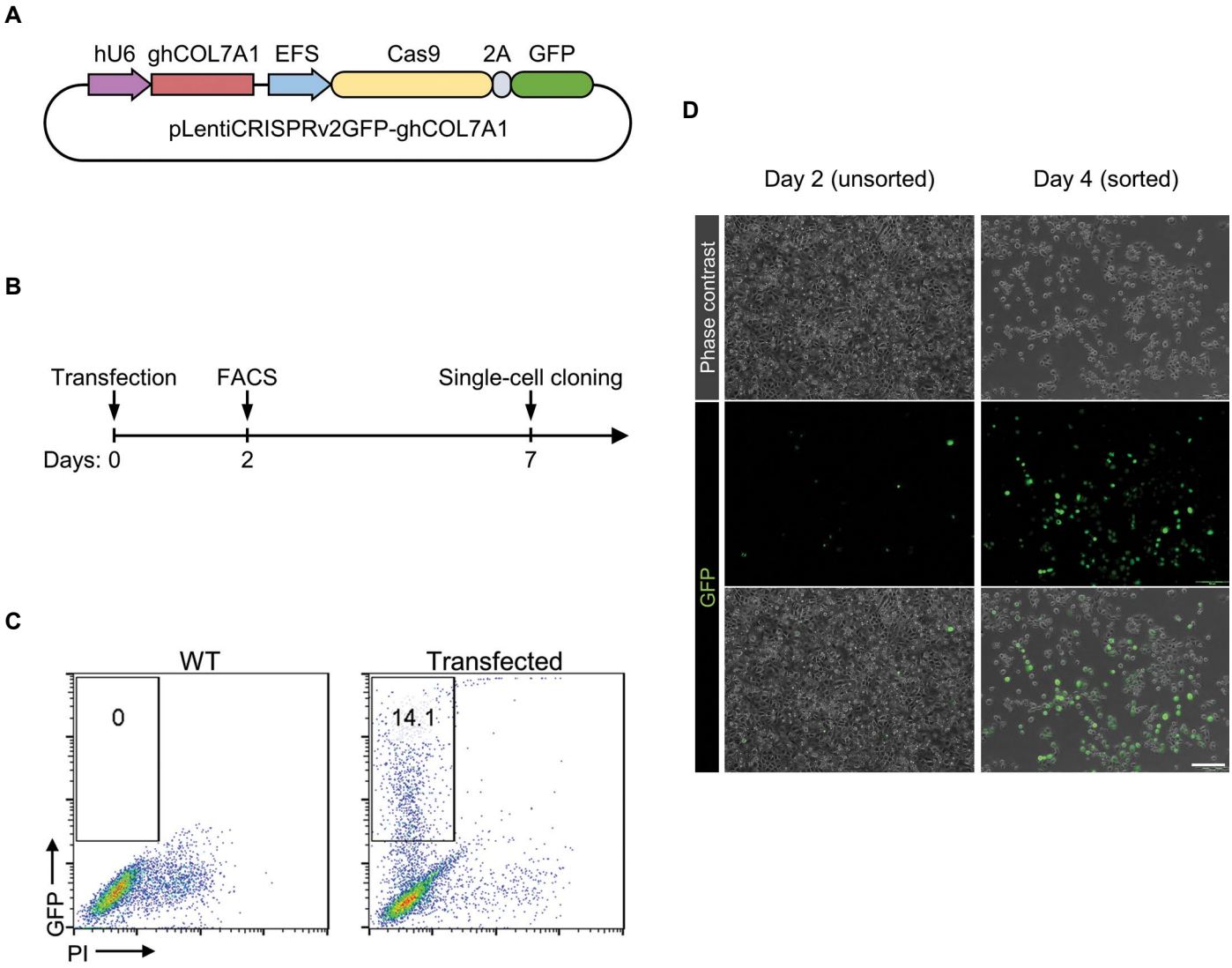

Fig.1: Transfection and isolation of GFP$^+$ cells. **A.** Schematic map of the CRISPR plasmid vector. gRNA was inserted in expression vector encompassing Cas9 and GFP sequence under U6 promoter. **B.** Diagram of the experimental procedure showing transfection, enrichment by fluorescence-activated cell sorting (FACS), and single-cell cloning by limited dilution. **C.** Viable GFP-expressing cells comprising 14% of the transfected keratinocytes were sorted to enrich the genome-edited cell population. **D.** Fluorescent microscopy of the pool population of cells, two days after transfection (before sorting), and enriched GFP$^+$ cells, two days after sorting (scale bar: 50 µm).

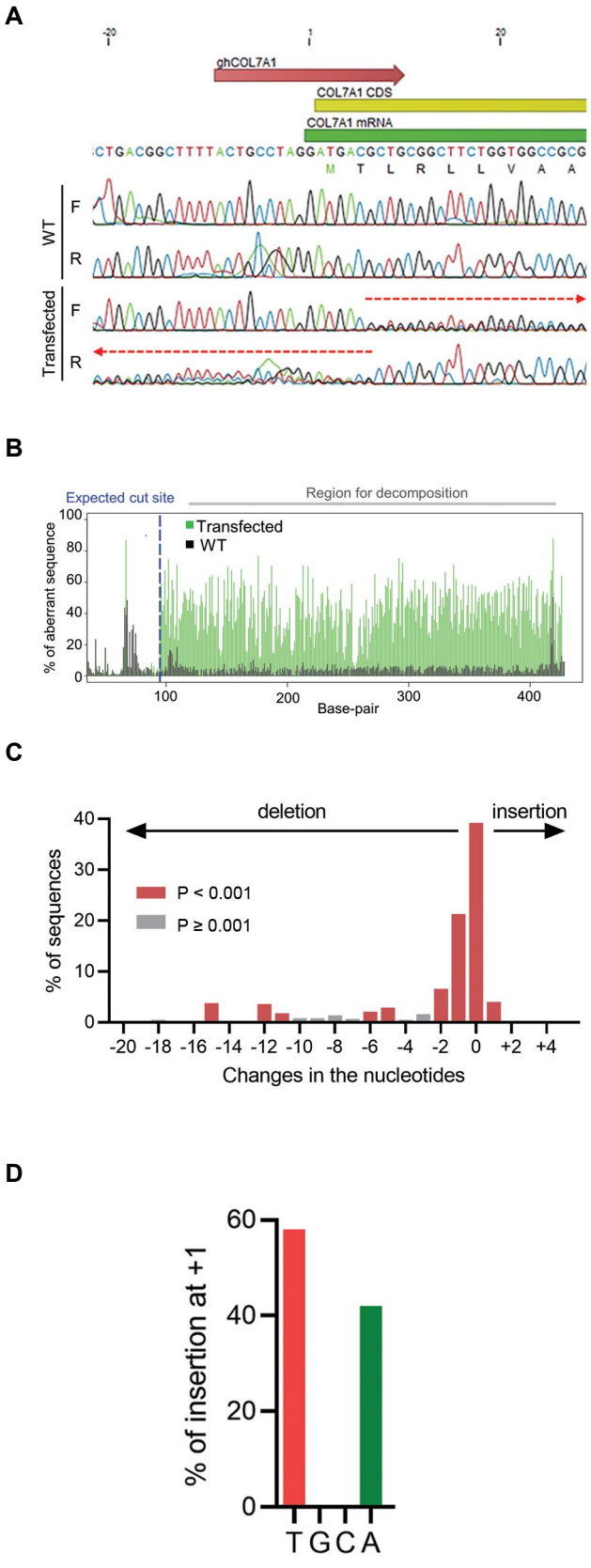

Fig.2: Sanger sequencing and decomposition analysis on the bulk population of transfected HEK001 cells. **A.** Sequencing on the bulk population of the transfected cells represents a composite sequence trace after the break site based on the direction of the indicated primer. **B.** Comparison of transfected bulk with untransfected cells revealed aberrant sequence after the break site. **C.** Decomposition analysis of changes in the targeted region shows frequency of mutations based on the number of nucleotides deleted from or inserted into the sequence. **D.** Out of all single nucleotide insertions, 58% was T and 42% was A. F; Forward primer, R; Reverse primer, and WT; Wild-type.

Sequencing analysis of the single-cell clones

To establish a homogeneous cell line with identified sequence, we isolated single-cell clones from the bulk transfected sequence. Out of 25 clones initially obtained from two 96-well plates, only nine showed normal expansion and they were subjected to further molecular analyses. Decomposition analysis of the target genomic sequence in these nine clones (Fig.3A) showed that only one clone (B6) contained the intact wild-type allele, while in three clones (B2, O3, and T7) more than two alleles were detected. Clone B1 showed a heterozygous genotype with single nucleotide insertion in one allele and an in-frame 15-nucleotide deletion in the other. The above-mentioned clones were excluded from the study, due to the presence of wild-type sequences, in-frame mutations, or possible heterogeneity. However, four other clones (namely clones B4, T5, T6, and T8) showed genotypes compatible with the complete abolition of the *COL7A1* function. Clones B4 and T8 had heterozygous genotypes with deleterious frameshift mutations in the both alleles (Fig.3B, C). A single-nucleotide deletion at positions +9 (ninth nucleotide after the transcription start site) and a two-nucleotide deletion at positions +7 to +8 in clone B4 and a single-nucleotide deletion at position +7 in clone T8 introduced frameshifts into the *COL7A1* coding sequence which resulted in altered amino acid sequence and ectopic stop codons. The second allele of clone T8 had a 7-nucleotide deletion (positions +1 to +7) eliminating the start codon. Clones T5 and T6 showed homozygous deletion of, respectively, 33 nucleotides (positions −26 to +8) and 32 nucleotides (positions −21 to +12) encompassing both the transcription start site and start codon of *COL7A1* gene (Fig.3C).

Off-target analysis

To ensure that the selected clones do not contain undesirable mutations due to the off-target activity of the CRISPR system, we performed an in-silico off-target prediction. Among 70 predicted off-target sites with four or fewer mismatched nucleotides (Table S2, See Supplementary Online Information at www.celljournal.org), only four were located in exonic sequences of *FAT3*, *ANKZF1*, *AXIN2*, and *NPHP4* genes, hence carrying the risk of unwanted mutations in a coding sequence. However, PCR-sequencing of these potential exonic off-target sites in the *COL7A1*-knockout cell lines showed no mutation when compared to the wild-type sequence (Fig.4).

Type VII collagen protein expression in selected knockout clones

Immunofluorescent staining was used to confirm the *COL7A1*-KO cell lines at the protein level. No expression of type VII collagen (COL7A1) was observed in the four clones selected in genotyping compared to the wild-type HEK001 keratinocytes in immunostaining and Western blot analysis results (Fig.5A, B). These results verified *COL7A1* deficiency predicted at sequence level on the four selected cell lines.

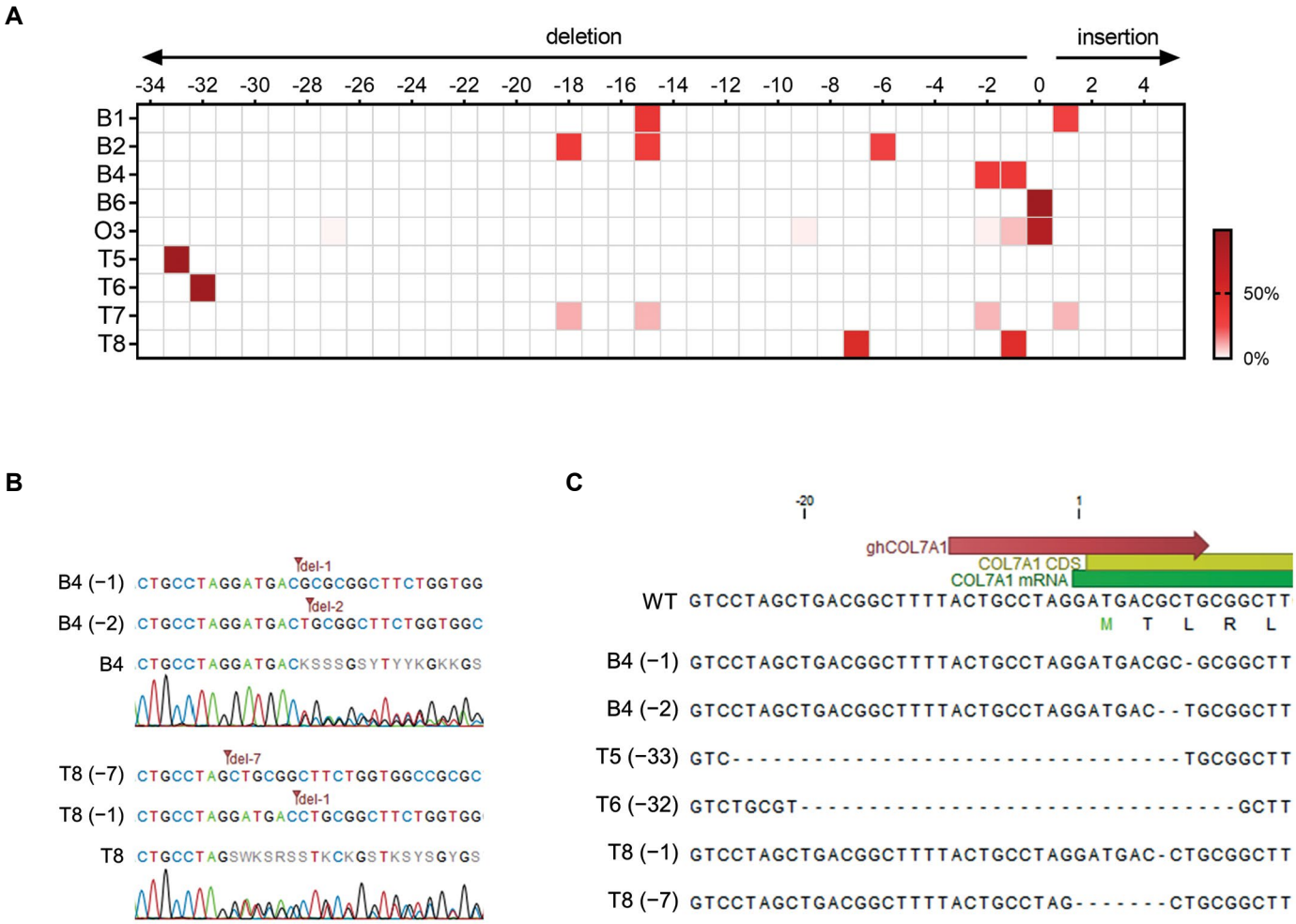

Fig.3: Genotyping of the single-cell clones. **A.** Heatmap summarizes the results of decomposition analysis on the sequences data obtained from nine single-cell clones shown on the vertical axis. Only the genotypes with statistically significant (P<0.001) frequency compared to the control sequence were depicted. **B.** Decomposition of alleles in two heterozygous clones (B4 and T8) with deleterious mutations. **C.** Deleterious alleles detected in four knockout clones with frameshift mutations in B4 (-1), B4 (-2).

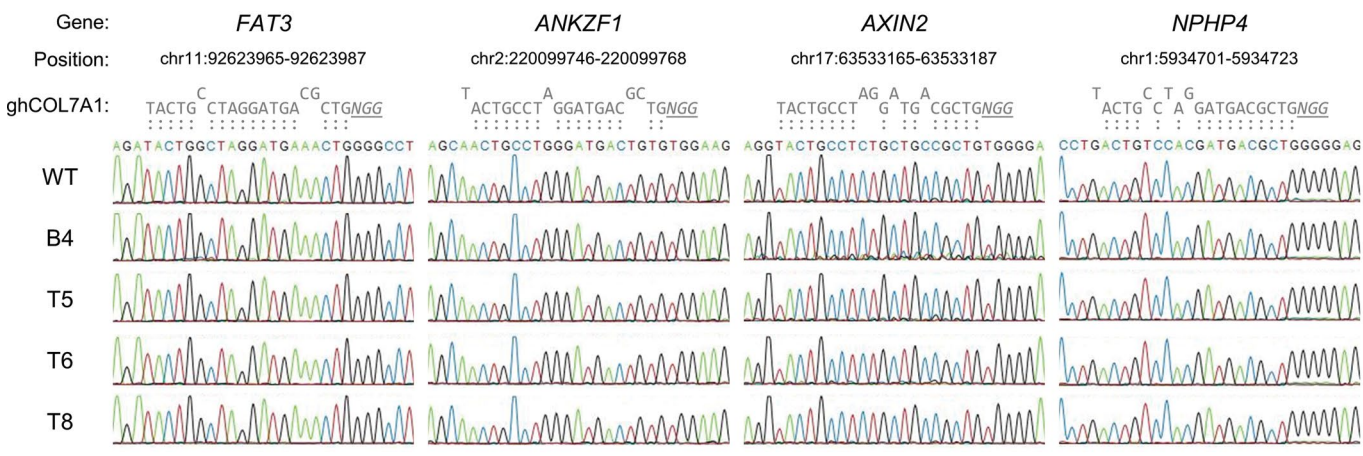

Fig.4: Investigating exonic potential off-target sites of ghCOL7A1 in knockout cell lines. Four predicted off-target sites in exonic sequences of *FAT3*, *ANKZF1*, *AXIN2*, and *NPHP4* genes were amplified by polymerase chain reaction (PCR) and subjected to DNA sequencing. Matched and mismatched nucleotides in comparison with ghCOL7A1 are shown above each sequence. No mutation was detected in any of these potential off-target sites.

Evaluation of cellular motility in the knockout cell lines

Since loss of COL7A1 deficiency is associated with increased cellular motility, and elevated risk of keratinocyte malignancy as well as invasiveness in RDEB patients (21-23), we sought to measure cell motility in our *COL7A1*-KO HEK001 model, as a functional indicator of *COL7A1* gene disruption. Using a scratch assay, we observed that the *COL7A1*-knockout HEK001 cells exerted significantly higher migration compared to the wild-type cells (Fig.6A, B).

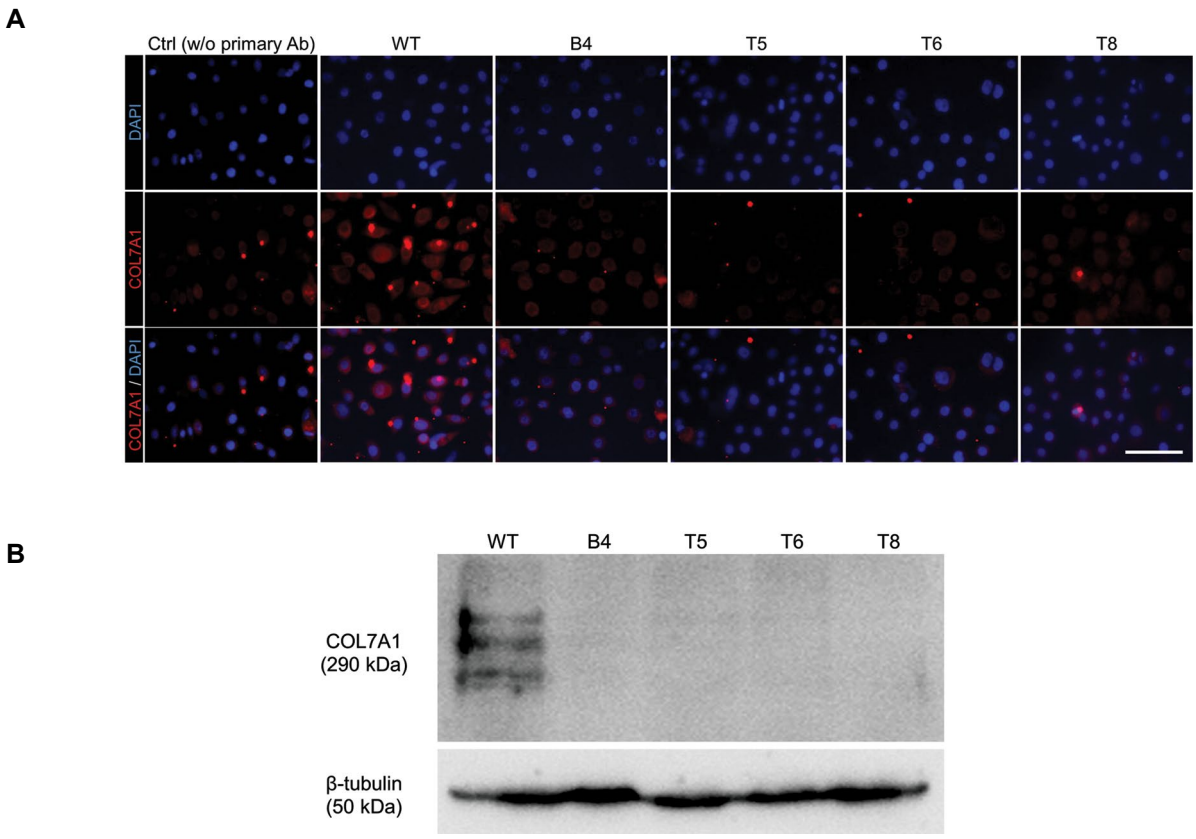

Fig.5: Evaluation of COL7A1 protein expression in the *COL7A1*-knockout HEK001 cell lines. **A.** Four knockout cell lines (B4, T5, T6, and T8) were stained with type VII collagen (COL7A1)-specific antibody along with wild-type (WT) HEK001 cells. COL7A1 protein expression was not detected in any of the knockout cell lines as compared to the WT cells. A representative negative control without primary antibody (Ctrl w/o primary Ab) was included for comparison (scale bar: 100 µm). **B.** Western blot analysis of COL7A1 protein expression in the wild-type and knockout HEK001 cell lines. Human β-tubulin served as an internal control.

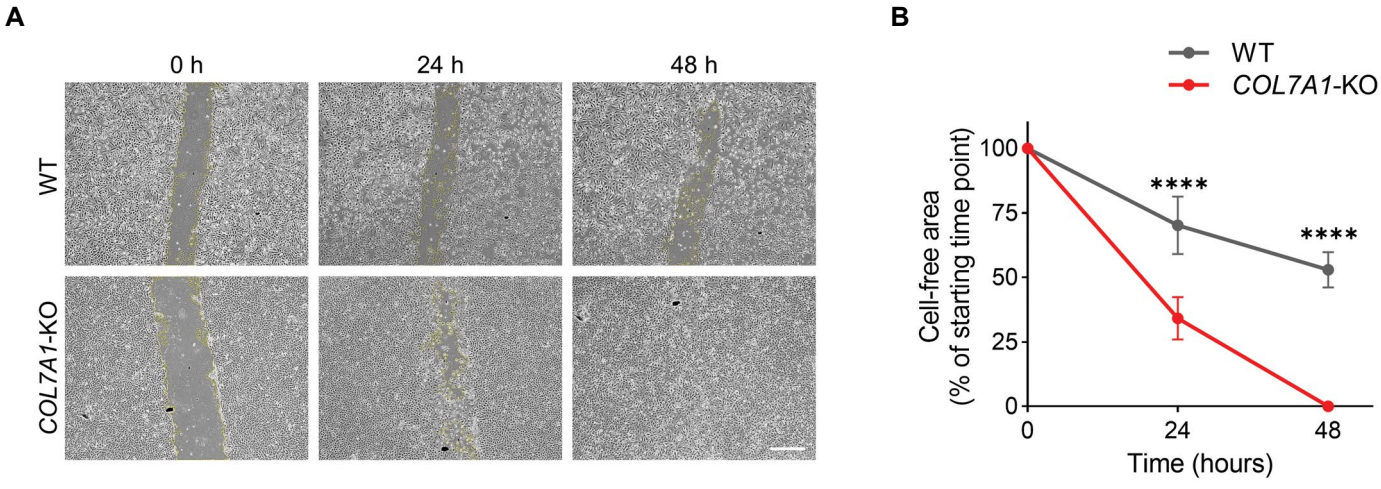

Fig.6: Assessment of cell motility by scratch assay in the wild-type (WT) and *COL7A1*-KO cells. **A.** Representative microscopic images of WT and one of the *COL7A1*-KO HEK001 cell lines (T6) at 0, 24, and 48 hours after wounding (scale bar: 100 µm). **B.** Quantitative comparison of cell migration and wound closure in WT and *COL7A1*-KO groups showed that *COL7A1*-KO HEK001 cells had obtained higher cell motility. Data presented as a percentage of the cell-free area of the starting time point ± SD (n=3). ****; P<0.0001 and h; Hour.

Discussion

Investigation of rare diseases, like EB, has challenges with the availability of the proper patients and ethical issues as well as practical difficulties, such as sampling, primary cell culture, and division potency of disease-specific cells. To obviate these problems, genetic modification in the desired gene to generate the disease model is favorable**.** In this study, we generated four immortalized keratinocyte cell lines harboring different characterized mutations of the *COL7A1* gene which can be used as a cellular model of RDEB.

The human *COL7A1* gene spans through more than 31 kb of chromosome 3 with 118 exons encoding a long polypeptide (around 2,944 amino acids) that gives rise to type VII collagen (24). Hundreds of *COL7A1* mutations have been detected in RDEB patients resulting in a variety of clinical manifestations with most severe forms correlating with the complete absence of the whole protein (25). Although amino acid substitution and truncated mutants can be found in some patients, these forms of the protein might be detected by antibody-based assays and therefore interferes with experimental investigations. Hence, to generate a straightforward experimental tool, we chose to completely eliminate type VII collagen expression by targeting the first exon in the proximity of the start codon and the transcription start site. The results showed that this strategy successfully resulted in the generation of multiple mutations in four generated cell lines, however, we showed that all four selected cell lines lacked the expression of COL7A1 protein. In the functional level, increased motility of the *COL7A1*-knocout cells was in line with the previous findings showing that RDEB keratinocytes had higher motility associated with increased susceptibility to keratinocyte malignancies in RDEB patients (21-23).

COL7A1 gene is expressed in both dermal fibroblasts and keratinocytes, while the latter is responsible for the majority of type VII collagen expressed in the skin (26). Therefore, several investigational cellular and molecular therapeutic strategies targeted keratinocytes in RDEB. Patient-derived immortalized keratinocytes have been generated as a cellular model for EB simplex (27) and RDEB (6). Although valuable for several studies, these cell lines lack the isogenic healthy counterparts. One disadvantage of patient-derived cell models compared to our approach is that they lack an isogenic control. Immortalized keratinocyte cell lines, derived from healthy donors, especially the HEK001 cell line, have been extensively characterized and used as valuable models for studying keratinocytes (28, 29). On the other hand, gene editing technologies, such as CRISPR/Cas9, can be readily applied to generate targeted mutations in human cells. This approach has been also used in skin-related studies to investigate several biological functions, such as keratinocyte development and homeostasis (30), signal transduction (31), adhesion (32), and epithelial differentiation (33, 34). In line with this approach, we employed CRISPR/Cas9 technology to generate new *COL7A1*-deficient HEK001 immortalized keratinocytes which closely resemble RDEB keratinocytes.

Although mouse models of RDEB have been generated and used for in vivo studies, rodent keratinocytes do not fully resemble human counterparts in terms of molecular mechanisms involved in EB, such as apoptotic and inflammatory pathways (35, 36). Targeting *COL7A1* by CRISPR/Cas9 in human primary keratinocytes has also been reported as a method to generate RDEB cellular model (7, 37). Whilst this method has the advantage of using primary keratinocytes, it has also some potential limitations, including the limited lifespan of primary keratinocytes, relatively labor-intensive procedure, generation of heterogenous mutations, persistent expression of gRNA and Cas9 by the integrative lentiviral vector, and the possibility of off-target mutations. Additionally, the efficiency of *COL7A1* knockout using CRISPR/Cas9 nucleoprotein in primary human keratinocytes was reported around 40% (8), while our approach allowed for the generation of homogenous *COL7A1* knockout cell lines. On the other hand, the major limitation of our approach is that immortalized keratinocytes do not fully represent some keratinocyte characteristics (e.g. differentiation and proliferation) which should be considered for future application of this cellular model. Moreover, immortalized keratinocytes might not be suitable for some in vivo experiments due to their constant proliferation. However, despite its inherent limitations, our strategy provided a more accessible, robust, and homogenous cellular model that may address some of the shortcomings in other cellular and animal models.

Conclusion

In this study, CRISPR/Cas9 technology was used to generate a keratinocyte model cell line for RDEB. The generated model cell lines not only can be used in experimental studies such as investigational cell and gene therapies, but also can potentially be applied to high-throughput screening of candidate drugs for symptomatic treatments such as wound healing, reduction in blister numbers, as well as amelioration of itch and pain. Moreover, our experimental strategy for CRISPR/Cas9-mediated gene editing in keratinocyte cell lines can be extended to the genes involved in the other types of EB, as well as the characterization and targeted modulation of pathogenic molecular cascades.

Acknowledgments

This work was supported by the funds from Royan Institute. The authors indicated no potential conflicts of interest.

Authors' Contributions

F.A., M.B.; Contributed to the design, implementation of the research, data analysis, and writing the manuscript. F.A., M.A., E.Y.; Carried out the experiments, contributed

to data analysis and interpretation. H.B., P.M.; Contributed to conceptualization of the study, interpreting the results, providing critical feedback, and finalizing the manuscript. All authors read and approved the final manuscript.

References

1. Has C, Nyström A, Saeidian AH, Bruckner-Tuderman L, Uitto J. Epidermolysis bullosa: Molecular pathology of connective tissue components in the cutaneous basement membrane zone. Matrix Biol. 2018; 71-72: 313-329.
2. Reichelt J, Koller U, De Rosa L, De Luca M, Bauer JW. Advances on potential therapeutic options for epidermolysis bullosa. Expert Opinion on Orphan Drugs. 2018; 6(4): 283-293.
3. Knaup J, Verwanger T, Gruber C, Ziegler V, Bauer JW, Krammer B. Epidermolysis bullosa - a group of skin diseases with different causes but commonalities in gene expression. Exp Dermatol. 2012; 21(7): 526-530.
4. Titeux M, Izmiryan A, Hovnanian A. The molecular revolution in cutaneous biology: emerging landscape in genomic dermatology: new mechanistic ideas, gene editing, and therapeutic breakthroughs. J Invest Dermatol. 2017; 137(5): e123-e129.
5. Afshar L, Aghayan HR, Sadighi J, Arjmand B, Hashemi SM, Basiri M, et al. Ethics of research on stem cells and regenerative medicine: ethical guidelines in the Islamic Republic of Iran. Stem Cell Res Ther. 2020; 11(1): 396.
6. Chamorro C, Almarza D, Duarte B, Llames SG, Murillas R, García M, et al. Keratinocyte cell lines derived from severe generalized recessive epidermolysis bullosa patients carrying a highly recurrent COL7A1 homozygous mutation: models to assess cell and gene therapies in vitro and in vivo. Exp Dermatol. 2013; 22(9): 601-603.
7. Fenini G, Grossi S, Contassot E, Biedermann T, Reichmann E, French LE, et al. Genome editing of human primary keratinocytes by CRISPR/Cas9 reveals an essential role of the NLRP1 inflammasome in UVB sensing. J Invest Dermatol. 2018; 138(12): 2644-2652.
8. Kocher T, March OP, Bischof J, Liemberger B, Hainzl S, Klausegger A, et al. Predictable CRISPR/Cas9-mediated COL7A1 reframing for dystrophic epidermolysis bullosa. J Invest Dermatol. 2020; 140(10): 1985-1993. e5.
9. Dabrowska M, Ciolak A, Kozlowska E, Fiszer A, Olejniczak M. Generation of new isogenic models of huntington's disease using CRISPR-Cas9 technology. Int J Mol Sci. 2020; 21(5): 1854.
10. Kaneski CR, Hanover JA, Schueler Hoffman UH. Generation of an in vitro model for peripheral neuropathy in Fabry disease using CRISPR-Cas9 in the nociceptive dorsal root ganglion cell line 50B11. Mol Genet Metab Rep. 2022; 31: 100871.
11. Martens MC, Edelkamp J, Seebode C, Schäfer M, Stählke S, Krohn S, et al. Generation and characterization of a CRISPR/Cas9-mediated SNAP29 knockout in human fibroblasts. Int J Mol Sci. 2021; 22(10): 5293.
12. Muñoz SS, Garner B, Ooi L. Generation of APOE knock-down SK-N-SH human neuroblastoma cells using CRISPR/Cas9: a novel cellular model relevant to Alzheimer's disease research. Biosci Rep. 2021; 41(2): BSR20204243.
13. Pavan E, Ormazabal M, Peruzzo P, Vaena E, Rozenfeld P, Dardis A. CRISPR/Cas9 editing for gaucher disease modelling. Int J Mol Sci. 2020; 21(9): 3268.
14. Serrano LJ, Garcia-Arranz M, De Pablo-Moreno JA, Segovia JC, Olivera-Salazar R, Garcia-Olmo D, et al. Development and characterization of a factor V-deficient CRISPR cell model for the correction of mutations. Int J Mol Sci. 2022; 23(10): 5802.
15. Concordet JP, Haeussler M. CRISPOR: intuitive guide selection for CRISPR/Cas9 genome editing experiments and screens. Nucleic Acids Res. 2018; 46(W1): W242-W245.
16. Basiri M, Behmanesh M, Tahamtani Y, Khalooghi K, Moradmand A, Baharvand H. The convenience of single homology arm donor DNA and CRISPR/Cas9-nickase for targeted insertion of long DNA fragment. Cell J. 2017; 18(4): 532-539.
17. Mohammadi P, Nilforoushzadeh MA, Youssef KK, Sharifi-Zarchi A, Moradi S, Khosravani P, et al. Defining microRNA signatures of hair follicular stem and progenitor cells in healthy and androgenic alopecia patients. J Dermatol Sci. 2021; 101(1): 49-57.
18. Greenfield EA. Single-cell cloning of hybridoma cells by limiting dilution. Cold Spring Harb Protoc. 2019; 2019(11).
19. Longo PA, Kavran JM, Kim MS, Leahy DJ. Single cell cloning of a stable mammalian cell line. Methods Enzymol. 2014; 536: 165-172.
20. Brinkman EK, Chen T, Amendola M, van Steensel B. Easy quantitative assessment of genome editing by sequence trace decomposition. Nucleic Acids Res. 2014; 42(22): e168.
21. Chen M, Kasahara N, Keene DR, Chan L, Hoeffler WK, Finlay D, et al. Restoration of type VII collagen expression and function in dystrophic epidermolysis bullosa. Nat Genet. 2002; 32(4): 670-675.
22. Gache Y, Baldeschi C, Del Rio M, Gagnoux-Palacios L, Larcher F, Lacour JP, et al. Construction of skin equivalents for gene therapy of recessive dystrophic epidermolysis bullosa. Hum Gene Ther. 2004; 15(10): 921-933.
23. Murauer EM, Gache Y, Gratz IK, Klausegger A, Muss W, Gruber C, et al. Functional correction of type VII collagen expression in dystrophic epidermolysis bullosa. J Invest Dermatol. 2011; 131(1): 74-83.
24. Van Agtmael T, Bruckner-Tuderman L. Basement membranes and human disease. Cell Tissue Res. 2010; 339(1): 167-188.
25. Kern JS, Kohlhase J, Bruckner-Tuderman L, Has C. Expanding the COL7A1 mutation database: novel and recurrent mutations and unusual genotype-phenotype constellations in 41 patients with dystrophic epidermolysis bullosa. J Invest Dermatol. 2006; 126(5): 1006-1012.
26. Ryynänen J, Sollberg S, Parente MG, Chung LC, Christiano AM, Uitto J. Type VII collagen gene expression by cultured human cells and in fetal skin. Abundant mRNA and protein levels in epidermal keratinocytes. J Clin Invest. 1992; 89(1): 163-168.
27. Morley SM, D'Alessandro M, Sexton C, Rugg EL, Navsaria H, Shemanko CS, et al. Generation and characterization of epidermolysis bullosa simplex cell lines: scratch assays show faster migration with disruptive keratin mutations. Br J Dermatol. 2003; 149(1): 46-58.
28. Sugerman PB, Bigby M. Preliminary functional analysis of human epidermal T cells. Arch Dermatol Res. 2000; 292(1): 9-15.
29. Bogen KT, Arnold LL, Chowdhury A, Pennington KL, Cohen SM. Low-dose dose-response for reduced cell viability after exposure of human keratinocyte (HEK001) cells to arsenite. Toxicol Rep. 2016; 4: 32-38.
30. Dahlhoff M, Gaborit N, Bultmann S, Leonhardt H, Yarden Y, Schneider MR. CRISPR-assisted receptor deletion reveals distinct roles for ERBB2 and ERBB3 in skin keratinocytes. FEBS J. 2017; 284(19): 3339-3349.
31. Gao S, Wang Z, Wang W, Hu X, Chen P, Li J, et al. The lysine methyltransferase SMYD2 methylates the kinase domain of type II receptor BMPR2 and stimulates bone morphogenetic protein signaling. J Biol Chem. 2017; 292(30): 12702-12712.
32. Wanuske MT, Brantschen D, Schinner C, Stüdle C, Walter E, Hiermaier M, et al. Clustering of desmosomal cadherins by desmoplakin is essential for cell-cell adhesion. Acta Physiol (Oxf). 2021; 231(4): e13609.
33. James CD, Das D, Morgan EL, Otoa R, Macdonald A, Morgan IM. Werner syndrome protein (WRN) regulates cell proliferation and the human papillomavirus 16 life cycle during epithelial differentiation. mSphere. 2020; 5(5): e00858-e00820.
34. Sobiak B, Leśniak W. Effect of SUV39H1 histone methyltransferase knockout on expression of differentiation-associated genes in HaCaT keratinocytes. Cells. 2020; 9(12): 2628.
35. Sollberger G, Strittmatter GE, Grossi S, Garstkiewicz M, Auf dem Keller U, French LE, et al. Caspase-1 activity is required for UVB-induced apoptosis of human keratinocytes. J Invest Dermatol. 2015; 135(5): 1395-1404.
36. Sand J, Haertel E, Biedermann T, Contassot E, Reichmann E, French LE, et al. Expression of inflammasome proteins and inflammasome activation occurs in human, but not in murine keratinocytes. Cell Death Dis. 2018; 9(2): 24.
37. Grossi S, Fenini G, Hennig P, Di Filippo M, Beer HD. Generation of knockout human primary keratinocytes by CRISPR/Cas9. Methods Mol Biol. 2020; 2109: 125-145.

Cell J
Cell Journal (Yakhteh)
Homepage: https://www.celljournal.org/
Original Article
Vol 25, No 10, October 2023, Pages: 674-687

Characterization of CAR T Cells Manufactured Using Genetically Engineered Artificial Antigen Presenting Cells

Ali Sayadmanesh, M.Sc.[1, 2], Mohammad Azadbakht, Ph.D.[2, 3], Kheirollah Yari, Ph.D.[4], Ali Abedelahi, Ph.D.[5], Hajar Shafaei, Ph.D.[1, 5], Dariush Shanehbandi, Ph.D.[6], Behzad Baradaran, Ph.D.[6*], Mohsen Basiri, Ph.D.[2, 7*]

1. Department of Applied Cell Sciences, Faculty of Advanced Medical Sciences, Tabriz University of Medical Sciences, Tabriz, Iran
2. Department of Stem Cells and Developmental Biology, Cell Science Research Center, Royan Institute for Stem Cell Biology and Technology, ACECR, Tehran, Iran
3. Department of Biology, Faculty of Science, University of Guilan, Rasht, Iran
4. Medical Biology Research Center, Health Technology Institute, Kermanshah University of Medical Sciences, Kermanshah, Iran
5. Department of Anatomical Sciences, Faculty of Medicine, Tabriz University of Medical Sciences, Tabriz, Iran
6. Immunology Research Center, Tabriz University of Medical Sciences, Tabriz, Iran
7. Advanced Therapy Medicinal Product Technology Development Center (ATMP-TDC), Royan Institute for Stem Cell Biology and Technology, ACECR, Tehran, Iran

Abstract

Objective: Chimeric antigen receptor (CAR) T cell therapy has recently emerged as a promising approach for the treatment of different types of cancer. Improving CAR T cell manufacturing in terms of costs and product quality is an important concern for expanding the accessibility of this therapy. One proposed strategy for improving T cell expansion is to use genetically engineered artificial antigen presenting cells (aAPC) expressing a membrane-bound anti-CD3 for T cell activation. The aim of this study was to characterize CAR T cells generated using this aAPC-mediated approach in terms of expansion efficiency, immunophenotype, and cytotoxicity.

Materials and Methods: In this experimental study, we generated an aAPC line by engineering K562 cells to express a membrane-bound anti-CD3 (mOKT3). T cell activation was performed by co-culturing PBMCs with either mitomycin C-treated aAPCs or surface-immobilized anti-CD3 and anti-CD28 antibodies. Untransduced and CD19-CAR-transduced T cells were characterized in terms of expansion, activation markers, interferon gamma (IFN-γ) secretion, CD4/CD8 ratio, memory phenotype, and exhaustion markers. Cytotoxicity of CD19-CAR T cells generated by aAPCs and antibodies were also investigated using a bioluminescence-based co-culture assay.

Results: Our findings showed that the engineered aAPC line has the potential to expand CAR T cells similar to that using the antibody-based method. Although activation with aAPCs leads to a higher ratio of $CD8^+$ and effector memory T cells in the final product, we did not observe a significant difference in IFN-γ secretion, cytotoxic activity or exhaustion between CAR T cells generated with aAPC or antibodies.

Conclusion: Our results show that despite the differences in the immunophenotypes of aAPC and antibody-based CAR T cells, both methods can be used to manufacture potent CAR T cells. These findings are instrumental for the improvement of the CAR T cell manufacturing process and future applications of aAPC-mediated expansion of CAR T cells.

Keywords: Artificial Antigen Presenting Cells, Chimeric Antigen Receptors, Immunotherapy, OKT3

Citation: Sayadmanesh A, Azadbakht M, Yari K, Abedelahi A, Shafaei H, Shanehbandi D, Baradaran B, Basiri M. Characterization of CAR T cells manufactured using genetically engineered artificial antigen presenting cells. Cell J. 2023; 25(10): 674-687. doi: 10.22074/CELLJ.2023.2001712.1304

Introduction

Adoptive cell therapy (ACT) is a type of personalized immunotherapy, in which a patient's immune cells are isolated and expanded outside the body, or in some cases modified, and then returned to the patient to boost the body's fight against diseases such as cancer (1-3). Chimeric antigen receptor (CAR) T cell therapy, as a type of adoptive cell transfer, is an innovative and promising approach in the field of cancer immunotherapy (4-6). CAR T cells are autologous T cells engineered to express target antigen-specific receptors with an intracellular CD3 domain fused to a stimulatory domain that does not require antigen-presenting cells to target malignant cells (7, 8). CAR T cells targeting CD19 and B-cell maturation antigen (BCMA) are currently being used to treat some hematological malignancies, including acute lymphoblastic leukemia (B-ALL), large B-cell lymphoma (LBCL), follicular lymphoma (FL),

Received: 06/May/2023, Revised: 22/June/2023, Accepted: 01/July/2023
*Corresponding Addresses: P.O.Box: 5166614766, Immunology Research Center, Tabriz University of Medical Sciences, Tabriz, Iran
P.O.Box: 16635-148, Department of Stem Cells and Developmental Biology, Cell Science Research Center, Royan Institute for Stem Cell Biology and Technology, ACECR, Tehran, Iran
Emails: baradaranb@tbzmed.ac.ir, basiri@royaninstitute.org

Royan Institute
Cell Journal (Yakhteh)

multiple myeloma (MM) and mantle cell lymphoma (MCL) that have been approved in the United States and Europe (6, 9, 10).

Ex vivo expansion of T cells requires activation through T cell receptor (TCR) and co-stimulatory signals, which is conventionally performed by bead- or surface-immobilized anti-CD3 and anti-CD28 antibodies. However, challenges such as the cost of manufacturing CAR T cells, disposable reagents with good manufacturing practice (GMP) quality, long-term preparation of pure antigen-specific and polyclonal $CD8^+$ T cells are the main obstacles to the clinical application of CAR T cell therapies. Therefore, one of the strategies aimed at improving the expansion and activation of T cells and minimizing the existing challenges has been the use of aAPCs to produce engineered T cells for clinical applications (11-13). One of the common approaches in this field is the use of the K562 cell line. Unlike anti-CD3/CD28 antibodies, the K562 aAPC approach is cost-effective and may include additional stimulatory molecules such as ICAM-1 and LFA-3 that are more readily capable of stimulating and interacting with T cells (14, 15). Other advantages of K562 aAPCs include the lack of MHC expression, the ability to grow in a serum-free environment, expanding the $CD8^+$ T cell population from donors in a short period of time, and the possibility of better immunological synapse formation due to the fluidity of the cell membrane (16, 17). Also, in previous studies conducted on humans, the use of K562 cell has been investigated and approved in terms of safety (18, 19). However, characterization and comparison of aAPC- and antibody-expanded T cells in terms of immunophenotype and functional properties is crucial to better understand the potential differences between these two methods.

In this study, we aimed to genetically engineer K562 cells with a membrane-bound anti-human CD3ε (OKT3) single-chain variable fragment (scFv) to create an aAPC cell line for ex vivo activation of T cells and CAR T cell generation. We also characterized CAR T cells generated with this cell line, comparing their immunophenotype and functional properties to CAR T cells manufactured with surface-immobilized anti-CD3 and anti-CD28 antibodies.

Materials and Methods

This study was approved by the Academic Research Ethics Committee of Tabriz University of Medical Sciences (IR.TBZMED.REC.1400.951). Informed consent was obtained from all blood donors involved in the study.

Construct preparation

A DNA sequence coding for a fusion protein consisting of of human CD5 signal sequence(nucleotines 73 to 135 of the GenBank accession number NM_014207), OKT3 scFv (nucleotines 64 to 810 of the GenBank accession number HM208751), and human CD8A hinge and transmembrane regions (nucleotines 1301 to 1516 of the GenBank accession number NM_001768) was synthesized (ShineGene, China) and recived in pUC57 plasmid. This fragment was then subcloned into a retroviral SFG.CNb30_opt.IRES.eGFP (Addgene, USA) at the NcoI and XhoI restriction sites. The retroviral CD19-CAR construct, comprising a CD19-specific FMC63 scFv, a CD8 hinge region, CD28 transmembrane and cytoplasmic regions, along with the cytoplasmic region of CD3 zeta, was sourced from the Royan Institute Plasmid Bank.

Cell lines

K562 and Raji cell lines were obtained from the American Type Culture Collection (ATCC, Manassas, VA, USA). K562 and Raji cells were maintained in RPMI 1640, supplemented with 10% FBS, GlutaMax (1X), penicillin (100 units/ml), and streptomycin (100 µg/ml, Gibco, Grand Island, NY, USA) and incubated at 37°C and 5% CO_2. The Platinum-Amphotropic (Plat-A) retroviral packaging cell line (Cell Biolabs, San Diego, CA, USA) was maintained in DMEM High Glucose (Dulbecco's Modified Eagle Medium), supplemented with 10% FBS, GlutaMax (1X), penicillin (100 units/ml) and streptomycin (100 µg/ml, Gibco, Country).

Retrovirus production

Retroviral particles were separately produced by transient transfection of Plat-A cells with the mOKT3 or CD19-CAR-encoding SFG plasmids (18 µg) in 100 mm tissue culture plates using Lipofectamine™ 3000 reagent (L3000075, Invitrogen, USA). Media were refreshed 16 hours post-transfection and supernatants containing retroviral particles were collected 48-72 hours after transfection. Viral supernatants were filtered through a 0.45 µm filter and used in transduction experiments.

aAPC line (OKT3-K562 cell line) production

K562 cells were cultured in non-tissue culture 24-well plate at the density of 2×10^5 per well. The cells were cultured overnight and then centrifuged at 400 g and re-suspended in mOKT3 vector-containing medum in the presence of 8 µg/ml Polybrene (Santa Cruz Biotechnology, sc-134220). After 12 hours, the medium was replaced with fresh complete medium and incubated for an additional 2 days at 37°C and 5% CO_2, and GFP expression was determined by fluorescent microscopy (Olympus, IX71). Transduced cells were cultured for 10 days (five passages) and then subjected to fluorescence-activated cell sorting (FACS) to obtain a uniform population of GFP-positive cell designed as OKT3-K562 cells (aAPC line).

Treatment aAPC with mitomycin C

The aAPCs were seeded in non-tissue culture 24-well plate at 1×10^6 cells per ml per well in complete medium, and were treated with 20 µg mitomycin C at different times (30, 60 and 90 minutes). In order to investigate the effect

of mitomycin C on cell proliferation, cells were washed with PBS and re-suspended in a complete medium, and counted for 4 consecutive days.

Co-culture of aAPCs with peripheral blood mononuclear cells

Initially, human peripheral blood mononuclear cells (PBMCs) were isolated from healthy donors using Ficoll-Paque density gradient centrifugation (Progen, 1114544). In each well of a 24-well plate, 1×10^6 isolated PBMCs were co-cultured with 1×10^6, 5×10^5, or 2.5×10^5 mitomycin C-treated aAPCs, corresponding for the PBMC:aAPC ratios of 1:1, 1:0.5, and 1:0.25, respectively. On day 1, CTL medium containing 100 IU/ml human IL-2 (R&D Systems, 202-IL-010/CF) was added to the plates and T cell expansion continued. Every two days, the cells were counted with a Neobar slide and splitted. Also, to determine whether T cells killed mitomycin C-treated aAPCs, they were co-cultured with PBMC cells at the ratio of 1:1, 1:0.5, and 1:0.25 (PBMC:aAPC). Considering that aAPCs express the GFP marker, on days 0, 1, and 2 the destroyed aAPCs were analyzed by flow cytometry. As a control group, 1×10^6 PBMCs were cultured in a 24-well plate pre-coated with anti-CD3 (Miltenybiotec, 130-093-387) and anti-CD28 (Miltenybiotec, 130-093-375) antibodies.

CAR T cell generation

To stimulate T cells, PBMCs were first isolated and divided into two groups: one group was cultured in a non-tissue culture 24-well plate pre-coated with anti-CD3 and anti-CD28 antibodies, and the other group was co-cultured with mitomycin C-treated aAPCs at the ratio of 1:0.5 (1×10^6 PBMCs: 0.5×10^6 aAPCs). The cells were cultured in 2 ml/well CTL medium containing RPMI1620 (Cytiva, SH3009601) and Click's medium (Fujifilm Irvine Scientific, 9195) in equal proportions supplemented with 1% GlutaMax (Gibco, 35050061) and 10% FBS (Gibco, 16140071). On day 1, we aspirated 1 ml of media from each well and added 1 ml of CTL media containing 200 IU/ml human IL-2 (R&D Systems) to a final concentration of 100 IU/ml. On day 3, the non-tissue culture 24-well plates were coated with 7 μg/ml RetroNectin (TAKARA) for 3 hours at 37°C. Then we aspirated RetroNectin solution and added 2 ml anti-CD19-CAR retroviral supernatants to each well and centrifuged the plates at 2000 g at 4°C for 90 minutes. The activated T cells were re-suspended at the concentration of 2×10^5 cells/well in 2 ml CTL media, at the final concentration of 100 IU/ml human IL-2, and centrifuged at 400 g for 10 minutes. During T cell expansion, the cells were split every two days with a CTL medium containing a final concentration of 50 IU/mL of IL-2.

Flow cytometry

T cells were stained for 30 minutes at 4°C with anti-human CD3-PE (Cyto Matin Gene, CMGCD3-P100) anti-CD3-PerCP (BD, 347344), anti-CD3-FITC (BD, 349201), anti-CD4-FITC (BD, 555346), anti-CD8-PE (Cyto Matin Gene, CMGCD8-P), anti-CD25-FITC (BioLegend, 302603), anti-CD69-PE (BioLegend, 310906), Fc-CD19-FITC (abcam, ab246020), anti-TIM-3-PE (BD, 583422), anti-PD-1-FITC (BioLegend, 329903), anti-CCR7 (BioLegend, 353216), anti-CD45RA (BD, 556627), CD56-PE (BD, 555516). The samples were washed with PBS and flow cytometry acquisition was performed on BD FACSCalibur (BD Biosciences, USA). 7-AAD was used for dead cell detection. (eBioscience, 00-6993-50). Analysis was performed using FlowJo software (Treestar, USA).

In vitro cytotoxicity assay

The cytotoxic activity of CAR T cells against target cells was determined by a luciferase-based and a flow cytometry-based cytotoxicity assays. The CAR T cells were incubated with firefly luciferace (ffluc)-expressing Raji cells at various effector to target (E:T) ratios in a flat bottom 96-well plate. After 6 h, 100 μl of 75 μg/ml of sigma D-luciferin (L6882, Sigma) was added to each well, and luciferase activity was measured immediately using an Alliance Q9 Advanced imaging system (UVITEC, UK). Untransduced T cells with ffluc-expressing Raji cells, as well as ffluc-expressing Raji cells without effector T cells, served as controls. The percentage of specific lysis was calculated according to the following formula: % specific lysis=100×(spontaneous cell death RLU- sample RLU)/(spontaneous death RLU-maximal killing RLU). For flow cytometry-based T cell cytotoxicity assay, CAR T cells, and untransduced T cells were added at a 1:5 effector to tumor cell ratio (25×10^4 T cells: 125×10^5 Raji cells) in untreated 6-well plates (Corning, 3736), where wells without effector cells served as untreated controls. Cells were co-cultured for 6 days in the presence of 2 mL complete media and on days 0, 3, and 6 the cells were harvested and stained with anti-CD3-PE antibody. As previously described (20), for quantifying cells by flow cytometry, 20 μL of CountBright™ Absolute Counting Beads (C36950; Invitrogen, Eugene, OR) were added, and for excluding the dead cells, 7-AAD staining was used. The acquisition was halted at 2000 beads.

Assessment of activation markers expression and IFN-γ release assay

CAR T cells and untransduced T cells prepared with aAPC and anti-CD3/CD28 were co-cultured with Raji cells at a ratio of 1:1 (1×10^5 cells) in a 24-well plate. After 24 hours, supernatants were harvested to measure the release of IFN-γ using a IFN-γ-specific ELISA according to the manufacturer's instructions (R&D Systems, DY28B05). To evaluate T cell activation markers, cells were stained with anti-CD25 and anti-CD69 antibodies and were analyzed by flow cytometry.

Statistical analyses

Statistical analysis was performed using GraphPad Prism software (V.8.4.1, GraphPad Software Inc.; San Diego, CA, USA) and P values were calculated by either

one-way or two-way ANOVA followed by Sidak's multiple comparisons test. In some cases that are indicated in the figure legends an unpaired t test was used. $P<0.05$ were considered statistically significant. All results are presented as mean ± standard deviation (SD).

Results

Generation of the aAPC line

To generate an aAPC line expressing mOKT3, we transduced K562 cells with a retroviral vector encoding mOKT3 along with a GFP reporter (Fig.1A). To confirm the transduction, K562 cells were examined for GFP expression using a fluorescent microscope 48 hours after transduction. After five passages, GFP-positive K562 cells were sorted by FACS to establish the aAPC line. Afterward, GFP expression was confirmed by fluorescent microscopy and flow cytometry in the aAPC line (sorted K562 transduced cells) in comparison with unsorted K562 transduced cells and untransduced K562 cells (Fig.1B). The results showed that the unsorted cells were transduced with an efficiency of about 10%, while 93% of them were positive for the GPF protein after sorting.

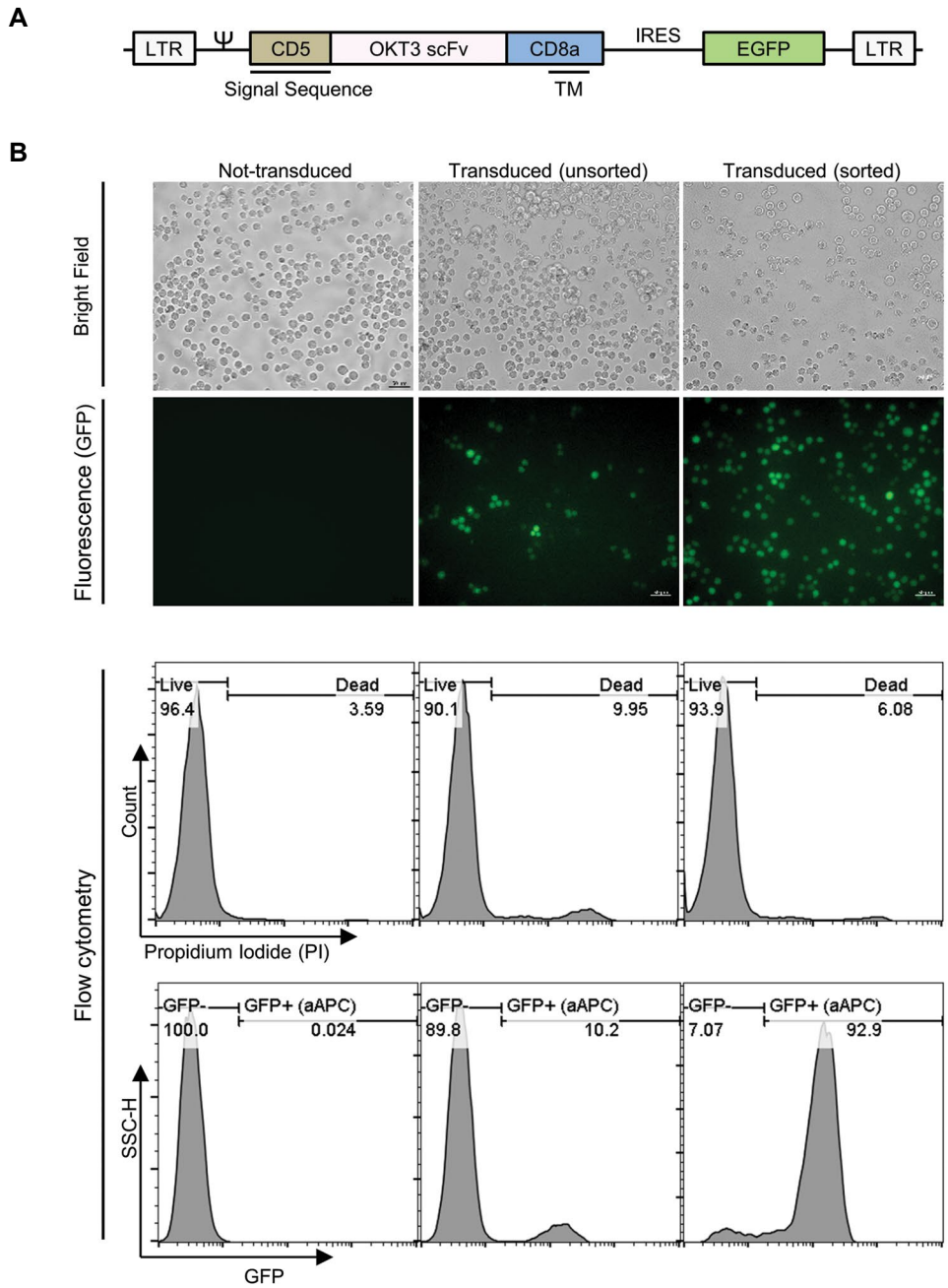

Fig.1: mOKT3 construct and generation of aAPC cell line. **A.** Schematic presentation of the mOKT3 construct containing a CD5 signal sequence, a synthetic gene coding for the OKT3 scFv, a CD8a transmembrane region, and IRES-EGFP in a SFG retroviral vector. **B.** OKT3 transduction on the K562 cell line was confirmed. The first and second panels from the top respectively: bright field and GFP fluorescent images of the untransduced, transduced, and sorted OKT3-K562 cells by fluorescent microscopy (scale bar: 50 µm). Third panel: total cell viability of corresponding cells before GFP+ gating. Fourth panel (lower panel): transduction efficiency was confirmed by flow cytometry.

Co-culture of aAPC with primary peripheral blood mononuclear cells

In order to use the aAPCs for T cell activation, we treated them with mitomycin C at different time points and cultured them for 4 days. The results of cell counting did not show any difference between the different times of cell treatment with mitomycin C, so the shortest time (30 minutes) was chosen as the incubation time for the rest of the experiments (Fig.2A). To investigate cluster formation of aAPC and T cells, we co-cultured PBMCs and mitomycin C-treated aAPCs in the ratio of 1:1, 1:0.5, and 1:0.25 (PBMC:aAPC) and one group was activated with anti-CD3/CD28 as a standard T cell activation protocol (Fig.2B). The results showed that at higher aAPC concentration, more clusters were formed, and at the 1:0.5 ratio the outcome was similar to the standard T cell activation method in terms of the amount of cluster formation (Fig.2C). Therefore, it seems that this ratio is suitable for cell activation. To measure the survival time of aAPCs in contact with the T cells, we measured the survival of aAPCs at the respective ratios on days 0, 1, and 2 (Fig.2D). The results showed that on day 2 after co-culture in the 1:1 ratio wells, more aAPCs are still alive, but at 1:0.5 and 1:0.25 ratios few live aAPCs are detectable (Fig.2E, F). Overall, according to the obtained results, the ratio of 1:0.5 was the most appropriate in terms of the cluster formation. In addition, considering that T cell transduction is performed on day 3 in most CAR T cell production protocols, the aAPCs did not persist in the culture after 3 days. Therefore, in the rest of the experiments, the ratio of 1:0.5 was chosen as a suitable ratio for activation of T cells.

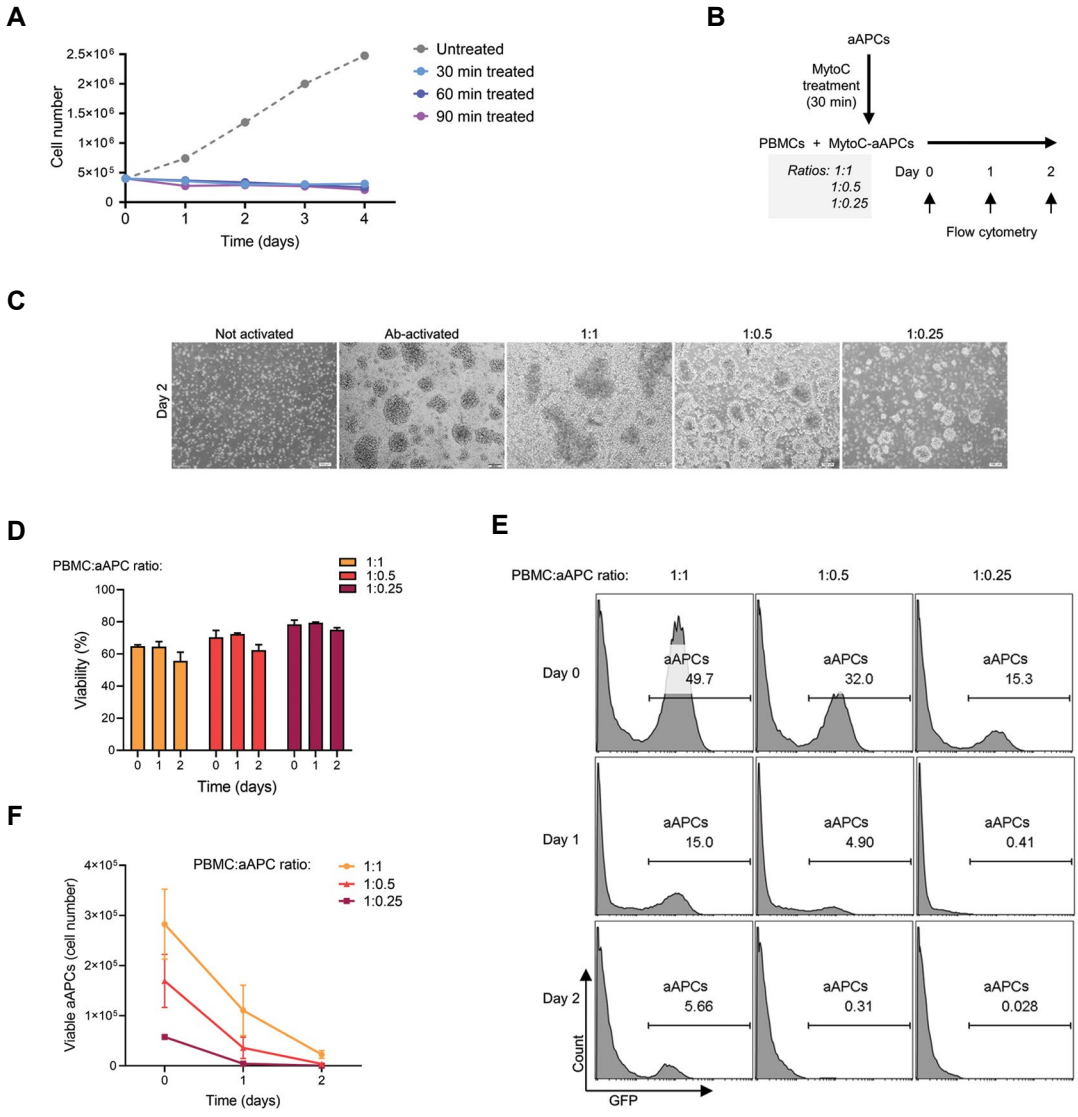

Fig.2: Co-culture of aAPC cells with PBMCs and their viability assay. **A.** Treatment of aAPC with mitomycin C (MytoC) for different durations showed that treated aAPC cells did not show proliferation. The data showed that aAPC cell lines treated with mitomycin C did not show proliferation for up to 4 days (n=1). **B.** Schematic of PBMC and aAPC co-culture in different ratios of 1:1, 1:0.5, and 1:0.25. **C.** Cluster formation of T cells after PBMCs co-cultured with mitomycin C treated-aAPC cells in different ratios (1:1, 1:0.5, and 1:0.25) and compared with standard T cell activation with anti-CD3/antiCD28 antibodies (Ab) (scale bar: 100 µm). **D.** Viability of co-cultured cells on day 2. **E.** Representitive data showing GFP expression among the viable cells in co-cultures, where GFP$^+$ cells represent aAPCs. The co-culture of aAPC cells with PBMCs at 3 time points showed that, on day 2, aAPC cells were eliminated in the ratio of 1:0.5 and 1:0.25, but in the ratio of 1:1, about 5% of the aAPC cells remained in the culture. **F.** Summery of data showing the quantified viable aAPC cells in different co-culture conditions. The ratios of 1:0.5 and 1:0.25 on day 2, the number of aAPC cells was greatly reduced and the majority of cells in the culture were eliminated (n=3). PBMCs; Peripheral blood mononuclear cells and aAPC; Artificial antigen presenting cell.

T cell expansion after aAPC-mediated activation

In order to evaluate the rate of T cell expansion with aAPC, we cultured PBMCs activated with aAPC, K562 (negative control), or anti-CD3/CD28 (positive control) for 7 days in the presence of IL-2 (Fig.3A). The cell counting results showed that PBMCs activated with aAPCs could expand similarly to the Ab-activated method (anti-CD3/CD-28 solution) and increased about 22 folds within 7 days. Also, lower rates of cell expansion were observed with K562 cells (Fig.3B). To determine the cell types expanded in the experimental groups, we used CD3 and CD56 markers. Our data showed that the aAPC activation resulted in a predominant $CD3^+$ T cell population similar to the anti-CD3/CD-28 group. The results also indicated that most of the cells that expanded after K562 co-culture are $CD3^-CD56^+$ NK cells (Fig.3C).

Immunophenotype of the T cells expanded with aAPC

To evaluate of effects of different activation methods on T cell immunophenotype, we stimulated PBMCs with aAPCs or anti-CD3/CD28 similar to the previous experiment (Fig.3A) and assessed the expression of different T cell markers after 7-8 days. We analyzed CD4 and CD8 markers to assess the effects of aAPC and Ab activation methods on T cell subpopulations. The analysis revealed that in the aAPC-activated group, $CD8^+$ T cytotoxic cells expanded more than $CD4^+$ T helper; instead, in the Ab-activated group, $CD4^+$ T helper cells expanded more than $CD8^+$ T cytotoxic cells (Fig.3D). Evaluation of the activation phenotype of T cells by CD25 and CD69 staining showed no difference in the $CD25^+CD69^+$ and $CD25^-CD69^-$ population between the aAPC and Ab groups. However, the proportion of $CD25^+CD69^-$ population was decreased in the aAPC group compared with the Ab group (Fig.3E). To compare the role of various activation methods on memory phenotype of T cells, the expression of CD45RA and CCR7 were measured using flow cytometry. As the results show in Figure 3F, aAPC-mediated activation increased the differentiation of T cells to T effector memory cells (TEM; $CD45RA^-CCR7^-$) when compared with Ab-mediated activation. Correspondingly, the proportion of naïve-like (TNL; $CD45RA^+CCR7^+$) sub-population was higher in the Ab-activated T cells. However, the percentages of central memory T cells (TCM; $CD45RA^-CCR7^+$) and $CD45RA^+$ effector memory T cells (TEMRA; $CD45RA^+CCR7^-$) were not significantly different between Ab and aAPC groups (Fig.3F). We did not observe any statistically significant difference in the expression of exhaustion markers PD-1 and TIM-3 between T cells activated by Ab or aAPC (Fig.3G).

CAR T cell generation by aAPC-mediated activation

In order to evaluate the application of aAPC line for manufacturing clinically relevant T cell products, we used a retroviral second-generation CD19-specific CAR construct to generate CD19 CAR T cells (Fig.4A, B). We were able to achieve transduction efficiencies higher than 80% with both aAPC-activated and Ab-activated T cells (Fig.4C). The expansion of the CAR transduced T cells in both aAPC and Ab groups was significantly higher than the T cells cultured with K562, which served as a negative control (Fig.4D).

The Effect of aAPCs-mediated activation on the immunophenotype of CAR T cells

To evaluate the expansion of $CD3^+$ T cell and NK cell population on day 3, activated T cells were transduced with CD19-CAR bearing retroviral, and CD3 and CD56 antibodies were used for cell staining on day 7. The data indicated that the aAPC-activated group induced the same level of expansion in $CD3^+$ T cells as the Ab-activated group, and there was no significant change in terms of expansion in the natural killer T (NKT) cell population ($CD3^+$ $CD56^+$) in the two groups (Fig.4E, F). Similar to what was observed with untransduced T cells, aAPCs expanded cytotoxic $CD8^+$ CAR T cells more than the Ab group (Fig.4G). We did not observe any difference in $CD25^+CD69^+$ CAR T cell population between aAPC and Ab groups, while the percentage of $CD25^+CD69^-$ CAR T cells was lower in aAPC group (Fig.4H). Although this result was consistent with the previous experiment using untransduced T cells (Fig.3E), the magnitude of difference in $CD25^+CD69^-$ sub-population between the two activation methods was lower in the case of CAR transduced T cells (1.6 fold) compared to untransduced T cells (>5 fold). As presented in Figure 4I, aAPC-mediated activation method resulted in increased TEM ($CD45RA^-CCR7^-$) and reduced TNL ($CD45RA^+CCR7^+$) percentages among CAR T cell population compared with the Ab-mediated activation method. No statistically significant difference was observed in TCM ($CD45RA^-CCR7^+$) and TEMRA ($CD45^+CCR7^-$) sub-populations. Moreover, the prevalence of PD-1 and TIM-3 expressing CAR T cells was not different between the two experimental groups (Fig.4J).

Assessment of activation and exhaustion characteristics of CAR T cells and the ability of antitumor activity

In order to evaluate the effect of aAPC-activation method on the CAR-mediated activation of CD19-CAR T cells, we co-cultured CAR T cells or untransduced T cells with $CD19^+$ target cells (Raji cells) at a ratio of 1:1 (Fig.5A). After 24 hours, we observed an extremely high IFN-γ level in the supernatant of co-cultured CAR T cells compared to untransduced T cells in aAPC and Ab groups. Also, CAR T cells activated with aAPC produced significantly higher IFN-γ compared to CAR T cells activated with Ab (Fig.5B). Also, CAR T cells activated with both aAPC and Ab showed increased expression of CD25 and CD69 activation markers compared with

untransduced T cells (Fig.5C). To measure CAR T cell exhaustion, a longer co-culture (16 days) with a higher number of target cells (E:T ratio of 1:5) was used (Fig.5A). The results showed that in both aAPC and Ab CAR T cell groups a higher percentage of cells co-expressed PD-1 and TIM-3 compared with the untransduced T cells, however, there was no difference between aAPC and Ab activation conditions (Fig.5D). Also, the results showed that the expression of TIM-3 in both groups of CAR T cells was higher than non-transduced T cells, although PD-1 expression was not different in the CAR T cells and untransduced T cells (Fig.S1, See Supplementary Online Information at www.celljournal.org).

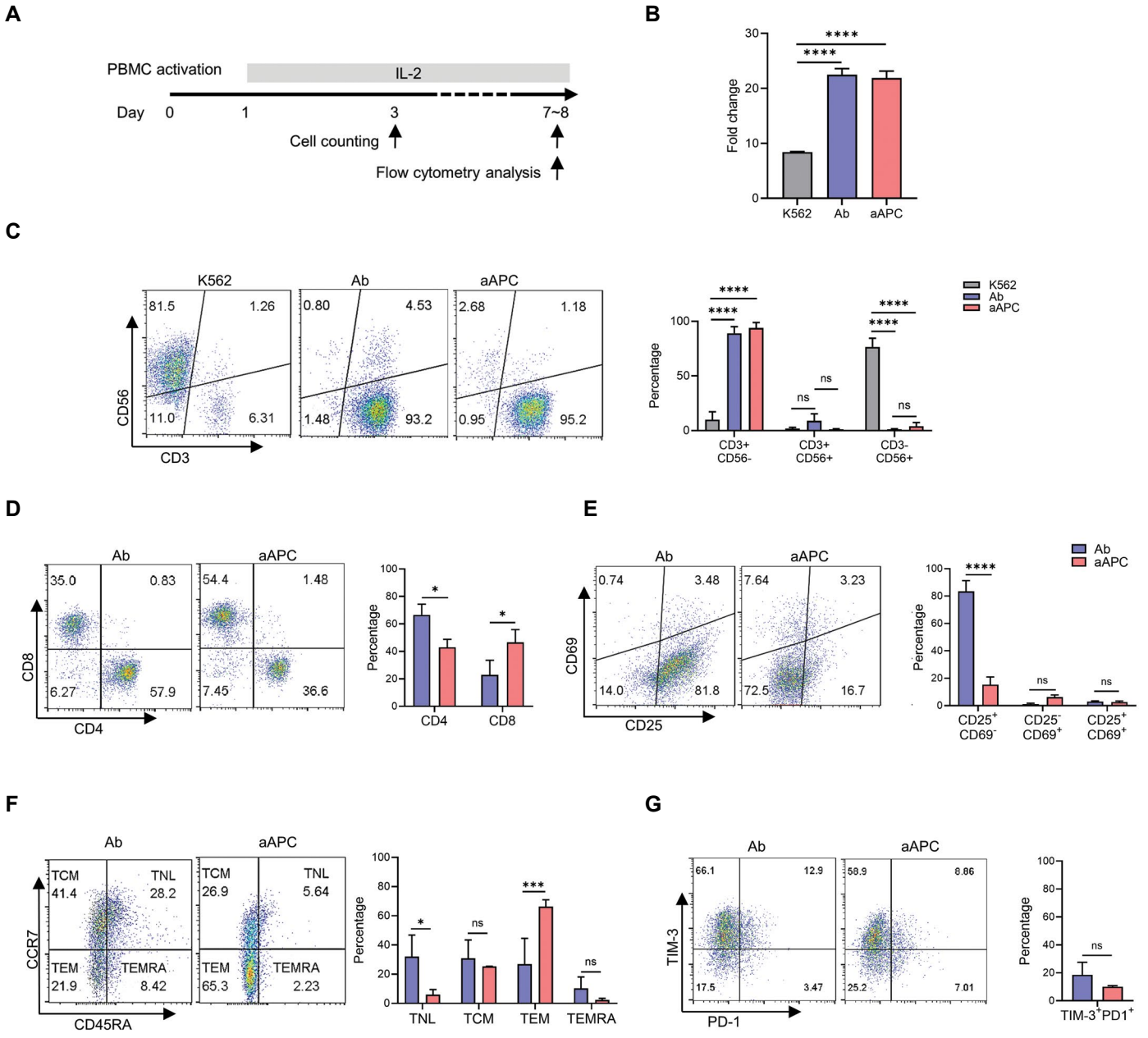

Fig.3: Expansion of T and NK cells and evaluation of markers of activation, exhaustion, and immunophenotype of T cells in aAPC activation method. **A.** Schematic illustration of the experiment for T cell activation with aAPC cells, anti-CD3/CD28 antibodies, and K562 cell line and cell expansion and staining. **B.** Fold expansion of activated T cells with aAPC cells, anti-CD3/CD28 antibodies (Ab), and K562 cell line as a negative control. Cell expansion was assessed from day 3 to day 7, where a 22-fold expansion was observed on day 4. **C.** Cells were stained with anti-CD56 and anti-CD3 antibodies to determine T cell and NK cell populations. The aAPC cells expanded T cells ($CD3^+CD56^-$) similarly to the Ab-activated method and in the two groups with no significant variation in the expansion of the NKT population ($CD3^+ CD56^+$). K562 cell line was not suitable for T cell expansion, but it was able to expand NK cells ($CD3^-CD56^+$). **D.** Analysis of T cells to determine the CD4/CD8 ratio showed that $CD8^+$ T cells were expanded at a higher level in the aAPC-activated method and $CD4^+$ T cells in the Ab-activated method. **E.** To assess CD25 and CD69 activation markers, cells were stained and measured by flow cytometry. The data showed no difference between the expression of $CD25^+CD69^+$ dual activation markers in aAPC- and Ab-activated methods, but the expression of $CD25^+CD69^-$ marker increased in Ab-activated method. **F.** Representative flow cytometry and quantification data for memory phenotype analysis of T cells on day 8. The aAPC activated method increased the differentiation of T cells into TEM cells, and the Ab-activated method increased the differentiation of T cells into TNL cells. **G.** The expression of PD-1 and TIM-3 exhaustion markers in different methods of activation measured by flow cytometry showed that T cell exhaustion markers were not significant in either groups (n=3). TNL; Naïve-like T cell, TCM; Central memory T cell, TEM; Effector memory T cell, TEMRA; $CD45RA^+$ effector memory T cell, ns; Not significant, *; P<0.05, ***; P<0.001, ****; P<0.0001, NK; Natural killer, NKT; Natural killer T, and aAPC; Artificial antigen presenting cell.

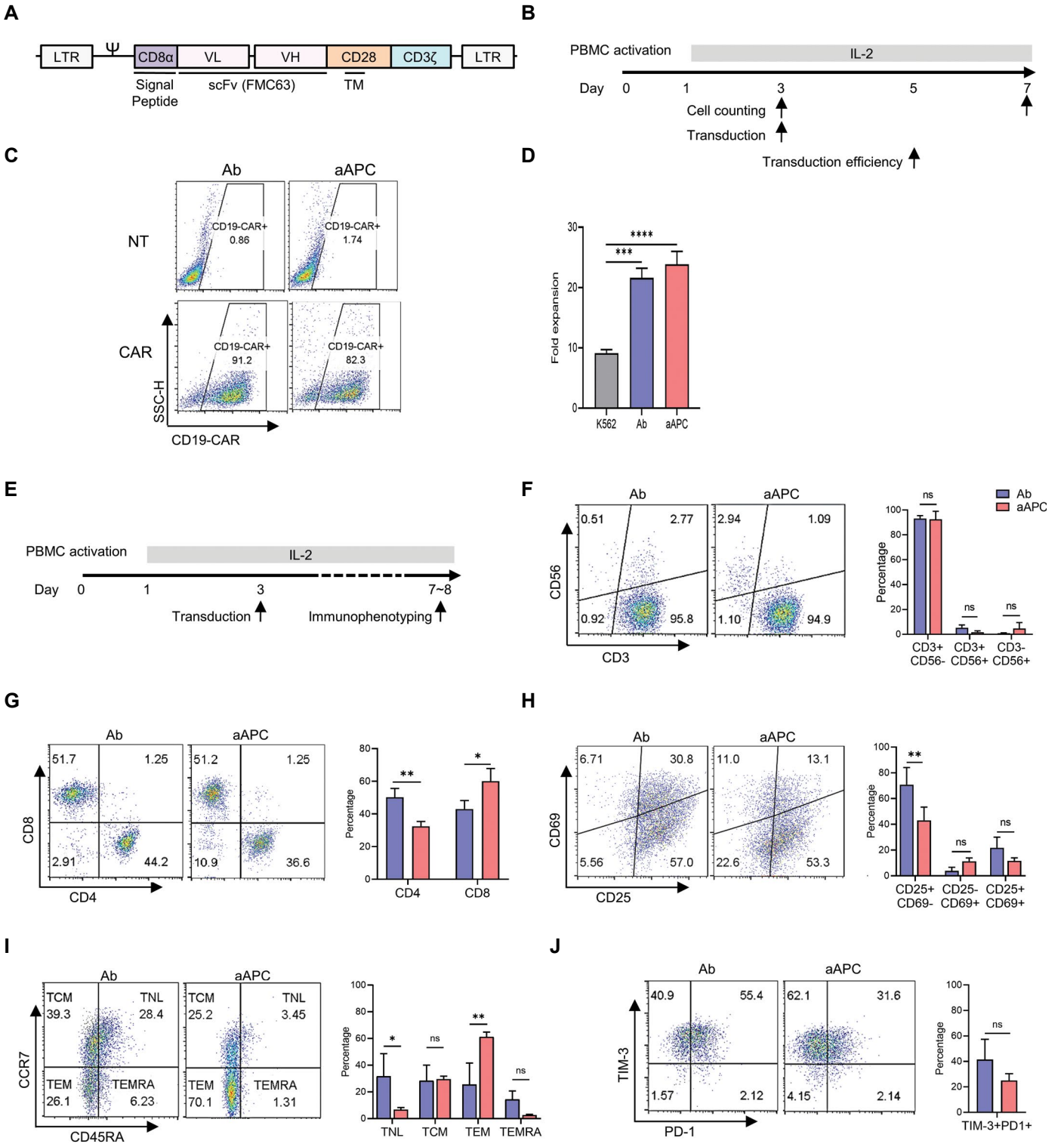

Fig.4: Design of CD19-CAR structure and the effect of aAPC and Ab activation methods on the expansion of CD19-CAR-positive cells and evaluation of their immunophenotype. **A.** Schematics of the anti-CD19 CAR construct with single-chain variable fragment (scFv) component (anti-CD19 antibody FMC63), CD28 co-stimulatory signaling domain, and CD3ζ. **B.** Experimental timeline. **C.** Cell surface CAR expression on transduced cells with CD19-CAR construct was determined by flow cytometry and comparison of transduction efficiency of CAR positive cells activated by aAPC and antibody (Ab) methods. **D.** Fold change of activated CD19-CAR positive cells with aAPC cell, anti-CD3/CD28 antibodies, and K562 cell line. Cell expansion was assessed from day 3 to day 7. **E.** Experimental timeline of T cell activation, transduction, cell expansion, and staining. **F.** Staining of cells with anti-CD56 and anti-CD3 to determine T and NK cell populations. Similar to the Ab-activated method, aAPC cells can expand CAR T cells ($CD3^+ CD56^-$) and have no significant changes in the expansion of the NKT population ($CD3^+CD56^+$). **G.** Analysis of T cells showed that $CD8^+$ CAR T cells were more expanded in the aAPC-activated method and $CD4^+$ CAR T cells in the Ab-activation method. **H.** Flow cytometry analysis of CD25 and CD69 activation markers of CAR T cells in aAPC- and Ab-activated methods. The data showed no difference between the expressions of $CD25^+CD69^+$ dual activation markers, and the expression of $CD25^+CD69^-$ marker increased in Ab-activated method. **I.** Representative flow cytometry and quantification data for memory phenotype of CAR T cells on day 8. In the aAPC-activated method, the differentiation of CAR T cells to TEM cells increased, and in the Ab activated method, the differentiation of CAR T cells to TNL cells increased. **J.** The expression of PD-1 and TIM-3 exhaustion markers of CAR T cell with different activation methods showed that the exhaustion markers were not significant in either group (n=3). TNL; Naïve-like T cell, TCM; Central memory T cell, TEM; Effector memory T cell, TEMRA; $CD45RA^+$ effector memory T cell, aAPC; Artificial antigen presenting cell, CAR T; Chimeric antigen receptor T cell, ns; Not significant, *; P<0.05, **; P<0.01, ***; P<0.001, and ****; P<0.0001.

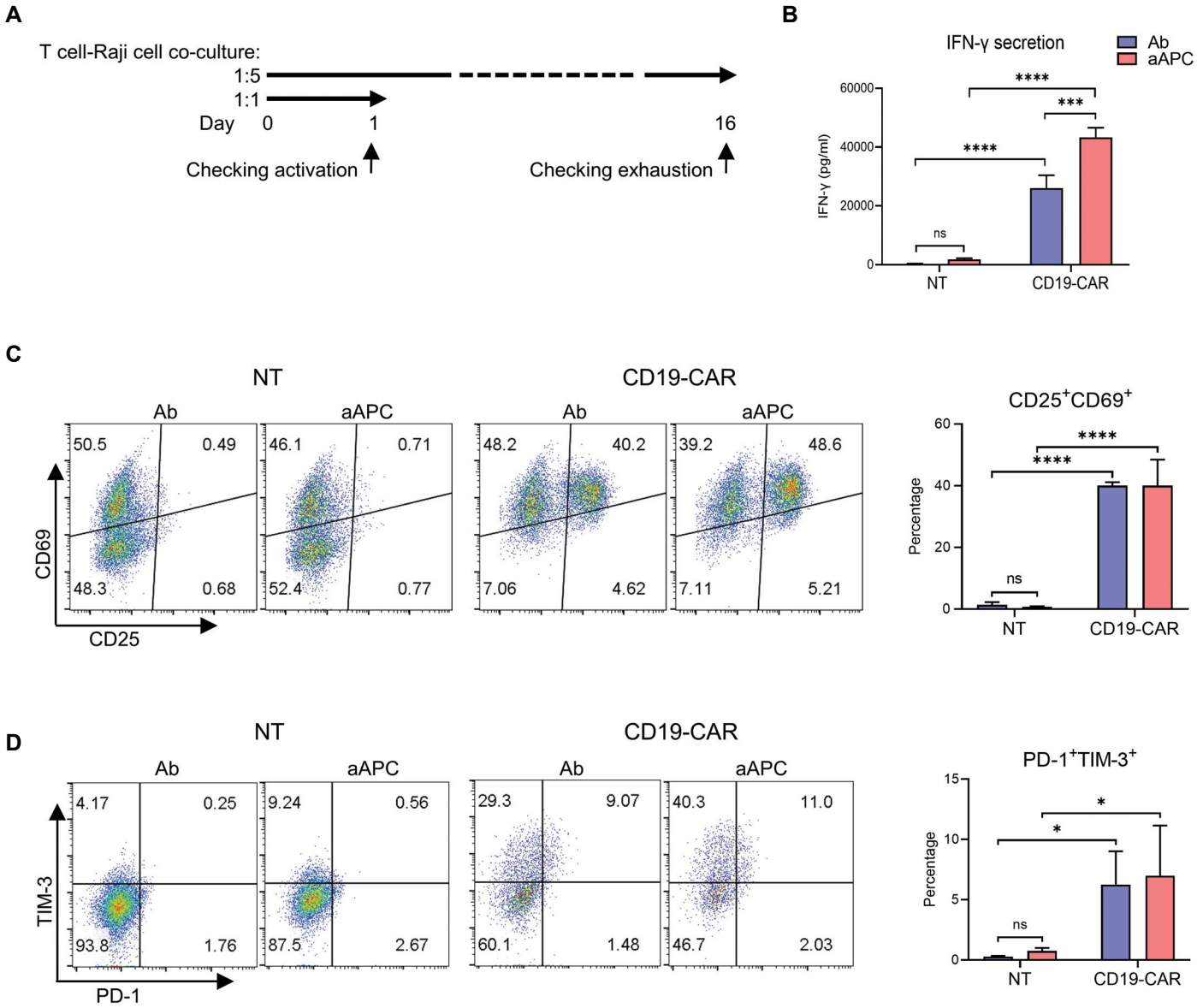

Fig.5: Antitumor effects and expression of activation and exhaustion markers in co-culture with target cells. **A.** Experimental timeline of co-culture of CAR T cells with Raji cells. **B.** Co-culture of CAR T cells with Raji cells at a ratio of 1:1 and collection of supernatants to evaluate IFN-γ release assay after 24 hours. The data showed that aAPC activated CAR T cells significantly produced IFN-γ compared with antibody (Ab) activated CAR T cells. **C.** CAR T cells and Raji cells were co-cultured at a ratio of 1:1 and after an overnight expression of CD25 and CD69 were measured by flow cytometry. The data showed that aAPC activated method similar to Ab-activated method can express activation markers. **D.** CAR T cells and Raji cells were co-cultured at a ratio of 1:5 (E:T). After 16 days, CAR T cells activated with aAPC cells express exhaustion markers PD-1 and TIM-3 upon long-term exposure to Raji cells, similar to Ab-activated method (n=3). IFN-γ; Interferon gamma, CAR T; Chimeric antigen receptor T cell, *; P<0.05, ***; P<0.001, and ****; P<0.0001.

Cytotoxicity of CAR T cells generated by aAPC-mediated activation

To investigate the cytotoxic function of aAPC CAR T cells, they were co-cultured with ffluc^{+} Raji cells at E:T ratios of 10:1, 5:1: 2.5:1, 1:1 and 0:1 in 96-well flat-bottom plates. Co-culture of untransduced T cells with tumor cells and tumor cells without effector cells were performed as a controls. After 6 hours of incubation cytotoxicity was measured in a luciferase-based assay. The results indicated that E:T-dependent cytotoxicity for aAPC- and Ab-drived CD19-CAR T cells were not significantly different in comparison to untransduced T cells (Fig.6A, B).

To further investigate the anti-tumor capacity of CAR T cells, a 6-day co-culture was performed with Raji cells at a higher ratio of target cells with an E:T of 1:5 (Fig.6C). The T cells and Raji calls were analyzed on days 0, 3 and 6 by CD3 staining (Fig.6D). Absolut quantification of the cell numbers using counting beads showed that both Ab- and aAPC-drived CAR T cells expanded in the course of co-culture, while untransduced T cells did not proliferate (Fig.6E). Additionally, the number of Raji cells were decreased in both Ab- and aAPC-drived CAR T cell groups, unlike the untransduced groups, which showed Raji cell growth (Fig.6F). In summary, both CAR T cells activated with either aAPC line or Ab were able to proliferate upon exposure to tumor cells and control the target cells at statistically indifferent rates.

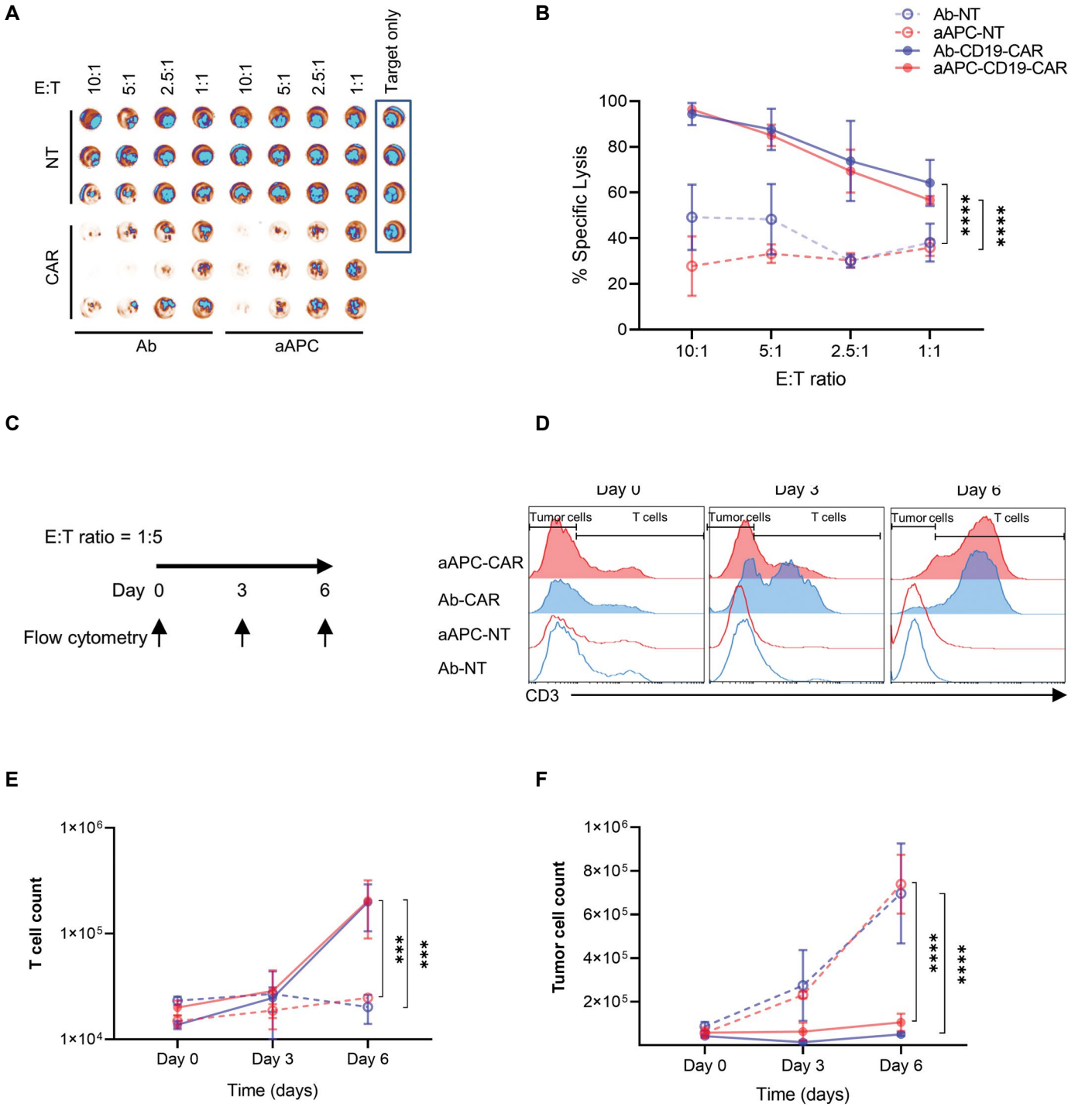

Fig.6: *In vitro* anti-tumor response of CD19-CAR T cells. **A, B.** Specific tumor cell lysis by CD19-CAR T cells. CD19-CAR T cells (CAR) and untransduced T cells (NT) were co-cultured with ffluc-expressing Raji cells at different effector to target (E:T) ratios and after 6 hours of incubation cell lysis was measured in a luciferase-based assay. The results indicated that specific lysis occurred with increasing numbers of CD19-CAR T cells, and aAPC-activated CAR T cells had similar specific lysis activity to antibody (Ab) activated CAR T cells. **C.** Experimental timeline of co-culture of CAR T cells with Raji cells for cytotoxicity. **D.** Representative flow cytometry histogram showing the cytotoxicity of CD19-CAR T cells at an E:T ratio of 1:5 for 6 days. Cells were harvested every 3 days for staining with anti-CD3 and the percentage of cell viability was measured with 7AAD. CAR T-mediated killing assays at 6 days into co-culture showed that the majority of Raji cells were eliminated. **E, F.** Number of T cells and tumor cells during co-culture. **E.** Proliferation of CD19-CAR T cells from panel D cultures occurred significantly higher than NT T cells. **F.** The number of eliminated Raji cells was significantly increased in co-culture with CD19-CAR T cells from panel D compared to co-culture with NT cells. The behavior of aAPC-activated CAR T cells in co-culture with tumor cells was comparable to that of Ab-activated CAR T cells (n=3). ***; P<0.001 and ****; P<0.0001.

Discussion

The importance of CAR T cell therapy compared to other treatments such as chemotherapy and conventional immunotherapies is that it shows better results in patients who have had multiple relapses (21, 22). In this treatment method, multiple infusions are not needed, and despite this, the treatment period is shorter and recovery is faster. So far, CAR T cell therapy for some blood cancers has

been able to overcome the limitations of other conventional treatments. Among current therapies, checkpoint blockade has shown better results, especially in solid tumors. However, combination therapy of CAR T cells with drugs, such as checkpoint blockade, has been proposed and may in fact provide desirable results (21-24).

In order to improve the activation and expansion of T cells for high-scale cultures, the use of aAPCs is a suitable and cost-effective approach (11-13). After dendritic cells (DC) were identified in the 1970s (25), one of the first strategies was to use them as natural APCs, which sense antigens and act as mediators for activation of other immune cells, especially T cells (26). DCs stimulate TCR and co-stimulatory signals on T cells through MHC expression molecules, and are a strong stimulus for T cell activation (27, 28). Many researchers have generated different types of engineered DCs to better expand T cells, however, limitations of this approach include inconsistency of antitumor responses among donors, reduced functionality and longevity of memory cells generated by this method (29-31). On the other hand, employing K562 aAPC for T cell activation offers several advantages beyond cost-effectiveness. These include the absence of MHC and inhibitory molecules and the presence of supplementary stimulatory molecules that foster enhanced stimulation of T cells (10, 11).

Thomas et al. (15) generated aAPCs that expressed anti-CD3CD28, which more rapidly induced T cells to enter the cell cycle and after 10 days of culture, expanded T cells fourfold more than with anti-CD3CD28-coated beads. By co-culturing aAPCs with PBMCs in different ratios, a cluster of aAPC and T cells was formed.

In our study, we engineered a K562 aAPC by constructing a membrane-bound OKT3 retroviral plasmid encoding OKT3-GFP. By co-culturing aAPCs with PBMCs in different ratios, clusters of aAPC and T cells were formed. We observed that large clusters were formed in the ratio of 1:1, but in a 1:0.5 ratio the size of the clusters formed was similar to the anti-CD3/CD28 standard T cell activation method. Since one of the important considerations in using aAPC for T cell stimulation is the duration of stimulation, aspersistent signaling causes cell exhaustion (32), we needed to investigate the disappearance of aAPCs in the co-cultures. In a previous study, the disappearance of irradiated aAPC from the co-culture was measured and adjusted at a ratio of 2:1, and the number of aAPC was determined by total cell count and flow cytometry. The number of irradiated aAPCs in the co-culture started to decrease on the first day and reached zero on the third day. Also, in our study we examined the disappearance of mitomycin C-treated aAPC in co-culture from day 0 to day 2 by total cell count and flow cytometry. We observed that on day 2, in a ratio of 1:1, some aAPCs were still alive, but in ratios of 1:0.5 and 1:0.25, aAPCs are almost eliminated by T cells. Due to the similarity in cluster size in 1:0.5 ratio with that in the Ab activated method, and the disappearance of aAPC on day 2, we chose this ratio for the next experiments.

The immunophenotyping results showed that activation of T cells with aAPC expands $CD3^+$ T cells similar to the Ab activation method, but in aAPC activation method $CD8^+$ T cells expand significantly more than $CD4^+$ T cells. In fact, when the CD19-CAR T cells produced by these methods were examined, these results were confirmed similar to untransduced T cells as shown previously by Butler et al. (33). They showed in their study that aAPC/mOKT3 promoted the expansion of $CD8^+$ T cells better than $CD4^+$ T cells. Bishwas Shrestha and colleagues replicated similar results, while generating aAPCs expressing anti-CD3, anti-CD28, and in combination with CD137L (34). Our generated aAPCs, on the other hand, express only anti-CD3, causing an increase specifically in $CD8^+$ T cell expansion.

When we evaluated T cell activation markers on day 7 without co-culture with tumor cells, there was no difference between the expression levels of $CD25^+CD69^+$ double positive and double negative markers, but the expression of $CD25^+CD69^-$ increased in the Ab activation method rather than the aAPC activation method. In a previous study, we found that after stimulation of T cells with anti-CD28, the expression level of CD25 was increased (35) and another study indicated that CD25 gene expression in T cells is rapidly induced upon TCR/CD28 co-stimulation through activation of NF-κB, NFAT, AP-1, and cAMP response element-binding protein/activating transcription factor (36). It is clear that our aAPCs express only anti-CD3 and lack the expression of CD28, and therefore the increase in CD25 expression was not the same as in the Ab activation group. It is important that the expression of activation markers increases after the exposure of T cell and CAR T cell to the tumor cell. Our data showed that the expression of these markers was significantly increased in CAR T cells activated with aAPC and Ab activated methods after exposure to tumor cells in a similar manner compared to the untransduced T cells.

To evaluate the effects of different activation methods on T cell memory phenotype, we analyzed untransduced T cells on day 8. The results indicate that aAPC activation method increased the population of TEM cells, but Ab activation method increased TNL cell population. It seems that exposure of T cells with aAPCs in the aAPC activation method has caused the differentiation of T cells in this group more towards the memory effector cells. There was no significant difference in the cell population of T central memory (TCM) and Terminally differentiated effector memory T (TEMRA) in the two activation methods. In the study that they used CD3/28/137L K562 aAPCs, they did not observe a significant difference in $CD8^+$ TCM and $CD8^+$ TEM between CD3/28/137L and aAPC beads, but they showed that activation of T cells with aAPCs resulted in a higher percentage of memory $CD8^+$ T cells (34). Also, Kawalekar et al. (37) observed similar results, where CAR T cells with 41BB/CD137L endodomain increased their oxidative phosphorylation characteristic of $CD8^+$ memory T cells. In contrast to

these two groups, activation with our aAPCs showed an increase in TEM cells in the total population of non-transduced T cells and CAR T cells. On day 8, we evaluated the expression of PD-1 and TIM-3 exhaustion markers on T cells in two activation methods and our findings showed that the exhaustion markers in the aAPC method are lower, but there is no significant difference in the expression level of the exhaustion markers with the Ab activation method. This outcome showed that aAPCs do not have a great effect on T cell exhaustion, like the standard activation method. In a previous study using K562 CD3/28/137L aAPCs, intrinsic glycolysis (ECAR) and oxidative phosphorylation mitochondrial index (OCAR) of $CD8^+$ T cells were measured to assess T cell exhaustion. They showed that $CD8^+$ T cells activated with aAPC CD3/28/137L K562 cells have a higher glycolytic phenotype, along with increased mitochondrial oxidation (34). Compared to this study, our aAPC only expressed anti-CD3 and also the type of cellular exhaustion measurement in that study is different from our method, as they only investigated cellular exhaustion on $CD8^+$ T cells, but we measured it on the whole cell population. The memory phenotype and exhaustion markers of CD19-CAR T cells produced by aAPC and Ab activation methods were similar to the results observed with untransduced T cells generated through these two methods.

To further assess antigen-mediated T cell activation, we exposed CD19-CAR T cells with Raji target cells at a 1:1 ratio. After overnight stimulation, we measured upregulation of the surface marker CD25/CD69. The results suggested that the CAR T cells produced by the aAPC method show a strong upregulation of CD25/CD69 when co-cultured with target cells, as well as the Ab activation method. These results indicate that CAR T cells are activated by aAPC when exposed to antigen-presenting cells, expressing specific activation markers as in the standard method. The IFN-γ release of the CAR T cells produced by both methods compared to untransduced T cells showed that CAR T cells were able to secrete a high level of IFN-γ after co-culture with the target cells. Interestingly, the CAR T cells produced by the aAPC method produced significantly higher levels of IFN-γ compared to the Ab activation method, showing that aAPC activation method induces T cells to further differentiate into effector memory (TEM) phenotype. Also when co-cultured aAPC activated CAR T cells with Raji cells at a 1:5 E:T ratio for 16 days, no difference was observed when compared to the Ab activated CAR T cells in terms of the expression levels of PD-1 and TIM-3 exhaustion markers. In a study in which aAPC produced anti-CD3 and anti-CD28 in combination with CD137L, compared to T cells stimulated with anti-CD3/CD28 beads, the aAPC-expanded CD8 T cell subpopulation expressed fewer markers of exhaustion (34), instead, we did not measure exhaustion markers in T cell sub-populations and only in the total T cell population.

In addition, we co-cultured CAR T cells with ffluc-expressing Raji cells at various E:T ratios and measured antitumor immune responses *in vitro* in a luciferase-based assay. We showed that CAR T cells activated with aAPC had ~95% specific lysis potency, but no significant lysis was observed for untransduced T cells. Also, the results show that CAR T cells activated with aAPC method have the same potency as CAR T cells activated by Ab. Also, we evaluated the anti-tumor capacity of CAR T cells through co-culturing them with Raji target cell at a higher E:T ratio (1:5) at 3 different time points. As it is clear in the results, the aAPC-activated CAR T cells eliminated the target cells in a period of 6 days, and the activated aAPC CAR T cells were equivalent to the standard method in terms of killing potential. We also counted the number of T cells and tumor cells by adding counting beads to the cell mixture of the co-culture and found that aAPC and Ab-activated CAR T cell subsets were able to proliferate when exposed to tumor cells, unlike untransduced T cells. The results showed that the proliferation of tumor cells co-cultured with untransduced T cells increased, but in the presence of both groups of CAR T cells, the tumor cells were killed and thus proliferation did not occur. Andrea Schmidts and colleagues used $CD3^+CD28^+$K562 aAPC as a T cell activator, and checked *in vitro* potency of aAPC-activated CD19-CAR T cells on Nalm6 and Jeko-1 target cells by luciferase-based assay. They successfully showed that aAPC-activated CD19-CAR T cells acted similar to the anti-CD3/CD28 bead-activated CD19-CAR T cells, which have potency in killing tumor cells. Compared to this study, in addition to the luciferase-based method, we used long-term co-culture and a high ratio of target cells to measure CAR T cell potency, as well as CAR T cell and target cell proliferation.

In a previous study, K562 aAPCs were generated that expressed anti-CD3/CD28 and, in addition, disrupted endogenous low-density lipoprotein receptor (LDLR) gene expression in these aAPCs, to prevent unwanted lentiviral transduction. They hypothesized that K562 cells are sensitive to transduction by lentiviral vectors due to constitutive expression of LDLR, and unwanted aAPC transduction may reduce desirable T cell transduction (14). In the current study, we used aAPC for the activation of T cells and after removing them by the T cells, on day 3 we transduced those T cells and observed a high rate of cell transduction (80-90%) as in the standard method of Ab activation. Therefore, our generated aAPC can be used as a candidate for activation and preparation of T cells for transduction as in the standard method and without reducing the transduction rate.

The safety of K562 cells was previously demonstrated in a phase 2 acute myeloid leukemia (AML) study, in which autologous leukemia cells were mixed with GM-CSF-secreting K562 cells and primed lymphocytes were re-infused through stem cell transplantation (18). In another study, patients with chronic myeloic leukemia (CML) received a series of intradermal vaccines containing irradiated K562/GM-CSF cells (19). Based on these trials that evaluated the safety of the irradiated-K562, it is hoped that engineered K562 cells may also be used for T

cell activation with cost-effective production and further expansion of $CD8^+$ T cells.

Conclusion

In summary, our findings suggest that the engineered OKT3 aAPC, as a simpler and more cost-effective approach, has the potential to expand large numbers of CAR T cells for immunotherapy of cancer patients. It was also shown that after the second day, we have no residual aAPCs in the culture, so it does not interfere with transduction of T cells, and its rate of transduction is comparable to the Ab activation method. It was also shown that this aAPC does not change the phenotype and exhaustion level of the CAR T cells and increases the proliferation of $CD8^+$ killer cells compared to the standard method. CAR T cells expanded by this method after exposure to target cells show significant expression of activation markers, and the potential of these cells in specific lysis and cytotoxicity in co-culture with a high proportion of target cells is competitive with the standard method. This aAPC cell has the potential to activate and expand T cells and is also proposed as a cost-effective way to generate CAR T cells for cancer studies. Overall, our results show that engineered aAPC cells similar to the standard Ab activation method can activate T cells and even further expand $CD8^+$ T cells, so this method is introduced as a cost-effective way to generate CAR T cells for cancer immunotherapy.

Acknowledgments

We thank all staff and technicians at Royan Institute for Stem Cell Biology and Technology for their technical assistance, especially Gene Therapy and CAR T cell team members. This research was supported by Tabriz University of Medical Sciences (grant code: 68848). The authors declare no conflict of interest.

Authors' Contributions

A.S., M.B.; Conceptualization, Data analysis, and Interpretation. A.S., M.A., M.B.; Performing the experiments and Data analysis. A.S., K.Y., A.A., H.S., D.S., B.B., M.B.; Interpretation of the results, Writing, Critical review, and Editing the manuscript. B.B., M.B.; Supervision and funding acquisition. All authors read and approved the final manuscript.

References

1. Rosenberg SA, Restifo NP. Adoptive cell transfer as personalized immunotherapy for human cancer. Science. 2015; 348(6230): 62-68.
2. Redeker A, Arens R. Improving adoptive T cell therapy: the particular role of T cell costimulation, cytokines, and post-transfer vaccination. Front Immunol. 2016; 7: 345.
3. Maus MV, Fraietta JA, Levine BL, Kalos M, Zhao Y, June CH. Adoptive immunotherapy for cancer or viruses. Annu Rev Immunol. 2014; 32: 189-225.
4. Mullard A. FDA approves first CAR T therapy. Nat Rev Drug Discov. 2017; 16(10): 669.
5. Morgan RA, Dudley ME, Wunderlich JR, Hughes MS, Yang JC, Sherry RM, et al. Cancer regression in patients after transfer of genetically engineered lymphocytes. Science. 2006; 314(5796): 126-129.
6. Noonan KA, Huff CA, Davis J, Lemas MV, Fiorino S, Bitzan J, et al. Adoptive transfer of activated marrow-infiltrating lymphocytes induces measurable antitumor immunity in the bone marrow in multiple myeloma. Sci Transl Med. 2015; 7(288): 288ra78.
7. Xu D, Jin G, Chai D, Zhou X, Gu W, Chong Y, et al. The development of CAR design for tumor CAR-T cell therapy. Oncotarget. 2018; 9(17): 13991-14004.
8. June CH, Sadelain M. Chimeric antigen receptor therapy. N Engl J Med. 2018; 379(1): 64-73.
9. Sterner RC, Sterner RM. CAR-T cell therapy: current limitations and potential strategies. Blood Cancer J. 2021; 11(4): 69.
10. Safarzadeh Kozani P, Safarzadeh Kozani P, Rahbarizadeh F. CAR-T cell therapy in T-cell malignancies: is success a low-hanging fruit? Stem Cell Res Ther. 2021; 12(1): 527.
11. Iyer RK, Bowles PA, Kim H, Dulgar-Tulloch A. Industrializing autologous adoptive immunotherapies: manufacturing advances and challenges. Front Med (Lausanne). 2018; 5: 150.
12. McCarron A, Donnelley M, McIntyre C, Parsons D. Challenges of up-scaling lentivirus production and processing. J Biotechnol. 2016; 240: 23-30.
13. Merten OW, Hebben M, Bovolenta C. Production of lentiviral vectors. Mol Ther Methods Clin Dev. 2016; 3: 16017.
14. Schmidts A, Marsh LC, Srivastava AA, Bouffard AA, Boroughs AC, Scarfò I, et al. Cell-based artificial APC resistant to lentiviral transduction for efficient generation of CAR-T cells from various cell sources. J Immunother Cancer. 2020; 8(2): e000990.
15. Thomas AK, Maus MV, Shalaby WS, June CH, Riley JL. A cell-based artificial antigen-presenting cell coated with anti-CD3 and CD28 antibodies enables rapid expansion and long-term growth of CD4 T lymphocytes. Clin Immunol. 2002; 105(3): 259-272.
16. Maus MV, Thomas AK, Leonard DG, Allman D, Addya K, Schlienger K, et al. Ex vivo expansion of polyclonal and antigen-specific cytotoxic T lymphocytes by artificial APCs expressing ligands for the T-cell receptor, CD28 and 4-1BB. Nat Biotechnol. 2002; 20(2): 143-148.
17. Prakken B, Wauben M, Genini D, Samodal R, Barnett J, Mendivil A, et al. Artificial antigen-presenting cells as a tool to exploit the immune 'synapse'. Nat Med. 2000; 6(12): 1406-1410.
18. Borrello IM, Levitsky HI, Stock W, Sher D, Qin L, DeAngelo DJ, et al. Granulocyte-macrophage colony-stimulating factor (GM-CSF)-secreting cellular immunotherapy in combination with autologous stem cell transplantation (ASCT) as postremission therapy for acute myeloid leukemia (AML). Blood. 2009; 114(9): 1736-1745.
19. Qin L, Smith BD, Tsai HL, Yaghi NK, Neela PH, Moake M, et al. Induction of high-titer IgG antibodies against multiple leukemia-associated antigens in CML patients with clinical responses to K562/GVAX immunotherapy. Blood Cancer J. 2013; 3(9): e145.
20. Yekehfallah V, Pahlavanneshan S, Sayadmanesh A, Momtahan Z, Ma B, Basiri M. Generation and functional characterization of PLAP CAR-T cells against cervical cancer cells. Biomolecules. 2022; 12(9): 1296.
21. Want MY, Bashir Z, Najar RA. T cell based immunotherapy for cancer: approaches and strategies. Vaccines (Basel). 2023; 11(4): 835.
22. Sheykhhasan M, Manoochehri H, Dama P. Use of CAR T-cell for acute lymphoblastic leukemia (ALL) treatment: a review study. Cancer Gene Ther. 2022; 29(8-9): 1080-1096.
23. Houot R, Schultz LM, Marabelle A, Kohrt H. T-cell-based Immunotherapy: adoptive cell transfer and checkpoint inhibition. Cancer Immunol Res. 2015; 3(10): 1115-1122.
24. Ramos CA, Heslop HE, Brenner MK. CAR-T cell therapy for lymphoma. Annu Rev Med. 2016; 67: 165-183.
25. Steinman RM, Cohn ZA. Identification of a novel cell type in peripheral lymphoid organs of mice. I. Morphology, quantitation, tissue distribution. J Exp Med. 1973; 137(5): 1142-1162.
26. Steinman RM. The dendritic cell system and its role in immunogenicity. Annu Rev Immunol. 1991; 9: 271-296.
27. Inaba K, Metlay JP, Crowley MT, Steinman RM. Dendritic cells pulsed with protein antigens in vitro can prime antigen-specific, MHC-restricted T cells in situ. J Exp Med. 1990; 172(2): 631-640.
28. Ye K, Li F, Wang R, Cen T, Liu S, Zhao Z, et al. An armed oncolytic virus enhances the efficacy of tumor-infiltrating lymphocyte therapy by converting tumors to artificial antigen-presenting cells in situ. Mol Ther. 2022; 30(12): 3658-3676.
29. Ratta M, Fagnoni F, Curti A, Vescovini R, Sansoni P, Oliviero B, et al. Dendritic cells are functionally defective in multiple myeloma: the role of interleukin-6. Blood. 2002; 100(1): 230-237.

30. Satthaporn S, Robins A, Vassanasiri W, El-Sheemy M, Jibril JA, Clark D, et al. Dendritic cells are dysfunctional in patients with operable breast cancer. Cancer Immunol Immunother. 2004; 53(6): 510-518.
31. Neal LR, Bailey SR, Wyatt MM, Bowers JS, Majchrzak K, Nelson MH, et al. The basics of artificial antigen presenting cells in T cell-based cancer immunotherapies. J Immunol Res Ther. 2017; 2(1): 68-79.
32. Wherry EJ. T cell exhaustion. Nat Immunol. 2011; 12(6): 492-499.
33. Butler MO, Imataki O, Yamashita Y, Tanaka M, Ansén S, Berezovskaya A, et al. Ex vivo expansion of human CD8+ T cells using autologous CD4+ T cell help. PLoS One. 2012; 7(1): e30229.
34. Shrestha B, Zhang Y, Yu B, Li G, Boucher JC, Beatty NJ, et al. Generation of antitumor T cells for adoptive cell therapy with artificial antigen presenting cells. J Immunother. 2020; 43(3): 79-88.
35. Vidán MT, Fernández-Gutiérrez B, Hernández-García C, Serra JA, Ribera JM, Pérez-Blas M, et al. Functional integrity of the CD28 co-stimulatory pathway in T lymphocytes from elderly subjects. Age Ageing. 1999; 28(2): 221-227.
36. Beyersdorf N, Kerkau T, Hünig T. CD28 co-stimulation in T-cell homeostasis: a recent perspective. Immunotargets Ther. 2015; 4: 111-122.
37. Kawalekar OU, O'Connor RS, Fraietta JA, Guo L, McGettigan SE, Posey AD Jr, et al. Distinct signaling of coreceptors regulates specific metabolism pathways and impacts memory development in CAR T cells. Immunity. 2016; 44(2): 380-390.

Cell J
Cell Journal(Yakhteh)
Homepage: https://www.celljournal.org/
Original Article
Vol 25, No 10, October 2023, Pages: 688-695

Role of The circ-HIPK3, circ-PVT1, miR-25, and miR-149 in Response of Breast Cancer Cells to Ionizing Radiation

Elahe Abdollahi, Ph.D.[1], Hossein Mozdarani, Ph.D.[1*]

Department of Medical Genetics, Faculty of Medical Sciences, Tarbiat Modares University, Tehran, Iran

Abstract

Objective: Determining cellular radiosensitivity of breast cancer (BC) patients through molecular markers before radiation therapy (RT) allows accurate prediction of individual's response to radiation. The aim of this study was therefore to investigate the potential role of epigenetic biomarkers in breast cancer cellular radiosensitivity.

Materials and Methods: In this experimental study, we treated two BC cell lines, MDA-MB 231 and MCF-7, with doses of 2, 4, and 8Gy of irradiation for 24 and 48 hours. Expression levels of circ-HIPK3, circ-PVT1, miR-25, and miR-149 were quantified using quantitative reverse-transcription polymerase chain reaction (qRT-PCR). Significance of the observations was statistically verified using one-way ANOVA with a significance level of $P<0.05$. Annexin V-FITC/PI binding assay was utilized to measure cellular apoptosis.

Results: The rate of cell apoptosis was significantly higher in MCF-7 cells compared to MDA-MB-231 cells at doses of 4Gy and 8Gy ($P=0.013$ and $P=0.004$, respectively). RNA expression analysis showed that circ-HIPK3 was increased in the MDA-MB-231 cell line compared to the MCF-7 cell line after exposure to 8Gy for 48 hours. Expression of circ-PVT1 was found to be higher in MDA-MB-231 cells compared to MCF-7 cells after exposure to 8Gy for 24 hours, likewise after exposure to 4Gy and 8Gy for 48 hours. After exposing 8Gy, expression of miR-25 was increased in MDA-MB-231 cells compared to MCF-7 cells at 24 and 48 hours. After exposing 8Gy dose, expression of miR-149 was increased in MCF-7 cells compared to MDA-MB-231 cells at 24 and 48 hours.

Conclusion: circ-HIPK3, circ-PVT1, and miR-25 played crucial roles in the mechanisms of radioresistance in breast cancer. Additionally, miR-149 was involved in regulating cellular radiosensitivity. Therefore, these factors provided predictive information about a tumor's radiosensitivity or its response to treatment, which could be valuable in personalizing radiation dosage.

Keywords: Breast Cancer, Ionizing Radiation, miR-149, miR-25

Citation: **Abdollahi E, Mozdarani H. Role of the circ-HIPK3, circ-PVT1, miR-25, and miR-149 in response of breast cancer cells to ionizing radiation. Cell J. 2023; 25(10): 688-695. doi: 10.22074/CELLJ.2023.1995943.1255**

Introduction

Breast cancer (BC) is the most diagnosed cancer among women globally and the primary cause of cancer-related fatalities in women (1). Radiation therapy (RT) is a common treatment used in approximately 50% of all cancer patients at some stage of their disease, as adjuvant therapy (2, 3). Ionizing radiation (IR) used in RT induces various types of DNA damage, including double-strand breaks (DSBs). DNA damage response (DDR) plays an important role in DSB repair and maintains genomic stability by protecting cells from apoptosis and malignancies (4). Levels of apoptosis are closely associated with cellular responses to IR. RNA expression can be involved in the epigenetic regulation of apoptosis (5). Circular RNAs (circRNAs) are a novel class of endogenous non-coding RNAs (ncRNAs) characterized by a closed-loop structure, which makes them resistant to degradation by RNases (6). This highlights the advantages of circRNA as a stable molecular biomarker for various types of cancer (7-12). circRNAs regulate expression of the related genes by specifically binding to microRNAs (miRNAs) and functioning as a sponge for them (13), thereby modulating expression of the target genes. miRNAs are a subtype of small non-coding RNA molecules, typically 20-25 nucleotides in length. They have been identified for their role in breast tumor development and regulation of radiation responses (7). miRNAs can influence tumor radiosensitivity through regulation of DDR (10).

Circular RNA homeodomain-interacting protein kinase 3 (circ-HIPK3 or hsa_circ_0000284) is produced through exon two back-splicing of the *HIPK3* gene located on chromosome 11 (14). Several studies showed that circ-HIPK3 was involved in progression of various types of cancer, including colorectal (15), glioblastoma (16), prostate (17), and breast cancers (18). High levels of

Received: 14/March/2023, Revised: 18/June/2023, Accepted: 16/July/2023
***Corresponding Address: P.O.Box: 14115-111, Department of Medical Genetics, Faculty of Medical Sciences, Tarbiat Modares University, Tehran, Iran**
Email: mozdarah@modares.ac.ir

Royan Institute
Cell Journal (Yakhteh)

circ-HIPK3 have been demonstrated in breast cancer; however, its expression was decreased when cancer cells underwent apoptosis. Overexpression of circ-HIPK3 has been shown to inhibit cell apoptosis in non-small-cell lung cancer (19), colorectal cancer (20), and BC (18). On the other hand, circRNA plasmacytoma variant translocation 1 (circ-PVT1 or hsa-circ-0001821) is a circRNAs molecule, originated from the *PVT1* gene, which is located on chromosome eight. This circRNA is formed through a process called exon two back-splicing. For convenience, this circRNA is referred to as circ-PVT1. Suppression of circ-PVT1 has been shown to promote BC cell apoptosis, while inhibiting proliferation, invasiveness, and migratory capacity (21).

Studies showed that circ-HIPK3 functioned as a miR-149 sponge, regulating activity of cancerous cells by controlling FOXM1 expression through miR-149-mediated regulation (19). circ-PVT1 enhanced FOXM1 expression by binding to miR-149-5p, thereby influencing the viability and migration of ovarian cancer cells (22). miR-149 is positively correlated with radiosensitivity in colorectal cancer (23).

Additionally, BC patients, who exhibited low serum miR-25-3p expression, had a higher overall survival rate compared to those with high serum miR-25-3p expression (24, 25). miR-25 has been identified as a contributing factor to radiosensitivity in lung cancer and therefore, it may serve as a potential target for enhancing effectiveness of the RT (25).

Using molecular markers can predict an individual's response to radiation and provide valuable insights into tumor sensitivity to radiation, as well as its potential response to treatment. This approach could be advantageous for customizing radiation dosage to optimize treatment outcomes. This would allow medical professionals to choose various treatment options, while reducing radiation-related harm in patients who are unlikely to benefit from treatment. For this purpose, we investigated potential involvement of these RNAs in response to the radiation and rates of apoptosis in BC cell lines. For the first time, we assessed expression levels of miR-149, miR-25, circ-PVT1, and circ-HIPK3 in two cell lines -one of which was resistant to radiation and the other one was sensitive to radiation. Finally, both cell lines were evaluated for apoptosis before and after irradiation.

Materials and Methods

This experimental study was conducted by ethical guidelines for laboratory cell line research and received approval from the Ethics Committee of the Research Department at Tarbiat Modares University in Tehran, Iran, ensuring compliance with ethical standards (IR.MODARES.REC.1400.176).

Cell culture

The MCF-7 and MDA-MB 231 human BC cells were obtained from the Pasteur Institute cell bank in Tehran, Iran. The cells were thawed from liquid nitrogen, washed, and cultured at a density of 1×10^6 cells per well in 6-well plates using Dulbecco's Modified Eagle medium (DMEM-F12) supplemented with 10% fetal bovine serum (FBS, Gibco, USA), penicillin, streptomycin, and glutamine (all from Gibco, USA). The cells were incubated at 37°C in a humidified atmosphere containing 5% CO_2.

Cell irradiation

The experiments were conducted at the Cancer Radiotherapy department in Pars Hospital (Tehran, Iran) using a Siemens Artiste linac that emitted 6 MV and 15 MV X-ray beams. Ten minutes before irradiation, the medium was replaced with a fresh complete medium to ensure proper backscatter. The cells were exposed to 6 MV and 15 MV photon radiation using a polystyrene phantom measuring $25\times25\times15$ cm³. The film exposures were performed using an open field size of 10×10 cm² at a depth of 5 cm. Two EBT3 films were used for each radiation beam. Each sheet was then cut into nine pieces with 6.8×8.5 cm² size. Therefore two films (one for each absorbed dose) were exposed to each X-ray at three dose levels: 2 Gy, 4 Gy, and 8 Gy. The other four films were considered zero-dose exposures.

Apoptosis detection by Annexin V-FITC/PI binding assay

Both cell lines (MDA-MB-231 and MCF-7 cells) were incubated for 24 and 48 hours after irradiation. Apoptotic cells were identified using the Annexin V-FITC Apoptosis Detection Kit from Sigma-Aldrich (USA). The target cells were detached using EDTA-free trypsin. To neutralize trypsin, serum containing DMEM (Gibco, USA) was used. The cells were then washed with 500 µl of flow buffer. After washing, 5 µl of fluorescein isothiocyanate (FITC)-labeled annexin V and 5 µl of propidium iodide (PI) were added to the tube containing the target cells. The mixture was then incubated at room temperature in dark for 15 minutes. Finally, cell apoptosis was measured using a BD FACSCalibur™ flow cytometer (BD Biosciences, USA) equipped with a fluorescence-activated cell sorter (FACS). Flowing software version 2.5.1 was used for data analysis.

Target selection

In this study, we investigated expression levels of hsa-miR-149, hsa-miR-25, circ-PVT1, and circ-HIPK3 in BC cell lines, as potential biomarkers for predicting radiosensitivity and radiotoxicity in BC patients undergoing radiotherapy. When selecting these non-coding RNAs, we had to consider various criteria, including their involvement in carcinogenesis and radio-responsiveness, as well as their expression in blood, rather than being tissue-specific. Furthermore, these miRNAs and circRNAs functioned within the same pathway and

exhibited interrelatedness. Based on these criteria, we selected RNAs that had previously been studied primarily in the cell lines and cancers other than BC, and that met all of the above criteria.

Designing primers

A stem-loop primer was designed for the reverse transcription of miRNAs. The primer sequences for the stem-loop used in this study are listed below:

hsa-miR-149:

5′-GTCGTACCAGTGCAGGGTCCCGA-3′
GGTATTCGCACTGGATACGACGGGAGT-3′

hsa-miR-25:

5′-GTCGTATCCAGTGCAGGGTCCGAGGTATTCG-CACTGGATACGACTCAGAC-3′

miRNA sequences were obtained from the miRBase database, and the primers were designed using the stem-loop method.

circRNA sequence was obtained from the circBase database. The junction region was identified using the circRNA Interactome database (Fig.1A, B), and primers were designed using divergent methods for both sides of the junction.

All primers were designed using the Primer3 database and validated using the Primer-BLAST tool. The primers list is presented in Table 1.

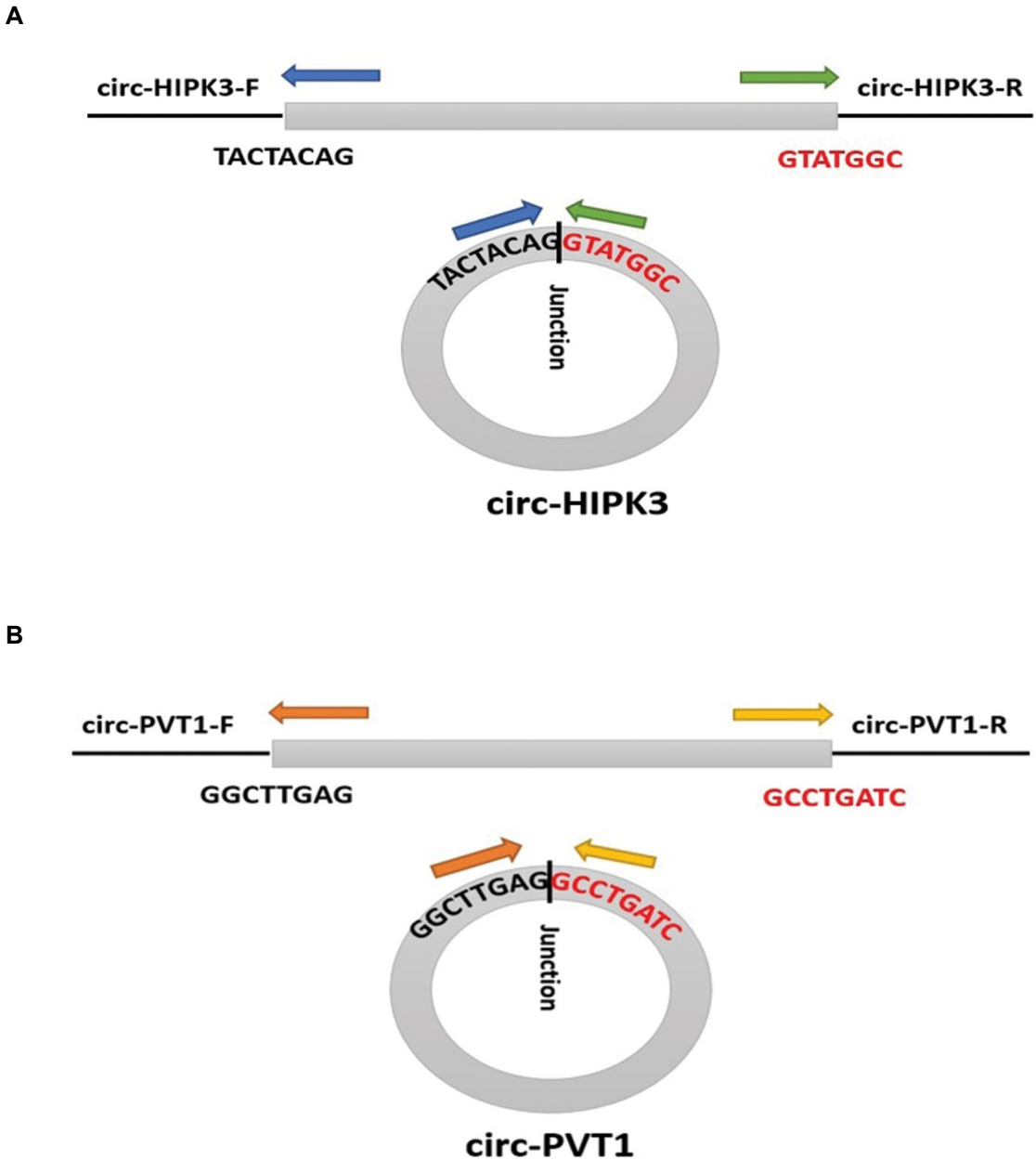

Fig.1: Scheme illustrating the production of circular RNAs and sequencing analysis of back-splicing junctions. **A.** circ-HIPK3 and **B.** circ-PVT1.

Table 1: Primer sequences utilized for quantitative reverse transcription polymerase chain reaction (qRT-PCR)

Target	Primer sequence (5′-3′)
circ-HIPK3	F: GGTCGGCCAGTCATGTATC
	R: ACTGCTTGGCTCTACTTTGAG
circ-PVT1	F: CTGCCAACTTCCTTTGGGTC
	R: AGGCACAGCCATCTTGAGG
miR-25	F: ACGATCTTTGCTCTTGTCTCG
	R: AATACCTCGGACCCTGCAC
miR-149	F: ACATCTGGCTCCGTGTCTTC
	R: AATACCTCGGACCCTGCAC
U6	F: CTCGCTTCGGCAGCACA
	R: AACGCTTCACGAATTTGCGT
GAPDH	F: ATGAGAAGTATGACAACAGCCTC
	R: CATGAGTCCTTCCACGATACC

RNA isolation and quantitative reverse transcription polymerase chain reaction

Total RNA was extracted from the cell lines using and TRIzol reagent (Invitrogen, Germany) following to the manufacturer's instructions. Purity and concentration of the RNA samples were determined using a NanoDrop ND-1000 spectrophotometer (Thermo Fisher Scientific, USA). For validation experiments, RNA was prepared and stored at -80°C. For cDNA synthesis, we utilized the qPCRBIO cDNA synthesis kit (PCR Biosystems Ltd., UK) and followed the manufacturer's protocol.

The reagents were gently mixed on ice. The reagents included miRNA, Stem-Loop RT primer (1 pM), and water. The mixture was then incubated at 70°C for five minutes. A mixture was prepared containing 5x first strand buffer, dNTP (10 mM each), and RNasin (40 units of MLV). The mixture was added to a tube and incubated at 16°C for 30 minutes and then at 60°C for 42 minutes using a PCR system (Eppendorf, Germany). The reaction was terminated by incubating it at 70°C for 5 minutes.

qRT-PCR reactions were conducted using a Step-One Plus RT-PCR thermal cycler (Applied Biosystems, USA) and SYBR Green qPCR Mix Reagent (Amplicon, Taiwan), in accordance with the manufacturer's instructions. Expressions of circ-PVT1 and circ-HIPK3 were normalized using *GAPDH*, as a reference gene, while expression of miR-25 and miR-149 was normalized using U6, as a reference gene. Each 20 µl reaction contained 10 µl of 2x Master Mix SYBR Green qPCR Mix Reagent (Amplicon, Taiwan), 0.5 µl of each primer (final concentration of 0.25 µM), 5 µl nuclease-free water and 4 µl cDNA. Nuclease-free water was included as a negative control in every qRT-PCR run to ensure that there was no contamination from non-template sources. We manually set the threshold value for all assays to determine the cycle threshold (Ct) value. The cycling conditions were as follows: an initial denaturation at 95°C for 20 seconds, followed by 40 cycles of 95°C for 5 seconds and 60°C for 30 seconds each. This was followed by a melting curve ranging from 60°C to 95°C, with fluorescence data being acquired every 0.3°C. To ensure specific amplification, we confirmed size of the amplicons by running them on a 2% agarose gel electrophoresis and analyzing the melting curve during the process. All reactions were performed in duplicate.

Statistical analysis

Statistical values are expressed as the mean ± SEM. The Shapiro-Wilk test was used to evaluate normality of the data distribution. Outliers were excluded from the analysis. Statistical analyses were conducted using GraphPad Prism 9.0 (GraphPad Software Inc.; San Diego, CA, USA). Multiple comparisons were analyzed using a single-factor ANOVA, followed by post-hoc comparisons using the Newman-Keuls test. A $P<0.05$ was considered statistically significant.

Results

Association of circ-HIPK3, circ-PVT1, miR-25, and miR-149 with radiation response

We aimed to analyze expression of circ-HIPK3, circ-PVT1, miR-25, and miR-149 in both radiosensitive and radioresistant BC cells, specifically MCF-7 and MDA-MB-231. We detected expression of circ-HIPK3, circ-PVT1, miR-25, and miR-149 in MCF-7 and MDA-MB-231 cells that were irradiated with 2Gy, 4Gy, and 8Gy X-rays using qRT-PCR.

We found that expression of circ-HIPK3 was significantly increased in MDA-MB-231 cells exposed to the dose of 8Gy for 48 hours, compared to the control group (expression ratio=18.16). The results of the non-parametric ANOVA test were statistically significant with $P<0.0001$.

A comparison of RNA expression between two cell lines showed a 72.64-fold increase of expression level in the MDA-MB-231 cell line compared to the MCF-7 cell line after 48 hours of exposure to the dose of 8Gy ($P<0.0001$). A comparison of circ-HIPK3 expression revealed a significant increase at radiation doses of 4Gy and 8Gy (14.76 and 6.01 times, respectively; $P<0.0001$ for both) in the MDA-MB-231 cell line after 48 hours (Fig.2A).

On the other hand, increases of circ-PVT1 expression level were observed in an MDA-MB-231 cell line at doses of 2Gy, 4Gy, and 8Gy after 24 and 48 hours, compared to the control. The expression ratios were 1.39, 1.61, 26.65, 1.23, 16.2, and 58.55, respectively. The results of the non-parametric ANOVA test were statistically significant with $P<0.0001$ for all of the tested variables. Moreover, a comparison between the two cell lines showed that after 24 hours of exposure to 8Gy radiation, and after 48 hours of exposure to 4Gy and 8Gy radiation, expression levels

of circ-PVT1 in the MDA-MB-231 cell line were 5.07, 7.3, and 9.5 times higher, respectively, than the MCF-7 cell line. The results of non-parametric ANOVA test were statistically significant with p-values of less than 0.0001 for the all three variables. In addition, expression level of circ-PVT1 was significantly higher in the MDA-MB-231 cell line after 24 hours exposure to radiation doses of 4Gy and 8Gy compared to 48 hours (10.56-fold and 2.19-fold, respectively). The results of non-parametric ANOVA test were statistically significant with p-values of less than 0.0001 for both variables (Fig.2B).

Furthermore, the expression of miR-25 in MDA-MB-231 cells was increased significantly at 24 and 48 hours post-exposure to 8Gy doses, with an expression ratio of 22.47 and 26.77, respectively, compared to the control group. The non-parametric ANOVA test results indicated statistical significance with p-values of less than 0.0001 for the both time-points. Findings showed that a dose of 8Gy increased miR-25 expression level by 449 and 535-fold in the MDA-MB-231 cell line, respectively, compared to the MCF-7 cell line after 24 and 48 hours (P<0.0001 for the both data, Fig.2C).

Moreover, an increase in miR-149 expression in the MCF-7 cell line was observed at dose of 8Gy after 24 and 48 hours, compared to the control. The expression ratios were 3.98, 3.98, and 5.86, respectively. The results of the non-parametric ANOVA test were statistically significant with P<0.0001 for all the tested variables.

Moreover, comparing the two cell lines at 8Gy demonstrated that expression level of miR-149 was 4.97 fold higher in the MCF-7 cell line after 24 hours and 6.51 fold higher after 48 hours, in contrast to the MDA-MB-231 cell line (P<0.0001 for the both data, Fig.2D).

Apoptotic rate

MCF-7 and MDA-MB-231 cells were cultured and then exposed to radiation. Morphological changes in the cells were observed under a light microscope (Fig.3). The data revealed that rate of apoptosis in the MCF-7 cell line was significantly higher in cells exposed to 4Gy and 8Gy compared to the control group after 24 hours (P=0.0002 and 0.0005, respectively). Results also showed that the cells receiving 8Gy had higher percentage of apoptotic cells compared to those receiving 2Gy and 4Gy at 24 hours. Additionally, the cells receiving 8Gy had higher percentage of apoptotic cells than those receiving control and 2Gy at 48 hours. It also showed a significant increase (P=0.016, P=0.032, P<0.0001 and P=0.01). The rate of cell apoptosis was significantly higher in the MCF-7 cell line, than the MDA-MB-231 cell line 24 hours after treatment with 8Gy radiation (P=0.007). The results also indicated that the MCF-7 cell line exhibited significantly higher levels of cell apoptosis compared to the MDA-MB-231 cell line after exposing to doses of 4Gy and 8Gy (P=0.013 and P=0.013, respectively, Fig.4).

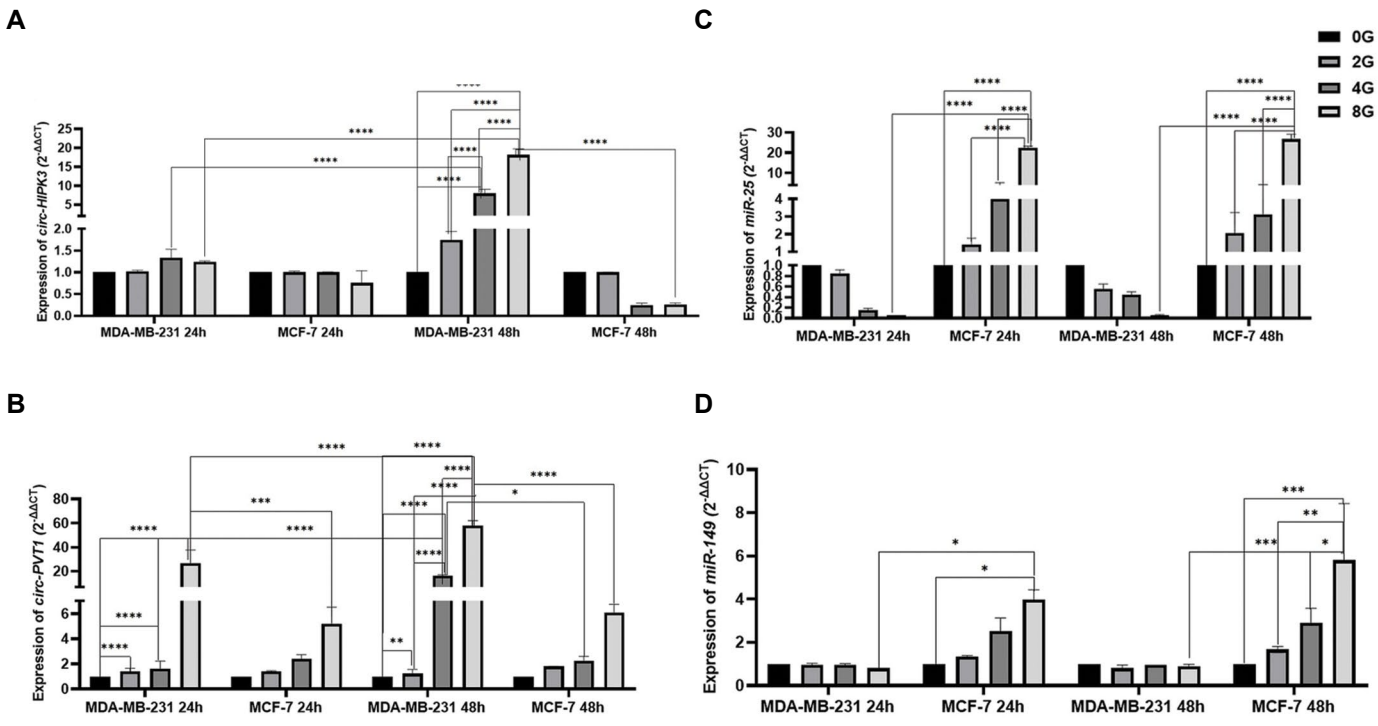

Fig.2: Comparison of the expression levels of RNAs in the control as well as irradiated MCF-7 and MDA-MB-231 cell lines (2Gy, 4Gy, and 8Gy) after 24- and 48 hours. **A.** circ-HIPK3, **B.** circ-PVT1, **C.** miR-25, and **D.** miR-149. The data was analyzed using Tukey's post-hoc one-way ANOVA. All experiments were performed three times. *; P<0.05, **; P<0.01, ***; P<0.001, and ****; P<0.0001.

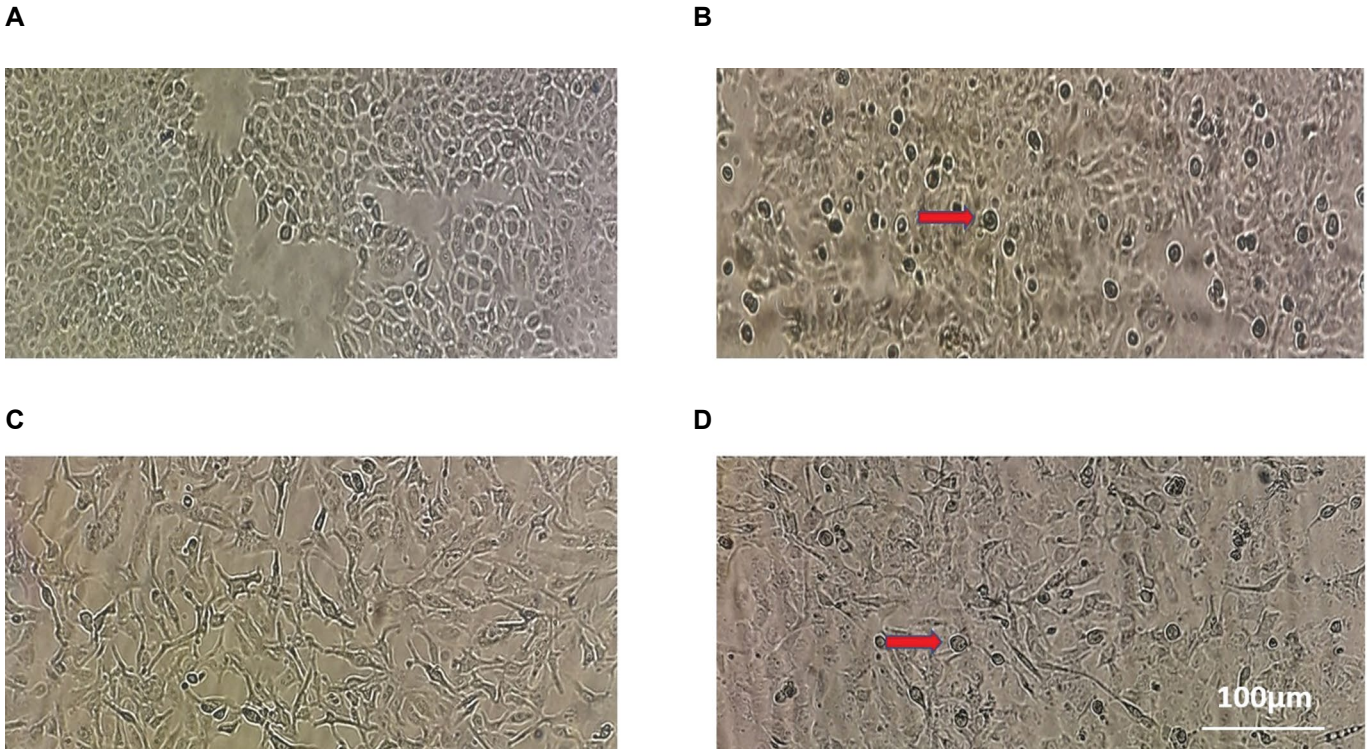

Fig.3: Morphological changes in cells observed under a light microscope. **A.** MCF-7 cells before irradiation. **B.** MCF-7 cells after irradiation. Apoptotic cells are indicated by red arrows. **C.** MDA-MB-231 cells before irradiation. **D.** MDA-MB-231 cells after irradiation. Apoptotic cells are indicated by red arrows. All experiments were performed three times (scale bar: 100 µm).

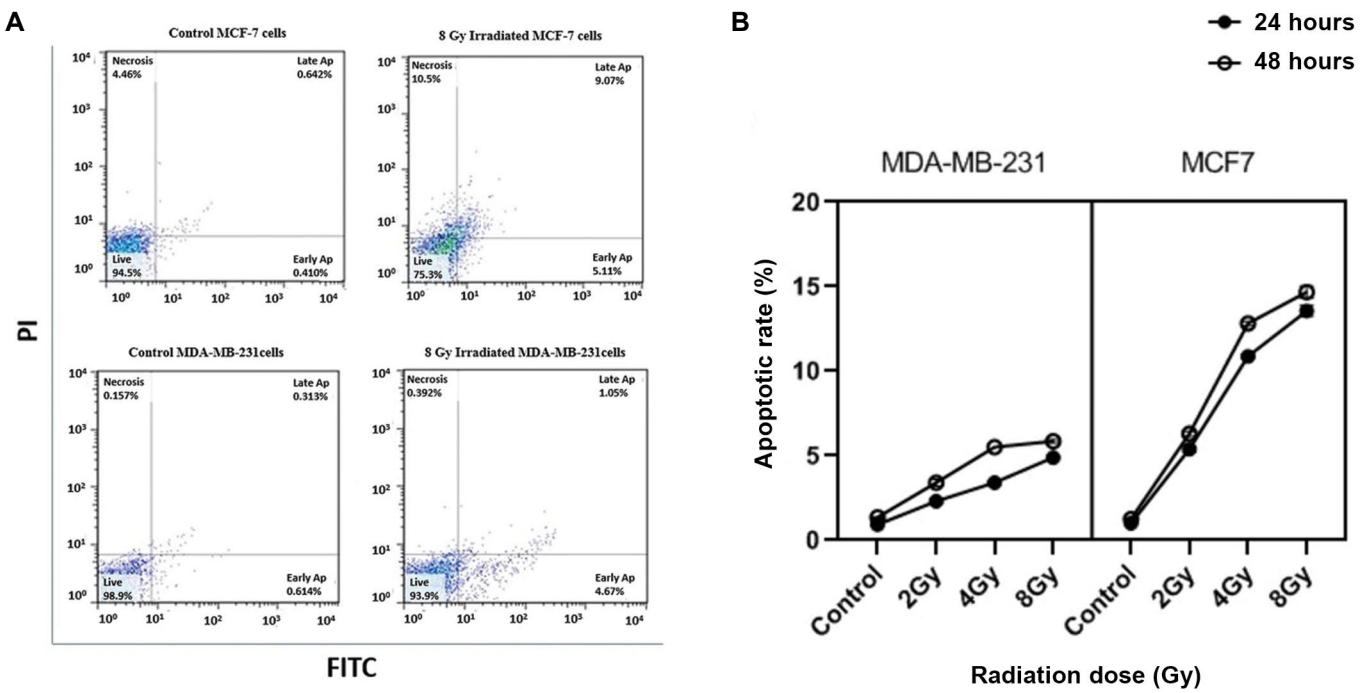

Fig.4: Flow cytometric analysis of apoptosis in cell lines. **A.** Detection of early and late apoptosis through flow cytometry assay using annexin V and PI staining. MCF-7 and MDA-MB-231 cells were exposed to 2, 4, and 8Gy of X-radiation for 24 and 48 hours, respectively. They were subsequently assessed using flow cytometry. MCF-7 cells were treated with medium alone as a control, without radiation. **B.** Rate of apoptosis in MCF-7 and MDA-MB-231 cells under radiation and control conditions. Data was analyzed using Tukey's post-hoc one-way ANOVA. All experiments were performed three times (scale bar: 100 µm).

Discussion

A potential avenue for radiosensitivity research involves developing risk models that incorporate genetic assays to predict a patient's response to radiation and the probability of experiencing radiation-induced side effects (26). This risk model can ultimately be combined with current predictors of radiosensitivity, such as radiation dose, developing the other diseases and conditions in addition to primary cancer, and volume of tissue exposed to radiation (27). The mechanism of RT involves directing X-rays at the affected area of body, which damages the double-stranded DNA. Healthy cells can repair this damage, while the cells with repair defects, such as cancer cells, undergo apoptosis and are eliminated. Previous studies have shown that rate of cell apoptosis was correlated with the level of radiation sensitivity (28). Moreover, cancer cells have high levels of reactive oxygen species (ROS) and they are selectively targeted for cell death by radiation. Degree of oxidative stress mediated by ROS is also linked to cellular radiosensitivity (29).

According to the results of this study, rate of cell apoptosis in the MCF-7 cell line following irradiation was significantly higher than the MDA-MB-231 cell line. This finding is consistent to the results obtained from another research (30).

Conducting the current study on additional cell lines would be beneficial to better establish role of radiation-sensitive or radiation-resistant RNAs. Additionally, conducting a functional study on the target proteins of these RNAs would provide more comprehensive understanding of their mechanisms. Unfortunately, limitations in this study prevented us from conducting such an investigation.

In the present study, we successfully demonstrated an increase in the expression levels of circ-HIPK3, circ-PVT1, and miR-25 in the MDA-MB-231 cell line, compared to the MCF-7 cell line after irradiation. Research indicated that circ-HIPK3, circ-PVT1, and miR-25 were highly expressed in specific types of malignancy, including BC (18, 19, 21). Previous studies demonstrated that circ-HIPK3 activated the NFκB/AKT pathway. Dysregulation of NFκB activity could cause alterations in the expression level of the genes regulated cell death, resulting in the upregulation of antiapoptotic and pro-survival genes, such as members of the Bcl-2 family, IAP proteins (XIAP, cIAP), and TNF receptor-associated factor (TRAF). Based on the previous studies which are in line with our findings, this dysregulation could also hinder apoptotic response to therapeutic agents (31, 32).

On the other hand, the previous studies showed that circ-PVT1 activated Arginase 2 (ARG2). This activation, in turn, inhibited BAX and activated bcl2, ultimately leading to inhibition of apoptosis (33). circ-PVT1 could regulate functions of PI3K/AKT, Wnt5a/Ror2, E2F2, and HIF-1α pathways. The AGR2-HIF-1α pathway, regulated by miR-29a-3p, was activated by circ-PVT1 in breast cancer, leading to increase of proliferation, invasion, and migration, while apoptosis was decreased. This suggested that circ-PVT1 functions as an oncogene in BC (34). Overexpression of circ-PVT1 enhanced expression of AGR2 and HIF-1α by inhibiting miR-29a-3p. During hypoxia, HIF-1α mediated an increase in Arg-II protein levels, which in turn increased production of mitochondrial ROS.

Another study showed that overexpressing miR-25 could decrease production of ROS and apoptosis in renal tubular epithelial cells by activating the PTEN/AKT pathway. These findings are consistent with the results of the current study (24, 35).

Furthermore, our findings demonstrated that expression of miR-149 was higher in the radiosensitive MCF-7 cell line compared to the MDA-MB-231 cell line. Additionally, the expression of miR-149 increased in parallel with higher rates of apoptosis. These results are consistent with the previous studies. Moreover, research studies demonstrated that miR-149 can efficiently inhibit migration and invasion of basal BC cells by targeting transcription factors SP1, FOXM1, and ZBTB2 (19). Previous studies revealed that overexpression of miR-149-5p led to reduction of the chaperonin TCP1 subunit 3 (CCT3) expression level. This reduction led to disruption of intracellular ROS homeostasis as well as redistribution of free amino acids for energy metabolism. This promoted apoptosis of tumor cells (36).

Conclusion

Our findings provided new evidence that circ-HIPK3, circ-PVT1, and miR-25 play crucial roles in the mechanisms of radioresistance in breast cancer. miR-149 was involved in cellular radiosensitivity and it may serve as a valuable factor for assessing cellular radiosensitivity *in vitro* for breast cancer. These factors could serve as a new therapeutic target for treatment of breast cancer. In future, additional studies should be conducted to investigate radiation sensitivity of patients with breast cancer. Establishing role of these factors as biomarkers for radiation sensitivity and resistance could provide valuable predictive information about tumor radiosensitivity or its response to treatment. This information could be used to personalize radiation dosing, making treatment more effective. This would enable clinicians to select from a variety of treatment options, while preventing radiation-induced toxicity in patients who are unlikely to benefit from the treatment.

Acknowledgments

This study was supported by the Tarbiat Modares University in Tehran, Iran, with a research ID: IG-39711. The authors sincerely appreciate the head and staff of the Oncology Department of Imam Khomeini Hospital for their valuable cooperation. The authors also thank all patients and healthy volunteers who participated in our study. We also thank H. Nosrati for irradiating the samples. There is no disclosed potential conflict of interest.

Authors' Contributions

E.A.; Collected samples, conducted experiments, analyzed data, and wrote the manuscript. H.M.; Designed and supervised the research plan, prepared and approved the final manuscript. All authors read and approved the final manuscript.

References

1. Jemal A, Bray F, Center MM, Ferlay J, Ward E, Forman D. Global cancer statistics. CA Cancer J Clin. 2011; 61(2): 69-90.
2. Delaney G, Jacob S, Featherstone C, Barton M. The role of radiotherapy in cancer treatment: estimating optimal utilization from a review of evidence-based clinical guidelines. Cancer. 2005; 104(6): 1129-1137.
3. Early Breast Cancer Trialists' Collaborative Group (EBCTCG); Darby S, McGale P, Correa C, Taylor C, Arriagada R, et al. Effect of radiotherapy after breast-conserving surgery on 10-year recurrence and 15-year breast cancer death: meta-analysis of individual patient data for 10,801 women in 17 randomised trials. Lancet. 2011; 378(9804): 1707-1716.
4. Liu X, Li F, Huang Q, Zhang Z, Zhou L, Deng Y, et al. Self-inflicted DNA double-strand breaks sustain tumorigenicity and stemness of cancer cells. Cell Res. 2017; 27(6): 764-783.
5. Jackson SP, Bartek J. The DNA-damage response in human biology and disease. Nature. 2009; 461(7267): 1071-1078.
6. Xu L, Lyu M, Yang S, Zhang J, Yu D. CircRNA expression profiles of breast cancer and construction of a circRNA-miRNA-mRNA network. Sci Rep. 2022; 12(1): 17765.
7. Zheng Q, Bao C, Guo W, Li S, Chen J, Chen B, et al. Circular RNA profiling reveals an abundant circHIPK3 that regulates cell growth by sponging multiple miRNAs. Nat Commun. 2016; 7: 11215.
8. Kong D, Shen D, Liu Z, Zhang J, Zhang J, Geng C. Circ_0008500 Knockdown improves radiosensitivity and inhibits tumorigenesis in breast cancer through the miR-758-3p/PFN2 axis. J Mammary Gland Biol Neoplasia. 2022; 27(1): 37-52.
9. Hu F, Peng Y, Fan X, Zhang X, Jin Z. Circular RNAs: implications of signaling pathways and bioinformatics in human cancer. Cancer Biol Med. 2023; 20(2): 104-128.
10. Zhang ZH, Wang Y, Zhang Y, Zheng SF, Feng T, Tian X, et al. The function and mechanisms of action of circular RNAs in urologic cancer. Mol Cancer. 2023; 22(1): 61.
11. Attwaters M. In vivo RNA base editing with circular RNAs. Nat Rev Genet. 2022; 23(4): 196-197.
12. He J, Xie Q, Xu H, Li J, Li Y. Circular RNAs and cancer. Cancer Lett. 2017; 396: 138-144.
13. Nielsen AF, Bindereif A, Bozzoni I, Hanan M, Hansen TB, Irimia M, et al. Best practice standards for circular RNA research. Nat Methods. 2022; 19(10): 1208-1220.
14. Zheng Q, Bao C, Guo W, Li S, Chen J, Chen B, et al. Circular RNA profiling reveals an abundant circHIPK3 that regulates cell growth by sponging multiple miRNAs. Nat Commun. 2016; 7: 11215.
15. Zeng K, Chen X, Xu M, Liu X, Hu X, Xu T, et al. CircHIPK3 promotes colorectal cancer growth and metastasis by sponging miR-7. Cell Death Dis. 2018; 9(4): 417.
16. Liu Z, Guo S, Sun H, Bai Y, Song Z, Liu X. Circular RNA CircHIPK3 elevates CCND2 expression and promotes cell proliferation and invasion through miR-124 in glioma. Front Genet. 2020; 11: 1013.
17. Chen D, Lu X, Yang F, Xing N. Circular RNA circHIPK3 promotes cell proliferation and invasion of prostate cancer by sponging miR-193a-3p and regulating MCL1 expression. Cancer Manag Res. 2019; 11: 1415-1423.
18. Zeng K, Chen X, Xu M, Liu X, Hu X, Xu T, et al. CircHIPK3 promotes colorectal cancer growth and metastasis by sponging miR-7. Cell Death Dis. 2018; 9(4): 417.
19. Lu H, Han X, Ren J, Ren K, Li Z, Sun Z. Circular RNA HIPK3 induces cell proliferation and inhibits apoptosis in non-small cell lung cancer through sponging miR-149. Cancer Biol Ther. 2020; 21(2): 113-121.
20. Luo N, Liu S, Li X, Hu Y, Zhang K. Circular RNA circHIPK3 promotes breast cancer progression via sponging MiR-326. Cell Cycle. 2021; 20(13): 1320-1333.
21. Ghafouri-Fard S, Khoshbakht T, Taheri M, Jamali E. A concise review on the role of CircPVT1 in tumorigenesis, drug sensitivity, and cancer prognosis. Front Oncol. 2021; 11: 762960.
22. Li M, Chi C, Zhou L, Chen Y, Tang X. Circular PVT1 regulates cell proliferation and invasion via miR-149-5p/FOXM1 axis in ovarian cancer. J Cancer. 2021; 12(2): 611-621.
23. Shi LP, Guo HL, Su YB, Zheng ZH, Liu JR, Lai SH. MicroRNA-149 sensitizes colorectal cancer to radiotherapy by downregulating human epididymis protein 4. Am J Cancer Res. 2018; 8(1): 30-38.
24. Zhao T, Meng W, Chin Y, Gao L, Yang X, Sun S, et al. Identification of miR253p as a tumor biomarker: regulation of cellular functions via TOB1 in breast cancer. Mol Med Rep. 2021; 23(6): 406.
25. He Z, Liu Y, Xiao B, Qian X. miR-25 modulates NSCLC cell radiosensitivity through directly inhibiting BTG2 expression. Biochem Biophys Res Commun. 2015; 457(3): 235-241.
26. Barnett GC, Wilkinson JS, Moody AM, Wilson CB, Twyman N, Wishart GC, et al. The Cambridge breast intensity-modulated radiotherapy trial: patient- and treatment-related factors that influence late toxicity. Clin Oncol (R Coll Radiol). 2011; 23(10): 662-673.
27. Tipatet KS, Davison-Gates L, Tewes TJ, Fiagbedzi EK, Elfick A, Neu B, et al. Detection of acquired radioresistance in breast cancer cell lines using Raman spectroscopy and machine learning. Analyst. 2021; 146(11): 3709-3716.
28. Dunne AL, Price ME, Mothersill C, McKeown SR, Robson T, Hirst DG. Relationship between clonogenic radiosensitivity, radiation-induced apoptosis and DNA damage/repair in human colon cancer cells. Br J Cancer. 2003; 89(12): 2277-2283.
29. Dayal R, Singh A, Pandey A, Mishra KP. Reactive oxygen species as mediator of tumor radiosensitivity. J Cancer Res Ther. 2014; 10(4): 811-818.
30. Wang W, Luo YP. MicroRNAs in breast cancer: oncogene and tumor suppressors with clinical potential. J Zhejiang Univ Sci B. 2015; 16(1): 18-31.
31. Li R, Wang X, Zhu C, Wang K. lncRNA PVT1: a novel oncogene in multiple cancers. Cell Mol Biol Lett. 2022; 27(1): 84.
32. Wang W, Nag SA, Zhang R. Targeting the NFκB signaling pathways for breast cancer prevention and therapy. Curr Med Chem. 2015; 22(2): 264-289.
33. Li R, Wang X, Zhu C, Wang K. lncRNA PVT1: a novel oncogene in multiple cancers. Cell Mol Biol Lett. 2022; 27(1): 84.
34. Wang J, Huang K, Shi L, Zhang Q, Zhang S. CircPVT1 promoted the progression of breast cancer by regulating MiR-29a-3p-mediated AGR2-HIF-1α pathway. Cancer Manag Res. 2020; 12: 11477-11490.
35. Li H, Zhu X, Zhang J, Shi J. MicroRNA-25 inhibits high glucose-induced apoptosis in renal tubular epithelial cells via PTEN/AKT pathway. Biomed Pharmacother. 2017; 96: 471-479.
36. Temiz E, Koyuncu İ, Sahin E. CCT3 suppression prompts apoptotic machinery through oxidative stress and energy deprivation in breast and prostate cancers. Free Radic Biol Med. 2021; 165: 88-99.

Cell J
Cell Journal (Yakhteh)
Homepage: https://www.celljournal.org/
Original Article
Vol 25, No 10, October 2023, Pages: 696-705

Unraveling The Effects of *DICER1* Overexpression on Immune-Related Genes Expression in Mesenchymal Stromal/Stem Cells: Insights for Therapeutic Applications

Hamid Reza Bidkhori, M.D., Ph.D.[1], Moein Farshchian, Ph.D.[2, 3], Halimeh Hassanzadeh, M.Sc.[2], Reza Jafarzadeh Esfehani, M.D., Ph.D.[4], Reihaneh Alsadat Mahmoudian, Ph.D.[5, 6], Mahdi Moradi Marjaneh, M.D., Ph.D.[7], Houshang Rafatpanah, Ph.D.[1*]

1. Immunology Research Centre, Division of Inflammation and Inflammatory Diseases, Mashhad University of Medical Sciences, Mashhad, Iran
2. Stem Cells and Regenerative Medicine Department, Academic Center for Education, Culture, and Research (ACECR) - Khorasan Razavi, Iran
3. Division of Oncology, Laboratory of Cellular Therapy, Department of Medical and Surgical Sciences for Children and Adults, University Hospital of Modena and Reggio Emilia, Modena, Italy
4. Blood Borne Infections Research Center, Academic Center for Education, Culture, and Research (ACECR) - Khorasan Razavi, Iran
5. Basic Sciences Research Institute, Mashhad University of Medical Sciences, Mashhad, Iran
6. Cancer Research Center, Mashhad University of Medical Sciences, Mashhad, Iran
7. Department of Infectious Disease, Faculty of Medicine, Imperial College London, London, United Kingdom

Abstract

Objective: The immunoregulatory properties of mesenchymal stromal/stem cells (MSCs) bring a promise for the treatment of inflammatory diseases. However, their ability to suppress the immune system is unstable. To enhance their effectiveness against immune responses, it may be necessary to manipulate MSCs. Although some dsRNA transcripts come from invading viruses, the majority of dsRNA has an endogenous origin and is known as endo-siRNA. DICER1 is a ribonuclease protein that can generate small RNAs to modulate gene expression at the post-transcriptional level. We aimed to evaluate the expression of several immune-related genes at mRNA and protein levels in MSCs overexpressing DICER1 exogenously.

Materials and Methods: In this comparative transcriptomic experimental study, the adipose-derived MSCs (Ad-MSCs) were transfected using the pCAGGS-Flag-hsDicer vector for the *DICER1* overexpression. Following the RNA extraction, mRNA expression level of *DICER1* and several inflammatory cytokines were examined. We performed a relative real-time polymerase chain reaction (PCR) assay and transcriptome analysis between two groups including DICER1-transfected MSCs and control MSCs. Moreover, media from the transfected MSCs were evaluated for various interferon response factors by ELISA.

Results: The overexpression of *DICER1* is associated with a significant increase in the mRNA expression level of *COX-2, DDX-58, IFIH1, MYD88, RNase L, TLR3/4*, and *TDO2* genes and a downregulation of the TSG-6 gene in MSCs. Moreover, the expression levels of *IL-1, 6, 8, 17, 18, CCL2, INF-γ, TGF-β*, and *TNF-α* were higher in the DICER1-transfected MSCs group.

Conclusion: It seems that the ectopic expression of *DICER1* in Ad-MSCs is linked to alterations in the expression level of immune-related genes. It is suggested that the manipulation of immune-related pathways in MSCs via the *Dicer1* overexpression could facilitate the development of MSCs with distinct immunoregulatory phenotypes.

Keywords: DICER1, Immunomodulation, Mesenchymal Stromal/Stem Cells, RNA-Sequencing

Citation: **Bidkhori HR, Farshchian M, Hassanzadeh H, Jafarzadeh Esfehani R, Alsadat Mahmoudian R, Moradi Marjaneh M, Rafatpanah H. Unraveling the effects of DICER1 overexpression on immune-related genes expression in mesenchymal stromal/stem cells: insights for therapeutic applications. Cell J. 2023; 25(10): 696-705. doi: 10.22074/CELLJ.2023.1988987.1221**

Introduction

Mesenchymal stromal/stem cells (MSCs) are a category of stem cells deemed to have a high potential for therapeutic stem cell applications and regenerative medicine (1). MSCs are a diverse population of cells that possess the ability to self-renew and differentiate into various mesenchymal lineages, such as cartilage, adipose tissue, and bone (2). There is enough evidence that MSCs have immunomodulatory properties and can modify immune responses and inflammatory environments (1).

Received: 01/February/2023, Revised: 12/June/2023, Accepted: 01/July/2023
***Corresponding Address: P.O.Box: 9177899191, Immunology Research Centre, Division of Inflammation and Inflammatory Diseases, Mashhad University of Medical Sciences, Mashhad, Iran**
Email: RafatPanahH@mums.ac.ir

Royan Institute
Cell Journal (Yakhteh)

The immunosuppressive function of MSCs is not stable, and they need to be activated for their immunosuppressive properties to be unlocked. MSCs are now referred to as "inflammation sensors" due to their interaction with the inflammatory environment and immunomodulatory properties. They can affect the immune system through direct cell-to-cell attachment, inflammatory factor secretion, and programmed cell death induction (2). There is a growing interest in finding new ways to enhance the therapeutic potential of MSCs in various clinical conditions.

Given that miRNAs are key regulators of gene expression and that MSC functions are heavily dependent on their transcriptome profiles. Therefore, it is reasonable to hypothesize that miRNAs could have a significant impact on the immunomodulatory properties of MSCs. Understanding these interactions may provide a manipulated miRNA profile that brings a new chance of MSC-based therapy. The miRNAs are produced from pri-miRNAs, which are generated by the RNA polymerase II in the nucleus, and then processed to pre-miRNAs and exported to the cytoplasm (3).

The Dicer protein is a multi-domain endoribonuclease that mainly known for its catalytic function in regulating gene expression and specificity for processing endogenous dsRNAs (4). This highly conserved RNase has a crucial role in various physiological and molecular pathways during development and stress resistance (5). Abnormal expressions of Dicer were demonstrated in different types of malignancies, with an increased expression found in the prostate, colorectal, and early lesions of lung adenocarcinoma and decreased expression found in breast and invasive lung adenocarcinoma (6-9). The dysregulation of Dicer is associated with poor survival, invasion, and metastasis (8, 10, 11). Most of the available data on the abnormal expression of Dicer is related to cancer cell lines, and there is not enough data about the role of Dicer in human stem cells. The under or overexpression of Dicer results in the differentiation potential of stem cells for miRNA biogenesis (12). The probable role of Dicer in the regulation of immunological properties of human stem cells has not been previously discussed, but it has been demonstrated that Dicer-deficient murine stem cells showed inappropriate proliferation and fail to express pluripotency markers (13).

Regarding the therapeutic potential of MSCs, it has been suggested that manipulation of these cells toward an enhancement of their therapeutic functions, may increase their efficacy in treating human diseases. Therefore, this study aimed to over-express the *DICER1* in human adipose-derived MSCs (Ad-MSCs) and investigate the effect of the ectopic expression of this gene on the expression of immune-related genes.

Material and Methods

The biomedical research Ethics Committee ACECR, Khorasan Razavi, Iran, approved this investigation (IR.ACECR.JDM.REC.1398.007). This study was performed on samples obtained from 3 healthy females who underwent a plastic surgery in the Day Clinic, (Khorasan Razavi, Iran). All participants signed an informed consent.

Isolation and culture of human MSCs derived from adipose tissue

Adipose-derived stromal/stem cells were provided by fresh, healthy lipoaspirate of patients who underwent a plastic surgery. In our lab, samples were washed with the phosphate-buffered saline buffer (PBS, Biowest, Germany), containing 0.1% penicillin-streptomycin (pen-strep, 15140122, Thermo Fisher Scientific, USA). They were then incubated in the presence of 0.1% collagenase type I (17100, Gibco, USA) at 37°C for one hour, followed by inactivation of the collagenase with the 10% fetal bovine serum (FBS, 11960044, Gibco, USA). After a centrifugation (600 g for 10 minutes) to remove adipose cell debris, the pellets were suspended in the Dulbecco's Modified Eagle Medium (DMEM, Gibco, USA), containing 10% FBS and 0.1% pen-strep. The cells were incubated in a 5% CO_2 at 37°C and the culture medium was changed every three days. Experiments were conducted using cells at passage number 3 from the lipoaspiration.

Flow cytometry analysis of Ad-MSCs surface markers

To confirm the purity and characterization of isolated Ad-MSCs, we investigated the (RNA or protein) expression of some specific mesenchymal stem cell surface markers, such as CD44, 73, 90, and 105, and also the hematopoietic cell-specific markers, including CD11b, CD34, and CD45 as. Briefly, 10^6 Ad-MSCs were suspended in the 250 µl cold PBS with 5% FBS and incubated at room temperature with the 1 µl of interested antibodies (BioLegend, Spain) for 1 hour in the dark. Then the expression of surface antigens was evaluated by a FACSCalibur flow cytometer (BD Bioscience, USA) and data were analyzed by FlowJo 7.6 software (Tree Star, Ashland, OR) (14).

Plasmid construction and cell transfection

The pCAGGS-Flag-hsDicer vector, including the human *DICER1* gene sequence, was obtained from Addgene (41584, USA). Then, the fluorescent ZsGreen marker-2A-Puromycin fragment inframe was derived and amplified from the pCDH-513b lentivirus vector (513B-1, System Biosciences, USA) and cloned in the pCAGGS-Flag-hsDicer vector (Fig.1). This cistronic construct simultaneously expresses *DICER1* was connected to the fluorescent ZsGreen marker and puromycin by the 2A peptide. Moreover, the pCDH-513b vector was applied as a control for transfection experiments (approximately up to 90% transfection efficiency in cells). All vectors were purified by using the QIAGEN Plasmid Maxi Kit (12162., USA), according to the manufacturer's instructions. MSCs were transfected by using the Lipofectamine 3000 reagent (L3000001, Thermo Fisher Scientific, USA)

according to the manufacturer's protocol. Briefly, the cells in several groups were transfected with 2500 ng (per 6-well plate) of the pCAGGS-Flag-hsDicer plasmid and a plasmid expressing the fluorescent ZsGreen marker as a control group, separately. The MSCs were selected with 2 ug/ml puromycin (A1113803, Thermo Fisher Scientific, USA) 48 hours post-transfection and the remaining cells were selected after 72 hours of treatment with puromycin.

RNA extraction and quantitative real-time polymerase chain reaction analysis

The extraction of total RNA, removal of DNA contamination using DNase I treatment, and subsequent cDNA synthesis were carried out using the Tripure reagent from Roche (Roche, Germany), the DNase Removal kit, and MMuLV Reverse Transcriptase from Thermo Fisher Scientific (Thermo Fisher Scientific, USA), respectively. All procedures were performed according to the manufacturers' instructions. Real-time PCR was performed by SYBR Green PCR Master Mix (A323402., AMPLIQON, Denmark) on a CFX-96 machine (Bio-Rad, USA) with specific primers for the candidate genes and data were normalized by the *RPLP0* housekeeping gene. The specific primer sequences and amplicon size of genes are demonstrated in the supplementary file. The fold change between 0.5 and 2 was interpreted as a normal expression. Since the efficiency of all primers was measured to be 90 to 110%, the $2^{-\Delta\Delta CT}$ method was utilized to compare the relative expression. The gene expression at the mRNA level was evaluated. Our selected genes were included , *COX-2* (a proliferation-related transcriptional factor), *DDX-58* (an antiviral innate immune response receptor RIG-I), *IFIH1* (an interferon-induced helicase C domain-containing protein), *MYD88* (a myeloid differentiation primary response), *RNase L* (an interferon-induced ribonuclease which destroys all RNA within both cellular and viral), *TLR3* (an RA-related important pattern recognition receptor), *TLR4* (a bacterial lipopolysaccharide pattern recognition receptor), *TDO2* (a systemic regulator of tryptophan levels).

Enzyme-linked immunosorbent assay

Concentrations of the secreted cytokines including IL-1, 4, 6, 8, 10, 17, 18, 23, INF-γ, TNF-α, TGF-β, and CCL2, in the supernatant of the Dicer-transfected MSCs were measured with the use of ELISA kit (KPG, Iran) according to the manufacturer's instructions. Briefly, the supernatant of transfected and non-transfected cells was added to the ELISA strip plates that were pre-coated with captured antibodies specific of each cytokine, and colorimetric absorbance was recorded at a wavelength of 450 nm. The MSCs were transfected with the GFP expressing vector, pCDH-513b plasmids, and non-transfected cells were applied as control groups.

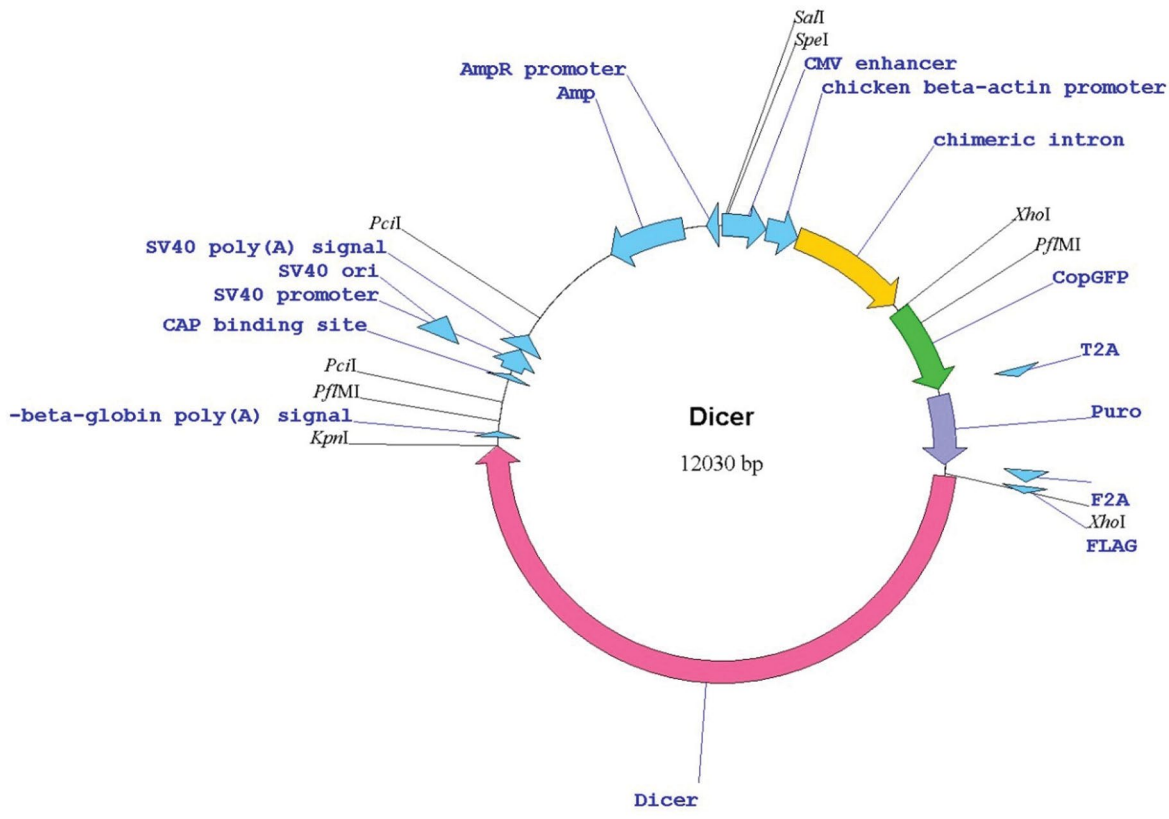

Fig.1: The genetic map of the pCAGGS-Flag-hsDicer construct that simultaneously express *DICER1* connected by a 2A peptide to the fluorescent ZsGreen marker.

RNA-sequencing by Illumina NovaSeq6000

RNA sequencing, mapping, and normalization were performed as previously described (15). Briefly, sequencing libraries were produced from 100 ng RNA sample, using KAPA RNA HyperPrep Kit (Kapa Biosystems, USA) with RiboErase (HMR) kit (Hoffmann-La Roche, Switzerland).

Then, paired-end reads (2×100 nucleotides) were attained for 4 samples, including 2 RNA samples of *DICER1* overexpressed MSCs and 2 of fluorescent ZsGreen markers overexpressed MSCs, on the Illumina NovaSeq 6000 platform (CeGaT company, Germany). The sequencing reads were aligned to the GRCh38 (hg38) human reference genome, using STAR 2.7.1, and the HTSeq package was run under the union mode. The differential expression of genes was identified by the DESeq2 package in R software from Bioconductor. The total RNA-sequencing data were deposited in the NCBI database under accession number (PRJNA681026).

Bioinformatics analysis

The GeneMANIA database (http://www.genemania.org) was used to identify the gene-to-gene interactions network and target genes correlated to DICER protein and immune genes. We also used NetworkAnalyst webserver (https://www.networkanalyst.ca) to find the expression network of differentially expressed genes (DEGs) and the most closely associated genes within the co-expression network and physical interaction.

Statistical analysis

The IBM SPSS 22 statistical software (La Jolla, USA) and GraphPad Prism 5.0 (La Jolla, USA) were used to perform the data analysis and figure drawing, respectively. A $P<0.05$ was considered to indicate a statistically significant difference. A One-Sample t test was used to compare the log2 fold change of qRT-PCR results.

Results

Characterization of Ad-MSCs analysis with flow cytometry

The MSCs derived from the adipose tissue were verified with their spindle-like shape examination and specific surface markers were identified. The expression levels of CD90, 44, 105, and 73 were 98.5, 98.2, 90.8, and 97.7%, respectively, whilst the expression of non-mesenchymal stem cell-specific markers, including CD11b, 45, and 34 were 4.22, 0.88, and 2.12%, respectively (Fig.2).

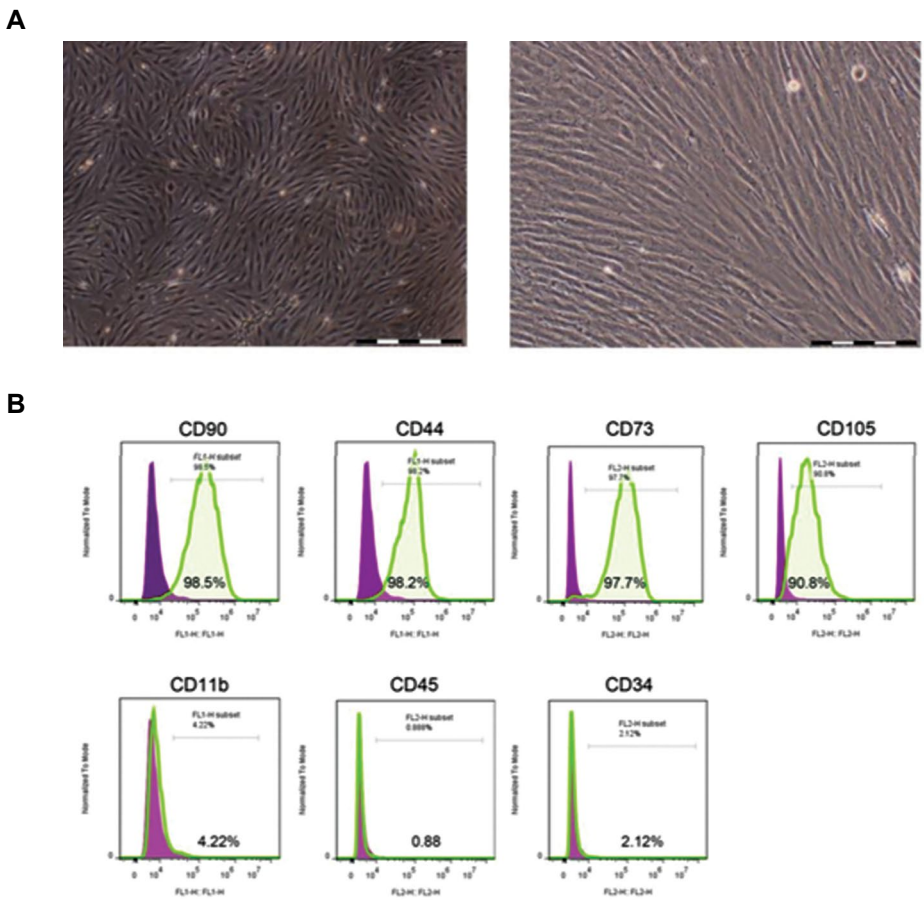

Fig.2: Characterization of human Ad-MSCs. **A.** Bright field images of cells at different magnifications showing a fibroblast-like morphology (scale bar: 500 µm (left) and 200 µm (right). **B.** Flow cytometry analysis shows almost all cultured Ad-MSCs (more than 90%) markers, including CD90, CD44, CD73, and CD105 expression, whereas a small portion of the cells expressed CD11b, CD45, and CD34 markers. We illustrated expressions of cell surface markers of Ad-MSCs that were compared with their respective isotype controls.

Overexpression of *DICER1* in MSCs

Using fluorescent microscopy, the transfection efficiency of the pCAGGS-Flag-hsDicer construct was compared with the pCDH513b fluorescent ZsGreen marker, following *DICER1* overexpression in MSCs. The transfection results of the pCAGGS-Flag-hsDicer and pCDH513b control transfected MSCs are revealed in Figure 3. Significant overexpression of *DICER1* was detected in the pCAGGS-Flag-hsDicer transfected MSCs in comparison with the pCDH513b control MSCs.

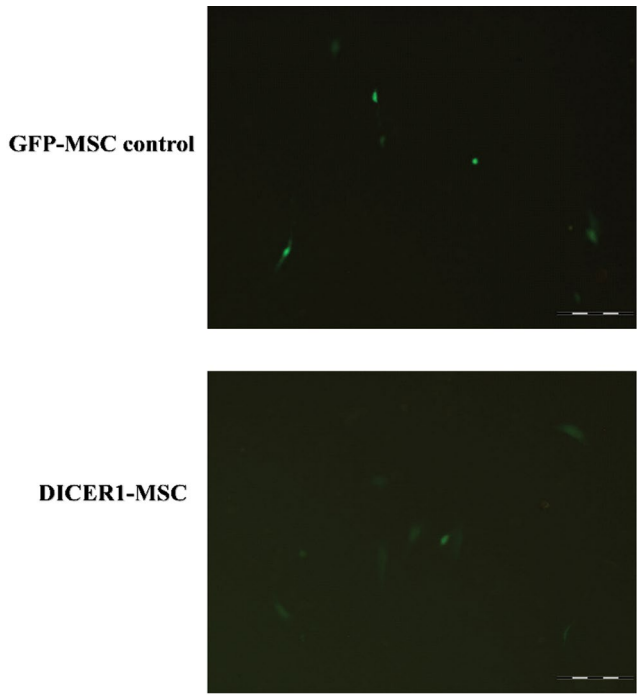

Fig.3: Ectopic expression of *DICER1* in MSCs. Fluorescence microscopy images of Ad-MSCs overexpressing pCDH-513b vector as a control (top) and also cells with ectopic expression of pCAGGS-Flag-hsDicer (bottom) (scale bar: 200 µm).

Overexpression of *DICER1* involved in the MSC-mediated immune regulation

By confirming the *DICER1* overexpression in Ad-MSCs, we evaluated the mRNA expression levels of 10 pro and anti-inflammatory cytokine genes by the qRT-PCR technique after triplicate examinations (Fig.4). Overexpression of *DICER1* led to a significant increase (P<0.0001) in the levels of mRNA expression of some genes, including *COX-2*, *DDX-58*, *IFIH1*, *MYD88*, *RNase L*, *TLR3*, *TLR4 and TDO2* (up to 3, 6, 4, 4.5, 3, 16, 4, 3 folds, respectively) in comparison with to the control cells. In addition, the overexpression of *DICER1* resulted in a significant reduction (P<0.05) in the expression of mRNA levels of *TSG-6*. The mRNA levels of *TSG-6* and *INF-γ* were decreased to 2.2 and 2 folds, respectively.

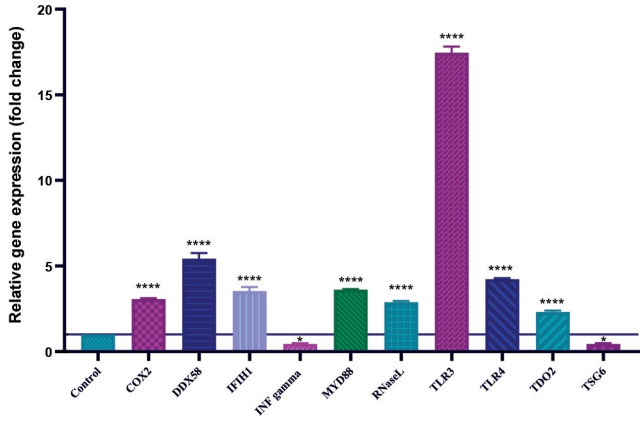

Fig.4: Ectopic expression of *DICER1* significantly impacts the mRNA expression of several immune-related genes in MSCs. The expression of all genes in the control group (GFP-MSCs) was set to a value of 1. When compared, the expression levels of these genes in Ad-MSCs with overexpressed *DICER1* gene were reported as relative values compared to the control group. RPLP0 was used as an intron control. The line parallel to the x-axis passes through one and the overexpression and downregulation of these genes in ASCs transfected with DICER1 were then compared with the control group. *; P<0.05 and ****; P<0.0001

To investigate the amount of pro and anti-inflammatory cytokines at the protein level of MSCs overexpressing *DICER1*, we determined the concentration of the secreted cytokines in each group's culture media by ELISA assay. The concentration of IL-4 (12.58 pg/mL), IL-10 (34.48 pg/mL), and IL-23 (24.32 pg/mL) were non − significantly less in the *DICER1*-transfected MSCs than the control group, whilst the concentrations of IL-1, 6, 8, 17, 18, CCL2, INF-γ, TGF-β, and TNF-α were higher in the *DICER1*-transfected MSCs group (28.19, 113.6, 156.2, 19.5, 42.44, 30.43, 25.12, 21.17, 45.45 pg/mL), respectively (Fig.5).

RNA-sequencing of *DICER1* overexpressing MSCs

The transcriptomes of o ur genetically modified MSCs were analyzed to determine if there were any changes in its gene expression and dsRNA related pathways. RNA sequencing was performed on the total RNA that was extracted from the duplication of MSC-GFP and MSC-DICER1 cells to identify the gene expression pattern. Our analysis revealed 527 significant DEGs between MSC-GFP and MSC-DICER1 cells (adjusted P<0.05, -1 <log2 Fold change <1). The most enriched gene terms in molecular function (MF) were extracellular matrix structure, organization, protein folding chaperone, cofactor binding/signaling receptor activator/receptor-ligand activity, and cell adhesion molecule binding, as shown in Figure S1A (See Supplementary Online Information at www.celljournal.org).

The metabolic processes of RNA molecules, including rRNA, mRNA, and ncRNA, as well as ribosome biogenesis, were found to be the most enriched in the biological process (BP) category (Fig.S1B, See Supplementary Online Information at www.celljournal.org). We did not

find an inclusive list of DEGs. Therefore, we evaluated the expression of some selected genes via qRT-PCR experiments. We concluded that the overexpression of some of genes, including *CDSN*, *POSTN*, and *HELLPAR*, plays a role in the stemness maintenance. Furthermore, *LCE1F*, *NTSR1*, *EPHA7*, *LRR1*, *ANKRD28* and *ZBTB12* were some of the most suppressed genes in our study. Most of the downregulated genes were involved in signal transduction pathways.

The significance of molecular function and BP is demonstrated in Table S1 (See Supplementary Online Information at www.celljournal.org).

Our analysis revealed that these DEGs are primarily involved in various biological processes, including the innate immune system, interferon response types α/β/γ, Toll-like receptor signaling, transport of mature mRNA independent of SLBP, transport of sugars, bile salts, organic acids, metal ions, and amine compounds, cytosolic sensing of pathogen-associated DNA, Th17 cell differentiation, NAD metabolism, PEDF signaling, ERK signaling, responses to bacterial infections, G-protein signaling via Ras family GTPases in kinase cascades, replication of viral genome, and ATM-dependent DNA damage response.

Although, the whole list of immunity related genes has not been found in the RNA-seq data, we considered a panel of genes to evaluate by qRT-PCR and ELISA at mRNA and protein levels. This panel contained the interferon response pathway genes, particularly those genes that were involved in the interferon response, α and/or β and/or γ types, ERK signaling, and Toll-like receptors. The results have demonstrated the dysregulation of innate immune response genes of the interferon response pathway. These genes included *IL-1*, *4*, *6*, *8*, *10*, *17*, *18*, *23*, *INF-γ*, *TNF-α*, *TGF-β*, *CCL2*, *COX-2*, *DDX-58*, *IFIH1*, *MYD88*, *RNase L*, *TLR3*, *TLR4*, *TDO2*, and *TSG-6*.

Our gene ontology analysis of mesenchymal stromal stem cells overexpressing *DICER1* showed that *DICER1* overexpression can affect various cellular processes. Particularly, we observed changes in heterochromatin-modifying enzymes, catalytic activity on RNA, and the formation of ribonucleoprotein complexes. These findings suggest that an immune function dysregulation may be an indirect result of the molecular changes associated with the DICER1 protein overexpression (Fig.6).

Gene co-expression network analysis

All *DICER1*, pro and anti-inflammatory cytokines and immunoregulatory genes were imported into the GeneMANIA database to generate the protein-protein interaction (PPI) network. The genes interaction was based on pathways, physical interactions, and genes co-expression. The data defined the biological functions of genes through the co-expression network. Our analysis revealed that the *DICER1* gene interacts with several gene markers, including *TARBP2*, *PRKRA*, and *ERCC3*, but not with cytokines. Moreover, anti-inflammatory and pro-inflammatory mediators interacted with several genes, including *TCN1*, *GNA1/2*, *PF4*, *GATA3*, *CBLAF*, *CUBN*, *IQGAP1*, *MAVS*, *CYLD*, *IRF5/7*, *TIRAP*, *LY96*, *IRAK1/2*, *TICAM2*, *IDO1/2*, *ECSIT*, and *MBL2*. These results confirmed the biological relevance between *DICER1* and genes expression of inflammatory cytokines (Fig.S2, See Supplementary Online Information at www.celljournal.org). The Network analysis revealed that NCBP1a protein was among the upregulated nodes. While, the NCBP1a protein is an mRNA-cap binding protein known for its role in transcription regulation by RNA polymerase II. Additionally, many genes associated with immune response were downregulated, in agreement with our earlier discussion. Our network analysis revealed that the NCBP1, an mRNA-cap binding protein, that is involved in transcription regulation by RNA polymerase II, was among the upregulated nodes. Additionally, many genes related to immune response were found to be downregulated, as previously discussed.

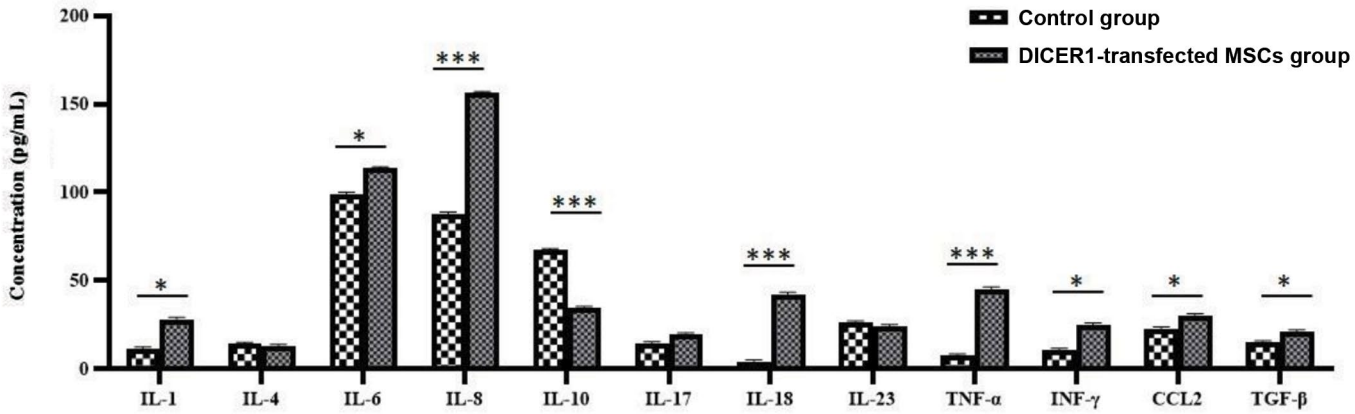

Fig.5: Cytokine expression analysis at protein level. The results indicate a significant difference in the expression of several cytokines, including IL-1, IL-6, IL-8, IL-10, IL-18, TNF-α, IFN-γ, CCL2 and TGF-β between DICER1-MSCs and the control group. Of these cytokines, only IL-10 was overexpressed in the control group in comparison with the DICER1 overexpressing cells. *; P<0.05 and ***; P<0.001.

A

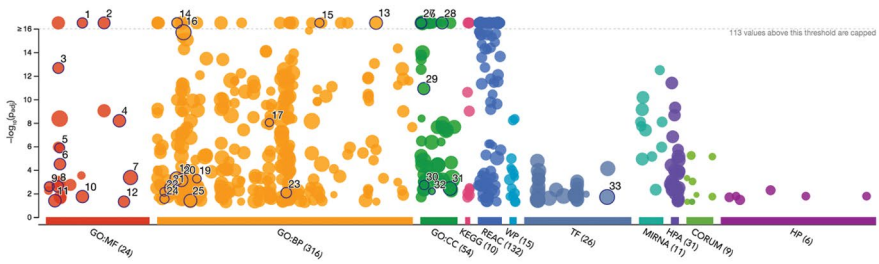

ID	Source	Term ID	Term Name	p_{adj} (query_1)
1	GO:MF	GO:0030527	structural constituent of chromatin	4.993×10^{-47}
2	GO:MF	GO:0046982	protein heterodimerization activity	5.557×10^{-20}
3	GO:MF	GO:0005201	extracellular matrix structural constituent	2.139×10^{-13}
4	GO:MF	GO:0050839	cell adhesion molecule binding	6.536×10^{-9}
5	GO:MF	GO:0005518	collagen binding	1.329×10^{-8}
6	GO:MF	GO:0008017	microtubule binding	3.178×10^{-5}
7	GO:MF	GO:0097367	carbohydrate derivative binding	4.321×10^{-4}
8	GO:MF	GO:0005125	cytokine activity	2.513×10^{-3}
9	GO:MF	GO:0003777	microtubule motor activity	2.536×10^{-3}
10	GO:MF	GO:0030545	signaling receptor regulator activity	1.808×10^{-2}
11	GO:MF	GO:0004672	protein kinase activity	4.071×10^{-2}
12	GO:MF	GO:0061134	peptidase regulator activity	4.837×10^{-2}
13	GO:BP	GO:1903047	mitotic cell cycle process	8.712×10^{-28}
14	GO:BP	GO:0006334	nucleosome assembly	1.646×10^{-27}
15	GO:BP	GO:0071459	protein localization to chromosome, centromer...	1.420×10^{-19}
16	GO:BP	GO:0007275	multicellular organism development	1.969×10^{-16}
17	GO:BP	GO:0045653	negative regulation of megakaryocyte different...	9.346×10^{-9}
18	GO:BP	GO:0006259	DNA metabolic process	5.209×10^{-4}
19	GO:BP	GO:0010575	positive regulation of vascular endothelial grow...	5.468×10^{-4}
20	GO:BP	GO:0006954	inflammatory response	7.201×10^{-4}
21	GO:BP	GO:0003013	circulatory system process	3.619×10^{-3}
22	GO:BP	GO:0002227	innate immune response in mucosa	7.166×10^{-3}
23	GO:BP	GO:0050830	defense response to Gram-positive bacterium	8.448×10^{-3}
24	GO:BP	GO:0002251	organ or tissue specific immune response	2.830×10^{-2}
25	GO:BP	GO:0009617	response to bacterium	4.033×10^{-2}
26	GO:CC	GO:0000786	nucleosome	5.419×10^{-40}
27	GO:CC	GO:0000775	chromosome, centromeric region	4.123×10^{-26}
28	GO:CC	GO:0062023	collagen-containing extracellular matrix	3.222×10^{-21}
29	GO:CC	GO:0005819	spindle	1.209×10^{-11}
30	GO:CC	GO:0005871	kinesin complex	1.895×10^{-3}
31	GO:CC	GO:0098590	plasma membrane region	3.724×10^{-3}
32	GO:CC	GO:0032133	chromosome passenger complex	6.374×10^{-3}
33	TF	TF:M03805_1	Factor: YB-1; motif: CCAMTCNGMR; match cla...	1.967×10^{-2}

version	e109_eg56_p17_1d3191d
date	4/22/2023, 11:48:25 AM
organism	hsapiens

B

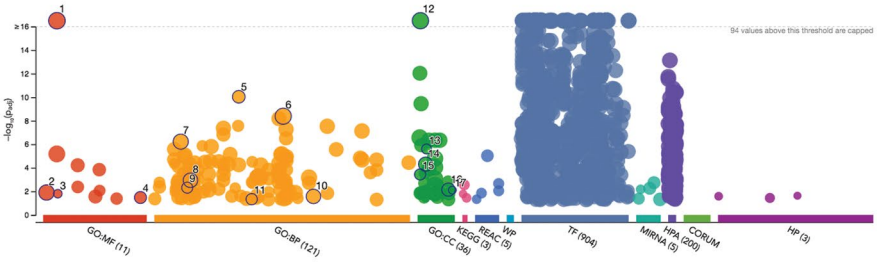

ID	Source	Term ID	Term Name	p_{adj} (query_1)
1	GO:MF	GO:0005515	protein binding	1.336×10^{-19}
2	GO:MF	GO:0003824	catalytic activity	1.247×10^{-2}
3	GO:MF	GO:0008171	O-methyltransferase activity	1.578×10^{-2}
4	GO:MF	GO:0140098	catalytic activity, acting on RNA	3.337×10^{-2}
5	GO:BP	GO:0034660	ncRNA metabolic process	9.153×10^{-11}
6	GO:BP	GO:0050794	regulation of cellular process	4.094×10^{-9}
7	GO:BP	GO:0007275	multicellular organism development	5.936×10^{-7}
8	GO:BP	GO:0010033	response to organic substance	1.144×10^{-3}
9	GO:BP	GO:0009451	RNA modification	4.860×10^{-3}
10	GO:BP	GO:0070887	cellular response to chemical stimulus	2.692×10^{-2}
11	GO:BP	GO:0042180	cellular ketone metabolic process	4.623×10^{-2}
12	GO:CC	GO:0005737	cytoplasm	2.451×10^{-17}
13	GO:CC	GO:0030684	preribosome	2.512×10^{-8}
14	GO:CC	GO:0030054	cell junction	4.883×10^{-5}
15	GO:CC	GO:0005681	spliceosomal complex	3.649×10^{-4}
16	GO:CC	GO:0099081	supramolecular polymer	7.067×10^{-3}
17	GO:CC	GO:1990124	messenger ribonucleoprotein complex	7.829×10^{-3}

version	e109_eg56_p17_1d3191d
date	4/22/2023, 11:50:17 AM
organism	hsapiens

Fig.6: The gene set enrichment analysis was performed using the g: Profiler web server on a set of differentially expressed genes identified in the *DICER1*-overexpressing MSCs. The top enriched gene ontology (GO) terms are displayed in a bubble plot, with the color indicating their level of significance, as measured by the -log10 of the P value. The size of each bubble represents the number of genes in the term. The x-axis shows different GO categories based on molecular function (MF), biological process (BP), and cellular components (CC), as well as different databanks. The y-axis shows the significance of the term, measured by the adjusted P value (q value). **A.** The pathway analysis of overexpressed genes revealed significant enrichment in several biological processes, including 'chromatin remodeling', 'cytokine activity', and 'extracellular matrix'. **B.** Downregulated genes involving in pathways such as 'RNA modification', 'spliceosome complex', and 'ncRNA metabolic process' are among the suppressed pathways.

Discussion

MSCs have been a promising target for cell regenerative therapy of numerous immune-mediated diseases and immune homeostasis due to their desirable characteristics, such as immunoregulatory features, multi-lineage differentiation ability, and directed tissue homing (16). Today, stem cell therapy is a fast-growing field, while the MSC draws attention to its potential. It seems that MSCs are safer and more easily applicable than stem cells from different sources. While the use of stem cells has shown effectiveness in treating various clinical conditions, transplantation of stem cells carries the risk of heterogeneity, genomic and chromosomal instability, as well as potential tumorigenesis *in vivo*. Although unfavorable outcomes are primarily caused by environmental host factors, enhancing the functions of MSCs through gene manipulation may help to overcome many of the shortcomings associated with transplantation (17).

The microenvironment surrounding MSCs influences the signalling pathway and cell polarization, leading to the secretion of potent soluble cytokine factors that prompt cells to adopt immunomodulatory and anti-inflammatory phenotypes. Additionally, this condition activates the immunosuppressive functions of MSCs, which has a critical role in their biological functions such as tissue repair (18). Several studies have evaluated the role of *DICER1* expression in stem cells. It has been demonstrated that the *DICER1* deficiency is linked to the type I interferons and PKR activation in murine embryonic stem cells (mESCs), making these cells more susceptible to the antiviral responses induced cytotoxicity that may be probably through a miRNA biogenesis deficiency. While the NF-κB pathway is the main factor in controlling the expression of interferons, the altered expression of some miRNAs, such as the miR-290 cluster, could be the reason for activating the NF-κB pathway in mESCs with the *DICER1* deficiency (13). Our findings support previous research showing that overexpressing DICER1 results in increased activity of the NF-κB pathway. Similar to its role in neural crest-derived stem cells, NF-κB acts as a key regulator of differentiation in MSCs, inhibiting the development of muscle and cartilage cells (19). It is noteworthy that this differentiation could be attributed to the inhibition of NF-κB signaling pathway, which leads to the counteraction of pro-inflammatory conditions (20). However, such a role is more likely to be context-dependent, as some studies reported that chondrogenesis could be induced without dysregulation even after blocking the NF-κB pathway (21).

Activation of NF-κB can lead to the proliferation, adhesion, and migration of MSCs. It can also trigger inflammatory responses and the production of cytokine such as IL-1, 2, 6, 8, 12, and TNF-α from these cells (22, 23).

It is noteworthy that the immunosuppressive properties of MSCs are related to their secretion factors, such as ILs, TGF-β, INF-γ, and TNF-α (24). Moreover, the silencing of *DICER* is linked to apoptosis and cell proliferation inhibition in myeloma and leukemia (6). The dysregulation of DICER has been associated with cell proliferation and tumor development in lung cancers (10). The decreased expression of *DICER* during aging and the development of age-related insulin resistance highlights its metabolic effect role in the adipose tissue (25).

We hypothesized that the overexpression of *DICER1* in MSCs may cause immune responses. It was suggested that inflammatory cytokines and chemokines, including IL-1, 4, 6, 8, 10, 17, 18, CCL2, TGF-β, INF-γ, and TNF-α, and immunoregulatory genes, including *COX-2*, *DDX-58*, *IFIH1*, *MYD88*, *RNase L*, *TLR3/4*, and *TDO2* may be considered as potential targets for stem cell therapy (24, 26, 27). In our previous study, we assessed the expression of certain immune related genes and found that pre-treating MSCs with B18R protein reduced their inflammatory response when stimulated with poly (I: C) and IFN-γ (28). Hosseini et al. indicated the critical roles of these pro- and anti-inflammatory cytokines and chemokines in the immune suppression (26). It has been confirmed that INF-γ, TNF-α, and IL-1 are crucial factors in initiating cytokine-inducing immunosuppression by MSCs. These cytokines contributing to an inflammatory response can change the immunosuppressive impacts of MSCs (29). Consistent with previous studies, our results indicated that the increase expression of IL-1 could modulate the expression of inflammatory cytokines. A high level of IFN-γ enhances the immunosuppressive capabilities of MSCs through the JAK/STAT1 signaling pathway and IDO1, indicating that cell therapy using MSCs primed with IFN-γ may be effective (30).

Remarkably, MSCs initiate the release of IFN-γ induced by IL-18, which could influence tissue regeneration and offer a new approach for anti-tumor therapy (31). The IL-8 promotes the therapeutic effects of MSCs on the bone regeneration, through the CXCR2-mediated PI3k/Akt signalling pathway (32). The TNF-α considerably suppresses an inflammation occurrence via increasing the levels of TGF-β and IL-10in MSCs (33). The overexpression of IL-10, an anti-inflammatory cytokine, in a normal homeostatic condition, can develop an autoimmune disease through an enhanced inflammatory response. Therefore, detecting key intermediates in various environments that regulate the IL-10 expression is a critical factor for preserving the balance of the immune response (34).

An increased TGF-β expression level acts as a crucial immunosuppressive factor that leads to an immune-modulator function via phosphorylation of Smad2/3, and induces macrophage M2-like polarization to inhibit the excessive inflammatory responses in MSCs (35). The production of IL-6 can result in the creation of anti-inflammatory M2 macrophages, inflammation through the NF-κB pathway, and the activation of transcription through STAT signaling pathways (36). Interestingly,

the CCL-2-secreted MSCs can be involved in therapeutic outcomes by facilitating macrophage repolarization, and result in reducing the inflammatory response through the local employment of macrophages (37). In line with previous studies, our data demonstrated that the IL-17-secreting MSCs promote an immunosuppression function in the cells with the *DICER1* overexpression nature (29). Together, these findings suggest that these cytokines secreted by MSCs may provide a novel approach to therapy by enhancing the therapeutic potential of these cells. In the present study, the overexpression of *DICER1* in Ad-MSCs did not affect the protein expression levels of IL-4 and 23.

Several pathways are involved in the regulation of the immune system through cytokine signalling, including signalling through interferon-α/β/γ, the IL-1/10 family, and the antiviral response triggered by genes stimulated by IFN (38). The increased expression level of *DDX-58*, an innate immune receptor gene, can lead to induce the interferon-α/β expression and the antiviral response was triggered by genes stimulated by IFN, and the IFIH1 (*MDA-5*) gene, which acts as an innate immune receptor, recognized RNA metabolites produced by RNase L, activating the interferon cascade. This is in line with our findings (39).

Given these observations, we propose that MSCs could improve the immunomodulatory properties by increasing the protein expression level of the *TSG-6* gene. Moreover, we hypothesized that the perturbation of cellular immunity by Dicer1 overexpression affects the expression and/or activation of TLRs which leads to trigger innate immune responses via the MYD88-dependent pathway. In this pathway, the activation of NF-κB and MAP kinase may have critical roles in the induction of inflammatory cytokines, such as *IL-1, 6*, and *TNF-α*. Also, the TIR domain-containing adaptor protein-inducing (IFNβ) dependent (TRIF) pathway and induce the type I interferon production (34).

Here, we suggested that the presence of an active stemness behavior and dynamic immunoregulatory nature of MSCs provides a complex context for the prediction of the transcriptional response by modulating the dsRNA response in these cells. The overexpression of *TLR4* can lead to generally overexpression of pro-inflammatory mediators, while *TLR3* induction results in the production of primary immunosuppressive mediators. It is proposed that stimulation of *TLR4* could imitate a pro-inflammatory environment (16). The *COX-2* increased expression level can propose its inhibition by overexpression of the *DICER1* gene that could be a therapeutic strategy for inflammation-mediated disorders (16, 40). Our data may suggest a dysregulation in the inflammatory cytokines and immunoregulatory genes through the expression of *DICER1* in MSCs, which may provide some knowledge of the immunoregulatory potential of these cells.

Conclusion

The overexpression of *DICER1* led to increased expression levels of some inflammatory and anti-inflammatory markers. This dysregulation could be due to inhibition and activation of some inflammatory, anti-inflammatory, and immunoregulatory capacities and alteration of RNA metabolism in human MSCs. It indicates that the *DICER1* manipulation can influence the production of pro-and anti-inflammatory cytokines.

Acknowledgments

This work was supported by a grant from the Iranian Ministry of Health and Medical Education (MoHME) (No. 96/548678) as a postdoctoral program at Mashhad University of Medical Sciences (MUMS, Hamid Reza Bidkhori). The experimental phase was conducted at and supported by the Academic Center for Education, Culture, and Research (ACECR)-Khorasan Razavi and MUMS laboratories. We are grateful for their financial support for this project. There is no conflict of interest in this study.

Authors' Contributions

H.R.B., M.F., H.R.; Designed the experiments. H.R.B., M.F., H.H.; Performed the experiments and collected data. M.F., R.J.E.; Analyzed data. M.M.M.; Performed the RNA sequencing and data analysis. H.R.B., R.J.E., H.H., R.A.M.; Prepared the draft of the manuscript. R.A.M.; Performed the experiments. H.R.; Supervised the study. All the authors approved the final version of the submitted manuscript.

References

1. Samsonraj RM, Raghunath M, Nurcombe V, Hui JH, van Wijnen AJ, Cool SM. Concise review: multifaceted characterization of human mesenchymal stem cells for use in regenerative medicine. Stem Cells Transl Med. 2017; 6(12): 2173-2185.
2. Ma S, Xie N, Li W, Yuan B, Shi Y, Wang Y. Immunobiology of mesenchymal stem cells. Cell Death Differ. 2014; 21(2): 216-225.
3. Boyd SD. Everything you wanted to know about small RNA but were afraid to ask. Lab Invest. 2008; 88(6): 569-578.
4. Murchison EP, Partridge JF, Tam OH, Cheloufi S, Hannon GJ. Characterization of dicer-deficient murine embryonic stem cells. Proc Natl Acad Sci USA. 2005; 102(34): 12135-12140.
5. Andika IB, Kondo H, Suzuki N. Dicer functions transcriptionally and posttranscriptionally in a multilayer antiviral defense. Proc Natl Acad Sci USA. 2019; 116(6): 2274-2281.
6. Bai Y, Qiu GR, Zhou F, Gong LY, Gao F, Sun KL. Overexpression of DICER1 induced by the upregulation of GATA1 contributes to the proliferation and apoptosis of leukemia cells. Int J Oncol. 2013; 42(4): 1317-1324.
7. Chiosea S, Jelezcova E, Chandran U, Luo J, Mantha G, Sobol RW, et al. Overexpression of dicer in precursor lesions of lung adenocarcinoma. Cancer Res. 2007; 67(5): 2345-2350.
8. Grelier G, Voirin N, Ay AS, Cox DG, Chabaud S, Treilleux I, et al. Prognostic value of dicer expression in human breast cancers and association with the mesenchymal phenotype. Br J Cancer. 2009; 101(4): 673-683.
9. Papachristou DJ, Korpetinou A, Giannopoulou E, Antonacopoulou AG, Papadaki H, Grivas P, et al. Expression of the ribonucleases Drosha, Dicer, and Ago2 in colorectal carcinomas. Virchows Arch. 2011; 459(4): 431-440.
10. Karube Y, Tanaka H, Osada H, Tomida S, Tatematsu Y, Yanagisawa K, et al. Reduced expression of dicer associated with poor prognosis in lung cancer patients. Cancer Sci. 2005; 96(2): 111-115.
11. Parizadeh SM, Jafarzadeh-Esfehani R, Hassanian SM, Parizadeh SMR, Vojdani S, Ghandehari M, et al. Targeting cancer stem cells as therapeutic approach in the treatment of colorectal cancer. Int J Biochem Cell Biol. 2019; 110: 75-83.
12. Pers YM, Maumus M, Bony C, Jorgensen C, Noël D. Contribution of microRNAs to the immunosuppressive function of mesenchymal stem cells. Biochimie. 2018; 155: 109-118.
13. Gurung C, Fendereski M, Sapkota K, Guo J, Huang F, Guo YL.

Dicer represses the interferon response and the double-stranded RNA-activated protein kinase pathway in mouse embryonic stem cells. J Biol Chem. 2021; 296: 100264.
14. Bidkhori HR, Bahrami AR, Farshchian M, Heirani-Tabasi A, Mirahmadi M, Hasanzadeh H, et al. Mesenchymal stem/stromal cells overexpressing CXCR4^{R334X} revealed enhanced migration: a lesson learned from the pathogenesis of WHIM syndrome. Cell Transplant. 2021; 30: 9636897211054498.
15. Farshchian M, Matin MM, Armant O, Geerts D, Dastpak M, Nakhaei-Rad S, et al. Suppression of dsRNA response genes and innate immunity following Oct4, Stella, and Nanos2 overexpression in mouse embryonic fibroblasts. Cytokine. 2018; 106: 1-11.
16. Hosseini SS, Mehrzad S, Hassanzadeh H, Kazemi M, Sanjar Moussavi N, Momeni Moghaddam M, et al. Vitamin E and hCG enhance the immunomodulatory properties of LPS-induced mesenchymal stem/stromal cells. Iran J Vet Sci Technol. 2021; 13(1): 64-74.
17. Damasceno PKF, de Santana TA, Santos GC, Orge ID, Silva DN, Albuquerque JF, et al. Genetic engineering as a strategy to improve the therapeutic efficacy of mesenchymal stem/stromal cells in regenerative medicine. Front Cell Dev Biol. 2020; 8: 737.
18. Sherman AB, Gilger BC, Berglund AK, Schnabel LV. Effect of bone marrow-derived mesenchymal stem cells and stem cell supernatant on equine corneal wound healing in vitro. Stem Cell Res Ther. 2017; 8(1): 120.
19. Sitcheran R, Cogswell PC, Baldwin AS Jr. NF-kappaB mediates inhibition of mesenchymal cell differentiation through a posttranscriptional gene silencing mechanism. Genes Dev. 2003; 17(19): 2368-2373.
20. Kaltschmidt C, Greiner JFW, Kaltschmidt B. The transcription factor NF-κB in stem cells and development. Cells. 2021; 10(8): 2042.
21. Hess K, Ushmorov A, Fiedler J, Brenner RE, Wirth T. TNFalpha promotes osteogenic differentiation of human mesenchymal stem cells by triggering the NF-kappaB signaling pathway. Bone. 2009; 45(2): 367-376.
22. Carrero R, Cerrada I, Lledó E, Dopazo J, García-García F, Rubio MP, et al. IL1β induces mesenchymal stem cells migration and leucocyte chemotaxis through NF-κB. Stem Cell Rev Rep. 2012; 8(3): 905-916.
23. Guan Y, Yao H, Wang J, Sun K, Cao L, Wang Y. NF-κB-DICER-miRs Axis Regulates TNF-α Expression in Responses to Endotoxin Stress. Int J Biol Sci. 2015; 11(11): 1257-1268.
24. Harrell CR, Fellabaum C, Jovicic N, Djonov V, Arsenijevic N, Volarevic V. Molecular mechanisms responsible for therapeutic potential of mesenchymal stem cell-derived secretome. Cells. 2019; 8(5): 467.
25. Brandão BB, Madsen S, Rabiee A, Oliverio M, Ruiz GP, Ferrucci DL, et al. Dynamic changes in DICER levels in adipose tissue control metabolic adaptations to exercise. Proc Natl Acad Sci USA. 2020; 117(38): 23932-23941.
26. Hosseini SS, Mehrzad S, Hassanzadeh H, Bidkhori HR, Mirahmadi M, Momeni-Moghaddam M, et al. Immunosuppressive effects of human chorionic gonadotropin (hCG) on mesenchymal stromal cells. J Cell Mol Res. 2020; 11(2): 90-98.
27. Mehrzad S, Hosseini SS, Momeni-Moghaddam M, Farshchian M, Hassanzadeh H, Mirahmadi M, et al. Vitamin E pretreatment of mesenchymal stem cells: the interplay of oxidative stress and inflammation. J Cell Mol Res. 2020; 11(2): 99-107.
28. Bidkhori HR, Farshchian M, Kazemi Noughabi M, Hassanzadeh H, Rafatpanah H. Alteration of immunoregulatory genes expression in mesenchymal stromal cells upon priming with B18R as an interferon binding protein. Iran J Basic Med Sci. 2023; 26(2): 241-247.
29. Han X, Yang Q, Lin L, Xu C, Zheng C, Chen X, et al. Interleukin-17 enhances immunosuppression by mesenchymal stem cells. Cell Death Differ. 2014; 21(11): 1758-1768.
30. Kim DS, Jang IK, Lee MW, Ko YJ, Lee DH, Lee JW, et al. Enhanced immunosuppressive properties of human mesenchymal stem cells primed by interferon-γ. EBioMedicine. 2018; 28: 261-273.
31. Liu X, Hu J, Sun S, Li F, Cao W, Wang YU, et al. Mesenchymal stem cells expressing interleukin-18 suppress breast cancer cells in vitro. Exp Ther Med. 2015; 9(4): 1192-1200.
32. Yang A, Lu Y, Xing J, Li Z, Yin X, Dou C, et al. IL-8 enhances therapeutic effects of BMSCs on bone regeneration via CXCR2-mediated PI3k/Akt signaling pathway. Cell Physiol Biochem. 2018; 48(1): 361-370.
33. Putra A, Ridwan FB, Putridewi AI, Kustiyah AR, Wirastuti K, Sadyah NAC, et al. The role of TNF-α induced MSCs on suppressive inflammation by increasing TGF-β and IL-10. Open Access Maced J Med Sci. 2018; 6(10): 1779-1783.
34. Iyer SS, Cheng G. Role of interleukin 10 transcriptional regulation in inflammation and autoimmune disease. Crit Rev Immunol. 2012; 32(1): 23-63.
35. Liu F, Qiu H, Xue M, Zhang S, Zhang X, Xu J, et al. MSC-secreted TGF-β regulates lipopolysaccharide-stimulated macrophage M2-like polarization via the Akt/FoxO1 pathway. Stem Cell Res Ther. 2019; 10(1): 345.
36. Wang Q, Ding G, Xu X. Immunomodulatory functions of mesenchymal stem cells and possible mechanisms. Histol Histopathol. 2016; 31(9): 949-959.
37. Whelan DS, Caplice NM, Clover AJP. Mesenchymal stromal cell derived CCL2 is required for accelerated wound healing. Sci Rep. 2020; 10(1): 2642.
38. Pfaff F, Hägglund S, Zoli M, Blaise-Boisseau S, Laloy E, Koethe S, et al. Proteogenomics uncovers critical elements of host response in bovine soft palate epithelial cells following in vitro infection with foot-and-mouth disease virus. Viruses. 2019; 11(1): 53.
39. Sanda C, Weitzel P, Tsukahara T, Schaley J, Edenberg HJ, Stephens MA, et al. Differential gene induction by type I and type II interferons and their combination. J Interferon Cytokine Res. 2006; 26(7): 462-472.
40. Basu A, Das AS, Sharma M, Pathak MP, Chattopadhyay P, Biswas K, et al. STAT3 and NF-κB are common targets for kaempferol-mediated attenuation of COX-2 expression in IL-6-induced macrophages and carrageenan-induced mouse paw edema. Biochem Biophys Rep. 2017; 12: 54-61.

Cell J
Cell Journal(Yakhteh)
Homepage: https://www.celljournal.org/
Original Article
Vol 25, No 10, October 2023, Pages: 706-716

Aberrant Expression of TET2 Accounts for DNA Hypomethylation in Varicocele

Hengameh Taghian Dinani, M.Sc.[1, 2], Nushin Naderi, Ph.D.[2], Marziyeh Tavalaee, Ph.D.[1, 2*], Farzaneh Rabiee, M.Sc.[3], Mohammad Hossein Nasr-Esfahani, Ph.D.[1, 2*]

1. ACECR Institute of Higher Education, Isfahan Branch, Isfahan, Iran
2. Department of Animal Biotechnology, Reproductive Biomedicine Research Center, Royan Institute for Biotechnology, ACECR, Isfahan, Iran
3. Department of Animal Biotechnology, Cell Science Research Center, Royan Institute for Biotechnology, ACECR, Isfahan, Iran

Abstract

Objective: Epigenetic modifications such as DNA methylation play a key role in male infertility etiology. This study aimed to explore the global DNA methylation status in testicular spermatogenic cells of varicocele-induced rats and consider their semen quality, with a focus on key epigenetic marks, namely 5-methylcytosine (5-mC) and 5-hydroxymethylcytosine (5-hmC), as well as the mRNA and proteins of ten-eleven translocation (TET) methylcytosine dioxygenases 1-3.

Materials and Methods: In this experimental study, 24 mature male Wistar rats (8 in each group) were assigned amongst the control, sham, and varicocele groups. Sperm quality was assessed, and DNA methylation patterns of testicular spermatogenic cells were investigated using reverse transcription-polymerase chain reaction (RT-PCR), western blot, and immunofluorescence techniques.

Results: Sperm parameters, chromatin and DNA integrity were significantly lower, and sperm lipid peroxidation significantly increased in varicocele-induced rats in comparison with control rats. During spermatogenesis in rat testis, 5-mC and 5-hmC epigenetic marks, and TET1-3 mRNA and proteins were expressed. In contrast to the 5-mC fluorescent signal which was presented in all testicular cells, the 5-hmC fluorescent signal was presented exclusively in spermatogonia and a few spermatids. In varicocele-induced rats, the 5-mC signal decreased in all cells within the tubules, whereas a strong signal of 5-hmC was detected in seminiferous tubules compared to the control group. As well, the levels of TET2 mRNA and protein expression were significantly upregulated in varicocele-induced rats in comparison with the control group. Also, our results showed that the varicocele-induced animals exhibited strong fluorescent signals of TET1-3 in testicular cells, whereas weak fluorescent signals were identified in the seminiferous tubules of the control animals.

Conclusion: Consequently, we showed TET2 upregulation and the 5-hmC gain at testicular levels are associated with varicocele and sperm quality decline, and therefore they can be exploited as potential biomarkers of spermatogenesis.

Keywords: DNA Methylation, Male Infertility, Sperm, Varicocele, 5-Methylcytosine

Citation: Taghian Dinani H, Naderi N, Tavalaee M, Rabiee F, Nasr-Esfahani MH. Aberrant expression of TET2 accounts for DNA hypomethylation in varicocele. Cell J. 2023; 25(10): 706-716. doi: 10.22074/CELLJ.2023.2000170.1284

Introduction

Varicocele as a public and remediable risk factor of male infertility, affects 15% of the general male population, within the infertile men cohort, the varicocele frequency is higher, being recognized in 35 to 50% of males with primary infertility, while in men with secondary infertility, it is 80% (1). Varicocele is the expansion and torsion of the scrotal venous pampiniform plexus which leads to pathological problems influencing particularly the left testicle (2). It is associated with a reduction of sperm count, motility, and normal morphology (3). Although various studies have recently been carried out on different aspects of varicocele, the varicocele etiology is multifactorial, and its physio-pathological mechanisms are uncertain (4). Overall, numerous factors such as oxidative stress, hypoxia, hyperthermia, apoptosis, and inflammation may be implicated (5, 6).

The alterability of clinical phenotypes related to varicocele proposes the attendance of indefinite related genetic factors and epigenetic alterations that may be significant in the varicocele etiology (3). DNA methylation is the most abundant epigenetic modification that directly influences the DNA, and it is necessitated for genomic imprinting, regulation of gene expression, sperm chromatin structure, and embryonic development (7). DNA methylation is regulated by the functional interaction between two enzyme families: DNA methyltransferases (DNMTs) and ten-eleven translocation (TET) methylcytosine dioxygenases, which regulate DNA methylation and demethylation, respectively. DNMTs catalyze the transfer of a methyl group from

Received: 15/April/2023, Revised: 19/June/2023, Accepted: 04/July/2023
*Corresponding Address: P.O.Box: 8165131378, Department of Animal Biotechnology, Reproductive Biomedicine Research Center, Royan Institute for Biotechnology, ACECR, Isfahan, Iran
Emails: m.tavalaee@royan-rc.ac.ir; mh.nasr-esfahani@royaninstitute.org

Royan Institute
Cell Journal (Yakhteh)

S-adenosylmethionine (SAM) to the C5 position of cytosine to produce 5-methylcytosine (5-mC), while TET proteins are Fe (II)/2-oxoglutarate-dependent dioxygenases that oxidize 5-mC to 5-hydroxymethylcytosine (5-hmC), 5-formylcytosine (5-fC), and 5-carboxylcytosine (5-caC) in DNA (8).

Abnormal DNA methylation can cause male infertility by leading to abnormal sperm parameters (9), this has been observed in men with varicocele too (1, 10, 11). Previous studies have shown that the severity of varicocele can affect the extent of sperm DNA methylation alteration (1, 12), which could be related to increased sperm DNA damage. This suggests that men with high-grade varicocele may be more likely to experience infertility (13).

Therefore, perception of pathophysiological mechanisms and cellular and molecular alterations during spermatogenesis in varicocele disorder is crucial in developing a remedy and for proper guidance and intervention. This study was designed to evaluate sperm parameters, sperm oxidative status, and the level of sperm DNA damage as well as testicular DNA methylation patterns in the rat model with varicocele induction.

Materials and Methods

Experimental design and animals

In this experimental study, 24 male Wistar rats weighing 150-200 g (two months of age) were purchased from the animal house belonging to the Royan Institute of Animal Biotechnology (Isfahan, Iran). Rats were held in the animal house in the standard environment, with a temperature of 22 ± 2°C, a humidity of 45-65%, and a 12-hr light/12-hr dark cycle, with access to water and food ad libitum. This experiment was ratified by the Ethics Committee of Royan Institute (IR.ACECR.ROYAN.REC.1400.049). After the acclimatization period (1 week), Wistar rats were randomly allocated into three experimental groups (eight rats per group): i. Control (with no intervention), ii. Sham (undergone a simple laparotomy), and iii. Varicocele (varicocele-induced).

Varicocele induction procedure

For the varicocele induction, rats were anesthetized via intraperitoneal injection of Ketamine (100 mg/kg) and Xylazine (10 mg/kg) using Guide for the Care and Use of Laboratory Animals (14). After the abdominal midline slice, the left renal vein, left adrenal vein, and left spermatic vein were then recognized. The undersurface of the left renal vein was attentively cleaned from adipose and connective tissues to make a channel and exposed in a medial site from the entry point of the left spermatic vein and left adrenal vein. Then, a 4-0 silk suture was elapsed through underneath the left renal vein and tied over a needle which had a 1 mm diameter and was set parallel to the left renal vein, next, the deletion of needles induces varicocele by enhancing the intravenous pressure lateral to the obstruction site, which was transferred to the pampiniform plexus. Lastly, the abdomen contents were rebounded, and the slice (in two layers) was closed by a 4-0 silk suture. In the sham group, partial ligation of the left renal vein was not carried out. The surgery was performed according to Turner's protocol (15).

Sample collection

Eight weeks after the progress of varicocele induction, all rats were sacrificed, and their left testis was dissected and washed, and then a portion of each testicular tissue was fixed with formalin 10% fixative for immunohistochemical evaluation, and the residuary testicular tissues were utilized for the western blot analysis. The left epididymides were dissected, and for sperm retrieval, the caudal epididymides were put in a petri dish containing 5 ml of sperm washing medium (VitaSperm™ Innovative Biotech, Tehran, Iran) at 37˚C with 5% CO_2 for 30 minutes (2).

Sperm parameters assessment

For sperm motility, ten microliters of sperm suspension were placed on pre-warmed clean slides, and then the motility of two hundred spermatozoa at random 10 microscopic fields was evaluated (CX31 OLYMPUS, Japan, 400× magnification). The percentages of motile (progressive and nonprogressive) sperm were recorded. For sperm concentration, ten microliters of diluted sperm suspension were assessed using a Makler chamber. Heads of sperm were considered in 5 rows by light microscopy (CX31 OLYMPUS, Japan, 400× magnification). The sperm concentration was shown as millions of sperm/mL. Sperm morphology was quantified by Eosin (1%, Merck, Germany) -Nigrosine (10%, Merck, Germany) staining. Forty microliters of Eosin were mixed with twenty microliters of sperm suspension. After 5 minutes, sixty microliters of Nigrosine were added. Thin smears were prepared with twenty microliters of sperm preparation on the slides. The morphology of two hundred spermatozoa was randomly assessed on the light microscope (CX31 OLYMPUS, Japan, 1000× magnification), afterward, the percentage of sperm abnormal morphology was reported (2).

Sperm lipid peroxidation evaluation

Sperm lipid peroxidation was evaluated by BODIPY $^{581/591}$ C11 dye. In brief, two million washed spermatozoa were exposed to a final concentration of 5 µM of BODIPY C11 dye for 30 minutes at 37˚C. Positive control was conducted for each sample by adding 2 mM H_2O_2 to the washed sample. The sperm lipid peroxidation percentage was quantified using a FACSCalibur (Becton Dickinson, San Jose, CA, USA) Flow Cytometer (16).

Sperm chromatin maturity and DNA integrity assessment

Aniline blue (AB), an acidic dye that interrelates

with lysine-rich histones, was exploited to evaluate the spermatic nucleus maturation level. In brief, after the smear preparation, the smears were fixed with 3% glutaraldehyde for 2 hr. Then, slides were dyed with AB (aqueous 5%) in 4% acetic acid (pH=3.5, 120 minutes), and then washed with phosphate-buffered saline (PBS 1X). A light microscope (CX31 OLYMPUS, Japan, 1000× magnification) was exhausted to assess the percentage of immature sperms with abnormal persistent histone content (AB-positive sperm). For each sample, at least two hundred spermatozoa were randomly considered. To improve our assessment of the ideal sperm nucleus structure, we also evaluated sperm nuclear chromatin protamination using chromomycin A3 (CMA3) staining. In brief, 20 µl of Carnoy solution (methanol/acetic acid, 3: 1) was added to 20 µl of sperm sample for 5 minutes at 4°C. After the smear provision, thereafter, the smears were treated with 150 µl CMA3 solution (0.25 mg/mL CMA3 in McIlvaine buffer [7 mL 0.1 M citric acid, 32.9 mL 0.2 M $Na_2HPO_4.7H_2O$, pH=7.0, containing 10 mM $MgCl_2$) for 2 hours. After washing with PBS 1X, microscopic investigations of the slides were completed by a fluorescent microscope (BX51 OLYMPUS, Japan, 1000× magnification) with suitable filters (460-470 nm). For each sample, a minimum of two hundred spermatozoa were randomly counted based on sperm with light yellow fluorescence ($CMA3^+$) that were considered spermatozoa with protamine deficiency (17). The Aridine orange (AO) staining was carried out to identify sperm DNA integrity. In this staining, after fixation of prepared smears with Carnoy's solution at 4°C, smears were then dyed with AO in citrate-phosphate buffer (80 ml 0.1 M citric acid+5 ml 0.3 M NaH_2PO_4, pH=2.5). Next step, the smears were washed with PBS 1X, and for each slide, two hundred sperm atozoa were randomly counted by a fluorescent microscope (BX51 OLYMPUS, Japan, 1000× magnification). The percentage of sperms with a red or orange nucleus was considered to display DNA damage (2).

Quantitative real time-polymerase chain reaction method

To isolate total RNA, 50 mg of rat testicular tissue, stored at -80°C, was homogenized with 1 ml of TRIzol reagent (Yekta Tajhiz Azma, Iran). The RNA quality and concentration were evaluated by a Thermo Scientific NanoDrop® ND-1000 spectrophotometer. The cDNA synthesis was performed by cDNA synthesis kit according to the manufacturer's instruction (Biotechrabbit™ cDNA Synthesis Kit), subsequent Real-time PCR was carried out by SYBR green (Yekta Tajhiz Azma, Iran) fluorescent dye by ABI (Applied Biosystems StepOnePlus™). All data were normalized to glyceraldehyde-3-phosphate dehydrogenase (GAPDH) and expressed as $2^{-\Delta\Delta Ct}$ (17). The list of primers is summarised in Table 1.

Western blot technique

In brief, after protein extraction of rat testicular tissues with the TRIzol reagent (Yekta Tajhiz Azma, Iran), the concentration of protein was identified by Bradford's assay. Protein samples were exposed to 10% sodium dodecyl sulfate-polyacrylamide gels (SDS-PAGE) and then transported to polyvinylidene difluoride (PVDF) membranes. The samples were probed with GAPDH (1:5000, MAB374), and antibodies against TET1 (1:6000, GTX124207), TET2 (1:50, ab94580), and TET3 (1:100, NBP2-20602) as formerly explained (18). Protein expression was detected via goat anti-rabbit IgG-horseradish peroxidase (HRP) secondary antibody (1: 5000, sc-2301), and identified by an enhanced chemiluminescence system (ECL, Santa Cruz, USA) following the manufacturer's instructions. Proteins expression was normalized for GAPDH expression as an internal control, and the signal quantification was attained via Image J software.

Immunofluorescence procedure

Immunofluorescence analysis was performed on fixed seminiferous tubules of rats using specific antibodies against 5-mC, 5-hmC, and TET1-3. This technique enabled the localization and evaluation of cytosine chemical modifications and the expression patterns of TET1-3 proteins. The rat testicular tissues were dissected and then fixed in 10% formalin buffer, embedded in paraffin wax, and then sections were cut (5 µm), deparaffinized, and rehydrated. Before the staining procedure, the slides were pre-heated for 25 minutes in an oven at 60°C (Samsung, Model CE117AE, South Korean) and then deparaffinized in Xylol (3x, each10 minutes), two times in 100% ethanol (each 5 minutes), in 96% ethanol (5 minutes) and 70% ethanol (5 minutes), and subsequently rehydrated. Next step, the slides were plunged in boiling citrate buffer (10% citrate buffer, pH=6) for 30 minutes, finally resumed to room temperature, and then rinsed in cold PBS (3x, each 5 minutes). After, all slides were immersed in 2% Triton X-100-PBS (5 minutes) and blocked by 3% bovine serum albumin (BSA) in 2% Triton X-100-PBS for 1 hour, and then subjected to the primary antibody against 5-mC (1:500, BI-MECY-0100), 5-hmC (1:500, NBP2-50099), TET1 (1:400, GTX124207), TET2 (1:400, ab94580), and TET3 (1:400, NBP2-20602) overnight at 4°C. Then, to be rinsed in PBS (3x, each 5 minutes) and subjected to secondary fluorescein isothiocyanate (FITC)-conjugated antibodies (AP124F, 1:200 for 5-mC, F1763; 1:300 for 5-hmC, and sc-2012; 1:80 for TET1-3) at room temperature for 1 hour. After washing with PBS, finally, the nuclei of testicular cells were stained using propidium iodide (PI). The testicular cells were imaged under a fluorescence microscope (BX51 OLYMPUS, Japan, 200× magnification) (18, 19).

Statistical analysis

The statistical analyses were carried out with SPSS software (SPSS Science, Chicago, IL, USA). Before statistical analysis, the normality of data was executed

with the Shapiro-Wilk test. All data were expressed as mean ± standard deviation (SD). One-way analysis of variance (ANOVA) with post hoc Tukey HSD was employed for sperm parameters data, while independent-sample t tests were used to identify differences between groups for reverse transcription-polymerase chain reaction (RT-PCR) and western blotting data. Graphs were shaped with GraphPad Prism statistical software package version 8 (San Diego, California, USA). P<0.05 were considered statistically significant. In this study, considering that there was no significant difference between the control and sham groups in sperm parameters, only the control group was used to evaluate gene and protein expression and immunofluorescence.

Results

Animal weight and testicular volume

As indicated in Figure 1A, the final body weight was reduced in the varicocele group (328.75 ± 50.18 g) in comparison with the control (351.87 ± 28.94 g) and sham (352.00 ± 35.74 g) groups, but the difference was not significant. While varicocele induction resulted in a significant reduction (1.07 ± 0.17 cm^3) in left testis volume compared to the control (1.38 ± 0.21 cm^3; P=0.04, Fig.1B), no significant difference was detected between the varicocele group and the sham group (1.34 ± 0.31 cm^3, P>0.05).

Sperm parameters

The results demonstrated that varicocele induction led to a significant decrease in the mean sperm concentration (24.50 ±7.24, Fig.1C) and motility (35.87 ± 8.72, Fig.1D) compared to the control (41.05 ± 15.13; P=0.02 and 60.75 ± 9.71; P=0.001, respectively) group. Also, in the varicocele condition, the mean percentage of sperm abnormal morphology (22.37 ± 5.57, Fig.1E) significantly increased in comparison with the control (13.64 ± 6.18, P=0.02) and sham (10.83 ± 4.98, P=0.004) groups.

Sperm lipid peroxidation, chromatin maturity, and DNA damage

As shown in Figure 2A, the varicocele induction resulted in a significant increase (50.85 ± 9.75) in the percentages of sperm lipid peroxidation in comparison with the control (20.50 ±10.18, P<0.001) and sham (15.14 ± 5.72, P<0.001) groups. The mean percentages of spermatozoa with abnormal persistence of histones in varicocele animals (15.00 ± 4.47, Fig.2B) were significantly higher than in control (7.14 ± 5.72, P=0.02) and sham (4.50 ± 2.50, P=0.003) animals. Besides, varicocele induction in rats led to a significant increase (23.83 ± 2.08, Fig.2C) in sperm protamine deficiency in comparison with sham (16.16 ± 1.75, P=0.006), while there was no significant difference between varicocele and control (19.50 ± 1.80) groups. Also, the mean percentages of spermatozoa with DNA damage were found to be remarkably higher in the varicocele (62.35 ± 6.96, Fig.2D) group compared to the control (12.68 ± 2.69, P<0.001) and sham (42.78 ± 3.12, P<0.001) groups.

The localization and expression levels of 5-mC and 5-hmC in the testicular tissue

Next, immunofluorescence staining of rat testicular tissue sections was performed to detect 5-mC and 5-hmC. A strong signal was detected for 5-mC from developing spermatogonia to spermatozoa in control animals (Fig.3A). However, the findings of this study demonstrated a decrease in the 5-mC signal from the cells at the basal membrane to the cells located in the lumen of the tubules in varicocele-induced rats (Fig.3B). The study's findings indicated that in control animals, the 5-hmC signal was present mostly in spermatogonia and a few spermatids during their developing stages (Fig.3C), while, in rats with varicocele induction (Fig. 3D), a strong immunofluorescence signal of 5-hmC was detected in the seminiferous tubules.

Table 1: Primer sequences of genes analyzed by real-time polymerase chain reaction

Name	Primer sequence (5′-3′)	Tm (°C)
Ten-eleven translocation (TET)1	F: GAAGCCCACAACTACCAC	56
	R: TTCCTAAATCTGCCTCGGTCA	
Ten-eleven translocation (TET)2	F: CCTTATTATACCCATCTAGGAGC	62
	R: TCCGATACACCCATTTAGCAA	
Ten-eleven translocation (TET)3	F: GGTCACAGCCTGCATGGACT	65
	R: AGCGATTGTCTTCCTTGGTCAG	
Glyceraldehyde-3-Phosphate Dehydrogenase (GAPDH)	F: TATGACTCTACCCACGGCAAG	54
	R: ATACTCAGCACCAGCATCACC	

Tm; primer melting temperature.

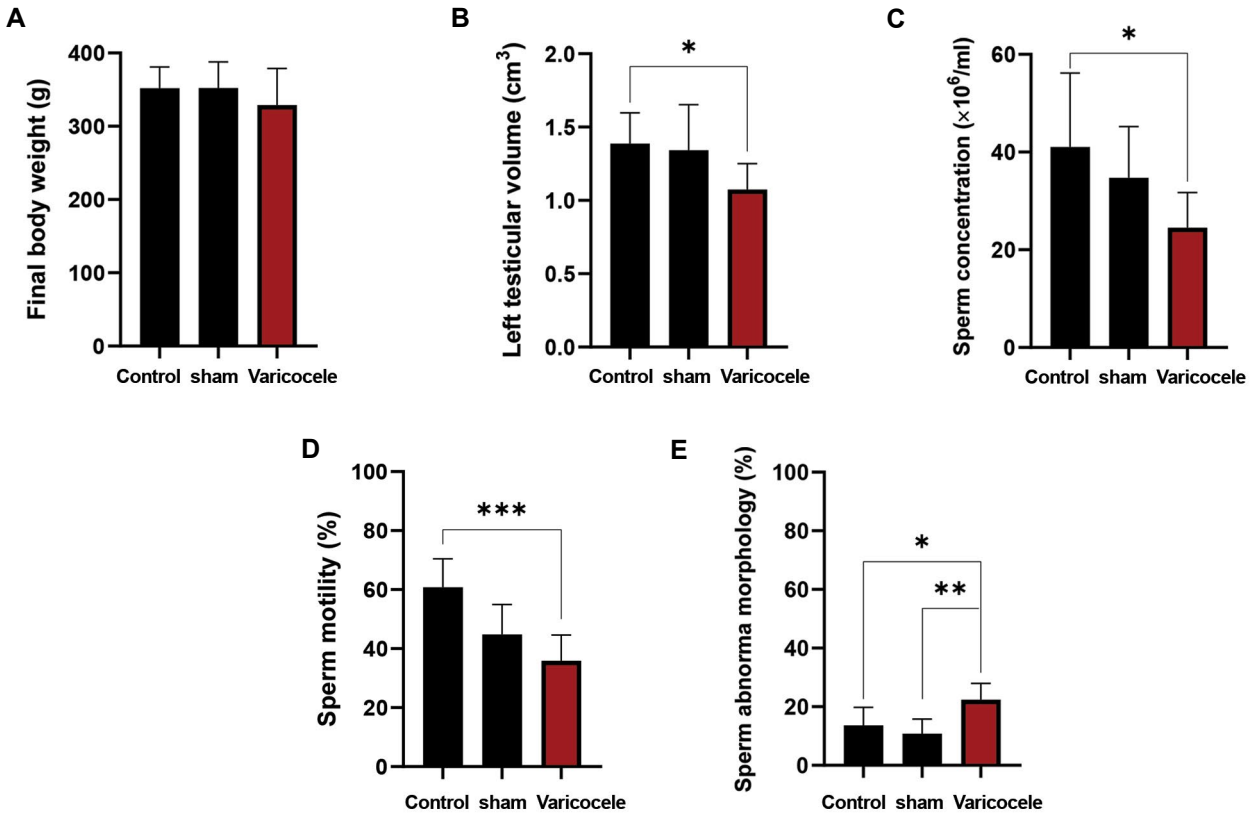

Fig.1: The effect of varicocele induction on the rat body weight, testicular volume, and sperm parameters. Comparison of mean **A.** Final body weight (g), **B.** Left testicular volume (cm^3), **C.** Sperm concentration (million /ml), **D.** Sperm motility (%,), and **E.** Sperm abnormal morphology (%) of varicocele induction group with control and sham groups. Data are mean ± standard deviation (SD) (n=8). *; P<0.05, **; P<0.01, and ***; P<0.001.

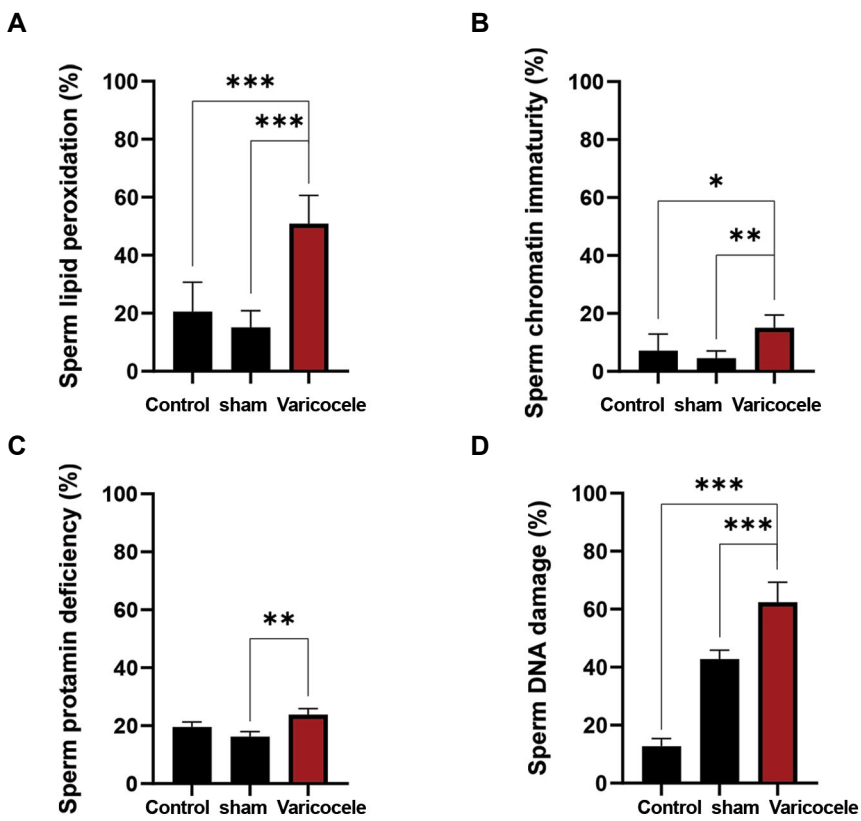

Fig.2: The effect of varicocele induction on the sperm lipid peroxidation and DNA integrity. Comparison of mean **A.** Sperm lipid peroxidation-BODIPY staining (%), **B.** Chromatin immaturity-Aniline blue staining (%), **C.** Protamine deficiency-Chromomycine A3 staining (%), and **D.** DNA damage-Acridine orange staining (%) of varicocele induction group with control and sham groups. Data are mean ± standard deviation (SD) (n=8). *; P<0.05, **; P<0.01, and ***; P<0.001.

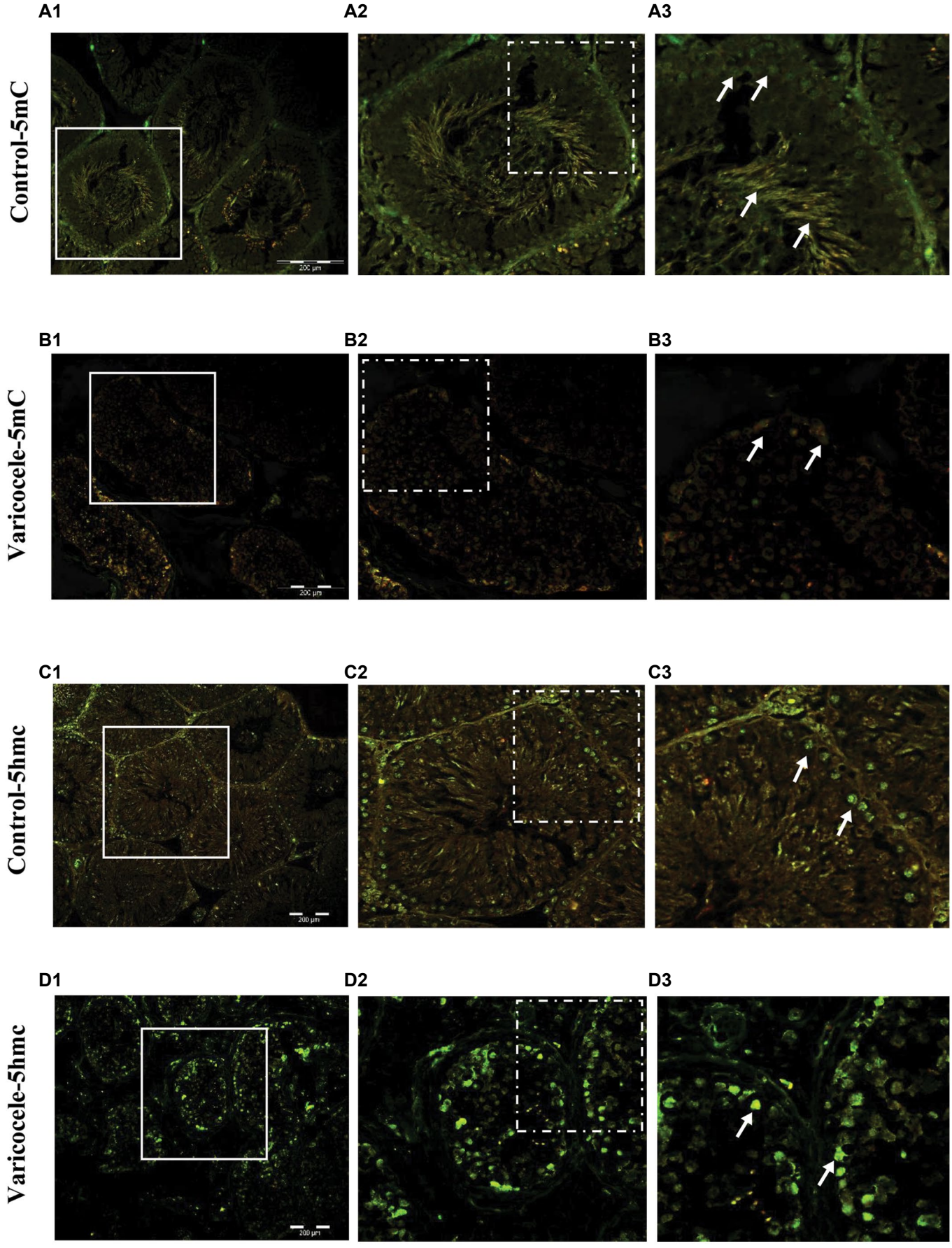

Fig.3: Varicocele increased hypomethylation. Immunofluorescent staining for 5-mC and 5-hmC. **A.** Note the high fluorescent signal (arrows) in the control group for 5-mC, **B.** Which is considerably decreased in the varicocele group. **C.** See the low fluorescent signal (arrows) in the control group for 5-mhC, **D.** Which is enhanced in the varicocele group (scale bar: 200 µm, magnification: 200×).

The levels of TET1-3 mRNA and TET2 protein expression

As represented in Figure 4A-C, the testicular tissue of rats with varicocele induction, expressed a significantly high level of TET2 mRNA (2.38 ± 0.35) in comparison with the control (1.00 ± 0.09, P<0.001) group, whereas no statistically significant differences were found in the expression levels of TET1 and TET3 mRNA between the varicocele and control group. Similarly, our findings presented that the TET2 expression at the protein level was significantly increased in varicocele-induced rats (1.68 ± 0.54) in comparison with the control (0.44 ± 0.33, P=0.03, Fig.4D, E) animals.

The localization and expression level of TET1-3 in the testicular tissue

The localization and expression levels of TET1-3 in the testis of rats were identified by immunofluorescence staining (Fig.5A-F). These results displayed that TET1-3 was present in different testicular cells, although with various distributions. Consistent with RT-PCR and western blot, the control animals exhibited weak fluorescent signals of TET1-3, especially TET2, in testicular cells (Fig.5A, C, E), whereas strong fluorescent signals were detected in seminiferous tubules of rats with varicocele induction (Fig.5B, D, E).

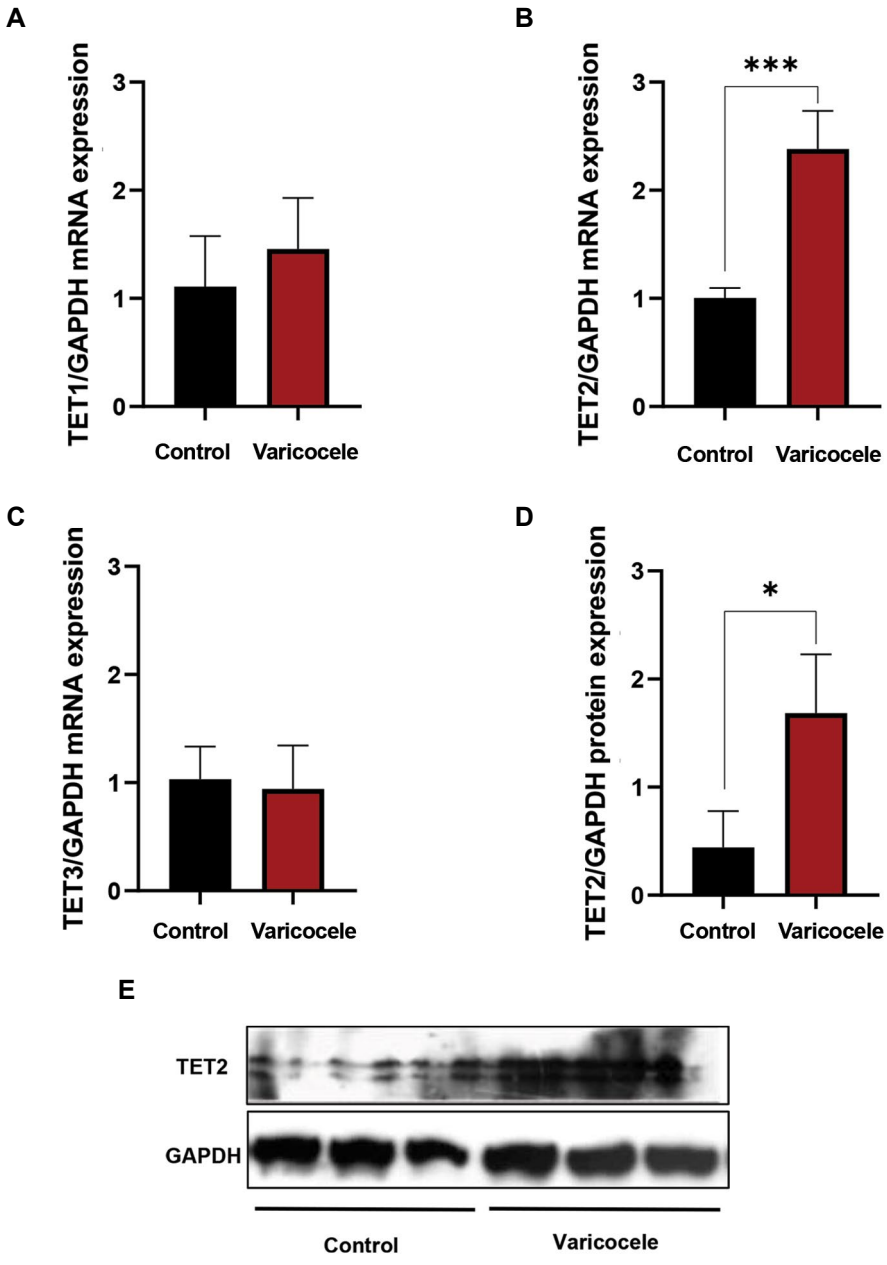

Fig.4: The effect of varicocele induction on the ten-eleven translocation (TET) methylcytosine dioxygenases 1-3 expressions in rat testicular tissue. Comparison of mean mRNA levels of **A.** TET1, **B.** TET2, **C.** TET3, and **D, E.** Protein level of TET2 of varicocele induction group with the control group. Data are mean ± standard deviation (SD) (n=4 for RT-PCR and n=3 for western blotting). *; P<0.05 and ***; P<0.001.

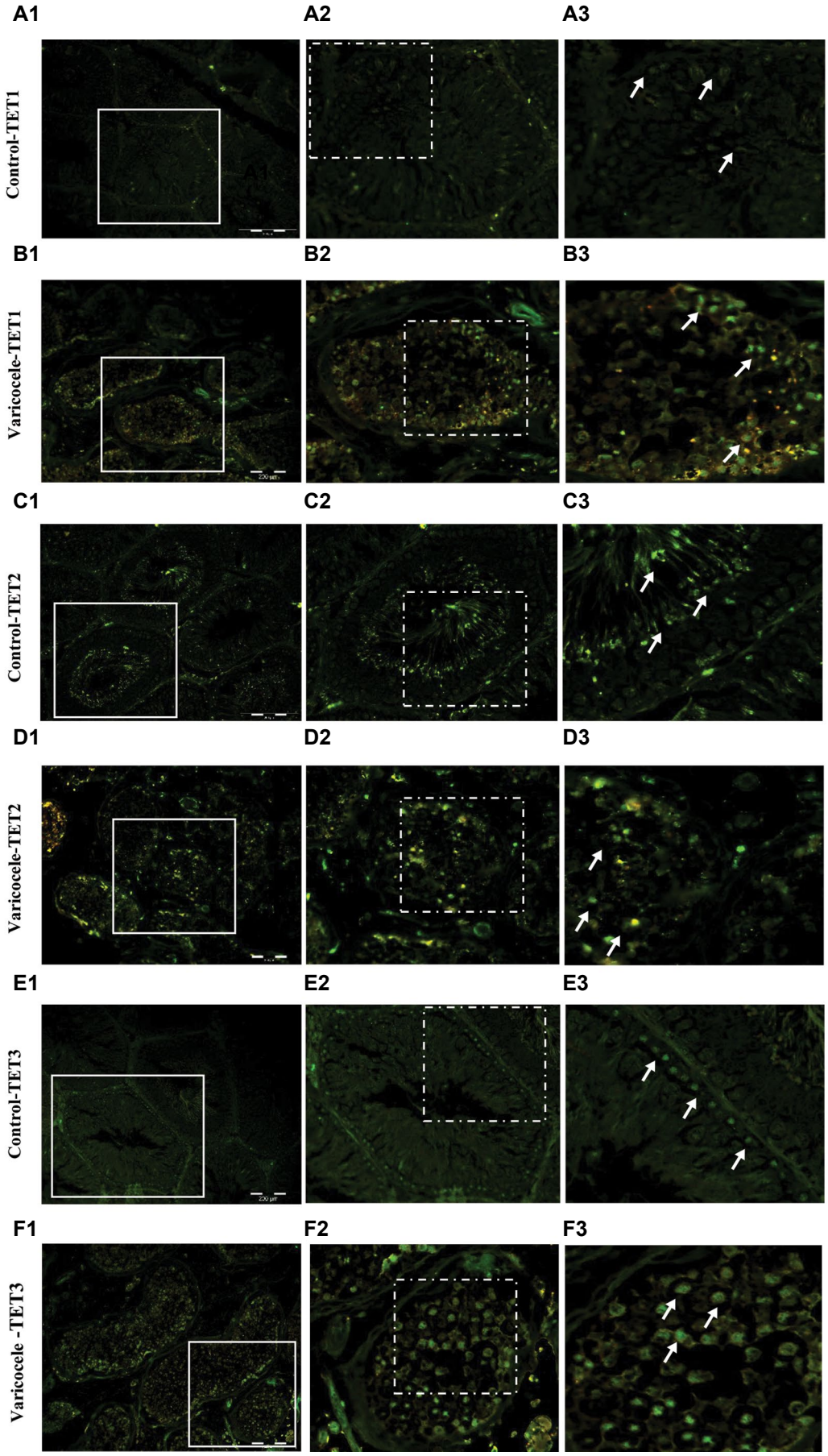

Fig.5: Varicocele induced ten-eleven translocation (TET) methylcytosine dioxygenases 1-3 enzyme activities in rat testicular tissue. **A-F.** Immunofluorescent staining for TET1-3. **A, C, E.** Note the weak fluorescent signal (arrows) of TET1-3 in the control group, **B, D, F.** Which is strong in the varicocele group (scale bar: 200 µm, magnification: 200×).

Discussion

One of the widespread risk factors for male infertility is varicocele as it negatively influences sperm parameters, sperm molecular and ultrastructural characteristics, and the testicular microenvironment (1). The varicocele etiology, the accurate effect of varicocele on male infertility, and the fundamental origins of the disturbance are still unclear; although literature has revealed that reactive oxygen species (ROS) and the subsequent oxidative stress perform a significant role in the pathogenesis of varicocele-related male infertility (4, 20, 21). However, the variety of phenotypes associated with varicocele proposes an intricate multifactorial disorder in which genetic, epigenetic, and environmental factors act a significant role in varicocele etiology (1). In particular, epigenetic modifications including DNA methylation, histone modifications, and non-coding RNAs have been found to adjust the transcription process and spermatogenesis (22).

In line with the literature, the results of the current study showed sperm with significantly lower sperm quality such as low sperm concentration, motility, and higher sperm abnormal morphology, chromatin immaturity, lipid peroxidation, and DNA damage for rats with varicocele induction in comparison with control animals.These sperm pathologies are mainly related to varicocele-induced oxidative stress (2, 5, 23, 24). Local testicular heat stress, hypoxia, and inflammation instigated by varicocele can break the regional oxidative balance, and stimulate oxidative stress and excessive ROS production, which is associated with insufficient sperm histone-protamine replacement and/or improper DNA methylation. One should mention that insufficient sperm histone-protamine replacement or poor sperm chromatin condensation performs an important role in DNA stability to ROS, which can influence the fertility ability in men and animals with varicocele (19, 20).

DNA methylation performs a key role in the regulation of gene expression and chromatin structure, which are important agents for spermatogenesis, sperm function, and embryonic development (1). Studies found a substantial negative correlation between global DNA methylation and DNA fragmentation in varicocele disorder (10) and damaged DNA is to a lesser extent prone to DNA methylation (25). While, a recent study revealed that prenatal exposure of male mice to a phytoestrogen-rich maternal diet in combination with a compromised redox system, resulted in global hypermethylation, and observed a positive correlation between DNA methylation and oxidative DNA damage in F1 generation testis and sperm, which these alterations may also influence F2 generation genetic integrity (26). It means that the persistent effects of maternal diets can be transferred later in life by DNA methylation changes. Therefore, one potential procedure that could serve as epigenetic cell memory, leading to differential gene expression, is DNA methylation (27).

The methylation of cytosine at the fifth carbon (5-mC) and the changed form of cytosine to 5-hmC are important epigenetic biomarkers that perform very critical roles in spermatogenesis (22). In this study, we performed immunofluorescence staining of testicular tissue sections to indicate 5-mC and 5-hmC localization and expression patterns. In accordance with previous results (28), 5-mC was present in all testicular cells, while 5-hmC was detectable almost exclusively in spermatogonia and only a few spermatids. The testicular histology analysis by Nettersheim et al. (29) revealed that human testicular tissue was marked by a high 5-hmC level in stem cell spermatogonia and a generally low 5-hmC level at the advanced differentiation stages. Besides, Gan et al. (30) showed elevated 5-hmC level was discovered in spermatogonia, which reduced to the round spermatid stage and enhanced anew in elongating spermatids and spermatozoa.

In our investigation, the fluorescent signal of 5-mC diminished in rats' testicular tissue with varicocele induction, this is in agreement with the literature, which exhibits lower 5-mC values in the rat model of varicocele (19), and in men with varicocele (11) and oligoasthenozoospermia (31). In contrast to 5-mC, the immunofluorescent signal of 5-hmC was represented at a high level in testicular spermatogenic cells in varicocele-induced rats in comparison with control rats. In confirmation of the results of our present study, it was established that a high 5-hmC level was adversely correlated with normal sperm head morphology whereas positively correlated with sperm DNA damage (28), therefore seems 5-mC and 5-hmC levels are related to impaired spermatogenesis, sperm parameters, as well as, sperm chromatin protamination and DNA integrity in testicular pathological conditions (31, 32) like varicocele.

Based on the literature, DNA hypomethylation is primarily carried out by decreasing DNMT activity and increasing TETs (33). Therefore, an important question is by what process perform testicular spermatogenic cells in animals with varicocele acquire 5-hmC? There are two pathways of 5-hmC formation: planned TETs-mediated 5-mC oxidation (8) and ROS attack on 5-mC under oxidative stress conditions and convert the 5-mC to 5-hmC (34).

In our current study, at the mRNA level, TET1 and 3 did not change but TET2 level significantly increased in rats with varicocele induction, and also at the protein level, TET2 showed relatively strong

expression. Interestingly, the TET2 protein structure differs from those of TET1 and TET3 and contains the IDAX CXXC4 domain that is crucial for CpG site detection, and downregulation of IDAX CXXC4 domain could result in TET2 overexpression and its improper recruitment to genomic regions where it is not normally found (35). Considering that the studies in this field are very limited, therefore, investigating the levels of TET2 and IDAX CXXC4 expression in normal and varicocele conditions will be important for future studies.

Another interesting point is that TET1 (36) and TET3 (37) are the maintenance DNA demethylases that do not deliberately decline the DNA methylation but especially avoid aberrant methylation extending into CpG islands in differentiated cells. Considering TET1 and 3 are recognized as maintenance demethylases, we did not see any significant difference in these gene expressions among the two groups. This might suggest that DNA methylation change in varicocele condition is not due to DNA maintenance aberration.

Also, our study in rats' testicular tissue sections of seminiferous tubules in the varicocele and control conditions showed that TET1-3 have almost the same distribution as 5-hmC, and TET1-3 proteins showed relatively strong fluorescent signals in the spermatogenic cells in varicocele-induced rats in comparison with control rats. Our results displayed that active DNA demethylation (18) in the testicular spermatogenic cells in varicocele condition involves the alteration of 5-mC to 5-hmC mediated by TET1-3, especially TET2, but we could not rule out the ROS attack on the conversion of the 5-mC to 5-hmC.

In addition to the above-described mechanisms of active DNA demethylation, there are possible alternative pathways of DNA demethylation including demethylase activity imagined for DNMTs enzymes in oxidizing redox conditions, in the presence of high calcium and low SAM levels (38). In the varicocele state owing to delayed blood flow and the presence of excessive iron sedimentation, spermatozoa are subjected to oxidative stress and nutritional restriction (3). Moreover, increase intracellular calcium ions, leading to endoplasmic reticulum stress and apoptosis, have been considered one of the molecular mechanisms related to varicocele (39). Based on this background, Rashidi et al. (12) have reported that despite the sperm DNA hypomethylation status in men with varicocele, DNMTs enzymes expression was enhanced at both RNA and protein levels, which can reflect demethylase activity of DNMTs in individuals with varicocele. Considering the varicocele state has three prerequisite circumstances for DNMTs to act as demethylase, therefore it can physiologically perform significant roles in gene expression via epigenetic modification.

According to this issue, the incidence of high sperm DNA damage is mainly made happen by ROS, therefore in patients with a high percentage of 5-hmC-positive spermatozoa, sperm hydroxylation can also be caused by ROS attack (28), because in post-testicular sperm maturation, sperm have strongly declined cytoplasm volume which makes their genetic and epigenetic patterns very susceptible to interior and exterior agents, including ROS (40). Hence, there is this hypothesis that a high 5-hmC level in varicocele condition at the testicular level could result from active DNA demethylation, and at post-testicular level could cause by spontaneous hydroxymethylation by ROS attack following the reduction of cytoplasm and the differentiation of spermatogenic cells to spermatozoa, and our experimental approach can discern between the two approaches.

Conclusion

Our results demonstrated that sperm parameters, chromatin and DNA integrity, and also testicular spermatogenic cells DNA methylation pattern were impaired by varicocele induction. In varicocele conditions, high 5-hmC formation in testicular spermatogenic cells may be induced by active DNA demethylation through TETs enzyme activities, especially TET2. In addition, the high sperm DNA damage occurrence, which is mainly caused by ROS attack, can represent spontaneous high hydroxymethylation of 5-mC by ROS and hypomethylation at the post-testicular level. Therefore, we suggest that measuring the 5-mC/5-hmC at testicular and post-testicular levels can be a beneficial way to create prognostic epidata in male infertility cases, particularly varicocele, and knowing the mechanisms intricated in epigenetic modification unties the way for targeted remedy of varicocele pathological condition.

Acknowledgments

We would like to express our gratitude to the staff of Isfahan Fertility and Infertility Center as well as the staff of the Department of Animal Biotechnology, Reproductive Biomedicine Research Center, Royan Institute for Biotechnology, ACECR, Isfahan, Iran. This research received no specific grant from any funding agency in the public, commercial, or not-for-profit sectors. The authors declare no conflict of interest.

Authors' Contributions

H.T.D.; Performed varicocele induction, sperm functional analysis, western blot technique, data analysis, and manuscript write. N.N.; Analyzed

the data, performed literature research, drafted the manuscript, revised the manuscript, and the final scientific manuscript revision. F.R..; Performed western blot technique, and analyzed the data. M.H.N.-E., M.T.; Contributed to the conception, design, and coordination of the study, data analysis, revised the manuscript, and performed the final scientific manuscript revision. All authors read and approved the final manuscript.

References

1. Santana VP, James ER, Miranda-Furtado CL, Souza MF, Pompeu CP, Esteves SC, et al. Differential DNA methylation pattern and sperm quality in men with varicocele. Fertil Steril. 2020; 114(4): 770-778.
2. Santana VP, Miranda-Furtado CL, de Oliveira-Gennaro FG, Dos Reis RM. Genetics and epigenetics of varicocele pathophysiology: an overview. J Assist Reprod Genet. 2017; 34(7): 839-847.
3. Sadeghi N, Erfani-Majd N, Tavalaee M, Tabandeh MR, Drevet JR, Nasr-Esfahani MH. Signs of ROS-associated autophagy in testis and sperm in a rat model of varicocele. Oxid Med Cell Longev. 2020; 2020: 5140383.
4. Zhang QF, Wang S, Zhang H, Liu QL, Wei Y, Deng W, et al. Effects of alpha-lipoic acid on sperm quality in patients with varicocele-related male infertility: study protocol for a randomized controlled clinical trial. Trials. 2022; 23(1): 1002.
5. Lorian K, Kadkhodaee M, Kianian F, Abdi A, Ranjbaran M, Ashabi G, et al. Long-term NaHS administration reduces oxidative stress and apoptosis in a rat model of left-side varicocele. Andrologia. 2020; 52(2): e13496.
6. Razi M, Tavalaee M, Sarrafzadeh-Rezaei F, Moazamian A, Gharagozloo P, Drevet JR, et al. Varicocoele and oxidative stress: New perspectives from animal and human studies. Andrology. 2021; 9(2): 546-558.
7. Rotondo JC, Lanzillotti C, Mazziotta C, Tognon M, Martini F. Epigenetics of male infertility: the role of DNA methylation. Front Cell Dev Biol. 2021; 9: 689624.
8. Onodera A, González-Avalos E, Lio CJ, Georges RO, Bellacosa A, Nakayama T, et al. Roles of TET and TDG in DNA demethylation in proliferating and non-proliferating immune cells. Genome Biol. 2021; 22(1): 186.
9. Li J, Xu J, Yang T, Chen J, Li F, Shen B, et al. Genome-wide methylation analyses of human sperm unravel novel differentially methylated regions in asthenozoospermia. Epigenomics. 2022; 14(16): 951-964.
10. Tavalaee M, Bahreinian M, Barekat F, Abbasi H, Nasr-Esfahani MH. Effect of varicocelectomy on sperm functional characteristics and DNA methylation. Andrologia. 2015; 47(8): 904-909.
11. Bahreinian M, Tavalaee M, Abbasi H, Kiani-Esfahani A, Shiravi AH, Nasr-Esfahani MH. DNA hypomethylation predisposes sperm to DNA damage in individuals with varicocele. Syst Biol Reprod Med. 2015; 61(4): 179-186.
12. Rashidi M, Tavalaee M, Abbasi H, Nomikos M, Nasr-Esfahani MH. Increased de novo DNA methylation enzymes in sperm of individuals with varicocele. Cell J. 2021; 23(4): 389-396.
13. Santana VP, Miranda-Furtado CL, Pedroso DCC, Eiras MC, Vasconcelos MAC, Ramos ES, et al. The relationship among sperm global DNA methylation, telomere length, and DNA fragmentation in varicocele: a cross-sectional study of 20 cases. Syst Biol Reprod Med. 2019; 65(2): 95-104.
14. NRC. Guide for the care and use of laboratory animals. 8th ed. Washington (DC): National Academies Press (US); 2011.
15. Turner TT. The study of varicocele through the use of animal models. Hum Reprod Update. 2001; 7(1): 78-84.
16. Aitken RJ, Wingate JK, De Iuliis GN, McLaughlin EA. Analysis of lipid peroxidation in human spermatozoa using BODIPY C11. Mol Hum Reprod. 2007; 13(4): 203-211.
17. Rahmani M, Tavalaee M, Hosseini M, Eskandari A, Shaygannia E, Sadeghi N, et al. Deferasirox, an iron-chelating agent, improves testicular morphometric and sperm functional parameters in a rat model of varicocele. Oxid Med Cell Longev. 2021; 2021: 6698482.
18. Ni K, Dansranjavin T, Rogenhofer N, Oeztuerk N, Deuker J, Bergmann M, et al. TET enzymes are successively expressed during human spermatogenesis and their expression level is pivotal for male fertility. Hum Reprod. 2016; 31(7): 1411-1424.
19. Salmani S, Razi M, Sarrafzadeh-Rezaei F, Mahmoudian A. Testosterone amplifies HSP70-2a, HSP90 and PCNA expression in experimental varicocele condition: Implication for DNA fragmentation. Reprod Biol. 2020; 20(3): 384-395.
20. Wang K, Gao Y, Wang C, Liang M, Liao Y, Hu K. Role of oxidative stress in varicocele. Front Genet. 2022; 13: 850114.
21. Majzoub A, Cho CL, Agarwal A, Esteves SC. Oxidative stress and varicocele pathophysiology series. In: Esteves Sc, Cho CL, MajzoubA Agarwal A, editors. Varicocele and male infertility: a complete guide. Cham: Springer International Publishing; 2019; 55-71.
22. Gao Y, Zhao Y, Zhang H, Zhang P, Liu J, Feng Y, et al. Pubertal exposure to low doses of zearalenone disrupting spermatogenesis through ERα related genetic and epigenetic pathways. Toxicol Lett. 2019; 315: 31-38.
23. Shaygannia E, Nasr-Esfahani MH, Sotoodehnejadnematalahi F, Parivar K. Is ferroptosis involved in ROS-induced testicular lesions in a varicocele rat model? Basic Clin Androl. 2021; 31(1): 10.
24. Hassanin AM, Ahmed HH, Kaddah AN. A global view of the pathophysiology of varicocele. Andrology. 2018; 6(5): 654-661.
25. Zhang Q, Zhang F, Gao HH, Zhang JM. Effects of varicocele on DNA methylation pattern of H19 and Snrpn gene in spermatozoa and behavioural characteristics of adult rat offspring. Andrologia. 2017; 49(1).
26. Godschalk RWL, Janssen MCM, Vanhees K, van Doorn-Khosrovani SBVW, van Schooten FJ. Maternal exposure to genistein during pregnancy and oxidative DNA damage in testes of male mouse offspring. Front Nutr. 2022; 9: 904368.
27. Bruno S, Williams RJ, Del Vecchio D. Epigenetic cell memory: the gene's inner chromatin modification circuit. PLoS Comput Biol. 2022; 18(4): e1009961.
28. Efimova OA, Pendina AA, Tikhonov AV, Parfenyev SE, Mekina ID, Komarova EM, et al. Genome-wide 5-hydroxymethylcytosine patterns in human spermatogenesis are associated with semen quality. Oncotarget. 2017; 8(51): 88294-88307.
29. Nettersheim D, Heukamp LC, Fronhoffs F, Grewe MJ, Haas N, Waha A, et al. Analysis of TET expression/activity and 5mC oxidation during normal and malignant germ cell development. PLoS One. 2013; 8(12): e82881.
30. Gan H, Wen L, Liao S, Lin X, Ma T, Liu J, et al. Dynamics of 5-hydroxymethylcytosine during mouse spermatogenesis. Nat Commun. 2013; 4: 1995.
31. Olszewska M, Kordyl O, Kamieniczna M, Fraczek M, Jędrzejczak P, Kurpisz M. Global 5mC and 5hmC DNA levels in human sperm subpopulations with differentially protaminated chromatin in normo- and oligoasthenozoospermic males. Int J Mol Sci. 2022; 23(9): 4516.
32. Montjean D, Zini A, Ravel C, Belloc S, Dalleac A, Copin H, et al. Sperm global DNA methylation level: association with semen parameters and genome integrity. Andrology. 2015; 3(2): 235-240.
33. Hernández-Cruz EY, Arancibia-Hernández YL, Loyola-Mondragón DY, Pedraza-Chaverri J. Oxidative stress and its role in Cd-induced epigenetic modifications: use of antioxidants as a possible preventive strategy. Oxygen. 2022; 2(2): 177-210.
34. Madugundu GS, Cadet J, Wagner JR. Hydroxyl-radical-induced oxidation of 5-methylcytosine in isolated and cellular DNA. Nucleic Acids Res. 2014; 42(11): 7450-7460.
35. Ko M, An J, Bandukwala HS, Chavez L, Aijö T, Pastor WA, et al. Modulation of TET2 expression and 5-methylcytosine oxidation by the CXXC domain protein IDAX. Nature. 2013; 497(7447): 122-126.
36. Jin C, Lu Y, Jelinek J, Liang S, Estecio MR, Barton MC, et al. TET1 is a maintenance DNA demethylase that prevents methylation spreading in differentiated cells. Nucleic Acids Res. 2014; 42(11): 6956-6971.
37. Santiago M, Antunes C, Guedes M, Iacovino M, Kyba M, Reik W, et al. Tet3 regulates cellular identity and DNA methylation in neural progenitor cells. Cell Mol Life Sci. 2020; 77(14): 2871-2883.
38. van der Wijst MG, Venkiteswaran M, Chen H, Xu GL, Plösch T, Rots MG. Local chromatin microenvironment determines DNMT activity: from DNA methyltransferase to DNA demethylase or DNA dehydroxymethylase. Epigenetics. 2015; 10(8): 671-676.
39. Li Y, Zhou T, Su YF, Hu ZY, Wei JJ, Wang W, et al. Prokineticin 2 overexpression induces spermatocyte apoptosis in varicocele in rats. Asian J Androl. 2020; 22(5): 500-506.
40. Aitken RJ, Gibb Z, Baker MA, Drevet J, Gharagozloo P. Causes and consequences of oxidative stress in spermatozoa. Reprod Fertil Dev. 2016; 28(1-2): 1-10.

Cell J
Cell Journal(Yakhteh)
Homepage: https://www.celljournal.org/
Original Article
Vol 25, No 10, October 2023, Pages: 717-726

The Potential Hepatoprotective Effect of *Vaccinium arctostaphylos* L. Fruit Extract in Diabetic Rat

Negar Saliani, Ph.D.[1], Shideh Montasser Kouhsari, Ph.D.[1]*, Maryam Izad, Ph.D.[2]

1. Department of Cellular and Molecular Biology, School of Biology, College of Science, University of Tehran, Tehran, Iran
2. Department of Immunology, School of Medicine, Tehran University of Medical Sciences, Tehran, Iran

Abstract

Objective: *Vaccinium arctostaphylos* has traditionally been employed in Iranian folk medicine to treat diabetes. However, the precise molecular mechanisms underlying its antidiabetic properties remain incompletely understood. The current experiment intended to explore the modulatory effects of *V. arctostaphylos* fruit ethanolic extract (VAE) on biochemical and molecular events in the livers of diabetic rats.

Materials and Methods: In this experimental study, male Wistar rats were randomly assigned to four groups: normal control, normal rats with VAE treatment, diabetic control, and diabetic rats with VAE treatment. Following 42 days of treatment, the impact of VAE on diabetes-induced rats was assessed by measuring various serum biochemical parameters, including insulin, free fatty acids (FFA), tumor necrosis factor-α (TNF-α), reactive oxygen species (ROS), and adiponectin levels. The activities of hepatic carbohydrate metabolic enzymes and glycogen content were determined. Additionally, expression levels of selected genes implicated in carbohydrate/lipid metabolism and miR-27b expression were evaluated. H&E-stained liver sections were prepared for light microscopy examination.

Results: Treatment with VAE elevated levels of insulin and adiponectin that reduced levels of FFA, ROS, and TNF-α in the serum of diabetic rats. VAE-treated rats exhibited increased activities of hepatic glucokinase (GK), glucose-6-phosphate dehydrogenase (G6PD), and glycogen concentrations, in conjunction with decreased activities of glucose-6-phosphatase (G6Pase) and fructose-1,6-bisphosphatase (FBPase). Furthermore, VAE significantly upregulated the transcription levels of hepatic insulin receptor substrate 1 (*Irs1*) and glucose transporter 2 (Glut2), while considerably downregulated the expression of peroxisome proliferator-activated receptor gamma (*Pparg*) and sterol regulatory element-binding protein 1c (*Srebp1c*). VAE remarkably enhanced the expression of miR27-b in the hepatic tissues of diabetic rats. Abnormal histological signs were dramatically normalized in diabetic rats receiving VAE compared to those in the diabetic control group.

Conclusion: Our findings underscore the hypoglycemic and hypolipidemic activities of *V. arctostaphylos* and assist in better comprehension of its antidiabetic properties.

Keywords: Diabetic Rat, Liver, miR27-b, *Vaccinium arctostaphylos*

Citation: Saliani N, Montasser Kouhsari Sh, Izad M. The potential hepatoprotective effect of Vaccinium arctostaphylos L. fruit extract in diabetic rat. Cell J. 2023; 25(10): 717-726. doi: 10.22074/CELLJ.2023.2004742.1328

Introduction

Diabetes mellitus is a serious metabolic disorder that is defined by elevated levels of blood glucose. This condition primarily stems from deficient insulin secretion, insulin action, or both which may arise from impaired metabolism of carbohydrates, proteins, and lipids in target tissues (1).

As the central metabolic organ, the liver serves a crucial biochemical function in maintaining glucose and lipid homeostasis and is profoundly impacted by diabetes. Chronic hyperglycemia and hyperlipidemia lead to inflammation and liver damage due to augmented oxidative stress and development of reactive oxygen species (ROS) (2). Accumulating evidence suggests that oxidative stress in the liver can initiate molecular alterations by influencing the expression of genes and micro-ribonucleic acids, potentially manifesting as liver dysfunction (3). Hepatic microRNAs (miRNAs) have emerged as critical regulators of glucose and lipid metabolism (4).

MiRNAs are small, approximately 22-nucleotide-long, evolutionarily conserved noncoding RNA molecules that negatively regulate the expression of target genes at the posttranscriptional level. They bind to mRNAs through base pairing to complementary sites, consequently leading to mRNA destabilization or translational repression. Expression profiling studies of miRNAs have confirmed their dysregulation during the onset and progression of a plethora of diseases, such as diabetes and metabolic disorders. Due to the pivotal roles of miRNAs in various aspects of glucose homeostasis and lipid metabolism, they are considered novel therapeutic targets and biomarkers

Received: 14/June/2023, Revised: 08/August/2023, Accepted: 28/August/2023
*Corresponding Address: P.O.Box: 14155-6455, Department of Cellular and Molecular Biology, School of Biology, College of Science, University of Tehran, Tehran, Iran,
Email: sh_montasser@ut.ac.ir

Royan Institute
Cell Journal (Yakhteh)

for the prognosis, diagnosis, and management of diabetes and its complications (5).

MiR-27b, a member of the miR-27 family, is functionally associated with multiple biological and pathogenic processes including angiogenesis, oxidative stress, inflammation, lipid metabolism, and adipogenesis (6). It has been shown that miR-27b is significantly upregulated in the serum of children with new-onset type 1 diabetes (7) and patients with type 2 diabetes (8). Notably, miR-27b is among the most profuse miRNAs in the liver. MiR-27b-induced alterations in hepatocytes contribute to various signaling pathways relevant to glucose and lipid metabolism and insulin sensitivity (4, 9). Interestingly, it has been shown that different dietary habits can influence the circulating and tissue miRNA signatures. Similarly, recent research on the molecular biology of diabetes has demonstrated that the incorporation of antidiabetic herbs into the diet alleviates diabetes by altering miRNA expression (10, 11).

There is abundant evidence for the identification of medicinal plants possessing antidiabetic properties, and several noteworthy findings have emerged in this field. However, the search for hypoglycemic phyto-bioactive compounds with free radical scavenging and antioxidant capabilities for the development of antidiabetic therapeutic agents remains ongoing. *Vaccinium arctostaphylos* is the only species of the *Vaccinium* genus (Ericaceae family) in northern regions of Iran, especially Ardebil province (known as *Qare-qat* and *Cyah-gileh* in Persian). The berries of *V. arctostaphylos* have traditionally been used in Iranian folk medicine as a remedy for diabetes, hypertension, and hyperlipidemia (12, 13). These effects are attributed to the potential antioxidant action of the fruit of *V. arctostaphylos*, owing to the presence of substantial quantities of flavonoids and anthocyanins (14). It has been reported that malvidin-3-O-β-glucoside has an inhibitory effects on pancreatic α-amylase (15).

These characteristics sparked our interest in acquiring comprehension of the diverse parameters that contribute to the mediation of antidiabetic activity. Accordingly, the main goal of this study was to examine the effects of *V. arctostaphylos* fruit on liver-related biochemical, molecular, and histological changes in an experimental rat model of diabetes. Furthermore, we aimed to investigate the role of miR-27b in hepatic lipid metabolism in this model. Additionally, we determined whether *V. arctostaphylos* effects were mechanistically driven by modulating expression of mir-27 and related genes.

Materials and Methods

Preparation of *V. arctostaphylos* fruit extract

Fresh and ripe fruits of *V. arctostaphylos* were collected from Ardabil Province, northwest of Iran. The specimen was identified by experts at the Central Herbarium of the Department of Botany, University of Tehran (Tehran, Iran). The fruits were rinsed thoroughly with distilled water for removing any adhering dust and air-dried in shaded areas at room temperature. The berries were then finely powdered and soaked in ethanol three times for 12 hours. The resulted ethanolic phase was filtered through Whatman No. 1 filter paper (Whatman, USA). The filtrate was concentrated at 40°C using a rotary evaporator (IKA, Germany) and freeze-dried to powder on an alpha 1-2 LDplus freeze dryer (Martin Christ, Germany) (16). The obtained extract, known as *V. arctostaphylos* ethanolic fruit extract (VAE), was stored in the dark at 4°C until further use.

Experimental animals

In this experimental study, healthy male albino Wistar rats (*Rattus norvegicus*) weighing 180-220 g and approximately two months old were provided by the School of Pharmacy, Tehran University of Medical Sciences (Tehran, Iran). They were acclimatized to the new laboratory environment for seven days prior to the commencement of the experiment. The rats were housed in a well-maintained and pathogen-free animal house under standard vivarium conditions (humidity 55 ± 5%; ambient temperature of 25 ± 2°C; constant 12-hour/12-hour light/dark cycle). They were fed standard chow pellets of known composition and provided clean drinking tap water ad libitum throughout the research period. The present study was reviewed and received approval from the Research Ethics Committees of the College of Sciences, University of Tehran (IR.UT.SCIENCE.REC.1402.005).

Induction of experimental Diabetes mellitus

Type 1 diabetes was induced by subcutaneous injection of freshly prepared alloxan monohydrate (Sigma Aldrich, USA) solution (120 mg/kg body weight, in cold 0.1 M citrate buffer, pH=4.5) to 18-hour fasted rats. An equal volume of citrate buffer without alloxan injected to non-diabetic group of rats for simulation of drug injection (17). Six hours after alloxan administration, a 20% glucose solution was injected intraperitoneally. The animals were then given access to a 5% glucose solution for the next 24 hours to overcome drug-induced fatal hypoglycemia (18). 72- hour post-alloxan treatment, hyperglycemia was confirmed using a portable glucometer (On Call Plus Blood Glucose Meter, USA), and rats with elevated blood glucose levels (>250 mg/dl) were deemed to be diabetic (17).

Experimental design

A total of 32 rats were stochastically aliquoted into four groups, each containing eight animals. These groups either were treated with vehicle (distilled water) alone or VAE as follows:

Normal control (NC): Healthy rats treated with vehicle alone.

Normal+VAE (N+VAE): Healthy rats treated with VAE at 400 mg/kg body weight.

Diabetic control (DC): Diabetic rats received vehicle.

Diabetic+VAE (D+VAE): Diabetic rats received VAE at 400 mg/kg body weight.

VAE was dissolved in distilled water (1 ml/rat) at the desired concentration immediately prior to each administration. VAE was administered by oral gavage to the respective groups for 42 consecutive days. The optimal dose of VAE (400 mg/kg body weight) was selected based on previous findings from our laboratory (16). During the experimental period, rats were monitored for physiological parameters, such as food and water intake, body weight, and blood glucose levels, at weekly intervals to investigate the stability of the diabetic condition. At the end of the treatment period, all rats were subjected to 12 hours of overnight fasting. Next, the rats were anesthetized intraperitoneally with a combination of ketamine (90 mg/kg) and xylazine (10 mg/kg) solution and humanely sacrificed (19). Thereafter, blood samples were collected via intracardiac puncture for biochemical analyses. Serum was prepared by coagulating blood samples at room temperature for 15-30 minutes and centrifugation at 1500 × g for 15 minutes. The supernatant sera were stored in aliquots at a temperature of -80°C. Immediately after dissection, tissue samples were separated, rinsed in ice-cold saline, frozen in liquid nitrogen, and kept at -80°C for subsequent biochemical and quantitative polymerase chain reaction (PCR)-based gene expression analyses. A portion of the tissues were fixed in 10% formalin (Merck, Germany) and subjected to histopathological examination.

Biochemical analysis

Serum insulin levels were estimated with a commercial rat insulin ELISA kit in accordance with the guidance provided by the manufacturer (Demeditec, Germany). The concentration of serum-free fatty acids (FFA) was quantified using an EnzyChrom™ free fatty acid kit (BioAssay Systems, USA). ELISA was performed to evaluate ROS levels in the serum of the experimental groups (MyBioSource, USA). The levels of serum and hepatic tumor necrosis factor-α (TNF-α), a proinflammatory cytokine, were measured in accordance with the manufacturer's protocol (RayBiotech, USA). A commercially available kit was used to determine adiponectin levels in the serum samples (Abcam, UK).

Determination of hepatic carbohydrate metabolic enzymes and glycogen

A portion of the harvested liver tissue underwent the process of homogenization in Tris-HCl buffer (100 mM, pH=7.4) centrifuged at 3000 × g for 10 minutes at the temperature of 4°C. The resultant supernatant was used to evaluate the carbohydrate-metabolizing enzyme activity. The protein content of the supernatant was estimated by the Bradford method (20). Hepatic glucokinase (GK), glucose-6-phosphate dehydrogenase (G6PD), glucose-6-phosphatase (G6Pase), and fructose-1,6-bisphosphatase (FBPase) activities and glycogen content in the liver of experimental rats were assessed according to previously described methods (21).

RNA extraction and real-time polymerase chain reaction analysis

To identify gene expression, total RNA was extracted from snap-frozen tissue samples using an RNX-Plus kit (SinaClon, Iran), followed by DNase I digestion (Yekta Tajhiz Azma, Iran). Agarose gel electrophoresis was employed to confirm the integrity of isolated RNA. A NanoDrop ND-1000 spectrophotometer (NanoDrop Technologies, USA) was utilized to quantify RNA concentration in all experimental groups. The purity of RNA samples was determined using an A260/A280 ratio of 1.8-2.0. Next, isolated total RNA (1 μg) was reverse-transcribed to obtain complementary DNA (cDNA) using a PrimeScript RT Reagent Kit according to the manufacturer's recommendations (TaKaRa, Japan). Real-time quantitative PCR (qPCR) was carried out using YTA SYBR Green qPCR Master Mix (Yekta Tajhiz Azma, Iran) on a StepOnePlus Real-Time PCR system (Applied Biosystems, USA) at optimized cycles. The cDNA was amplified with gene-specific primer pairs (SinaClon, Iran), as listed in Table S1 (See Supplementary Online Information at www.celljounal.org). Melting curve analysis was applied to verify primer specificity. Each reaction was run in triplicate. Transcription of the β-actin (*Actb*) housekeeping gene was employed as the internal control for normalization. The relative target mRNA expression was determined via the $2^{-\Delta\Delta Ct}$ method (22).

MicroRNA extraction and real-time polymerase chain reaction for miR-27b

To evaluate the effect of VAE administration on miR-27b expression levels, the homogenized liver suspension was applied to extract total miRNA using a miRNA isolation kit following the manufacturer's protocol (Favorgen, Taiwan). Polyadenylation and reverse transcription were performed according to the manufacturer's recommendations using a miRCURY LNA Universal cDNA Synthesis Kit II (Exiqon, Denmark). Tissue-derived miR-27b expression levels (mature sequence, 5′-UUCACAGUGGCUAAGUUCUGC-3′) were analyzed by qPCR using ExiLENT SYBR Green master mix (Exiqon, Denmark). PCR assays were performed in triplicate for each sample utilizing the StepOnePlus Real-Time PCR system. Hepatic expression of miR-27b was normalized to that of U6 small nuclear RNA (U6 snRNA) and calculated using the $2^{-\Delta\Delta CT}$ method.

Histological analysis

The effects of VAE on the histopathological alterations in the liver were evaluated. The excised liver tissues were washed with normal saline, immediately fixed in a 10% neutral formalin solution for 48 hours, and routinely processed for histological examination using the paraffin method. Paraffin-embedded tissues were cut into serial sections with 5 μm thickness and separately stained with Hematoxylin and Eosin (H&E) dye. The slides were examined under a light microscope (Olympus Corp., Japan), and images captured using a digital camera (23).

Statistical analysis

All data are presented as mean ± standard deviation (SD). To conduct statistical analysis, data were evaluated by one-way analysis of variance (ANOVA) followed by Tukey's post hoc test using GraphPad Prism software version 8.4.3 (La Jolla, CA, USA). Statistical significance was set at $P<0.05$.

Results

Effect of VAE on the clinical parameters

Alterations in food and water intake, body mass gain, and blood glucose levels were monitored in all experimental rats during the 42-day treatment period. Food, water intake and blood glucose levels in diabetic animals were considerably increased compared to the NC group (P=0.00, Figs.S1, S2, S3, See Supplementary Online Information at www.celljounal.org). Compared to the NC groups, untreated diabetic rats exhibited marked loss of body weight (P=0.00, Fig.S4, See Supplementary Online Information at www.celljounal.org). Treatment of diabetic animals with VAE remarkably ameliorated these parameters.

Effect of VAE on the levels of serum insulin, free fatty acid, and reactive oxygen species

The levels of serum insulin, FFA, and ROS of control and experimental rats are enumerated in Table 1. The ELISA test showed that the serum insulin level was dramatically diminished (P=0.000) in untreated diabetic rats compared to normal controls at the end of the 42-day study period. The insulin level of VAE-treated diabetic rats was elevated notably in comparison to the corresponding controls (P=0.04).

As shown, DC rats exhibited elevated levels of serum FFA compared to normal rats (P=0.02). A marked decline in the serum FFA levels was observed in diabetic rats following VAE administration (P=0.03).

ROS levels were drastically raised in control diabetic animals compared to NC rats (P=0.000). However, in animals receiving VAE, the serum levels of ROS were significantly diminished compared to diabetic controls (P=0.006).

Effect of VAE administration on serum and hepatic TNF-α levels

To elucidate whether TNF-α levels were affected by VAE administration, the serum and hepatic levels of TNF-α were evaluated in all experimental groups. Figure 1A, B represent that serum and hepatic levels of TNF-α in diabetic animals were considerably higher than those in the NC group (P=0.000). Nevertheless, oral administration of VAE remarkably decreased serum and hepatic TNF-α levels (P=0.009 and P=0.046, respectively).

Effect of VAE administration on serum adiponectin levels

Figure 1C shows the effect of VAE on serum adiponectin levels in all experimental groups. Diabetic rats demonstrated a significant diminution in adiponectin concentration in comparison to the NC group (P=0.001). Administration of VAE to diabetic rats remarkably increased serum adiponectin level (P=0.012).

Effect of VAE on activities of hepatic carbohydrate metabolic enzymes and glycogen content

Table 2 exhibits the impact of VAE treatment on carbohydrate metabolic enzyme activities and glycogen levels in the liver of normal and alloxan-induced diabetic rats. DC rats demonstrated a prompt decline in the activity of GK (P=0.000) and G6PD (P=0.002) and a concomitantly significant elevation in the activity of G6Pase (P=0.04) and FBPase (P=0.005) compared to NC rats. The altered activities of these enzymes reverted to near-normal values after VAE administration.

Compared to the NC group, hepatic glycogen concentration was significantly diminished (P=0.002) in diabetic rats. The treatment of diabetic animals with VAE showed remarkable amelioration in hepatic glycogen storage (P=0.04).

Table 1: Effect of VAE on serum insulin levels and other variables

Groups	Normal control	Normal+VAE	Diabetic control	Diabetic+VAE
Serum insulin (μU/mL)	15.21 ± 0.98	14.84 ± 1.43	4.90 ± 0.82***	7.63 ± 1.25≠
Serum FFA (mg/mL)	70.76 ± 3.14	74.29 ± 5.66	151.14 ± 3.25*	92.88 ± 7.41≠≠
Serum ROS (U/ml)	3.34 ± 0.25	3.86 ± 0.81	31.62 ± 5.63***	11.27 ± 8.03≠≠

Each value represents the mean ± SD of eight rats per group. Evaluation was performed by one-way ANOVA followed by post hoc Tukey's test. *; P<0.05, ***; P<0.001, in comparison to the normal control group, ≠; P<0.05, ≠≠; P<0.01, in comparison to the diabetic control group, FFA; Free fatty acids, and ROS; Reactive oxygen species.

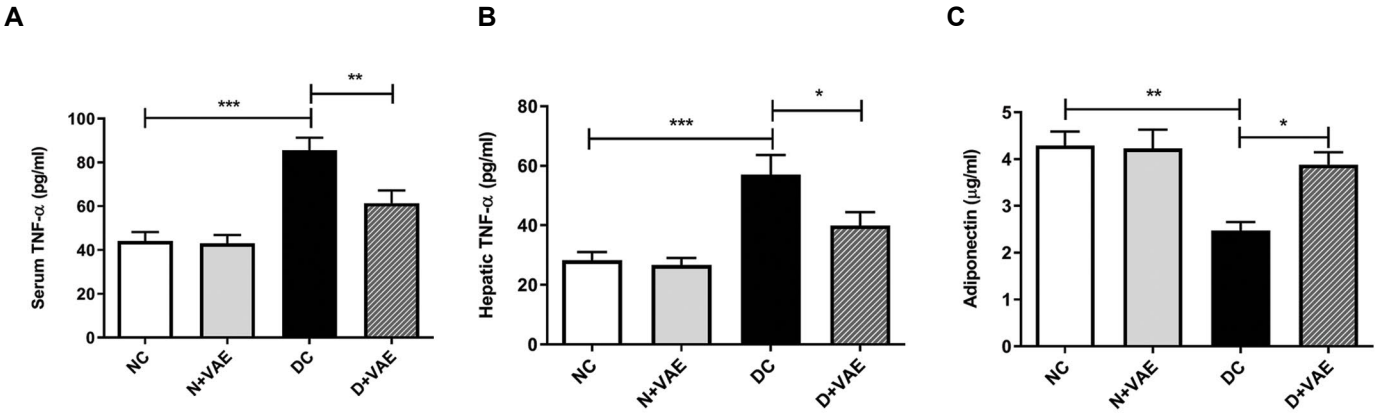

Fig.1: Effect of VAE on TNF-α and adiponectin levels in normal and experimental rats. **A.** Serum TNF-α levels, **B.** Hepatic TNF-α levels, and **C.** Serum adiponectin levels. Bars represent the mean ± SD of eight rats per group. Evaluation was carried out by one-way ANOVA followed by post hoc Tukey's test. *; P<0.05, **; P<0.01, ***; P<0.001: statistical differences in comparison to the diabetic control group, TNF-α; Tumor necrosis factor-α, NC; Normal control, N+VAE; Normal rats subjected to VAE treatment, DC; Diabetic control, and D+VAE; Diabetic rats subjected to VAE treatment.

Table 2: Effect of VAE on the activities of carbohydrate metabolic enzymes and glycogen content in the liver of all experimental rats

Groups	GK[a]	G6PD[b]	G6Pase[c]	FBPase[d]	Liver glycogen[e]
Normal control	0.19 ± 0.01	4.73 ± 0.12	0.17 ± 0.01	0.34 ± 0.02	45.24 ± 3.61
Normal+VAE	0.18 ± 0.04	4.77 ± 0.27	0.16 ± 0.01	0.32 ± 0.03	47.16 ± 4.05
Diabetic control	0.09 ± 0.01***	2.51 ± 0.23**	0.28 ± 0.01*	0.57 ± 0.04**	21.17 ± 2.18**
Diabetic+VAE	0.14 ± 0.02≠	3.01 ± 0.36≠	0.21 ± 0.02≠≠	0.39 ± 0.03≠	34.28 ± 3.23≠

Each value represents the mean ± SD of eight rats per group. Evaluation was carried out by one-way ANOVA followed by post hoc Tukey's test.*; P<0.05, **; P<0.01, ***; P<0.001, in comparison to the normal control group, ≠; P<0.05, ≠≠; P<0.01, in comparison to the diabetic control group, GK; Glucokinase, G6PD; Glucose-6-phosphate dehydrogenase, G6Pase; Glucose-6-phosphatase, FBPase; Fructose-1,6-bisphosphatase, [a]; µmol of glucose phosphorylated/hour/mg protein, [b]; nmol of NADPH formed/minute/mg protein, [c]; µmol of Pi liberated/minute/mg protein, [d]; µmol of Pi liberated/hour/mg protein, and [e]; mg/g tissue.

Effect of VAE on expression of key genes associated with glucose and lipid metabolism

To investigate the effect of VAE administration on the expression of genes involved in hepatic glucose and lipid metabolism, qPCR was performed in all experimental groups. These results revealed a dramatically reduced amount of insulin receptor substrate 1 (*Irs1*) expression in DC rats compared to that in NC animals (P=0.000). However, the expression levels of *Irs1* significantly enhanced in VAE-treated diabetic rats in contrast to the DC groups that did not receive treatment (P=0.025, Fig.2A). Glucose transporter 2 (GLUT2) plays an essential role in liver glucose transport (24). The transcription level of *Glut2* was notably downregulated in diabetes-induced rats in comparison to normal controls (P=0.002). On the other hand, the administration of VAE to diabetic group of rats led to a marked increase in *Glut2* expression levels (P=0.029, Fig.2B).

The expression of peroxisome proliferator-activated receptor gamma (*Pparg*) was found to be significantly upregulated in the liver of diabetic rats compared to that in normal controls (P=0.003). The treatment of diabetic rats with VAE considerably downregulated *Pparg* expression (P=0.032, Fig.2C). Diabetic rats displayed a drastic increase in the transcription level of sterol regulatory element-binding protein 1c (*Srebp1c*) compared to NC rats (P=0.000). VAE administration ameliorated the alloxan-induced increase in *Srebp1c* gene expression (P=0.03, Fig.2D).

Effect of VAE on expression levels of hepatic miR-27b

Next, we identified the potential effect of VAE on the expression levels of hepatic miR-27b. qPCR analysis was performed to examine the modulatory impact of VAE on the expression of miR-27b in all experimental groups. The hepatic expression of miR-27b was significantly lower in DC rats than in normal controls (P=0.0018). Meanwhile, VAE-treated diabetic rats showed a significant upregulation in miR-27b expression levels compared to untreated diabetic group (P=0.045, Fig.3).

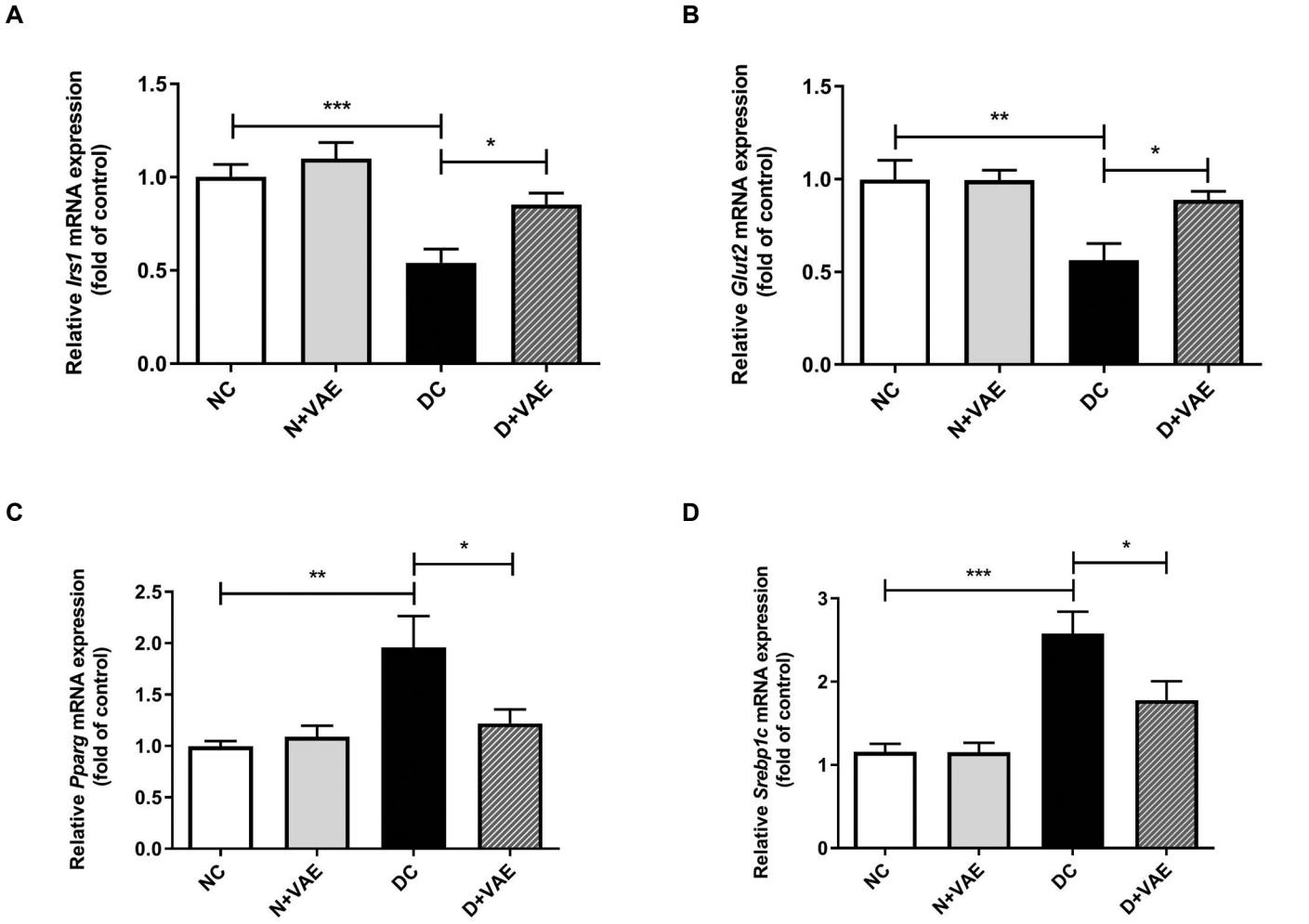

Fig.2: Effect of VAE on hepatic expression of key glucose and lipid metabolism-associated genes. **A.** *Irs1*, **B.** *Glut2*, **C.** *Pparg*, and **D.** *Srebp1c* expression levels. Bars represent the mean ± SD of eight rats per group. Evaluation was performed by one-way ANOVA followed by post hoc Tukey's test. *; P<0.05, **; P<0.01, ***; P<0.001: statistical differences in comparison to the diabetic controls, NC; Normal control, N+VAE; Normal rats subjected to VAE treatment, DC; Diabetic control, and D+VAE; Diabetic rats subjected to VAE treatment.

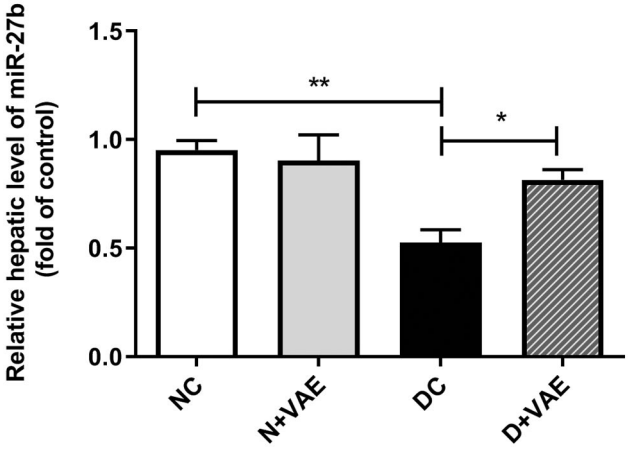

Fig.3: Effect of VAE on hepatic expression levels of miR-27b in normal and experimental rats. Bars represent the mean ± SD of eight rats per group. Evaluation was accomplished by one-way ANOVA followed by post hoc Tukey's test. *; P<0.05, **; P<0.01: statistical differences in comparison to the diabetic control group, NC; Normal control, N+VAE; Normal rats subjected to VAE treatment, DC; Diabetic control, and D+VAE; Diabetic rats subjected to VAE treatment.

Effect of VAE on histopathology of liver

To elucidate whether hepatic biochemical and molecular alterations lead to structural modifications at the microscopic level, a histological assessment was performed. Figure 4 illustrates the morphological features of the liver tissues of control and experimental rats. Photomicrographs of hepatic tissues from NC and normal rats treated with VAE displayed a well-preserved cellular architecture with normal nuclei and cytoplasm (Fig.4A, B). In comparison to the NC groups, histological abnormalities were observed in the liver tissues of DC rats characterized by disintegrated hepatic cells, degeneration, and mild inflammation accompanied by moderate fatty changes (Fig.4C). Treatment with VAE resulted in a near-normal hepatocyte arrangement with minimal inflammatory damage and fatty degeneration (Fig.4D). These findings imply that VAE treatment can ameliorate abnormal morphology in diabetic rats.

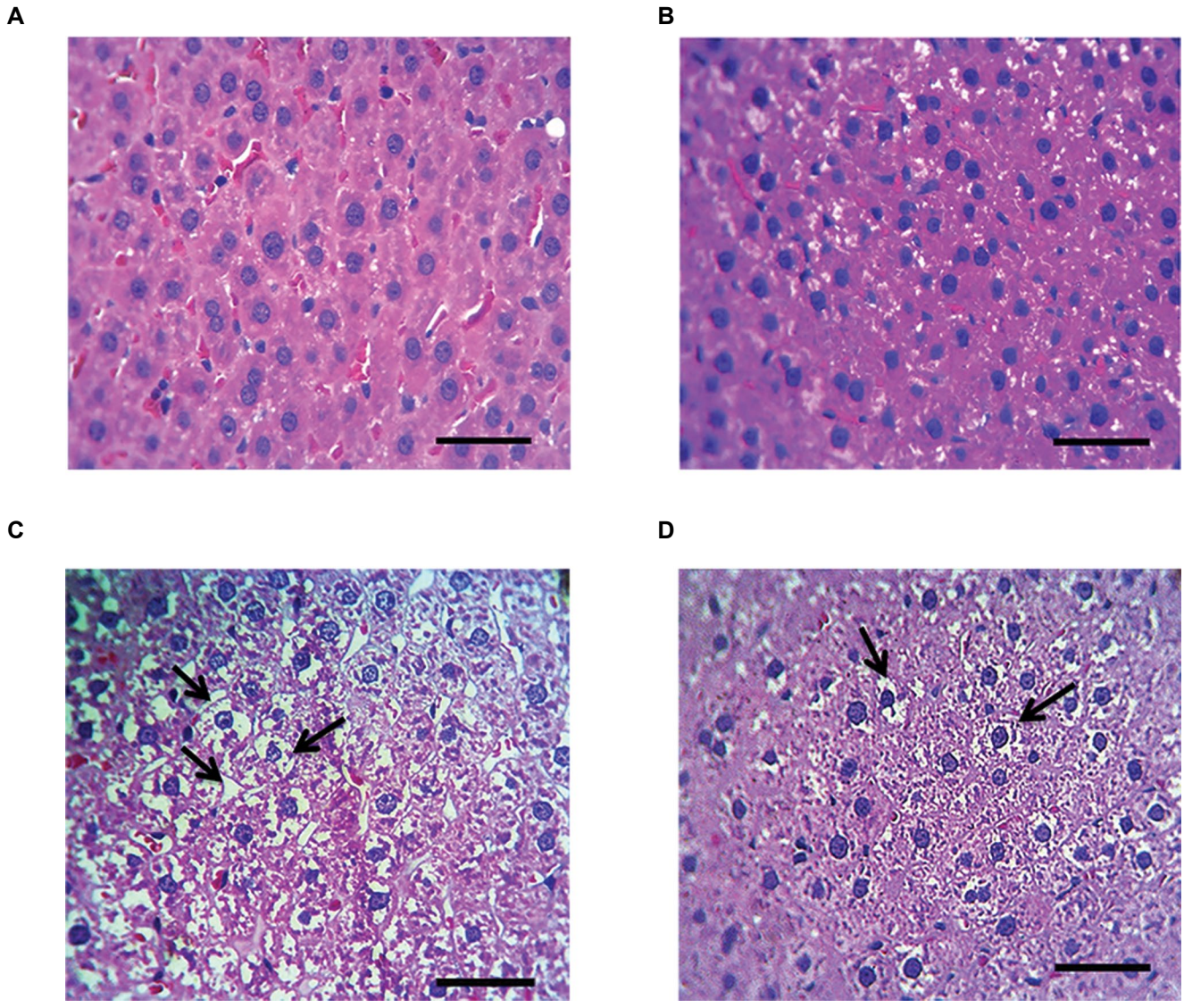

Fig.4: Histopathological observations of H&E-stained liver sections from normal and experimental rats (×40, scale bar: 150 µm). **A.** Normal control rats, **B.** Normal rats subjected to VAE treatment, **C.** Diabetic control rats, and **D.** Diabetic rats subjected to VAE treatment. Arrows indicate fatty changes.

Discussion

Diabetes is a heterogeneous metabolic disorder characterized by hyperglycemia arising from impaired carbohydrate metabolism and insulin secretion (1). The ultimate goal of all diabetes remedies is to normalize glycemia and improve health status. There is a rising trend toward the use of traditional medicinal plants for the diabetes treatment.

The antidiabetic therapeutic properties of *V. arctostaphylos* fruit have been tested in several clinical trials (12, 13). Administration of the hydroalcoholic extract of *V. arctostaphylos* berries to type 2 diabetic patients reduced hyperglycemic conditions through decreasing fasting blood sugar and HbA1c levels (13). The previous research conducted by this group showed that ethanolic fruit extract of *V. arctostaphylos* improved blood sugar levels, lipid profiles, and antioxidant enzymes activities in Allegan-induced diabetic rats (16). In light of these findings, the present investigation aimed to provide new insights into understanding other antidiabetic properties of *V. arctostaphylos*. This study examined the effects of *V. arctostaphylos* fruit on the mechanism of actions involved in hepatic glucose regulation and lipid metabolism. Moreover, to ascertain the molecular mechanisms mediating VAE antidiabetic properties, the expression of key metabolic genes as long as miR-27b were investigated at both transcriptional and posttranscriptional levels.

Liver dysfunction is among the foremost complications of Diabetes mellitus. The activities of key regulatory enzymes relevant to hepatic glycolysis, gluconeogenesis, and glycogenesis are altered in diabetes. GK is the first rate-limiting enzyme in the glycolytic pathway that transfers a phosphoryl group from ATP to glucose, resulting in glucose-6-phosphate. It is well-established that restored GK activity correlates with an overall improvement in glucose homeostasis (21). Our findings

indicated that hepatic GK activity was remarkably lower in diabetic rats than in normal controls. Decreased activity of GK is attributed to insulin deficiency as a repercussion of alloxan-mediated β-cell cytotoxicity and degeneration. However, the administration of VAE to diabetic rats improved the activity of this enzyme.

G6PD is the rate-limiting enzyme of the hexose monophosphate shunt that maintains anabolic biosynthesis and redox homeostasis. In diabetic conditions, the decrease in G6PD activity and subsequent NADPH levels makes the cells more susceptible to oxidative stress (25). According to our data, G6PD activity increased significantly in diabetic rats upon treatment with VAE.

G6Pase controls the last step of gluconeogenesis and dephosphorylates glucose-6-phosphate to glucose and free phosphate. Insufficient insulin levels elevate G6Pase activity and endogenous glucose production, thereby giving rise to diabetic complications (21). In the present work, diabetic rats exhibited high activity of G6Pase, while oral administration of VAE restored the enzyme activity close to normal levels. FBPase is responsible for the second irreversible step in gluconeogenesis and catalyzes the hydrolytic dephosphorylation of fructose-1,6-bisphosphate to fructose-6-phosphate, representing a promising target for glycemic control. Diabetes impairs the suppression of FBPase, leading to excessive hepatic glucose output and hyperglycemia (26). Our data revealed VAE decreased the activity of this gluconeogenic enzyme in diabetic rats.

The current study showed that the concentration of hepatic glycogen, the principal storage form of carbohydrates, was declined in diabetic animals compared to normal controls. The administration of VAE considerably augmented glycogen concentration in the livers of control diabetic rats. Overall, our aforementioned findings were consistent with those of studies reporting the beneficial effects of herbal supplements on hepatic glycogen and carbohydrate metabolizing enzymes in diabetic models (27).

Adiponectin is the most common adipokine synthesized by adipose tissue and possesses antidiabetic, anti-inflammatory, and anti-atherogenic properties. Low adiponectin levels correlate with insulin resistance, obesity, and fatty liver disease. The antidiabetic effects of adiponectin are thought to be partially mediated by abrogating the expression of phosphoenolpyruvate carboxylase (PEPCK) and G6PD which reduce the synthesis and release of endogenous glucose from liver cells (28). Chemically-induced diabetic rats showed reduced levels of circulating adiponectin (29), and these findings corroborate our observations in the diabetes-induced group. However, a dramatic increase was observed in diabetic rats treated with VAE compared to corresponding controls. Similarly, in a study by Dadgar et al. (30), the potential effect of herbal extracts was reported in elevating adiponectin levels in diabetic rodents. Adiponectin and TNF-α exhibit an inverse correlation (31). This notion could explain our findings, where we observed increased levels of TNF-α in both the serum and hepatic tissues of the untreated diabetic group. Supporting these findings, Ingaramo et al. (32) demonstrated elevated levels of TNF-α and its receptor in the livers of diabetic rats. Results of this study imply that supplementation with *V. arctostaphylos* fruit extract reduced TNF-α levels, thus highlighting its potent anti-inflammatory properties.

From a molecular point of view, we examined the expression levels of *Irs1* (upstream of insulin signaling) and *Glut2* in the livers of experimental animals to determine how VAE activates insulin signaling and glucose uptake. IRS1 plays a vital role in insulin-mediated responses, and decreased mRNA levels of *Irs* could potentially lead to the progression of insulin resistance and diabetes (11). Our data revealed a significant decrease in hepatic *Irs1* expression after toxic alloxan treatment. However, VAE administration increased the mRNA expression of *Irs1*, thereby promoting downstream signaling. It might be speculated that VAE may partially exert its antidiabetic effects by upregulating *Irs1* levels.

As evidenced, circulating glucose is taken up by GLUT2 in the liver. Reduced expression of hepatic *Glut2* impairs glucose uptake (24). We observed a diminution in hepatic *Glut2* mRNA levels in control diabetic animals. However, VAE administration significantly upregulated *Glut2* expression in the livers of diabetic rats compared to that in the untreated diabetic group. Collectively, VAE upregulated *Irs1* and *Glut2* and promoted liver function for glucose uptake.

Lipid perturbation can be a risk factor for diabetes. In this study, we investigated the expression levels of *Pparg* and *Srebp1c* to comprehend the hepatic lipid metabolism in diabetes-induced rats.

PPARγ is required for metabolic balance and has garnered considerable interest owing to its diverse functions in glucose and lipid metabolism. Studies using rodent models have demonstrated that PPARγ activation is critically associated with the development of hepatic steatosis and lipotoxicity (33). In this study, the DC group exhibited overexpression of *Pparg* compared to the normal controls. These results are in accordance with those of previous in vivo experiments (34). Modulation of *Pparg* expression by herbal compounds (35) supports the VAE-induced depletion of *Pparg* in diabetic rats.

SREBP1c is a crucial transcription factor that is involved in fatty acid biosynthesis. It has been reported that overexpression of *Srebp1c* increases the expression of lipogenic-associated genes, including fatty acid synthase (*Fasn*) and acetyl-CoA carboxylase (*Accca*), accumulating intracellular triglycerides within lipid droplets in hepatocytes (36). The findings of this research indicated the upregulation of hepatic *Srebp1c* in the diabetic state. This is consistent with earlier reports on diabetic rodent models (34). In this study, VAE administration effectively attenuated *Srebp1c* expression close to normal values, reducing lipid synthesis and droplet formation, as

supported by our histological findings.

The crucial role of miR-27b as a key metabolic regulator in hepatic lipid metabolism has been well-established in animal and human research (9). Ji et al. (37) reported that *in vitro* inhibition of miR-27b reestablished cytoplasmic lipid droplet formation in rat hepatic stellate cells. Bioinformatic and experimental target gene analyses demonstrated that miR-27b directly and indirectly regulates key genes involved in hepatic lipid metabolism [e.g., *Pparg*, *Srebp1c* (38)], and insulin signaling in hepatocytes (4). Notably, miR-27b attenuates hepatic glucose output by modulating the expression of gluconeogenic enzymes such as G6Pase. Our data revealed that miR-27b abundance was depleted in the livers of diabetic rats. Imperatively, the results of the current research indicated that VAE treatment stimulate miR-27b expression in diabetic animals.

Qin et al. found that a flavonoid derivative (Fla-CN) regulated miR-27 expression in the liver and adipose tissues of high-fat diet-induced obese mice (39). Therefore, it is plausible to speculate that VAE exerts its hepatoprotective effects by enhancing miR-27b expression and downregulating the expression of its target genes.

In view of the above findings, it is hypothesized that hepatic gene expression changes elicited by alloxan during the 42-day study period could slightly shift the metabolic status of liver cells toward fatty acid storage and dyslipidemia, as reinforced by our histological observations. DC rats in this study showed histopathological alterations, such as hepatocellular necrosis, inflammation, and fat droplets, compared to normal liver sections. Similar results were obtained in a previous experiment (40). In contrast, VAE administration significantly reduced these abnormalities and improved the liver histoarchitecture, suggesting the tissue-protective nature of VAE.

Conclusions

Taken together, the results of the current biochemical and expression-based study add to the picture of the antidiabetic properties of *V. arctostaphylos* fruit. These findings shed light on the mechanisms of action underlying the hepatoprotective effects of VAE. VAE efficiently ameliorates hyperglycemia, dyslipidemia, oxidative stress, and inflammatory states.

This study provides further scope to evaluate the effects of VAE at the molecular level. Apart from improving hepatic carbohydrate metabolizing enzymes activity and glycogen content, VAE also governs the expression of genes involved in glucose and lipid homeostasis in liver. According to our findings, it can be asserted that VAE may alleviate diabetes-induced hepatic lipotoxicity by upregulating miR-27b and modulating the expression of its target genes, which are correlated with lipid metabolism. These results are consistent with our hepatic histopathological assessment.

Acknowledgments

The authors would like to thank the personnel of the Department of Cellular and Molecular Biology of the University of Tehran for their guidance and assistance. The financial support from the Iran National Science Foundation (No. 92044182) is gratefully acknowledged.

Authors' Contributions

Sh.M.K.; Conceptualization, Validation, Writing, Review, Editing, Supervision, and Project administration. N.S.; Methodology, Software, Formal Analysis, Investigation, Data curation, Writing, Original draft preparation, and Visualization. M.I.; Data Curation, Writing, Review, and Editing. All authors read and approved the final version of the article.

References

1. Bereda G. Risk factors, complications and management of diabetes mellitus. Am J Biomed Sci Res. 2022; 16 (4): 409-412.
2. Li Y, Mai Y, Qiu X, Chen X, Li C, Yuan W, Hou N. Effect of long-term treatment of Carvacrol on glucose metabolism in Streptozotocin-induced diabetic mice. BMC Complement Med Ther. 2020; 20(1): 142.
3. Klieser E, Mayr C, Kiesslich T, Wissniowski T, Fazio PD, Neureiter D, et al. The crosstalk of mirna and oxidative stress in the liver: from physiology to pathology and clinical implications. Int J Mol Sci. 2019; 20(21): 5266.
4. Benito-Vicente A, Uribe KB, Rotllan N, Ramírez CM, Jebari-Benslaiman S, Goedeke L, et al. miR-27b modulates insulin signaling in hepatocytes by regulating insulin receptor expression. Int J Mol Sci. 2020; 21(22): 8675.
5. Saliani N, Montazersaheb S, Montasser Kouhsari S. Micromanaging glucose tolerance and diabetes. Adv Pharm Bull. 2017; 7(4): 547-556.
6. Chen WJ, Yin K, Zhao GJ, Fu YC, Tang CK. The magic and mystery of microRNA-27 in atherosclerosis. Atherosclerosis. 2012; 222(2): 314-323.
7. Nielsen LB, Wang C, Sørensen K, Bang-Berthelsen CH, Hansen L, Andersen ML, et al. Circulating levels of microRNA from children with newly diagnosed type 1 diabetes and healthy controls: evidence that miR-25 associates to residual beta-cell function and glycaemic control during disease progression. Exp Diabetes Res. 2012; 2012: 896362.
8. Wang S, Ai H, Liu L, Zhang X, Gao F, Zheng L, et al. Micro-RNA-27a/b negatively regulates hepatic gluconeogenesis by targeting FOXO1. Am J Physiol Endocrinol Metab. 2019; 317(5): E911-E924.
9. Vickers KC, Shoucri BM, Levin MG, Wu H, Pearson DS, Osei-Hwedieh D, et al. MicroRNA-27b is a regulatory hub in lipid metabolism and is altered in dyslipidemia. Hepatology. 2013; 57(2): 533-542.
10. Shin PK, Kim MS, Park SJ, Kwon DY, Kim MJ, Yang HJ, et al. A traditional korean diet alters the expression of circulating micrornas linked to diabetes mellitus in a pilot trial. Nutrients. 2020; 12(9): 2558.
11. Gharib E, Montasser Kouhsari S, Izad M. Punica granatum L. fruit aqueous extract suppresses reactive oxygen species-mediated p53/p65/miR-145 expressions followed by elevated levels of irs-1 in alloxan-diabetic rats. Cell J. 2018; 19(4): 520-527.
12. Soltani R, Hakimi M, Asgary S, Ghanadian SM, Keshvari M, Sarrafzadegan N. Evaluation of the effects of vaccinium arctostaphylos l. fruit extract on serum lipids and hs-CRP levels and oxidative stress in adult patients with hyperlipidemia: a randomized, double-blind, placebo-controlled clinical trial. Evid Based Complement Alternat Med. 2014; 2014: 217451.
13. Kianbakht S, Abasi B, Dabaghian FH. Anti-hyperglycemic effect of Vaccinium arctostaphylos in type 2 diabetic patients: a randomized controlled trial. Forsch Komplementmed. 2013; 20(1): 17-22.
14. Huang H, Luo Y, Wang Q, Zhang Y, Li Z, He R, et al. Vaccinium as potential therapy for diabetes and microvascular complications. Nutrients. 2023; 15(9): 2031.
15. Nickavar B, Amin G. Bioassay-guided separation of an alpha-amylase inhibitor anthocyanin from Vaccinium arctostaphylos berries. Z Naturforsch C J Biosci. 2010; 65(9-10): 567-570.

16. Feshani AM, Kouhsari SM, Mohammadi S. Vaccinium arctostaphylos, a common herbal medicine in Iran: molecular and biochemical study of its antidiabetic effects on alloxan-diabetic Wistar rats. J Ethnopharmacol. 2011; 133(1): 67-74.
17. Gharib E, Montasser Kouhsari S. Study of the antidiabetic activity of punica granatum l. fruits aqueous extract on the alloxan-diabetic wistar rats. Iran J Pharm Res. 2019; 18(1): 358-368.
18. Gargouri M, Hamed H, Akrouti A, Dauvergne X, Magné C, El Feki A. Effects of Spirulina platensis on lipid peroxidation, antioxidant defenses, and tissue damage in kidney of alloxan-induced diabetic rats. Appl Physiol Nutr Metab. 2018; 43(4): 345-354.
19. Bagheri Y, Barati A, Nouraei S, Jalili Namini N, Bakhshi M, Fathi E, et al. Comparative study of gavage and intraperitoneal administration of gamma-oryzanol in alleviation/attenuation in a rat animal model of renal ischemia/reperfusion-induced injury. Iran J Basic Med Sci. 2021; 24(2): 175-183.
20. Bradford MM. A rapid and sensitive method for the quantitation of microgram quantities of protein utilizing the principle of protein-dye binding. Anal Biochem. 1976; 72: 248-254.
21. Murali R, Srinivasan S, Ashokkumar N. Antihyperglycemic effect of fraxetin on hepatic key enzymes of carbohydrate metabolism in streptozotocin-induced diabetic rats. Biochimie. 2013; 95(10): 1848-1854.
22. Montazersaheb S, Kabiri F, Saliani N, Nourazarian A, Avci ÇB, Rahbarghazi R, et al. Prolonged incubation with Metformin decreased angiogenic potential in human bone marrow mesenchymal stem cells. Biomed Pharmacother. 2018; 108: 1328-1337.
23. Bagheri Y, Sadigh-Eteghad S, Fathi E, Mahmoudi J, Abdollahpour A, Namini NJ, et al. Hepatoprotective effects of sericin on aging-induced liver damage in mice. Naunyn Schmiedebergs Arch Pharmacol. 2021; 394(12): 2441-2450.
24. Thorens B. GLUT2, glucose sensing and glucose homeostasis. Diabetologia. 2015; 58(2): 221-232.
25. Çelik R, Mert H, Comba B, Mert N. Effects of cinnamaldehyde on glucose-6-phosphate dehydrogenase activity, some biochemical and hematological parameters in diabetic rats. Biomarkers. 2022; 27(3): 270-277.
26. Mata R, Flores-Bocanegra L, Ovalle-Magallanes B, Figueroa M. Natural products from plants targeting key enzymes for the future development of antidiabetic agents. Nat Prod Rep. 2023; 40(7): 1198-1249.
27. Lee J, Noh S, Lim S, Kim B. Plant extracts for type 2 diabetes: from traditional medicine to modern drug discovery. Antioxidants (Basel). 2021; 10(1): 81.
28. Ruan H, Dong LQ. Adiponectin signaling and function in insulin target tissues. J Mol Cell Biol. 2016; 8(2): 101-109.
29. Guo Z, Xia Z, Yuen VG, McNeill JH. Cardiac expression of adiponectin and its receptors in streptozotocin-induced diabetic rats. Metabolism. 2007; 56(10): 1363-1371.
30. Dadgar H, Kermanshahi H, Jaafari MR, Javadmanesh A. Effects of curcumin and its nan-omicelle form on body weight, insulin resistance, adiponectin, and blood parameters of streptozotocin-induced diabetic rats. Iran J Vet Sci Technol. 2022; 14(3): 38-45.
31. Xu A, Wang Y, Keshaw H, Xu LY, Lam KS, Cooper GJ. The fat-derived hormone adiponectin alleviates alcoholic and nonalcoholic fatty liver diseases in mice. J Clin Invest. 2003; 112(1): 91-100.
32. Ingaramo PI, Ronco MT, Francés DE, Monti JA, Pisani GB, Ceballos MP, et al. Tumor necrosis factor alpha pathways develops liver apoptosis in type 1 diabetes mellitus. Mol Immunol. 2011; 48(12-13): 1397-1407.
33. Gavrilova O, Haluzik M, Matsusue K, Cutson JJ, Johnson L, Dietz KR, et al. Liver peroxisome proliferator-activated receptor gamma contributes to hepatic steatosis, triglyceride clearance, and regulation of body fat mass. J Biol Chem. 2003; 278(36): 34268-34276.
34. Lin CH, Wu JB, Jian JY, Shih CC. (-)-Epicatechin-3-O-β-D-allopyranoside from Davallia formosana prevents diabetes and dyslipidemia in streptozotocin-induced diabetic mice. PLoS One. 2017; 12(3): e0173984.
35. Wu L, Guo C, Wu J. Therapeutic potential of PPARγ natural agonists in liver diseases. J Cell Mol Med. 2020; 24(5): 2736-2748.
36. Stoeckman AK, Towle HC. The role of SREBP-1c in nutritional regulation of lipogenic enzyme gene expression. J Biol Chem. 2002; 277(30): 27029-27035.
37. Ji J, Zhang J, Huang G, Qian J, Wang X, Mei S. Over-expressed microRNA-27a and 27b influence fat accumulation and cell proliferation during rat hepatic stellate cell activation. FEBS Lett. 2009; 583(4): 759-766.
38. Hsu CC, Lai CY, Lin CY, Yeh KY, Her GM. MicroRNA-27b Depletion Enhances Endotrophic and Intravascular Lipid Accumulation and Induces Adipocyte Hyperplasia in Zebrafish. Int J Mol Sci. 2017; 19(1): 93.
39. Qin N, Chen Y, Jin MN, Zhang C, Qiao W, Yue XL, et al. Anti-obesity and anti-diabetic effects of flavonoid derivative (Fla-CN) via microRNA in high fat diet induced obesity mice. Eur J Pharm Sci. 2016; 82: 52-63.
40. Lucchesi AN, Cassettari LL, Spadella CT. Alloxan-induced diabetes causes morphological and ultrastructural changes in rat liver that resemble the natural history of chronic fatty liver disease in humans. J Diabetes Res. 2015; 2015: 494578.

Cell J
Cell Journal(Yakhteh)
Homepage: https://www.celljournal.org/
Original Article
Vol 25, No 10, October 2023, Pages: 727-737

Integrative Bioinformatics Analysis of The Cell Division Cycle and Ribosomal Pathways in The Rat Varicocele: Implications for Drug Discovery

Ali Nasr-Esfahani, M.D.[1], Ali Valipour Motlagh, M.Sc.[2], Minoo Adib, Ph.D.[3], Kosar Pashaei, M.D.[1], Mohammad Hossein Nasr-Esfahani, Ph.D.[4*]

1. Isfahan Fertility and Infertility Center, Isfahan, Iran
2. Department of Animal Biotechnology, Cell Science Research Center, Royan Institute for Biotechnology, ACECR, Isfahan, Iran
3. Department of Immunology, Medical School, Isfahan University of Medical Sciences, Isfahan, Iran
4. Department of Animal Biotechnology, Reproductive Biomedicine Research Center, Royan Institute for Biotechnology, ACECR, Isfahan, Iran

Abstract

Objective: Varicocele is a common cause of male infertility, affecting a substantial proportion of infertile men. Recent studies have employed transcriptomic analysis to identify candidate genes that may be implicated in the pathogenesis of this condition. Accordingly, this study sought to leverage rat gene expression profiling, along with protein-protein interaction networks, to identify key regulatory genes, related pathways, and potentially effective drugs for the treatment of varicocele.

Materials and Methods: In this in-silico study, differentially expressed genes (DEGs) from the testicular tissue of 3 rats were screened using the edgeR package in R software and the results were compared to 3 rats in the control group. Data was obtained from GSE139447. Setting a -1<LogFC>1 and P<0.05 as cutoff points for statistical significance, up and down-regulated genes were identified. Based on Cytoscape plugins, protein-protein interaction (PPI) networks were drawn, and hub genes were highlighted. ShinyGO was used for pathway enrichment. Finally, effective drugs were identified from the drug database.

Results: Among the 1277 DEGs in this study, 677 genes were up-regulated while 600 genes were down-regulated in rats with varicocele compared to the control group. Using protein-protein interaction networks, we identified the top five up-regulated genes and the top five down-regulated genes. Enrichment analysis showed that the up-regulated genes were associated with the cell division cycle pathway, while the down-regulated genes were linked to the ribosome pathway. Notably, our findings suggested that dexamethasone may be a promising therapeutic option for individuals with varicocele.

Conclusion: The current investigation indicates that in varicocele the cell division cycle pathway is up-regulated while the ribosome pathway is down-regulated compared to controls. Based on these findings, dexamethasone could be considered a future candidate drug for the treatment of individuals with varicocele.

Keywords: Cell Division Cycle, RNA-SEQ, Varicocele

Citation: **Nasr-Esfahani A, Valipour Motlagh A, Adib M, Pashaei K, Nasr-Esfahani MH. Integrative bioinformatics analysis of the cell division cycle and ribosomal pathways in the rat varicocele: implications for drug discovery. Cell J. 2023; 25(10): 727-737. doi: 10.22074/CELLJ.2023.2004771.1329**

Introduction

Varicocele occurs in around 15 to 20% of all males and is reported in about 40% of infertile males. It is characterized by the abnormal enlargement of veins within the scrotum's pampiniform plexus which serve to drain oxygen-depleted blood from the testicles. Varicocele is commonly observed in the left testis and typically arises during or after puberty, likely owing to rapid testicular growth and the consequent need for increased blood supply (1). While varicocele typically does not severely impede blood flow, some individuals may experience venous backflow within the network of veins, leading to the development of varicocele and consequent male infertility. Interestingly, varicocele is also prevalent in fertile individuals, thus making the question of varicocelectomy a highly debated topic in the field of andrology, pertaining to when, why, and in whom surgical intervention should be undertaken (2).

In order to resolve these uncertainties, a comprehensive investigation into the factors that underlie varicocele is required. To this end, multiple studies have been conducted, with the majority of researchers suggesting that reactive oxygen species (ROS), resulting from increased testicular temperature, serve as the primary contributing factor. Given the role of ROS in the development of varicocele-induced male infertility, a growing number of researchers have explored the use of

Received: 14/June/2023, Revised: 03/July/2023, Accepted: 04/July/2023
***Corresponding Address: P.O.Box: 8159358686, Department of Animal Biotechnology, Reproductive Biomedicine Research Center, Royan Institute for Biotechnology, ACECR, Isfahan, Iran**
Email: mh.nasr-esfahani@royaninstitute.org

Royan Institute
Cell Journal (Yakhteh)

antioxidants as a potential therapeutic strategy to enhance fertility outcomes in affected males (3). However, recent studies suggest that it may not be "oxidative stress" but rather "reductive stress" that leads to increased ROS in the sperm of individuals with varicocele (4). To deepen our understanding of the etiology of varicocele, numerous research groups have taken advantage of an animal model of varicocele to evaluate the molecular and cellular mechanisms involved (5).

Members of our research team recently conducted a comprehensive review varicocele and oxidative stress with new insight to both human and animal studies in which we summarized the findings of numerous investigations into the mechanisms underlying varicocele-related infertility. Our review highlighted several cellular mechanisms that may contribute to the pathophysiology of varicocele, including ionic imbalance, hypoxia, hyperthermia, and impaired blood flow, all of which may ultimately result in severe, chronic oxidative and nitrosamine stress (5).

Despite extensive studies at the cellular and molecular levels, limited transcriptomic and proteomic analyses have been conducted in the field of varicocele. No single gene or single nucleotide polymorphism (SNP) directly associated with varicocele has been identified thus far to fully explain its common etiology. To gain a comprehensive understanding, researchers need to expand their focus to include transcriptomic and epigenetic analyses.

Our aim in this study was to find epigenetic regulatory mechanisms underlying varicocele by integrating the transcriptome and miRNA profiles of testicular tissue from rats with induced varicocele. Such identification of dysregulated gene expression patterns may contribute to the development of effective treatment strategies (6). Specifically, in this study, we analyzed the GSE139447 dataset, including control, varicocele, and treated varicocele groups. Our aim was to investigate differential gene expression in samples from varicocele and treated varicocele groups compared to controls. We constructed protein-protein interaction (PPI) networks to identify hub genes with significant interactions. Enrichment analysis using rat databases showed that cell division and ribosome pathways were prominently affected among the up-regulated and down-regulated genes respectively. Based on findings from these analyses, we utilized drug databases to identify candidate drugs for the treatment of varicocele.

Materials and Methods

Data collection and differential gene expression analysis

In this in silico analysis, we utilized RNA-Seq data obtained from an experimental study conducted at the Department of Human Anatomy and Histology and Embryology at Fujian Medical University in China. The dataset (GSE139447) consisted of nine rat testis tissues, including three samples from left varicocele testes, three normal samples and three varicocele treated with 300 mg/kg Morinda officinalis polysaccharide (MOP). As in the study by Zhang et al. (7), the rats used in this study were 67weekold Sprague Dawley rats, weighing 200 ± 10 g. Varicocele was induced by partial ligation of the left renal vein. The time post-analysis was 12 weeks, which is equivalent to chronic human varicocele commonly occurring on the left side.

RNA from the GSE139447 data set was extracted from the left testis using Trizol reagent and the quantity and quality of RNA was checked using nanodrop. The total RNA from each sample was used to prepare the RNA sequencing library. Random primed was used for first strand cDNA synthesis. This was followed by adaptor ligation and PCR amplification (7).

The GSE139447 normalized files, determined using Illumina HiSeq 4000 (Rattus norvegicus), were obtained directly from the Gene Expression Omnibus database. By utilizing the “edgeR” package in R software and by considering the counts per million (CPM) criterion (CPM less than 10 in 70% of samples), genes with low expression and close to zero were removed from the normalized data. A boxplot was used to measure the quality control of the normalized data. Differential expression analysis was then performed to compare differences between varicocele samples and normal samples. Genes with a $P<0.05$ and $|logFC|\geq 1$ and $|logFC|<-1$ were defined as candidate genes. Volcano plots indicated differentially expressed genes (DEGs) using the "ggplot2" package in R software. A volcano plot is a type of scatterplot in which each point on the graph represents a gene. The log2-fold differences between the groups are plotted on the x-axis and the P value differences are plotted on the y-axis. The horizontal dashed line represents the significance threshold specified in the analysis.

Protein-protein interaction network and module analysis

One of the best tools for detecting PPI, is the Search Tool for the Retrieval of Interacting Genes (STRING), which is an online tool for recognizing and assessing PPI. The Cytoscape 3.9.1 application was used to establish a PPI network among the selected genes using the STRING plugin. Subsequently, the Molecular Complex Detection (MCODE) plugin was used to cluster the PPI network based on the following criteria: degree cutoff=2, node score cutoff=0.2, k-core=2, and max depth=100. Finally, we employed the CytoHubba plugin in Cytoscape to identify hub genes using 11 topological analysis methods for ranking nodes in the PPI network. In our study, hub genes were classified based on the maximal clique centrality (MCC) method. The MCC method was chosen because it captures essential proteins in both high-degree and low-degree regions, making it more effective than other methods.

Enrichment analysis

Pathway enrichment analysis helps researchers gain

mechanistic insight into gene lists generated from genome-scale (omics) experiments. ShinyGO, developed based on different R/Bioconductor packages, is a graphical web application that shows the functional acuteness of a set of genes. In this study, three enrichment databases including GO (molecular function, biological process, cellular component), KEGG, and Reactome were used for the identification of gene-related pathways via the ShinyGO (http://bioinformatics.sdstate.edu/go/) application. For the enrichment analysis, we set P<0.05 as the cutoff for statistical significance.

Drug discovery

Drug discovery can be described as the process of recognizing chemical entities that have the potential to become therapeutic agents. Several drug databases have been developed to introduce the drugs and explain the influence of the drugs on patients, and on the role of key genes in different diseases. To determine drugs that could target our selected genes, we made use of some of these drug databases including DTC, TdgClinicalTrial, GuideToPharmacology, ChemblInteractions and NCI. The GSE139447 dataset consisted of three treated samples with Morinda officinalis polysaccharide MOP and three untreated samples. We used this study to evaluate the influence of MOP on the expression levels of key candidate genes in rat varicocele samples (7). Thus, differential expression analysis was performed between three varicocele samples treated with MOP and three varicocele samples, as control, using the "edgeR" package. P<0.05 were considered sufficient to determine that the effectiveness of the drug on the genes was significant.

Statistics

All the analyses were performed using packages in R language 4.1.1 and Bioconductor packages in R software. GraphPadPrisme9 (Dotmatics, USA) was used for constructing the plots and performing the t test analyses. Cytoscape software (version 4.1, The Institute of Systems Biology, USA) was used to draw and categorize the data obtained. It is worth noting that the Limma package used the moderated t test.

Results

Indicating differentially expressed genes

Differential expression analysis showed a total of 1,277 different genes (P<0.05, |log2FC|≥ 1, |log2FC|< -1), of which expression of 677 different genes were up-regulated and expression of 600 different genes was down-regulated (Fig.1, Table S1, See Supplementary Online Information at www.celljournal.org).

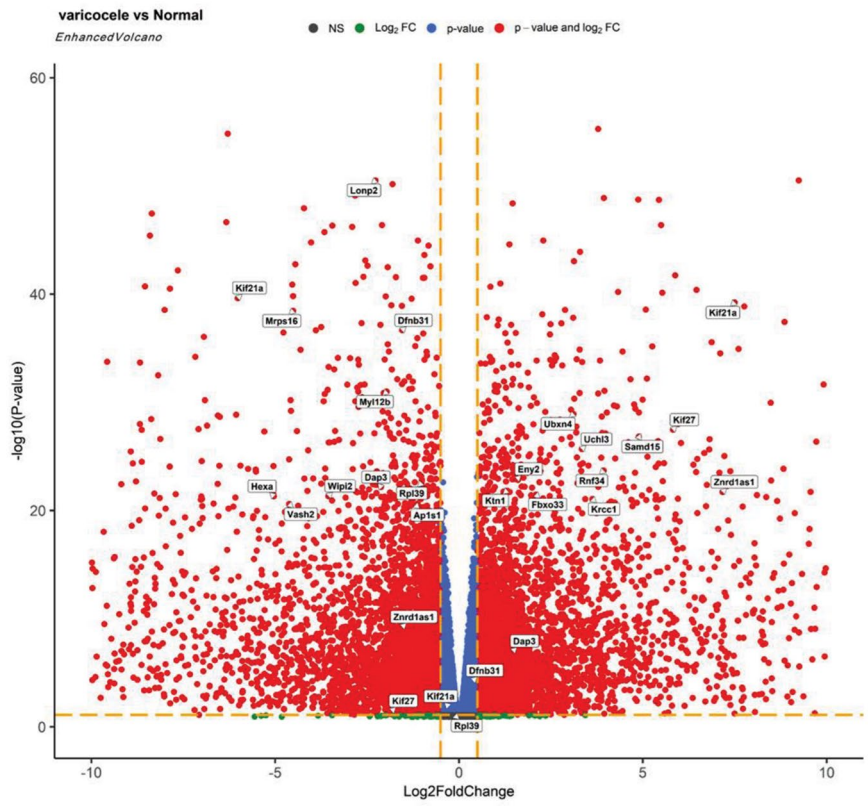

Fig.1: Differentially expressed genes in varicocele compared to normal samples. The expression level of differentially expressed genes (DEGs) was visualized using a volcano plot where the red dots represent the up-regulated genes and the down-regulated genes. Blue dots represent genes that not meet our criteria. The yellow line indicates P value and LogFC cutoffs. The LogFC>1, <-1 and P<0.05 was considered the cut point for statistical significance.

PPI network and generelated clustering module construction

To explore potential interconnections among the identified DEGs, we constructed PPI networks separately for up- and down-regulated genes based on the STRING database. Our analysis revealed that the up-regulated network consisted of 281 nodes and 710 edges, while the down-regulated network contained 181 nodes and 777 edges (Fig.2A, B). We selected the top modules for up- and down-regulated networks based on the highest MCODE score (Table S2, See Supplementary Online Information at www.celljournal.org). The top 5 genes among 30 cluster-related genes with the highest MCC score were designated as the top hub genes for the up-regulated network (*BUB1, SMC4, CENPE, KIF11,* and *ASPM*) and the down-regulated network (*RPL11, RPS15, RPS19, RPS55,* and *RPS2*) (Fig.3A, B, Table S3, See Supplementary Online Information at www.celljournal.org).

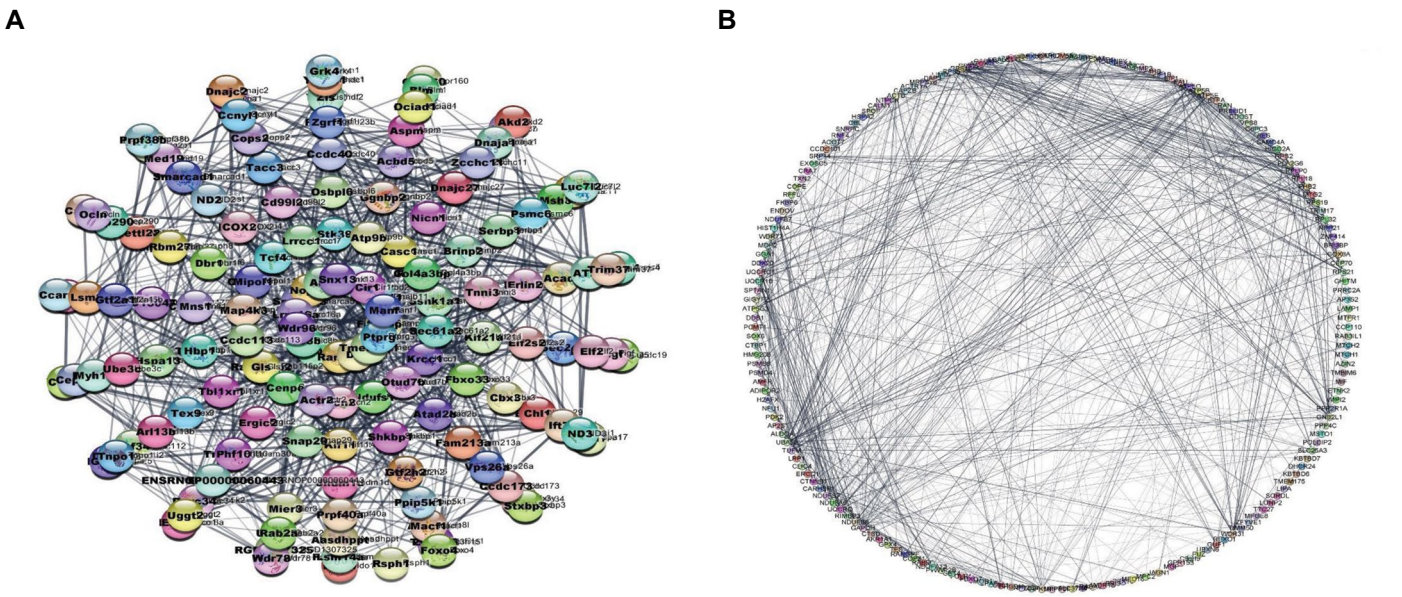

Fig.2: Protein-protein interaction networks. **A.** Up-regulated and **B.** Down-regulated genes.

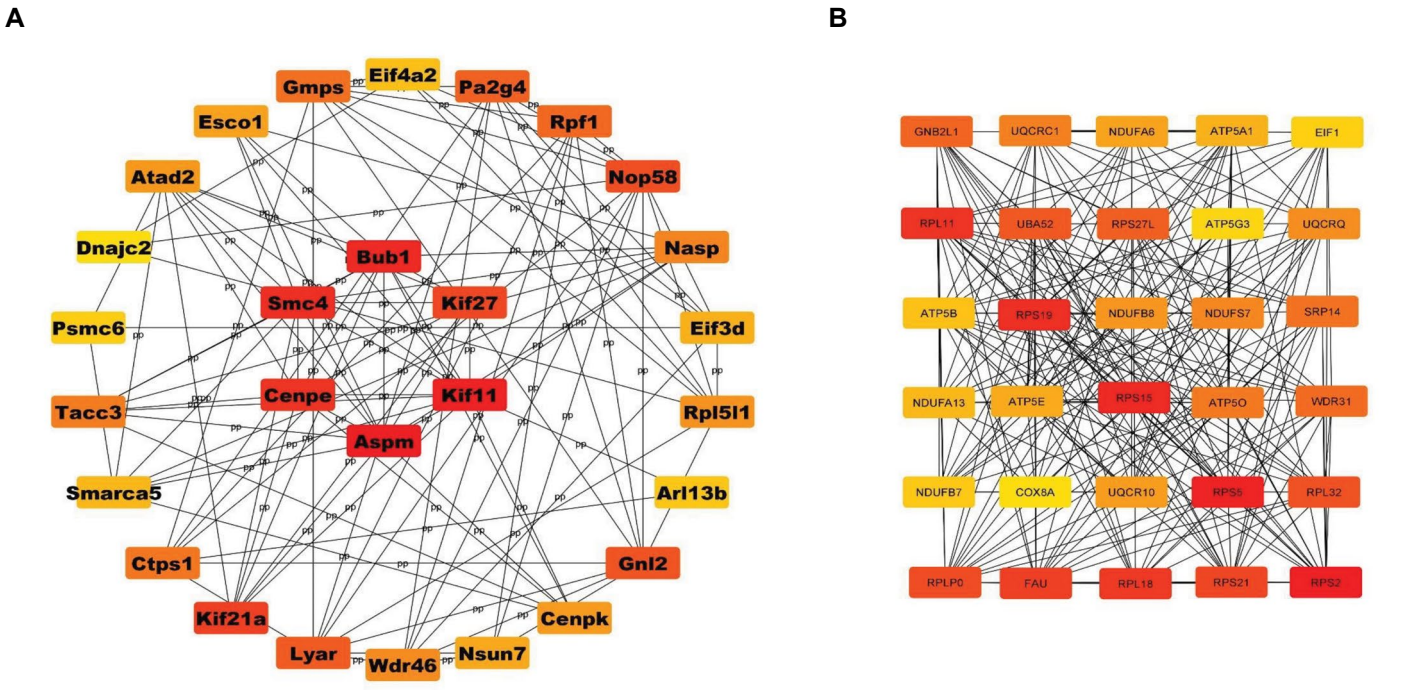

Fig.3: Identification of top hub genes using the Cytohubaa plugin in Cytoscape. **A.** Top hub up-regulated and **B.** Down-regulated genes. Darker colors represent higher Cytohubba scores.

Enrichment analysis for top hub genes

We utilized the ShinyGO online tool to perform functional annotation and pathway enrichment analysis of the top hub genes. To identify pathways related to selected genes with an adjusted P<0.05, KEGG, GO Biological Process, GO Molecular Function, GO Cellular Component, and Reactome datasets were used. The three top terms in each database for up- and down-regulated genes were highlighted based on the P value (Fig.4A-I). For up-regulated genes, the top KEGG pathways included the Cell cycle, oocyte meiosis, and progesterone-mediated oocyte maturation. The top GO Biological Process terms included nuclear division, organelle fission, and mitotic nuclear division. The top GO molecular function terms included microtubule motor activity, cytoskeletal motor activity, and ATP binding. The top GO Cellular Component terms included the chromosome, centromeric region, and mitotic spindle. Additionally, the top Reactome pathways were kinesins, COPI-dependent Golgi-to-ER retrograde traffic, and Golgi-to-ER retrograde transport. For down-regulated genes, the top pathways related to the GO Biological Process were translation, peptide biosynthesis, and peptide metabolism. The top GO Molecular Function terms included structural components of ribosomes, structural molecule activity proteins, and ubiquitin-protein transferase inhibitor activity. The top GO Cellular Component terms included ribosomes, small ribosomal subunits, and ribosomal subunits. The top Reactome pathways were l13a-mediated translational silencing of ceruloplasmin expression, SRP-dependent co-translational protein targeting to membranes, and eukaryotic translation initiation. Notably, the down-regulated genes were not significantly enriched in the KEGG pathway (Fig.4A-I). Therefore, our investigation showed that most varicocele-related pathways were involved in cell division and ribosomal pathways.

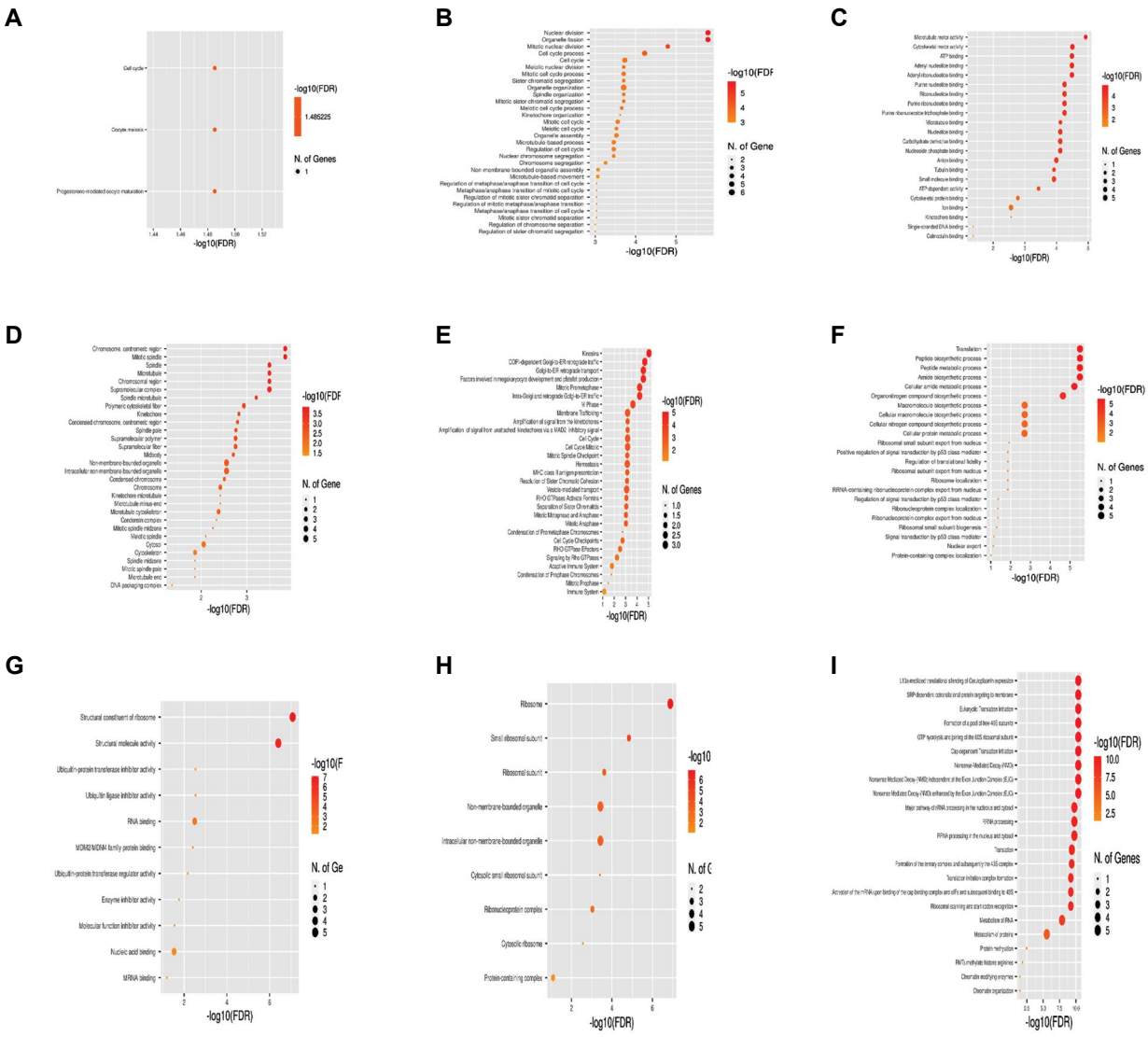

Fig.4: Enrichment analysis based on top hub up- and down-regulated genes. **A.** Dot plots represent top up-regulated genes in five selected pathways including KEGG, **B.** GEO biological process, **C.** Molecular function, **D.** Cellular component and **E.** Reactome datasets. **F.** Down-regulated genes include biological processes, **G.** Molecular function, **H.** Cellular component, and **I.** Reactome datasets. A P<0.05 was used to denote statistical significance.

Identification of suitable drugs

Recognizing drugs that could change the expression level of key genes with altered expression in varicocele could reduce the severity of this disease. Based on the Drug Gene Interaction Database (DGIdb) and the score obtained, drugs that could affect the expression level of candidate genes in varicocele patients were identified. The GSE139447 study was used to evaluate the effect of MOP on our candidate genes (Materials and Methods). Our results showed that among the up-regulated candidate genes, the expression levels of *BUB1, SMC4, CENP-E*, *ASPM*, were up-regulated by the effect of the MOP drug on varicocele samples, while the expression level of *KIF11* was not changed significantly. In addition, the expression of *RPS5* and *RPL11* were up-regulated significantly by the effect of MOP on varicocele samples, while the expression of *RPS19* was down-regulated significantly, and the expression of *RPS2* and *RPS15* were not significantly changed (Fig.5A-J). Our results indicated that the expression level of *KIF11* was lowered by some drugs like DIMETHYLENASTRON, CHEMBL392369, CHEMBL409102, ISPINESIB, AZD-4877, and LITRONESIB, some of which have been reported to have inhibitory roles. Furthermore, our results showed that the expression level of *RPS19* could be increased by DEXAMETHASONE (Table 1). Therefore, our outcomes suggested that MOP could have strong effects on the master genes in varicocele and could potentially impede its progression.

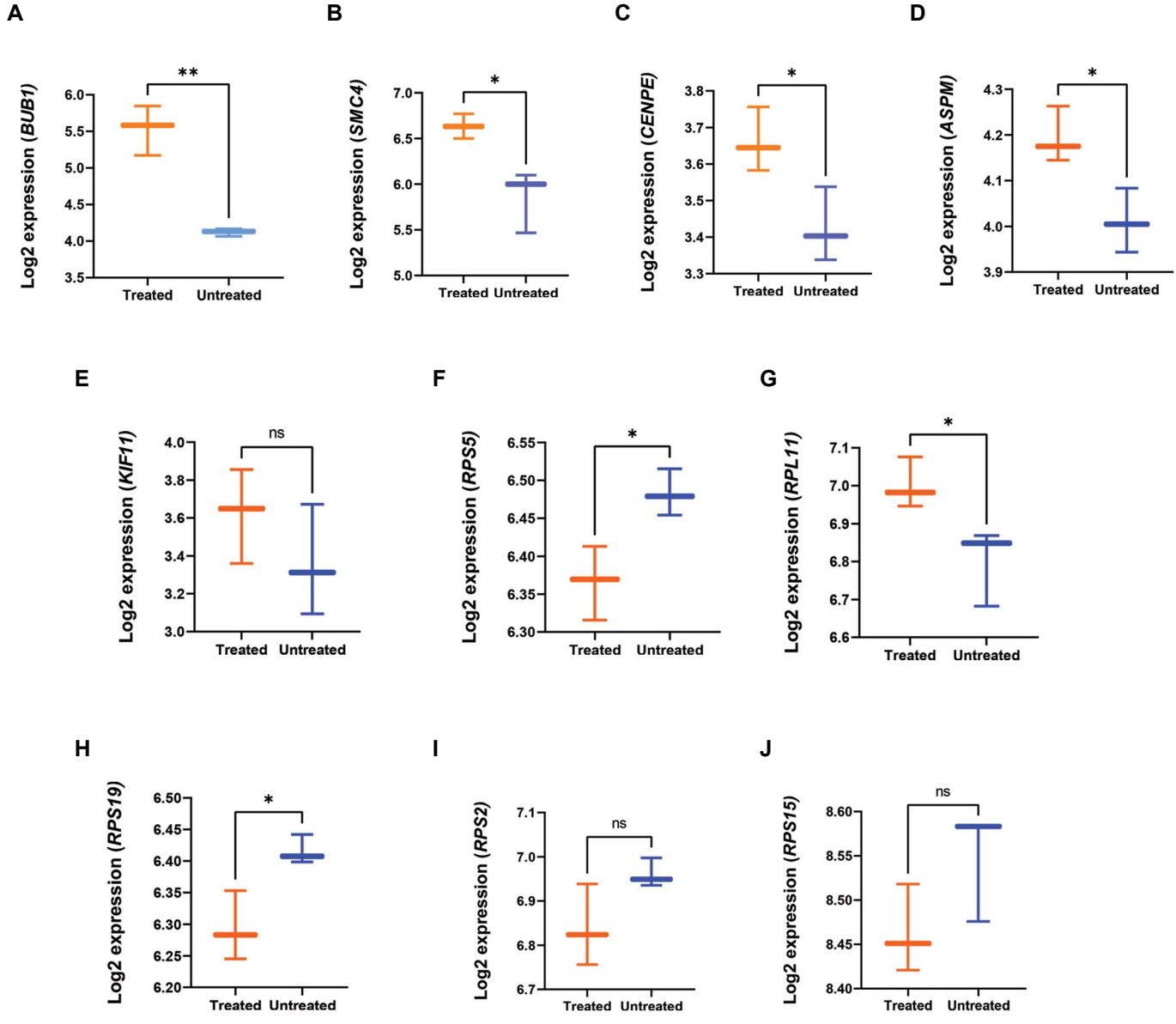

Fig.5: The effect of Morinda officinalis polysaccharide (MOP) on the expression levels of candidate genes. **A-E.** The effect of MOP drug on the expression levels of up-regulated and **F-J.** Down-regulated genes using the normalized count from the GSE139447 study. The Limma moderate t test was used to evaluate the degree of significance with the cutoff for statistical significance set at P<0.05, *; P<0.05, **; P≤0.01, and ns; P>0.05.

Table1: List of drugs effective on the candidate genes based on approved databases

Drug name	Score	Database	PMIDs	GENE	Specific action
DIMETHYLENASTRON	12.73	DTC	20138511	*KIF11*	Inhibitor
CHEMBL392369	12.73	DTC	19167222	*KIF11*	Inhibitor
CHEMBL409102	12.73	DTC	21344920	*KIF11*	Inhibitor
ISPINESIB	12.73	TdgClinicalTrial	NA	*KIF11*	Inhibitor
AZD-4877	12.73	GuideToPharmacology	NA	*KIF11*	Inhibitor
LITRONESIB	6.37	ChemblInteractions	NA	*KIF11*	Inhibitor
DEXAMETHASONE	5.89	NCI	15755903	*RPS19*	Stimulatory

NA; Not available.

Discussion

Varicocele is recognized as the primary and most remediable cause of male infertility. Nevertheless, some varicocele-affected men can procreate without intervention. This apparent contrast in fertility outcomes between varicocele-afflicted men who father at least one child and those who are infertile has remained a largely unresolved issue in the field of andrology (8). While obtaining semen and especially testicular biopsy from varicocele patients who have fathered a child can be challenging, animal models offer an alternative approach to deepen our understanding of the underlying causes of varicocele. The rat model has been widely utilized to explore the cellular and molecular mechanisms underlying varicocele and to advance our comprehension of this condition. Nevertheless, there is still potential for a more comprehensive approach (5).

In this study we utilized the transcriptomic profile of GSE139447 to investigate differentially expressed genes. Our analysis found 1,277 differentially expressed genes, including 677 up-regulated genes and 600 down-regulated genes. To identify key genes, we constructed PPI networks and obtained several modules. Using the cytohubba plugin, we identified the hub genes for the up- and down-regulated genes. The top five up-regulated hub genes were *BUB1, SMC4, CENPE, KIF11*, and *ASPM*, all of which are related to the cell division cycle. The top down-regulated genes were *RPL11, RPS15, RPS19, RPS5*, and *RPS2*, which are all involved in ribosomal pathways.

The findings of this study showed that all five of the top hub genes were intricately linked to the mechanism of cell division. It can be comprehended that even slight fluctuations in temperature can disrupt the organization of microtubules, which can ultimately lead to severe cellular consequences (9). These genes include:

BUB1 is a key protein mediating spindle-checkpoint activation and plays a key role in the inhibition of the anaphase-promoting complex/cyclosome (APC/C). Therefore, it is not surprising that a SNP in this gene predisposes humans to disease or affects drug response. In addition, BUB1 plays a central role in centromere cohesion and spindle assembly checkpoint (SAC). In human oocytes, the activity *BUB1* decreases with age while concomitantly the inter-kinetochore distances of bivalent chromosomes strongly increase with age (10). The consequence of this is aberrant sister chromatid separation in meiosis I, leading to aneuploidy (10, 11). Therefore, up-regulation of *BUB1* could be considered as a compensatory mechanism to overcome the heat-induced spindle-checkpoint aberrations in varicocele.

SMC4 one of the other up-regulated hub genes identified in this study, is another component of cohesion within multi-unit protein complexes (12). These complexes are involved in the maintenance of the chromosome family and are associated with "spermatoproteasomes" (13, 14). In this regard, the miRNAs related to *SMC4* have been shown to be differentially expressed between fertile and infertile males with abnormal semen parameters. Therefore, up-regulation of this gene is possibly another compensatory approach to reduce anomalies in mitotic and meiotic divisions by overcoming aberrant protein degradation.

The precise regulation of protein homeostasis is crucial for the proper functioning of specific protein groups during different stages of spermatogenesis. The inactivation or degradation of these proteins at specific stages is necessary for the step-wise progression of spermatogenesis. This process involves unique protein degradation events that are facilitated by testis-associated proteasome isoforms, known as “spermatoproteasomes”. Dysfunctions in these spermatoproteasomes have been linked to the pathogenesis of male infertility related to the ubiquitin-proteasome system, and may also be associated with chromatin defects that contribute to abnormal sperm morphology (12, 15, 16).

CENP-E similar to *BUB1*, regulates chromosome alignment and mediates kinetochore-microtubule attachment (17, 18). The specific inhibition of this protein significantly disrupts spermatogenesis and

can result in the arrest of the cell cycle, chromosome misalignment, spindle disorganization, and, ultimately, the formation of aneuploid cells. Moreover, the disruption of *CENP-E* function can lead to defects in spermatid formation, including impaired sperm head condensation and tail formation. For instance, Baccetti et al. (19) demonstrated that men with varicocele commonly exhibit mean frequencies of disomies and diploidy outside the normal range, indicating a severe disturbance in meiotic segregation.

KIF11 is involved in various kinds of spindle dynamics including chromosome positioning, centrosome separation, and establishing a bipolar spindle during cell mitosis (20). Thus, *KIF11* plays a crucial role in facilitating the proper progression of meiosis during spermatogenesis. Studies have shown that exposure to plasticizers can reduce its expression in male rat offspring. In addition, during spindle formation, its expression is altered in spermatogenesis-arrested mutant mice. Therefore, it serves as a pre-meiotic marker in germ cells and is essential for normal nuclear meiotic events (21).

Single-cell transcriptional analysis revealed that *KIF11* is notably overexpressed in spermatogonia and primary spermatocytes, as compared to other testicular cells. In these cells, the low expression of *KIF11,* as compared to cells with high expression of *KIF11*, cyclin binding, apoptotic processes, toxic substance binding, biological adhesion, DNA replication, identical protein binding, nuclear outer membrane of the endoplasmic reticulum membrane network, and the cell cycle are significantly enriched (20). Therefore, it is of note that *KIF11* is not only required for mitosis and meiosis but also is fundamental to a number of other biological functions, such as axonal transport in sperm motility.

ASPM is one of the genes involved in the regulation and evolution of brain size in primates and its mutation is associated with microcephaly and major defects in both male and female germlines (22). *ASPM* plays a central role in processes such as mitotic and meiotic spindle regulation, ciliary and flagellar function, and is essential for proper brain development. Given its critical role in these processes, it is not surprising that mutations in *ASPM* can lead to infertility. In the context of varicocele, the upregulation of *ASPM* may serve as a compensatory mechanism to improve the process of spermatogenesis

In summary, our analysis identified five up-regulated hub genes that are associated with cell division. Interestingly, the down-regulation of these genes is expected upon the reversal of varicocele, indicating that their up-regulation serves as a compensatory mechanism to rectify cell division-related disorders in the state of varicocele. However, in the long term, lack of recovery from varicocele, may possibly lead to a gradual decrease in the expression of these genes. The consequence of this depletion in these genes could result in reduced sperm count and motility, increased sperm abnormalities, and germline depletion in both human and rat models. It is important to note that the dataset used in this study was derived from rats with chronic varicocele, which is similar to the chronic condition observed in humans. In contrast, the only other available transcriptomic study in the literature utilized an acute rat model of varicocele. The observed differences between these two studies may be attributed to the distinction between the chronic and acute models. Although no transcriptomic analyses of human varicocele have been conducted yet, it would be intriguing to examine how future human studies align with the chronic or acute rat model, providing valuable insights into the condition in humans.

As stated above, the up-regulation of these genes is likely to be related to compensatory mechanisms, and to maintain spermatogenesis in surviving seminiferous tubules. Therefore, it is worth noting that MOP, which is also believed to have anti-inflammatory effects, increased the expression of these five up-regulated genes, of which 4 were significant. Observing that MOP in the state of varicocele increases the expression of these compensatory genes gives hope for remedying varicocele. Based on data presented in Table 1, it was interesting to note that 6 out of the 7 predicted drugs targeted *KIF11* via inhibitory action. Considering that *KIF11* is a pre-meiotic marker, its reduced expression may also be an alternative way to save pre-meiotic cells from entering a defective process of spermatogenesis; an hypothesis which needs future consideration.

Four of the top down regulated genes are associated with ribosomes, which are macromolecular machines involved in protein synthesis and composed of small and large 40S and 60S subunits, consisting of four RNA species and approximately eighty structurally distinct proteins. The "ribosome filter hypothesis" proposes that the specific functions of ribosomal proteins may make ribosomes selective for mRNA translation in a cell type- or tissue-specific manner, such as in the testis (23). By doing so, it minimizes the energy resources or cost of generating misfolded proteins at the earliest stages and occurs during ER-stress (24). This has important implications considering that seventy percent of cell energy is used for protein synthesis. In this analysis, the five down-regulated genes are:

RPL11 has been shown to be up-regulated in the normozoospermic group, as compared to the asthenozoospermic group. Moreover, in men with idiopathic infertility, antioxidant supplementation has been reported to increase the expression of this transcript, indicating its potential therapeutic value in the management of male infertility (25).

However, the deficiency of *RPL11* has been associated with reduced p53 responses and high C-MYC levels (RPL11-3). In the case of varicocele, the reduced expression of RPL11 may serve as a compensatory mechanism to transiently inhibit apoptosis induced by the condition. It is important to note that RPL11 is among the sperm-intact RNAs delivered to the zygote during

fertilization (RPL11-2), and its reduced level may have an impact on zygote quality (26).

RPS15 mutations rewire the translation program of primary CLL cells by reducing their translational efficiency. In addition, mutations in the C-terminal tail of human RPS15 have been shown to induce defective translation and impair the late pre-40S maturation step in the cytoplasm, the consequence of which could be reduced protein synthesis in varicocele (27).

In this regard, transcriptomic assessment of individuals with Klinefelter syndrome showed that RPS15 was among the hub genes in sperm, with higher expression observed in the control group. Interestingly, its expression showed a downward trend from SSC cells to sperm, indicating its potential role in spermatogenesis in normal individuals (28).

It was interesting to note that the expression of *RSP19*, a ribosomal protein, was reduced when sperm were exposed to the stress of both slow and rapid freezing (29, 30). It was also interesting to note that in an integrative network analysis of proteins, nine of the 10 hubs were cytoplasmic ribosomal proteins and *RPS19* was among these 9 hub genes (31). Gur and Breitbart (32) state that, despite spermatozoa being relatively transcriptionally and translationally silent, some studies have reported the existence of de novo protein synthesis under capacitation conditions. These proteins may be important for the replacement of some degraded proteins during capacitation events and their impairment may account for reduced motility, actin polymerization, acrosomal reaction, and *in vitro* fertilization. Therefore, low levels of ribosomal proteins, like *RPS19*, occurring in varicocele may account for poor-sperm quality.

RPS5 is another ribosomal protein shown to be down-regulated in asthenozoospermic and normozoospermic men compared to fertile or control groups (33). This statement indicates the critical role of ribosomes in producing healthy sperm and highlights the association between defects in their biogenesis and various diseases. It has been suggested that the copy number of ribosomal DNA is correlated with gene expression variation and mitochondrial DNA abundance in humans. As mitochondria have their own translational machinery and the down-regulation of ribosomal proteins could affect the assembly of ribosomes in mitochondria, it is possible that the consequence of reduced *RPS15* expression could lead to mitochondrial dysfunction in spermatozoa and, thereby, oxidative stress (34).

RPS2 has also been reported to be down-regulated during cryopreservation stress in human sperm (35). In addition, Talluri et al. (35) showed the expression of *RPS2* to be lower in low-fertile vs high-fertile bulls. They also concluded that this might be related to the role of the ribosomes in mitochondrial biogenesis which also accounts for oxidative stress.

Taken together, the analysis of both up-regulated and down-regulated hub genes, particularly those involved in mitotic and meiotic machinery for the up-regulated genes, and ribosomal machinery for the down-regulated genes, shows the significance of these biological processes in varicocele. However, a search in PubMed and Google suggests that these processes have not received much attention in the context of varicocele, despite their importance as highlighted in this network analysis. On the other hand, literature surveys have demonstrated that oxidative-reductive imbalance, endoplasmic stress, and altered metabolism are central factors in the biological and molecular pathways underlying varicocele pathophysiology (5). Differences observed through various biological approaches have contributed to the observed complexity of the pathophysiology of varicocele. However, these differences also provide an opportunity for further investigation to determine which biological or molecular pathways have a major impact on the infertility associated with varicocele. In this regard, a comparative study conducted by Xu et al. (36) evaluated the proteome profile of testicular tissues in rats with varicocele and after varicocelectomy. The study reported significant changes in the expression of several proteins, including 40S ribosomal protein S24, 60S ribosomal protein L38, and 60S ribosomal protein L32, which were ranked as the top first, fourth, and eighth proteins, respectively, in terms of the magnitude of the change in their expression in varicocele. This finding further confirms the effect of varicocele on protein machinery.

In addition, the study carried by Zhu et al. (37) which assessed key genes in varicocele rats via high-throughput sequencing and bioinformatics showed that oxidative stress-induced cell death and amyotrophic lateral sclerosis are the two major pathway involved in varicocele. These findings are consistent with the literature on the acute model of varicocele (8 weeks after surgery), while the data from this study pertains to the chronic model of varicocele (12 weeks), which resembles chronic varicocele in humans. Additionally, our study may shed light on the role of oxidative-reductive stress, ER stress, hypoxia, and related mechanisms that may be secondary to the altered regulation of these hub genes. Our study is the first bioinformatics study of chronic varicocele in a rat model. Differences between the two studies are likely to be related to difference between the acute vs the chronic model.

Considering the temperature sensitivity of mitotic and meiotic spindles, the up-regulation of genes related to the meiotic and mitotic machinery to improve the integrity of cell division is understandable. However, the altered or reduced expression of genes related to ribosomal biosynthesis is intriguing and novel, as it evidently affects protein biosynthesis. In this regard, it has been demonstrated that free ribosomal proteins regulate the Mdm2/p53 axis, leading to DNA damage, cell cycle arrest, apoptosis, and autophagy. Therefore, reduced expression of ribosomal proteins may inhibit the Mdm2/p53 axis, reducing the ability of the testis to remove DNA-damaged cells, and allowing processes like cell

cycle arrest, apoptosis, and autophagy to be executed.

Based on the Drug Gene Interaction Database analysis, Dexamethasone is the only predicted drug that targets ribosomes. However, it is interesting to note that MOP seems to increase the expression of *RPS5* and *RPS11*, while decreasing the expression of *RPS19*. In contrast, changes in the expression of *RPS15* and *RPS2* were insignificant (38).

It is noteworthy that dexamethasone has been demonstrated to decrease inflammation-induced oxidative and nitrosative stresses in a rat model of varicocele. In their study, Khosravanian et al. (39) showed that dexamethasone safeguarded testicular endocrine functions and facilitated the process of spermatogenesis. However, the effect of dexamethasone on ribosomal proteins in the context of varicocele remains to be investigated. Despite prior studies by Wang et al. (40) on teratozoospermia and by Zhang et al. (41) on asthenozoospermia, proposing a connection between ribosomal function and male infertility, the role and function of ribosomes in varicocele has not been explored. This is significant, given that varicocele is a well-known and treatable cause of male infertility. In this regard, unexpectedly, the second largest family of proteins, after the nucleoproteins, identified in the isolated human sperm nucleus corresponds to the ribosomal proteins (42). In addition, the background literature shows that among the ribosomal protein, *RPS6* regulates the viability of Sertoli cells in blood-testis barrier dynamics in rats, and deficiency of Rpl10lin in male mice and humans results in infertility (43-45). Collectively, these finding indicate that the disruption of ribosome biogenesis should be considered as one of the possible causes of male infertility. Considering the fact that ribosomal proteins constitute the second largest family of proteins in sperm, their reduced expression may be related to their abundance rather than their functions. This may also be true for other proteins, and, taken together, the functional importance of these findings requires validation.

Given the highly condensed and transcriptionally inert nature of the sperm nucleus, mitochondrial machinery is likely to be the sole player in translational processes within the sperm. As such, the altered transcription of ribosomal proteins may significantly impact mitochondrial function, which in turn may partially account for the oxidative-reductive stress observed in varicocele. The abundance of ribosomal protein in the sperm nucleus is not surprising, as it has been reported to be present in the cell nuclei of other eukaryotic cell types. The assembly of the 40S and 60S ribosomal subunits typically occurs in the nucleolar compartment of the nucleus, with later maturation events occurring in the nucleoplasm and cytoplasm. This suggests that altered ribosomal function in the context of varicocele could have implications beyond mitochondrial dysfunction, potentially impacting nucleolar and cytoplasmic processes as well (46, 47). This suggests that the sperm nucleus could potentially serve as a reservoir for ribosomal proteins that may play a role after fertilization, although further research is needed to explore this possibility. Alternatively, it is possible that these ribosomal proteins are simply remnants of spermatogenic differentiation.

Conclusion

Based on the results obtained in this study, it appears that cell division and ribosomal pathways are the most severely affected in chronic varicocele, and although the existing literature partly supports the outcome of this study, lab verification remains to be ascertained. The difference between this study and the only previous study on rat varicocele is likely to be related to the differences between the acute vs the chronic model of varicocele; an hypothesis which also needs verification. In addition, this type of study generates hypotheses for future lab studies and testing of candidate drugs, like dexamethasone, to remedy the damage induced by varicocele. It is important to note that this study was limited to rat models, and further research in humans is needed to validate these findings.

Acknowledgements

We also thank our colleagues for their support with and helpful discussions about the study. There is no financial support and conflict of interest in this study.

Authors' Contributions

A.V.M.; Design, Conceptualization and Methodology of the study was undertaken. M.A.; Data mining, Formal analysis, and Investigation. A.N.-E., K.P.; Carried out the literature search and helped with interpretation and writing of the manuscript. M.H.N.-E.; Supervision, Validation, Visualization, Reviewed, Edited and Approved. All authors read and approved the final manuscript.

Reference

1. Paduch DA, Skoog SJ. Current management of adolescent varicocele. Rev Urol. 2001; 3(3): 120-133.
2. Cozzolino DJ, Lipshultz LI. Varicocele as a progressive lesion: positive effect of varicocele repair. Hum Reprod Update. 2001; 7(1): 55-58.
3. Arab D, Doustmohammadi H, Ardestani Zadeh A. Dietary supplements in the management of varicocele-induced infertility: a review of potential mechanisms. Andrologia. 2021; 53(1): e13879.
4. Swain N, Samanta L, Agarwal A, Kumar S, Dixit A, Gopalan B, et al. Aberrant upregulation of compensatory redox molecular machines may contribute to sperm dysfunction in infertile men with unilateral varicocele: a proteomic insight. Antioxid Redox Signal. 2020; 32(8): 504-521.
5. Razi M, Tavalaee M, Sarrafzadeh-Rezaei F, Moazamian A, Gharagozloo P, Drevet JR, et al. Varicocoele and oxidative stress: new perspectives from animal and human studies. Andrology. 2021; 9(2): 546-558.
6. Ni K, Steger K, Yang H, Wang H, Hu K, Chen B. Sperm protamine mRNA ratio and DNA fragmentation index represent reliable clinical biomarkers for men with varicocele after microsurgical varicocele ligation. J Urol. 2014; 192(1): 170-176.
7. Zhang L, Zhao X, Wang W. lncRNA and mRNA sequencing of the left testis in experimental varicocele rats treated with Morinda officinalis polysaccharide. Exp Ther Med. 2021; 22(4): 1136.
8. Jensen CFS, Østergren P, Dupree JM, Ohl DA, Sønksen J, Fode M. Varicocele and male infertility. Nat Rev Urol. 2017; 14(9): 523-533.

9. Nishio K, Yamazaki M, Taniguchi M, Besshi K, Morita F, Kunihara T, et al. Sensitivity of the meiotic stage to hyperthermia during in vitro maturation of porcine oocytes. Acta Vet Hung. 2017; 65(1): 115-123.
10. Lagirand-Cantaloube J, Ciabrini C, Charrasse S, Ferrieres A, Castro A, Anahory T, et al. Loss of centromere cohesion in aneuploid human oocytes correlates with decreased kinetochore localization of the sac proteins Bub1 and Bubr1. Sci Rep. 2017; 7: 44001.
11. Marchetti F, Venkatachalam S. The multiple roles of Bub1 in chromosome segregation during mitosis and meiosis. Cell Cycle. 2010; 9(1): 58-63.
12. Gómez L, Felipe-Medina N, Condezo YB, Garcia-Valiente R, Ramos I, Roig I, et al. Spermatoproteasome-deficient mice are proficient in meiotic DNA repair but defective in meiotic exit. bioRxiv. 2018; 384354. Available from: https://www.biorxiv.org/content/10.1101/384354v1.full.pdf (3 Aug 2018).
13. Siddiqui NU, Rusyniak S, Hasenkampf CA, Riggs CD. Disruption of the Arabidopsis SMC4 gene, AtCAP-C, compromises gametogenesis and embryogenesis. Planta. 2006; 223(5): 990-997.
14. Xiong Y, Yu C, Zhang Q. Ubiquitin-proteasome system-regulated protein degradation in spermatogenesis. Cells. 2022; 11(6): 1058.
15. Salas-Huetos A, Blanco J, Vidal F, Godo A, Grossmann M, Pons MC, et al. Spermatozoa from patients with seminal alterations exhibit a differential micro-ribonucleic acid profile. Fertil Steril. 2015; 104(3): 591-601.
16. Wen FP, Guo YS, Hu Y, Liu WX, Wang Q, Wang YT,et al. Distinct temporal requirements for autophagy and the proteasome in yeast meiosis. Autophagy. 2016; 12(4): 671-688.
17. Abrieu A, Kahana JA, Wood KW, Cleveland DW. CENP-E as an essential component of the mitotic checkpoint in vitro. Cell. 2000; 102(6): 817-826.
18. She ZY, Yu KW, Zhong N, Xiao Y, Wei YL, Lin Y, et al. Kinesin-7 CENP-E regulates chromosome alignment and genome stability of spermatogenic cells. Cell Death Discov. 2020; 6: 25.
19. Baccetti BM, Bruni E, Capitani S, Collodel G, Mancini S, Piomboni P, et al. Studies on varicocele III: ultrastructural sperm evaluation and 18, X and Y aneuploidies. J Androl. 2006; 27(1): 94-101.
20. Hara-Yokoyama M, Kurihara H, Ichinose S, Matsuda H, Ichinose S, Kurosawa M, et al. KIF11 as a potential marker of spermatogenesis within mouse seminiferous tubule cross-sections. J Histochem Cytochem. 2019; 67(11): 813-824.
21. Cannarella R, Condorelli RA, Mongioì LM, La Vignera S, Calogero AE. Molecular biology of spermatogenesis: novel targets of apparently idiopathic male infertility. Int J Mol Sci. 2020; 21(5): 1728.
22. Pulvers JN, Bryk J, Fish JL, Wilsch-Bräuninger M, Arai Y, Schreier D, et al. Mutations in mouse Aspm (abnormal spindle-like microcephaly associated) cause not only microcephaly but also major defects in the germline. Proc Natl Acad Sci USA. 2010; 107(38): 16595-16600.
23. Mauro VP, Edelman GM. The ribosome filter redux. Cell Cycle. 2007; 6(18): 2246-2251.
24. Sitron CS, Brandman O. Detection and degradation of stalled nascent chains via ribosome-associated quality control. Annu Rev Biochem. 2020; 89: 417-442.
25. Bansal SK, Gupta N, Sankhwar SN, Rajender S. Differential genes expression between fertile and infertile spermatozoa revealed by transcriptome analysis. PLoS One. 2015; 10(5): e0127007.
26. Sun YH, Wang A, Song C, Shankar G, Srivastava RK, Au KF, et al. Single-molecule long-read sequencing reveals a conserved intact long RNA profile in sperm. Nat Commun. 2021; 12(1): 1361.
27. Chan D, Delbès G, Landry M, Robaire B, Trasler JM. Epigenetic alterations in sperm DNA associated with testicular cancer treatment. Toxicol Sci. 2012; 125(2): 532-543.
28. He H, Huang T, Yu F, Chen K, Guo S, Zhang L, et al. KIF2C affects sperm cell differentiation in patients with Klinefelter syndrome, as revealed by RNA-Seq and scRNA-Seq data. FEBS Open Bio. 2022; 12(8): 1465-1474.
29. Corda PO, Silva JV, Pereira SC, Barros A, Alves MG, Fardilha M. Bioinformatic approach to unveil key differentially expressed proteins in human sperm after slow and rapid cryopreservation. Front Cell Dev Biol. 2022; 9: 759354.
30. Fu L, An Q, Zhang K, Liu Y, Tong Y, Xu J, et al. Quantitative proteomic characterization of human sperm cryopreservation: using data-independent acquisition mass spectrometry. BMC Urol. 2019; 19(1): 133.
31. Prakash MA, Kumaresan A, Sinha MK, Kamaraj E, Mohanty TK, Datta TK, et al. RNA-Seq analysis reveals functionally relevant coding and non-coding RNAs in crossbred bull spermatozoa. Anim Reprod Sci. 2020; 222: 106621.
32. Gur Y, Breitbart H. Protein synthesis in sperm: dialog between mitochondria and cytoplasm. Mol Cell Endocrinol. 2008; 282(1-2): 45-55.
33. Choucair F. Unraveling the sperm transcriptome by next generation sequencing and the global epigenetic landscape in infertile men. 2018. Avialable from: https://theses.hal.science/tel-01958881/preview/2018AZUR4058.pdf (6 Sep 2018).
34. Gibbons JG, Branco AT, Yu S, Lemos B. Ribosomal DNA copy number is coupled with gene expression variation and mitochondrial abundance in humans. Nat Commun. 2014; 5: 4850.
35. Talluri TR, Kumaresan A, Sinha MK, Paul N, Ebenezer Samuel King JP, Datta TK. Integrated multi-omics analyses reveals molecules governing sperm metabolism potentially influence bull fertility. Sci Rep. 2022; 12(1): 10692.
36. Xu F, Gao QQ, Zhu LL, Jiang HS, Chen H, Xu ZP, et al. Impact of varicocelectomy on the proteome profile of testicular tissues of rats with varicocele. Andrologia. 2018; 50(2).
37. Zhu J, Ou N, Song Y, Hu R, Zhang W, Liang Z, et al. Identification and verification of key genes in varicocele rats through high-throughput sequencing and bioinformatics analysis. Andrologia. 2020; 52(9): e13662.
38. Kang J, Brajanovski N, Chan KT, Xuan J, Pearson RB, Sanij E. Ribosomal proteins and human diseases: molecular mechanisms and targeted therapy. Signal Transduct Target Ther. 2021; 6(1): 323.
39. Khosravanian H, Razi M, Farokhi F, Khosravanian N. Simultaneous administration of dexamethasone and vitamin e reversed experimental varicocele-induced impact in testicular tissue in rats; correlation with Hsp70-2 chaperone expression. Int Braz J Urol. 2015; 41(4): 773-790.
40. Wang X, Ma S, Mao M, Li C, Shen X, Xu S, et al. RNA-sequencing and bioinformatics analysis of long noncoding RNAs and mRNAs in the prefrontal cortex of mice following repeated social defeat stress. Biomed Res Int. 2019; 2019: 7505260.
41. Zhang T, Wu J, Liao C, Ni Z, Zheng J, Yu F. System analysis of teratozoospermia mRNA profile based on integrated bioinformatics tools. Mol Med Rep. 2018; 18(2): 1297-1304.
42. de Mateo S, Castillo J, Estanyol JM, Ballescà JL, Oliva R. Proteomic characterization of the human sperm nucleus. Proteomics. 2011; 11(13): 2714-2726.
43. Jiang L, Li T, Zhang X, Zhang B, Yu C, Li Y, et al. RPL10L is required for male meiotic division by compensating for RPL10 during meiotic sex chromosome inactivation in mice. Curr Biol. 2017; 27(10): 1498-1505. e6.
44. Mok KW, Mruk DD, Cheng CY. rpS6 regulates blood-testis barrier dynamics through Akt-mediated effects on MMP-9. J Cell Sci. 2014; 127(Pt 22): 4870-4882.
45. Tu C, Meng L, Nie H, Yuan S, Wang W, Du J, et al. A homozygous RPL10L missense mutation associated with male factor infertility and severe oligozoospermia. Fertil Steril. 2020; 113(3): 561-568.
46. Antoine M, Reimers K, Wirz W, Gressner AM, Müller R, Kiefer P. Identification of an unconventional nuclear localization signal in human ribosomal protein S2. Biochem Biophys Res Commun. 2005; 335(1): 146-153.
47. Schmidt C, Lipsius E, Kruppa J. Nuclear and nucleolar targeting of human ribosomal protein S6. Mol Biol Cell. 1995; 6(12): 1875-1885.

Cell J
Cell Journal(Yakhteh)
Homepage: https://www.celljournal.org/
Commentary
Vol 25, No 10, October 2023, Pages: 738-740

A Shadow of Knowledge in Stem Cell Science

Sarina Omid-Shafiei, B.Sc.[1], Moustapha Hassan, Ph.D.[2], Andreas K. Nüssler, Ph.D.[3], Mustapha Najimi, Ph.D.[4*], Massoud Vosough, M.D., Ph.D.[1, 2*]

1.Department of Regenerative Medicine, Cell Science Research Center, Royan Institute for Stem Cell Biology, ACECR, Tehran, Iran
2. Experimental Cancer Medicine, Department of Laboratory Medicine, Karolinska Institute, Stockholm, Sweden
3. Department of Traumatology, Siegfried Weller Institute, University of Tubingen, BG Tubingen, Tubingen, Germany
4. Laboratory of Pediatric Hepatology and Cell Therapy, Institute of Experimental and Clinical Research (IREC), UC Louvain, Brussels, Belgium

Abstract

"Theory of Forms" implies that a genuine version of creatures exists beyond the shapes in this world. Stem cell technology has adopted developmental cues to mimic real life. However, the functionality of the lab-made cells is far from primary ones. Perhaps it is time to switch from analytical to systematic perspective in stem cell science. This may be the way to define new horizons based on the systematic perspective and convergence of science in stem cell biology, bridging the current gap between the shadows of real knowledge in current research and reality in future.

Keywords: Theory of Forms, Stem Cell Science, Systems Biology

Citation: **Omid-Shafiei S, Hassan M, K. Nüssler AK, Najimi M, Vosough M. A shadow of knowledge in stem cell science. Cell J. 2023; 25(10): 738-740. doi: 10.22074/CELLJ.2023.2005680.1346**

Greek philosopher Plato implies that beyond all creatures and shapes in this world, there is a far more genuine version of them. How we appear physically is merely an image and a fairly unwitting imitation of the original forms in the "realm of forms" or the "Realm of Ideas". This philosophical theory is named "The theory of Forms or the theory of Ideas" (1, 2).

Human life begins when a fertilized egg passes through the different developmental stages followed by the differentiation of embryonic stem cells to a great number of different cells with varied physiological functions (3, 4). Thanks to the rapid advances in stem cell research during the past four decades, scientists were able to successfully generate a variety of somatic cells by applying the knowledge gained from embryo development. Experimental stem cell differentiation protocols have adopted developmental cues and mimicked micro-environmental and spatiotemporal conditions required for natural development that control most of the cell's fates (5, 6).

However, the functionality of the experimentally generated somatic-like cells is far less than that observed from primary cells both *in vitro* and in living organisms. Hence, the lab-made cells should be considered as tentative, simple, and superficial replicas of the original cells. For instance, stem cell-derived neurons have many similarities with primary neurons in terms of morphological features and they can recapitulate basic physiological functions such as electrical conductivity. However, they lack the advanced capabilities of primary neurons (7). Human activities are controlled by the nervous system; neurons perceive specific stimuli and fire signals that regulate all of a being's actions. Although activation of lab-made neurons does produce an electrical action potential, it does not generate philosophy, critical thinking, rational conclusions, feelings, emotions, intellectual pondering, and many other complicated actions when we pile up billions of them. More specifically, tiny neurons located in the pre-frontal cortex of the human brain, generate concepts and reflect them as meaningful words and emotional fluctuations such as love, passion, misery, grief, and other empathic and mental connections that are tangible and transparent to others. All this convoluted relativity is something that is not present in *in vitro* generated nerve cells (8). We are all aware of limitations of a single cell to perform a distinct physiologic function and we admire the fact that combination of cells in certain clusters enable them to do physiologic activity."

Received: 26/June/2023, Revised: 17/September/2023, Accepted: 30/September/2023
***Corresponding Addresses: Laboratory of Pediatric Hepatology and Cell Therapy, Institute of Experimental and Clinical Research (IREC), UC Louvain, Brussels, Belgium**
Department of Regenerative Medicine, Cell Science Research Center, Royan Institute for Stem Cell Biology, ACECR, Tehran, Iran
Emails: mustapha.najimi@uclouvain.be, masvos@royaninstitute.org

Royan Institute
Cell Journal (Yakhteh)

Since 1998, despite massive efforts to propose pluripotent stem cell (PSC) technology as a promising platform in regenerative medicine, few translational studies reached clinical trials. The heterogeneity of PSC-derived cells in terms of maturity, possible terato-/tumorigenicity, and their poor physiological performance are the main obstacles to reaching their broad application (9). Thus, two major questions can be highlighted:

1. Is it time to summarize our achievements and to reconsider our perspectives and expectations in stem cell research?

2. Could a different standpoint serve as a game changer in this regard?

From a philosophical point of view, current research is based on breaking down complex processes into smaller parts in order to easily understand them, which is called "analytical approach" (10). Therefore, cells were studied as microscopic units of living organisms to understand life's complexity. On the other hand, "systemic approach" enables scientists to handle complex systems with a global perspective without focalizing on details in order to reach equivalent complexity, and without oversimplifying the reality. From a philosophical perspective, this approach corresponds to the holistic school of thought (11).

Thus, there is a philosophical dilemma as to whether the cells represent the whole living thing or if the living system can only be comprehended by the holistic view. Certainly, both views are logical to some extent, however, the pivotal question remains unanswered. Does the living system as a whole, as parts or as cells contain other components that we are not able to understand using the present methodologies and techniques? In other words, does life at molecular or cellular level or even the whole organism itself have any other esoteric forms? Or simply, does the living organism as a "whole" have properties that are more than "the sum" of its components?

Historically, "reductionism" was a step ahead of the subjectivity and holistic views of ancient philosophers. This improved human observation and its confirmation but it also led to a paradox because it relied on parts and not the whole. The historic disagreements between Plato and Aristotle were mostly because of the subjective nature of their observations and their holistic views without experimental confirmation due to lack of modern tools.

After years of research, current knowledge enables scientists to create an environment mimicking reality which is a demo version of real life with living cells. Thus, the situation is like the shape of words drawn by an under-the-school-age child without having any insight into the meaning or the actual message behind them.

Comprehending the complexity of inter- and intracellular reactions and the dynamic cross-talk between the living cells and their microenvironment would provide a new horizon for a better understanding of life. "Systems biology" and "optimization approaches" such as "artificial intelligence" (AI) are interdisciplinary fields in science that can process big data and simplify complicated phenomena (12-14). Both advanced technologies, and their related databases are constantly being expanded and updated. High-tech instruments and in-use software packages generate big data and enable researchers to focus more on data-driven hypotheses rather than idea-driven ones (15). This approach enables scientists to investigate precise hypotheses followed by an exact analytical process in order to reach accurate results/answers without any prejudice and bias.

If systems biology is complemented with a holistic view and philosophy of existence, as well as a reductionist approach, it may present a realistic picture of natural phenomena. Then, stem cells will be viewed as biological substrate for the perfect growth/repair of an organism. The reductionist approach will describe the roles of individual mechanisms in the whole organism and system biology could have its missing puzzle solved with this.

Organoid technology (16-18), microfluidics (19, 20), and OMICS approaches (21) have provided reliable models to investigate the complexity and translation of vast data pools of biological molecules into structures and physiological functions. Human on a chip is a great example for this approach. All these modules together, can on one hand, open new windows for the better understanding of real life and on the other hand, bridge the gap between analytical and systemic approaches.

At present, interdisciplinary approaches and networking in form of collaborating across traditional disciplinary boundaries may help scientists to envisage different perspectives in order to solve their challenges. This, in turn, will help scientists save time and money as well as redefine current challenges beyond their limitations, which may provide innovative solutions based on a new understanding of complex phenomena.

However, even the modern technologies and approaches, in the future, will face the central challenge of "control volume". Does the smallest entity studied in the Petri dish or the highly complex whole organism have other unknown or hidden facets beyond their reach? Is there any other form or realm of existence like that mentioned by Plato some thousand years ago?

In summary, significant progress has been made in the field of stem cell research throughout the years. Still, we are facing the same limitations as for the other configurations in *in vitro* cell culture. Thus, lab-made cells still cannot describe a character in the frame of an overall physiological function like metabolism regulation. Still acting as shadows of their real-life counterparts, these cells are a preliminary version of primary cells in Mother Nature. Thus, lab-made cells cannot describe a character in the frame of a complex activity such as writing a poem or generating images as a result of the excitement of photoreceptor cells in the retina.

In the big data era, scientists need to collaborate more on systematic approaches to understand the complexities of

life and think beyond the current box of knowledge using advanced approaches such as AI to facilitate analysis and interpretation of big data and validate them. What scientists have achieved until now is of great value, but it should not be forgotten that there could be shadows or frames far away from the actual physical forms that exist in the realm of nature. Perhaps it is time to reconsider our current analytical approach in stem cell science to better design the strategy of their applications in regenerative medicine. This may be the way to define new horizons based on the systematic perspective and convergence of science in stem cell biology, bridging the current gap between the shadows of real knowledge in current research and reality in future.

Acknowledgments

Authors would like to express their gratitude to their colleagues at Regenerative Medicine Department, Royan Institute and Experimental Cancer Medicine, Karolinska Institute, as well as Siegfried Weller Institute, and UC Louvain. Also, we would like to thank Prof. MR Heydari, Dr. Faezeh Shekari, Dr. Roya Solhi, Dr. Meghdad Yeganeh, Dr. Fatemeh Mehryab, Ibrahim Ghoytasi, and Sina Vosough for their critical discussion and support. There is no financial support and conflict of interest in this study.

Authors' Contributions

S.O.-S.; Drafted manuscript and contributed in development of the concept. A.K.N., M.H., M.N.; Developed and discussed the idea. M.V., A.K.N., M.H., M.N.; Critically edited manuscript. M.V.; Conceived the idea, developed and discussed the subject and finalized the manuscript.

References

1. Dancy RM. Plato's introduction of forms. Cambridge: Cambridge University Press; 2004.
2. Ross WD. Plato's theory of ideas. Oxford: Clarendon Press; 1951.
3. Rossant J, Tam PPL. Early human embryonic development: Blastocyst formation to gastrulation. Dev Cell. 2022; 57(2): 152-165.
4. Vosough M, Omidinia E, Kadivar M, Shokrgozar MA, Pournasr B, Aghdami N, et al. Generation of functional hepatocyte-like cells from human pluripotent stem cells in a scalable suspension culture. Stem Cells Dev. 2013; 22(20): 2693-2705.
5. Zakrzewski W, Dobrzyński M, Szymonowicz M, Rybak Z. Stem cells: past, present, and future. Stem Cell Res Ther. 2019; 10(1): 68.
6. Zahmatkesh E, Ghanian MH, Zarkesh I, Farzaneh Z, Halvaei M, Heydari Z, et al. Tissue-specific microparticles improve organoid microenvironment for efficient maturation of pluripotent stem-cell-derived hepatocytes. Cells. 2021; 10(6): 1274.
7. Riemens RJM, van den Hove DLA, Esteller M, Delgado-Morales R. Directing neuronal cell fate in vitro: achievements and challenges. Prog Neurobiol. 2018; 168: 42-68.
8. Rouleau N, Murugan NJ, Kaplan DL. Toward studying cognition in a dish. Trends Cogn Sci. 2021; 25(4): 294-304.
9. Liu G, David BT, Trawczynski M, Fessler RG. Advances in pluripotent stem cells: history, mechanisms, technologies, and applications. Stem Cell Rev Rep. 2020; 16(1): 3-32.
10. Jones RH. Reductionism: analysis and the fullness of reality. Bucknell University Press; 2000.
11. Marshall A. The unity of nature: wholeness and disintegration in ecology and science. London: Imperial College Press; 2002.
12. Yue R, Dutta A. Computational systems biology in disease modeling and control, review and perspectives. NPJ Syst Biol Appl. 2022; 8(1): 37.
13. Camacho DM, Collins KM, Powers RK, Costello JC, Collins JJ. Next-generation machine learning for biological networks. Cell. 2018; 173(7): 1581-1592.
14. Bhardwaj A, Kishore S, Pandey DK. Artificial intelligence in biological sciences. Life (Basel). 2022; 12(9): 1430.
15. Mazzocchi F. Could big data be the end of theory in science? A few remarks on the epistemology of data-driven science. EMBO Rep. 2015; 16(10): 1250-1255.
16. Kim J, Koo BK, Knoblich JA. Human organoids: model systems for human biology and medicine. Nat Rev Mol Cell Biol. 2020; 21(10): 571-584.
17. Zahmatkesh E, Khoshdel-Rad N, Mirzaei H, Shpichka A, Timashev P, Mahmoudi T, et al. Evolution of organoid technology: lessons learnt in co-culture systems from developmental biology. Dev Biol. 2021; 475: 37-53.
18. Heydari Z, Moeinvaziri F, Agarwal T, Pooyan P, Shpichka A, Maiti TK, et al. Organoids: a novel modality in disease modeling. Biodes Manuf. 2021; 4(4): 689-716.
19. Ingber DE. Human organs-on-chips for disease modelling, drug development and personalized medicine. Nat Rev Genet. 2022; 23(8): 467-491.
20. Ramezankhani R, Solhi R, Chai YC, Vosough M, Verfaillie C. Organoid and microfluidics-based platforms for drug screening in COVID-19. Drug Discov Today. 2022; 27(4): 1062-1076.
21. Pieters VM, Co IL, Wu NC, McGuigan AP. Applications of omics technologies for three-dimensional in vitro disease models. Tissue Eng Part C Methods. 2021; 27(3): 183-199.